



University
of Glasgow

Caldwell, Jane Cochrane (2006) Ventricular fibrillation in ischaemia and its defibrillation. PhD thesis

<http://theses.gla.ac.uk/6196/>

Copyright and moral rights for this thesis are retained by the author

A copy can be downloaded for personal non-commercial research or study, without prior permission or charge

This thesis cannot be reproduced or quoted extensively from without first obtaining permission in writing from the Author

The content must not be changed in any way or sold commercially in any format or medium without the formal permission of the Author

When referring to this work, full bibliographic details including the author, title, awarding institution and date of the thesis must be given.

Ventricular Fibrillation in Ischaemia and its Defibrillation

A thesis submitted in fulfilment of the degree of

Doctor of Philosophy

to

University of Glasgow

Faculty of Medicine

By

Jane Cochrane Caldwell

BSc (Hons), MB ChB (Hons), MRCP

Department of Medical Cardiology, Glasgow Royal Infirmary

&

Institute of Biomedical and Life Sciences, University of Glasgow

2006





IMAGING SERVICES NORTH

Boston Spa, Wetherby
West Yorkshire, LS23 7BQ
www.bl.uk

**PAGE NUMBERS CLOSE TO
THE EDGE OF THE PAGE.
SOME ARE CUT OFF**

Abstract

The aim of this thesis was to i) study the effect of principal components of ischaemia on electrical activity during ventricular fibrillation and on defibrillation success, and ii) identify the electrophysiological mechanisms underlying these effects.

ECG signals were recorded from isolated, Langendorff-perfused rabbit hearts to establish the relationship between dominant frequency and myocardial perfusion during ventricular fibrillation. Lower perfusion rates produced faster rates of dominant frequency decline, to lower steady state values. Optically mapping the anterior epicardial surface demonstrated heterogeneity of dominant frequency in ventricular fibrillation. During low-flow ischaemia, the dominant frequency reduction was restricted to the left ventricle. Application of individual ischaemic components during ventricular fibrillation demonstrated that raised $[K^+]_{EC}$, but not hypoxia or acidic pH_{EC} , reproduced the ischaemic reduction of dominant frequency in the ECG, pseudoECG and over the left ventricular epicardial surface. In contrast, minimum defibrillation energies were increased by hypoxia and acidic pH_{EC} , and not by raised $[K^+]_{EC}$.

The dominant frequency heterogeneity during ventricular fibrillation in low-flow ischaemia and raised $[K^+]_{EC}$ was not due to differential prolongation of repolarisation or post-repolarisation refractoriness in the left ventricle. Monophasic action potential studies showed that APD_{90} was reduced to similar degrees in each ventricle by low-flow ischaemia and raised $[K^+]_{EC}$. Effective refractory period was not altered in either ventricle by either condition. Low-flow ischaemia decreased conduction velocity in the left, but not the right ventricle. Conduction velocities were unaltered by raised $[K^+]_{EC}$ in either ventricle. The activation threshold of the left ventricle was increased in low-flow ischaemia and raised $[K^+]_{EC}$, whilst the threshold of the right ventricle was unchanged. The increased activation threshold was associated with decreased upstroke velocity and diastolic depolarisation.

In conclusion, this thesis demonstrates that in ventricular fibrillation, the decreased ECG dominant frequency in low-flow ischaemia is predominantly due to slowing of electrical activity in the left ventricle, associated with an elevation in the activation threshold by raised $[K^+]_{EC}$. The differential threshold change in left compared to right ventricle, probably results from differential inhibition of I_{Na} . This thesis hypothesises that greater expression of Kir2.x in the left compared to right ventricle, as previously demonstrated in guinea pig, could underlie the observed electrical heterogeneity in the rabbit.

Table of contents

1	Introduction	22
1.1	Ventricular Fibrillation.....	23
1.1.1	Clinical Relevance.....	23
1.1.2	Electrophysiology of VF	25
1.2	Defibrillation by electric countershock	35
1.2.1	Mechanism of action	35
1.2.2	Assessment of defibrillation energies.....	38
1.2.3	Factors affecting successful defibrillation.....	40
1.3	Techniques for studying electrophysiology of VF	43
1.3.1	Intact vs. isolated.....	43
1.3.2	Global ECG.....	43
1.3.3	Microelectrode.....	45
1.3.4	Monophasic Action Potentials.....	46
1.3.5	Optical mapping	47
1.4	Aims and hypothesis	51
2	Methods	52
2.1	Preparation for Langendorff perfusion.....	53
2.2	Pacing and ECG	53

2.3	VF induction.....	54
2.4	Defibrillation	56
2.5	Optical mapping.....	56
2.6	Analysis of VF.....	59
2.6.1	Frequency analysis of VF.....	59
2.6.2	Amplitude analysis in VF.....	61
2.6.3	Analysis of conduction velocity.....	61
2.7	Monophasic action potential	67
2.7.1	MAP duration and restitution.....	67
2.7.2	Effective refractory period	70
2.8	Floating microelectrode.....	70
2.9	Statistical analysis	71
3	VF frequency in ischaemia.....	73
3.1	Introduction	74
3.2	Method.....	74
3.2.1	Statistical analysis	75
3.3	Results	76
3.3.1	ECG DF time-course with varied perfusion.....	76
3.3.2	Optical measurements in VF during control and low-flow ischaemia	78
3.4	Discussion	81

3.4.1	Time-course of VF DF with varied perfusion	81
3.4.2	Spontaneous VF conversion in zero-flow ischaemia	81
3.4.3	Spatiotemporal Organisation	83
4	VF frequency & isolated ischaemic components	88
4.1	Introduction	89
4.2	Methods	89
4.2.1	Statistical analysis	90
4.3	Results	91
4.3.1	Hypoxia	91
4.3.2	Acidic pH _{EC}	92
4.3.3	Raised [K ⁺] _{EC}	95
4.4	Discussion	97
4.4.1	Hypoxia	98
4.4.2	Acidic pH _{EC}	99
4.4.3	Raised [K ⁺] _{EC}	100
5	Monophasic action potential duration and restitution in low-flow ischaemia & raised [K ⁺] _{EC}	103
5.1	Introduction	104
5.2	Methods	104
5.3	Results	105

5.3.1	40ml/min vs. 6ml/min	105
5.3.2	5mM $[K^+]_{EC}$ vs. 8 & 10mM $[K^+]_{EC}$	109
5.4	Discussion	111
6	Effective refractory period, pacing threshold and dV/dt_{max} in low-flow ischaemia and raised $[K^+]_{EC}$	113
6.1	Introduction	114
6.1.1	Prolongation of post-repolarisation refractoriness	114
6.1.2	Raised threshold for activation	114
6.2	Methods	115
6.3	Results	116
6.3.1	Effective Refractory period (ERP)	116
6.3.2	Activation threshold	118
6.3.3	Maximum Upstroke Velocity	119
6.4	Discussion	120
6.4.1	Prolongation of post-repolarisation refractoriness	121
6.4.2	Raised threshold for activation	122
7	Alterations in conduction velocity	124
7.1	Introduction	125
7.2	Methods	125
7.2.1	Apparent CV measurements in VF	125

7.2.2	Traditional measurements of CV.....	126
7.3	Results	127
7.3.1	Apparent CV in VF	127
7.3.2	Traditional CV measurements.....	129
7.4	Discussion	129
7.4.1	Apparent CV and traditional CV discrepancy.....	130
7.4.2	Traditional CV	132
8	Changes in the amplitude of the VF signal with time	134
8.1	Introduction	135
8.2	Methods	135
8.3	Results	137
8.3.1	VF amplitude in control conditions.....	137
8.3.2	VF amplitude in low-flow ischaemia	139
8.3.3	VF amplitude in hypoxia.....	141
8.3.4	VF amplitude in acidic pH _{EC}	141
8.3.5	VF amplitude in raised [K ⁺] _{EC}	143
8.3.6	Relationship between amplitude and DF.....	146
8.4	Discussion	147
8.4.1	VF amplitude in control conditions.....	147
8.4.2	VF amplitude in low-flow ischaemia	149

8.4.3	VF amplitude in hypoxia	150
8.4.4	VF amplitude in acidic pH_{EC}	151
8.4.5	VF amplitude in raised $[K^+]_{EC}$	152
8.4.6	Relationship between frequency, organisation and amplitude	153
8.4.7	Conclusion	154
9	Membrane potential during VF	155
9.1	Introduction	156
9.2	Methods	156
9.3	Results	158
9.4	Discussion	162
9.4.1	Reduced systolic depolarisation in VF during control conditions	163
9.4.2	No amplitude increase in low-flow ischaemia or raised $[K^+]_{EC}$	164
9.4.3	Diastolic depolarisation in raised $[K^+]_{EC}$	164
10	Minimum defibrillation energies	166
10.1	Introduction	167
10.2	Methods	167
10.3	Results	169
10.3.1	Minimum defibrillation energy (MDE)	169
10.3.2	DF and MDE	170
10.3.3	Coefficient of variance	171

10.4	Discussion	172
10.4.1	MDE in low-flow ischaemia	172
10.4.2	MDE in hypoxia	175
10.4.3	MDE in acidic pH_{EC}	176
10.4.4	MDE in raised $[K^+]_{EC}$	178
10.4.5	MDE in infarcted hearts during zero-flow ischaemia	179
10.4.6	Lack of relationship between DF and MDE	181
10.4.7	Coefficient of variation as measure of dispersion of repolarisation	182
11	Synopsis	183
11.1	Spatiotemporal heterogeneity in dominant frequency	184
11.2	Electrophysiological mechanism of dominant frequency heterogeneity	185
11.2.1	(i) Prolongation of repolarisation	185
11.2.2	(ii) Prolonged of post-repolarisation refractoriness	186
11.3	(iii) Reduced conduction velocity	186
11.3.1	(iv) Raised activation threshold	187
11.4	Amplitude changes in VF	188
11.4.1	Control conditions	188
11.4.2	Low-flow ischaemia, hypoxia and acidic pH_{EC}	189
11.4.3	Raised $[K^+]_{EC}$	189
11.5	Minimum defibrillation energy	190

	10
11.6 Future work	191
11.6.1 Diastolic depolarisation	191
11.6.2 Heterogeneity of I_{K1} in rabbit	191
11.6.3 Voltage - calcium interactions during VF in low-flow ischaemia	192
11.7 Clinical Relevance.....	192
11.7.1 Reversal of hypoxia and acidosis	192
11.7.2 Antero-posterior vs. Antero-lateral paddle position.....	193
12 Appendix	194
13 List of reference.....	213

List of tables

Table 1.1 Summary of techniques for investigation of VF	44
Table 3.1 Ventricular DF during control (40ml/min) and low-flow ischaemia (6ml/min).	79
Table 4.1 Ventricular DF during VF in various individual ischaemic components compared to control and low-flow ischaemia.	92
Table 7.1 Mean apparent CV at 0s and 480s.....	128
Table 8.1 Percentage change in VF amplitude in LV and RV.	138
Table 10.1 Energy settings of Ventak ECD and the corresponding voltage, energy and waveform delivered.	169

List of figures

Figure 1.1 Frequency analysis of VF	25
Figure 1.2 Triggered activities	26
Figure 1.3 Formation of a wavebreak (anatomical)	27
Figure 1.4 APD restitution curves	29
Figure 1.5 Relationship between steepness of APD restitution curve and wave stability ..	29
Figure 1.6 Relationship between spiral wave dynamics and ECG dominant frequency during VF	30
Figure 1.7 Spatiotemporal distribution of VF frequencies as short-lived frequency blobs.	31
Figure 1.8 Two types of VF	32
Figure 1.9 Virtual electrodes in unipolar stimulation.....	38
Figure 1.10 Virtual electrodes on bipolar stimulation.....	39
Figure 1.11 Shock-induced phase singularity	39
Figure 1.12 Defibrillator waveforms.....	40
Figure 1.13 Transmembrane recordings from isolated myocytes	41
Figure 1.14 Origins of the ECG	44
Figure 1.15 Hypothesis of genesis of MAP recording by contact electrode	47
Figure 1.16 Diagram of voltage-sensitive spectral shift.....	48
Figure 1.17 Comparison of microelectrode and optical upstroke	49
Figure 1.18 Influence of magnification in optical mapping.....	49

Figure 1.19 Voltage resolution and signal-to-noise ratio (SNR).....	50
Figure 2.1 Langendorff perfusion apparatus	55
Figure 2.2 Photographs of the optical mapping chamber.....	57
Figure 2.3 Chemical structure of RH237	58
Figure 2.4 Diagram of the optical mapping set-up.....	58
Figure 2.5 Fourier Transform equation	59
Figure 2.6 The Fourier Transform illustrated.....	60
Figure 2.7 Illustration of peak identification in ECG, optical and microelectrode recordings	62
Figure 2.8 Illustration of the different possible pathways of epicardial activation	63
Figure 2.9 Illustrations of CV calculation from epicardial pacing and the radial approach to CV assessment.....	65
Figure 2.10 Illustration of linear approach to CV assessment	66
Figure 2.11 Point method for assessing CV	67
Figure 2.12 MAP recording.....	68
Figure 2.13 APD restitution as assessed by simulated VF	69
Figure 2.14 Assessment of MAPD.....	69
Figure 2.15 Illustration of S ₁ S ₂ protocol to assess ERP	70
Figure 2.16 Microelectrode apparatus.....	72
Figure 3.1 Time-course of ECG DF with varying perfusion rates as expressed by fractional change of starting DF	76

Figure 3.2 Time course of ECG DF in non-infarcted hearts (n = 4) and 8-week infarct model hearts (n = 4) during total global ischaemia	77
Figure 3.3 Time-course of psECG DF during control (40ml/min) and low-flow ischaemia (6ml/min), expressed as the fractional change of starting DF.....	78
Figure 3.4 DF maps during VF in control (40ml/min) and low-flow ischaemic (6ml/min) conditions	79
Figure 3.5 Investigation of the sharp transition of DF at the LV/RV boundary	80
Figure 3.6 Apex-to-base repolarisation	84
Figure 4.1 Solution transition time.....	90
Figure 4.2 DF time-course during hypoxia compared to control (40ml/min) and low-flow ischaemia (6ml/min).....	92
Figure 4.3 Time-courses of DF during VF with acidic pH _{EC} (pH 6.7 & pH 6.3) compared to control (pH 7.4, 40ml/min) and low-flow ischaemia (6ml/min).....	93
Figure 4.4 Typical DF maps during VF in low-flow ischaemia, raised [K ⁺] _{EC} , hypoxia and acidic pH _{EC} taken at 0s and 480s.....	94
Figure 4.5 Time-course of ECG DF and psECG DF during VF in raised [K ⁺] _{EC} (8mM and 10mM) compared to control (40ml/min) and low-flow ischaemia (6ml/min).	96
Figure 5.1 Assessment of MAPD ₉₀	105
Figure 5.2 MAP recordings from the anterior epicardial surface of the LV and RV	106
Figure 5.3 MAPD ₉₀ restitution curves during low-flow ischaemia.....	107
Figure 5.4 Mean MAPD ₉₀ restitution plots	108
Figure 5.5 MAPD ₉₀ in control (C) and low-flow ischaemia (6ml/min).....	109
Figure 5.6 MAPD ₉₀ in control (C), 8mM [K ⁺] _{EC} and 10mM [K ⁺] _{EC}	110

Figure 6.1 Transmembrane recordings during VF	115
Figure 6.2 Illustration of S ₁ S ₂ protocol to assess ERP	116
Figure 6.3 Plot of mean ERP in control (C), low-flow ischaemia, 8mM [K ⁺] solution and 10mM [K ⁺] solution	117
Figure 6.4 Post-repolarisation refractoriness.....	118
Figure 6.5 Fractional change of threshold voltage required to capture the respective ventricle at BCL 300ms.....	119
Figure 6.6 Percentage change in MAP upstroke velocity during low-flow ischaemia and perfusion with 8mM [K ⁺] solution or 10mM [K ⁺] solution	120
Figure 7.1 Apparent CV in VF	128
Figure 7.2 Bar plot of absolute traditional CV	130
Figure 7.3 Illustration of different pathways of epicardial activation	132
Figure 8.1 Amplitude and DF changes during VF under control conditions (n = 7)	138
Figure 8.2 Effects of dye degradation on optical signal amplitude.....	139
Figure 8.3 Amplitude changes during VF in low-flow ischaemia (n = 7) and hypoxia (n = 6).....	140
Figure 8.4 Colour-coded maps of fractional change in optical signal amplitude during VF	142
Figure 8.5 ECG and psECG amplitude during VF in acidic pH _{EC}	143
Figure 8.6 ECG and psECG amplitude during VF in 8mM (n = 6) and 10mM (n = 5) [K ⁺] solutions.....	144
Figure 8.7 Spatiotemporal progression of amplitude during VF in 8mM [K ⁺] solution...	145

Figure 8.8 Scattergrams of fractional change in VF amplitude against fractional change in VF DF.....	146
Figure 9.1 Sample microelectrode recordings.....	157
Figure 9.2 Transition time to wash in different $[K^+]$ solutions in the microelectrode set-up	158
Figure 9.3 Dominant frequency during control, low-flow ischaemia and $8mM [K^+]_{EC}$..	159
Figure 9.4 Membrane Potential during baseline pacing at BCL 180ms (Pace 180) and VF in control conditions.....	160
Figure 9.5 Membrane Potential during baseline pacing in control conditions (Pace 180) and during VF in low-flow ischaemia.....	161
Figure 9.6 Membrane potential during baseline pacing in control conditions (Pace 180) and during VF in $8mM [K^+]$ solution.....	162
Figure 9.7 Plot of mean membrane potential and amplitude change at 7 – 9 minutes with respect to baseline pacing at BCL 180s.....	163
Figure 9.8 Illustration of earliest and latest activation within a single pixel in regular pacing and VF	165
Figure 10.1 Diagram of the defibrillation set-up.....	168
Figure 10.2 Plot of mean MDE \pm SE	170
Figure 10.3 Scattergram of psECG DF vs. MDE.....	171
Figure 10.4 The coefficient of variance of the optical DF	171
Figure 10.5 Mean fractional change in coefficient of variance.....	172
Figure 10.6 Voltage- Ca^{2+} interactions.....	178
Figure 10.7 Bar charts of MDE and ECG DF	181

Acknowledgements

Throughout this work I have been supported and guided by Profs Smith and Cobbe, and Dr Burton. Godfrey, you have been an inspiration in so many ways, a fabulous sounding board, a diplomatic example and a great friend. Francis, thank-you for your programming skills, and those entertaining lunch-time conversations. Prof, thank-you for your continuous encouragement, your financial support in the early days, and your wisdom in writing and presenting.

To all in the lab, thank-you for making this an enjoyable time. In particular, thanks to Lisa for coffee and gab times, and for being such a great support. Aileen, for those confessional animal sacrifices, thank-you.

Author's declaration

Coronary artery ligation on the rabbits was carried out by the technical staff (Mrs Diane Smillie, Mr Michael Dunne and Mr Graham Deuchar) at the Department of Medical Cardiology Glasgow Royal Infirmary under the supervision of Dr. Martin Hicks. All the experimental work contained in this thesis was undertaken by me. The material has not been submitted previously for any other degree. Some of the results presented have been published during the period of study, details of which are below.

Publications

Caldwell JC, Burton FL, Smith GL, Cobbe SM. Heterogeneity of ventricular fibrillation dominant frequency during global ischaemia in isolated rabbit hearts – accepted by Journal of Cardiovascular Electrophysiology (Appendix).

Caldwell JC, Burton FL, Cobbe SM, Smith GL. Heterogeneity of ventricular fibrillation dominant frequency during global ischaemia in isolated rabbit hearts. *Heart Rhythm* 2006 3(5):S17.

Caldwell JC, Burton FL, Cobbe SM, Smith GL. Electrophysiology characteristics of isolated perfused rabbit hearts during ventricular fibrillation. *J. Mol. Cell. Cardiol.* 2005 39(1):196.

Caldwell JC, Burton FL, Cobbe SM, Smith GL. Optical Mapping of isolate rabbit heart reveals differential responses of left and right ventricle to global ischaemia during ventricular fibrillation SSEM May 2005 – published in *Scottish Medical Journal* 2006: (51)3 .

Caldwell JC, Burton FL, Cobbe SM, Smith GL. The effects of perfusion rate on the dominant frequency of ventricular fibrillation in the isolated rabbit heart. *J Physiol* 2004: 557P(C11).

Abbreviations

AED	Automatic External Defibrillator
AF	Atrial Fibrillation
AP	Action Potential
APD	Action Potential Duration
ARP	Absolute Refractory Period
BCL	Basic Cycle length
BDM	2,3-Butane-Dione Monoxime
CCD	Charged-coupled device
CFT	Continuous Fourier Transform
CPR	Cardio-Pulmonary Resuscitation
CV	Conduction Velocity
DAD	Delayed After Depolarisation
DF	Dominant Frequency
DFT	Defibrillation Threshold
DI	Diastolic Interval
dV/dt_{\max}	Maximum rate of depolarisation/upstroke velocity
EAD	Early After Depolarisation
ECG	Electrocardiogram

E_k	Reversal Potential. Membrane potential at which current switches from inward to outward.
ERP	Effective Refractory Period
FFT	Fast Fourier Transform
$I_{Ca(L)}$	L-type calcium current
$I_{Cl,vol}$	Volume-regulated chloride current
I_K	Delayed rectifier current. Potassium current
I_{K1}	Inward rectifier current. This potassium current conducts inwards more readily than outwards.
I_{Kr}	Rapid component of I_K
I_{Ks}	Slow component of I_K
I_{Kto}	Transient outward potassium current
I_{Na}	Fast sodium current
KCl	Potassium chloride
$[K^+]_{EC}$	Extracellular potassium concentration
Kir2.x	Proteins responsible for I_{K1} current. Subtypes of this protein channel are Kir2.1, Kir2.2 and Kir2.3
LAD	Left Anterior Descending artery
LV	Left Ventricle
MAP	Monophasic Action Potential
MAP ₅₀	Time to 50% repolarisation

MAP ₇₅	Time to 75% repolarisation
MAP ₉₀	Time to 90% repolarisation
MDE	Minimum Defibrillation Energy
MF	Median Frequency
NA	Numerical Aperture
psECG	pseudoECG
RA	Right Atrium
RV	Right Ventricle
SEM	Standard Error of the Mean
SR	Sarcoplasmic Reticulum
TAP	Transmembrane Action Potential
ULV	Upper Limit of Vulnerability
VE	Virtual Electrode
VF	Ventricular Fibrillation
VFI	Ventricular Fibrillation Interval
VT	Ventricular Tachycardia

1 Introduction

The aim of this introduction is to provide an overview of the phenomena of ventricular fibrillation and electrical defibrillation, to describe the electrophysiological processes that are thought to underlie these processes, and how they are affected by acute ischaemia.

1.1 Ventricular Fibrillation

1.1.1 Clinical Relevance

1.1.1.1 Definition

Ventricular fibrillation (VF) is a cardiac arrhythmia in which the electrical activity of the ventricles is chaotic and uncoordinated. This results in the loss of cardiac output and death, unless corrective measures are undertaken (1). Although in humans VF can be precipitated by a wide variety of conditions, ranging from electric shocks to drug overdoses, it is usually seen in the context of coronary artery disease.

1.1.1.2 Mortality data

Coronary artery disease is the leading cause of premature death in the UK, resulting in the deaths of over 105,000 people in 2004 (2). Of these, 30% died suddenly before reaching hospital, presumably from VF (3). VF is also a common consequence of mild to moderate left ventricular systolic dysfunction (4, 5).

1.1.1.3 Treatment

Surviving VF depends on the quick re-establishment of a rhythm compatible with perfusion, usually by the application of an electric defibrillation shock. Although the probability of successful outcome from defibrillation is directly related to the duration of the VF arrest (6), interventions to minimise this duration have not consistently shown improvements of survival rates. One example is the introduction of automated external defibrillators (AED) into public places. The use of AEDs by non-medical but trained individuals, shortens the time to first defibrillation shock, as it is no longer necessary to wait for the arrival of a paramedic crew. However, AED introduction has not resulted in the expected survival rate improvements (7-9). The efficacy of the "shock-first" approach was also brought into question by animal (10-12) and clinical research (9, 13) which showed that survival from more prolonged VF arrests was improved by an initial period of cardiopulmonary resuscitation (CPR) prior to defibrillation. To this end, the UK

Resuscitation Council changed its guidelines; rather than advocating immediate defibrillation on diagnosis of VF, the guidelines now recommend 2 minutes of CPR prior to first defibrillation attempt in unwitnessed out-of-hospital arrests (14).

1.1.1.4 Clinical VF progression

A three-phase model of VF progression has been proposed (15, 16): - (i) an initial “electrical phase” (0 – 4 mins), where little metabolic deterioration occurs and immediate defibrillation gives the best chance of survival, (ii) an intermediary “circulatory phase” (c. 4 – 10 mins) where the metabolic consequences of failed myocardial perfusion reduce the success of defibrillation, but are limited enough to be partially reversed by CPR. It should be noted that even when performed optimally, CPR can only restore 25% of perfusion to the heart (17), and is inherently hypercarbic/hypoxic if using “mouth-to-mouth” ventilation (18). (iii) Longer duration VF (“metabolic phase”) results in systemic consequences of ischaemia; the release of vasodilatory cytokines and translocation of gut bacteria leading to sepsis. Such sequelae prevent long-term survival even if defibrillation is successful.

As the immediate intervention for each VF phase is different, it is important to establish which phase a patient is in. Trying to determine the VF phase from bystander accounts of duration is at best an estimate. Alternatively, the VF phase can be related to parameters derived from the surface ECG, which also correlate with VF duration and resuscitation outcome. In non-perfused VF in animal models, the amplitude of the ECG waveform reduces with time (19). However, the assessment of ECG amplitude is not a useful clinical tool as large amplitude variations can occur with differing lead placements and body habitus (20). Analysing the ECG in the frequency domain negates these problems. As shown in figure 1.1, and described more fully in chapter 2.5.1, using Fast Fourier Transform (FFT) to convert the ECG signal into its constituent frequencies, allows the identification of the dominant or peak frequency (DF), and the median frequency (MF). Such frequency analysis in non-perfused VF has shown that the DF, the MF and amplitude spectrum area (AMSA = area under frequency power spectrum) are related to the VF duration, and probability of successful defibrillation, in both animal and clinical studies (21-34). For this reason, in this thesis the time-course of VF will primarily be examined in the frequency domain.

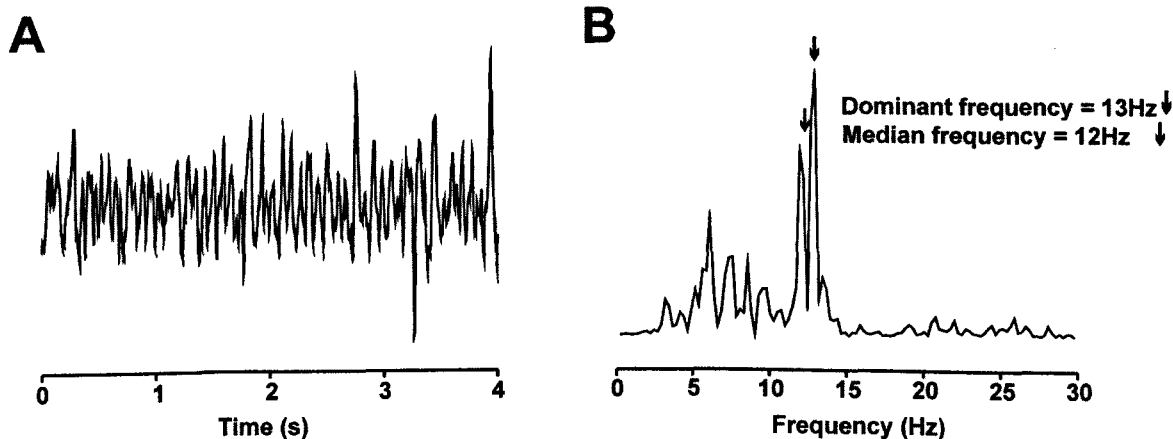


Figure 1.1 Frequency analysis of VF. Panel A: ECG during VF. Panel B: Power Spectrum of (A) created by Fast Fourier Transform (FFT).

1.1.2 Electrophysiology of VF

1.1.2.1 Onset of VF

1.1.2.1.1 Initiation of Ventricular Tachycardia (VT)

The qualitative description of VF has a long history (for review see (35)). Using cinematography, Wiggers described an initial regular VT, which quickly degenerated into the chaotic contractions of VF (36). Electrical mapping techniques demonstrated that this VT is characterised either by a single spiral wave or a figure-of-eight re-entry (37). Precipitation of such waves requires (i) a trigger and (ii) a potential pathway to support re-entry (38).

(i) Triggering is thought to occur by early or delayed after-depolarisations (EADs, DADs). As shown in figure 1.2, these oscillations in membrane potential either occur during the action potential (AP), as in EADs, or immediately after it, as in DADs. Both EADs and DADs frequently occur in electrolyte disturbances (low $[K^+]_{EC}$, $[Ca^{2+}]_{EC}$, $[Mg^{2+}]_{EC}$, and pH) or anti-arrhythmic therapy (39, 40), and are more common in the context of heart failure (41, 42).

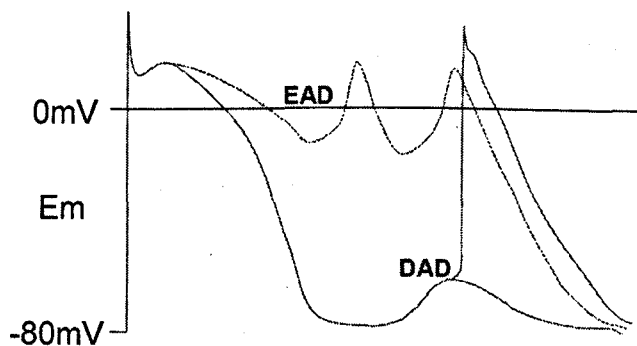


Figure 1.2 Triggered activities. Early After Depolarisations (EADs) occur prior to full repolarisation of the action potential. Delayed After Depolarisations (DADs) occur after full repolarisation of the membrane potential. Both are associated with electrolyte disturbances, drug therapy and heart failure. (Adapted from (40)).

(ii) At the simplest level, re-entry is the rotation of the cardiac impulse around an unexcitable obstacle, resulting in repetitive activation of the heart. The frequency of repetition is dependant on the conduction velocity of the activation and the length of the pathway around the obstacle. In order for re-entry to be established there must be a) unidirectional conduction block, which can be anatomical or functional, and b) a match between the conduction velocity and the length of the potential circuit to allow re-excitation.

a) Unidirectional conduction block - 1. Anatomical – Disease processes that disrupt the myocardial fibre arrangement and/or produce interstitial fibrosis can result in anatomical conduction block (e.g. chronic myocardial infarction) (43). Figure 1.3 illustrates the formation of figure-of-eight re-entry at an anatomical conduction block, and how the formation of re-entry is also dependant on the surrounding tissue excitability. If the tissue is of normal excitability, the wave simple reunites after the obstruction (Figure 1.3(i)). If excitability is reduced the wave-ends cannot unit, and so they become detached and form two counter-rotating spiral waves (Figure 1.3(ii)). 2. Functional – functional blockade results from the dispersion of repolarisation and conduction, as determined by restitution dynamics. This source of heterogeneity is also important in the degeneration of VT into VF, and will be discussed in section 1.1.2.1.3.

b) Re-excitation – In order to allow re-activation of the re-entry pathway by the circling activation, the rotational time around the circuit must be longer than the recovery interval throughout the pathway. This can be accomplished either through a relatively long pathway, a relatively slow conduction velocity or a relatively short refractory period.

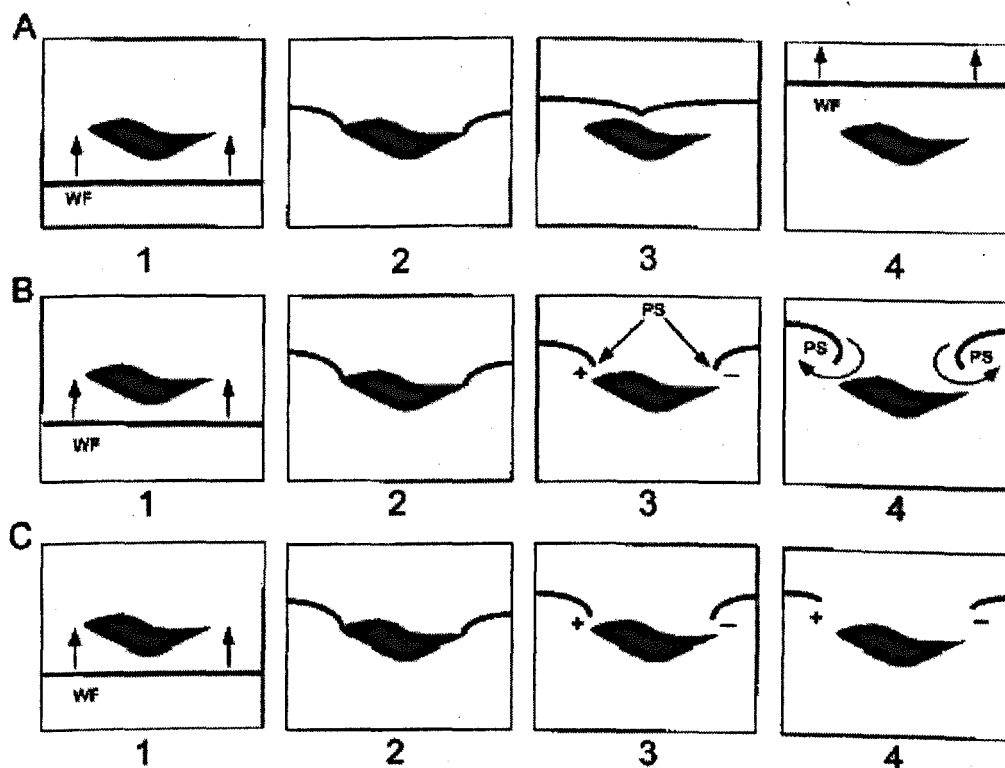


Figure 1.3 Formation of a wavebreak (anatomical). In all panels, a wavefront (WF) is moving upward to interact with an unexcitable obstacle, shown in black. Panel A: Normal excitability, upon reaching the obstacle, the wavefront splits in two. The two newly formed wavefronts circumnavigate the obstacle, without detaching from it, and then merge into a common wave front that continues moving upward, apparently undisturbed by its interaction with the discontinuity. Panel B: Lower excitability. The two broken wave fronts (wavelets) now detach from the obstacle, resulting in the formation of a singularity point (PS = phase singularity) at the broken end of each wavelet. This leads to two counter rotating vortices (figure-of-eight re-entry). Panel C: When excitability is too low, the two broken waves are unable to rotate, and instead undergo decremental conduction. (Adapted from (35)).

1.1.2.1.2 Degeneration into VF

Once established, VT may degenerate into VF. For this to occur, the re-entrant wavefront must fragment into numerous daughter waves. This process of wavebreak occurs in the context of spatial heterogeneity in electrophysiological properties such as conduction velocity and refractoriness (Figure 1.3). Some heterogeneity exists in the structurally normal heart; there are differences in the electrophysiological properties depending on location (apex or base, left ventricle (LV) or right ventricle (RV)), and depth in the tissue (epicardial through to endocardial) (44). These differences are enhanced further by sympathetic stimulation (45). Heterogeneity is increased in the abnormal heart. In left ventricular systolic dysfunction, stretch of the myocytes by dilation causes increases in the magnitude and dispersion of refractoriness (46). Early in acute myocardial infarction, ischaemia causes electrophysiological changes such as slowed conduction velocity (CV), depolarization of the resting potential, and reduced action potential amplitude (47). These

alterations can occur in patches, and may interdigitate with non-ischaemic tissue, thus increasing heterogeneity.

1.1.2.1.3 Restitution

An important contributor to the development of heterogeneity is restitution. Restitution is the phenomenon whereby the action potential duration (APD) and CV vary according to the length of the preceding diastolic interval (DI = the interval between electrical impulses). When the heart rate increases, the DI shortens. The AP therefore reaches the cell in a different stage of ion channel activation/inactivation. The result is shortening of the APD and reduction of the CV. Thus restitution produces rate-related changes of APD and CV.

Restitution is an important functional property, allowing the heart rate to increase during exercise without conduction blockade or consequent arrhythmias. However, the consequently ever-changing nature of APD and CV can lead to heterogeneity. The kinetics of restitution relationships are represented by plotting APD or CV against DI (Figure 1.4). With APD restitution, the gradient of the curve determines the stability of the activation. Figure 1.4 shows that at low activation rates (e.g. during normal sinus rhythm) the slope is shallow (<1), whereas at higher activation rates, such as those seen in VF, the curve is very steep (>1). Shallow gradients of restitution (<1) reflect a stable situation. As shown in figure 1.5A, if the restitution slope is <1 , changes in DI/heart rate produce ever reducing changes in APD, and the quick re-establishment of a new steady state. In contrast, steep gradients (>1) result in instability. As illustrated in figure 1.5B, with restitution slopes >1 even small changes in DI will have a dramatic effect on the APD, and result in conduction failure.

Restitution kinetics vary throughout the normal myocardium (48, 49). This heterogeneity of repolarisation/refractoriness and CV can lead to functional unidirectional conduction block, and hence wavebreak (50-52). Drugs which flatten the restitution curve (i.e. increase stability) have been shown to prevent the transition of VT to VF, and convert VF to VT (Figure 1.4) (53-55).

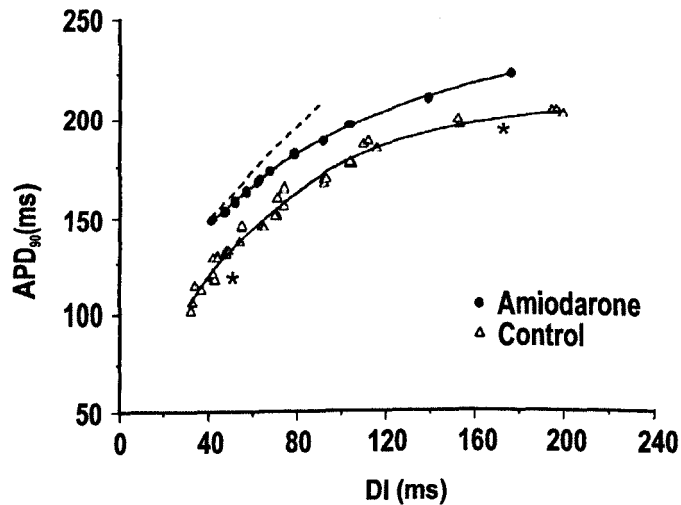


Figure 1.4 APD restitution curves. Restitution dynamics are assessed by plotting APD vs. DI. Under control conditions the slope of the curve is < 1 at longer DI (*), and > 1 at shorter DI (*). During amiodarone administration the slope of the curve is flattened. This stabilisation of the restitution dynamics prevents the transition of VT to VF. (Adapted from (54)).

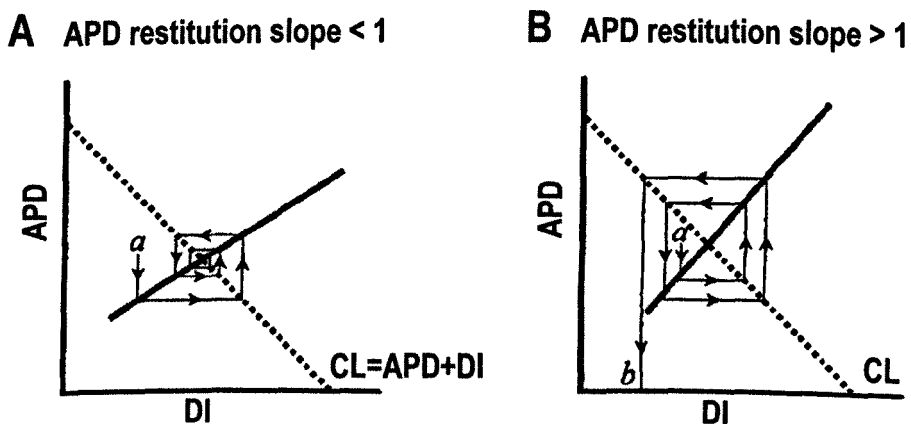


Figure 1.5 Relationship between steepness of APD restitution curve and wave stability. Panel A: For slopes < 1 , a small shift (a) that shortens DI results in and even smaller change in APD. This ever-decreasing pattern of changes continues until a new equilibrium is established. Panel B: For slopes > 1 , a similar small shift (a) produces a larger change in DI and a subsequent greater change in APD. This amplification circuit continues until the DI is too short to generate an APD (b) and conduction fails (i.e. wavebreak occurs). (Adapted from (56)).

1.1.2.1.4 Cardiac memory

Another phenomenon that is interlinked with restitution, and may also be important in VF, is cardiac memory. The myocardium is imprinted by the pattern of previous activations. That is it appears to remember what activation pattern has happened before (57). Therefore not only the preceding DI influences the APD, but the previous APD, and the antecedent DIs and APDs of several earlier cycles (58, 59). This phenomenon appears to be important

in maintaining VF in the first few seconds, but not thereafter (59). As this thesis is investigating prolonged episodes of VF, cardiac memory will not be evaluated.

1.1.2.2 Maintenance of VF

The mechanism of VF maintenance remains the subject of debate. Originally it was thought that VF was maintained by multiple wavelets; these wavelets, moving along ever-changing pathways, resulted in wave collision (extinction) and wavebreak (generation of new daughter waves) (56). More recently, an alternative mechanism of VF maintenance has been proposed. In this hypothesis, the driving force in VF is a single, rapidly firing spiral wave (or “mother rotor”) lying deep within myocardium. As the activation spreads from this source, and encounters tissues with longer refractory periods, wavebreak results, with the production of multiple wavelets as epiphenomena. Supporting this, optical mapping has demonstrated that (i) a relatively small numbers of drifting rotors can give rise to an ECG resembling VF (60), (ii) the dominant frequency (DF) of the ECG power spectra correlated to the cycling periodicity of the dominant/mother rotor (61, 62) (Figure 1.6) and (iii) in VF the electrical activity across the heart is divided into discrete DF domains, the fastest of which was consistently located in the anterior aspect of the LV (63).

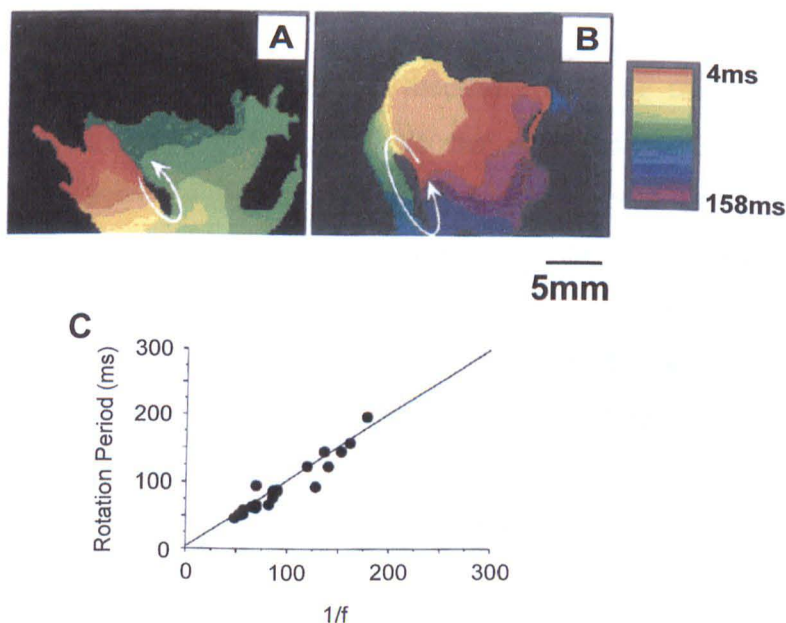


Figure 1.6 Relationship between spiral wave dynamics and ECG dominant frequency during VF. Panel A: In control conditions a single wave is shown rotating counterclockwise, with a rotation period of 54ms. **Panel B:** After 5 minutes of global ischaemia, a spiral wave was shown rotating counterclockwise with a rotation period of 158ms. In the adjacent colour bar each colour band corresponds to 4.2 ms of activity. Red represents the earliest activation and purple the latest activation. **Panel C:** Plot of rotation period against inverse of dominant frequency (1/f) demonstrates a strong inverse correlation between DF and rotational period of spiral wave dynamics. (Adapted from(62)).

Other groups have failed to demonstrate such fixed DF domains (64-66). Choi et al. found that in all areas of the epicardium the frequency power spectra were broad with multiple peaks. This made determination of the DF equivocal, and suggested the existence of multiple wavelets rather than a single mother rotor (65). Instead, as shown in figure 1.7, they demonstrated the existence of dynamically changing frequency “blobs” that were short lived, and could be altered pharmacologically (66).

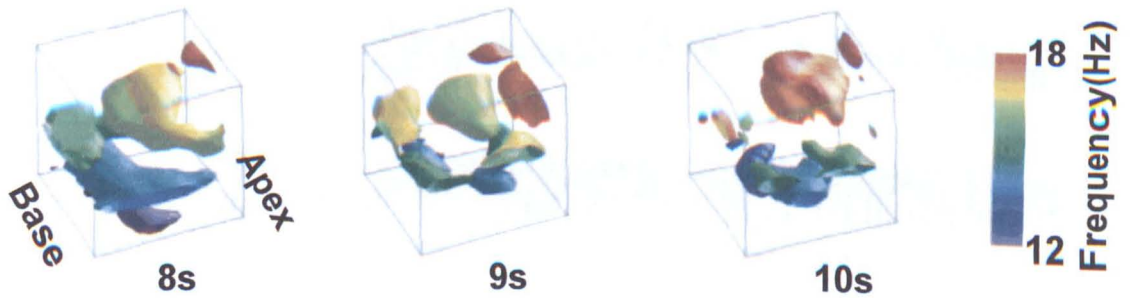


Figure 1.7 Spatiotemporal distribution of VF frequencies as short-lived frequency blobs. By performing time-frequency analysis across the anterior surface of the rabbit heart, Choi et al. did not find discrete domains, but rather identified ever-changing frequency blobs. The illustrated colour-coded plots are of frequency (z-axis) against spatial location (x & y axes). (Adapted from (66)).

1.1.2.2.1 Possibility of 2 types of VF

By demonstrating evidence to support both mechanisms of VF maintenance, Wu et al. proposed a unifying theory of two types of VF that occur under different circumstances (55, 67). Figure 1.8 shows the results of this study, where VF was optically mapped whilst changing the gradient of the APD and CV restitution curves independently. This was accomplished through increasing concentrations of methoxyverapamil, a Ca^{2+} and Na^{+} channel blocker. The baseline "fast" VF (type 1), consisted of multiple wandering wavelets, wave-wave interaction and continuous new re-entry (DF c.18 Hz, Figures 1.8A(i), B(i) & C(i)). Low methoxyverapamil concentrations inhibit the slow calcium inward current ($I_{\text{Ca(L)}}$) and thus flatten the APD restitution curve. Perfusing the preparation with low methoxyverapamil concentrations converted the type 1 VF to VT with a stationary spiral wave (Figures 1.8 A(ii) & B(ii)). Higher methoxyverapamil concentrations inhibit the fast sodium inward current (I_{Na}), thereby reducing myocardial excitability as well as steepening and broadening of the CV restitution curve. In the preparation, increasing the methoxyverapamil concentrations produced wavebreak such that VT now degenerated into VF (Figures 1.8A(iii), B(iii) & C(ii)). Optically this appeared as a single, long wavefront that failed to propagate in certain areas; wave-wave

interaction and generation of new re-entry were rarely observed. ECG recordings at these higher concentrations showed slow (type 2) VF (DF c.12 Hz).

As these 2 different types of VF can be attained in the same heart, it raises the possibility that both mechanisms (i.e. the multiple wavelets and the “mother rotor”) operate but at different points in the progression of VF in ischaemia (68-70).

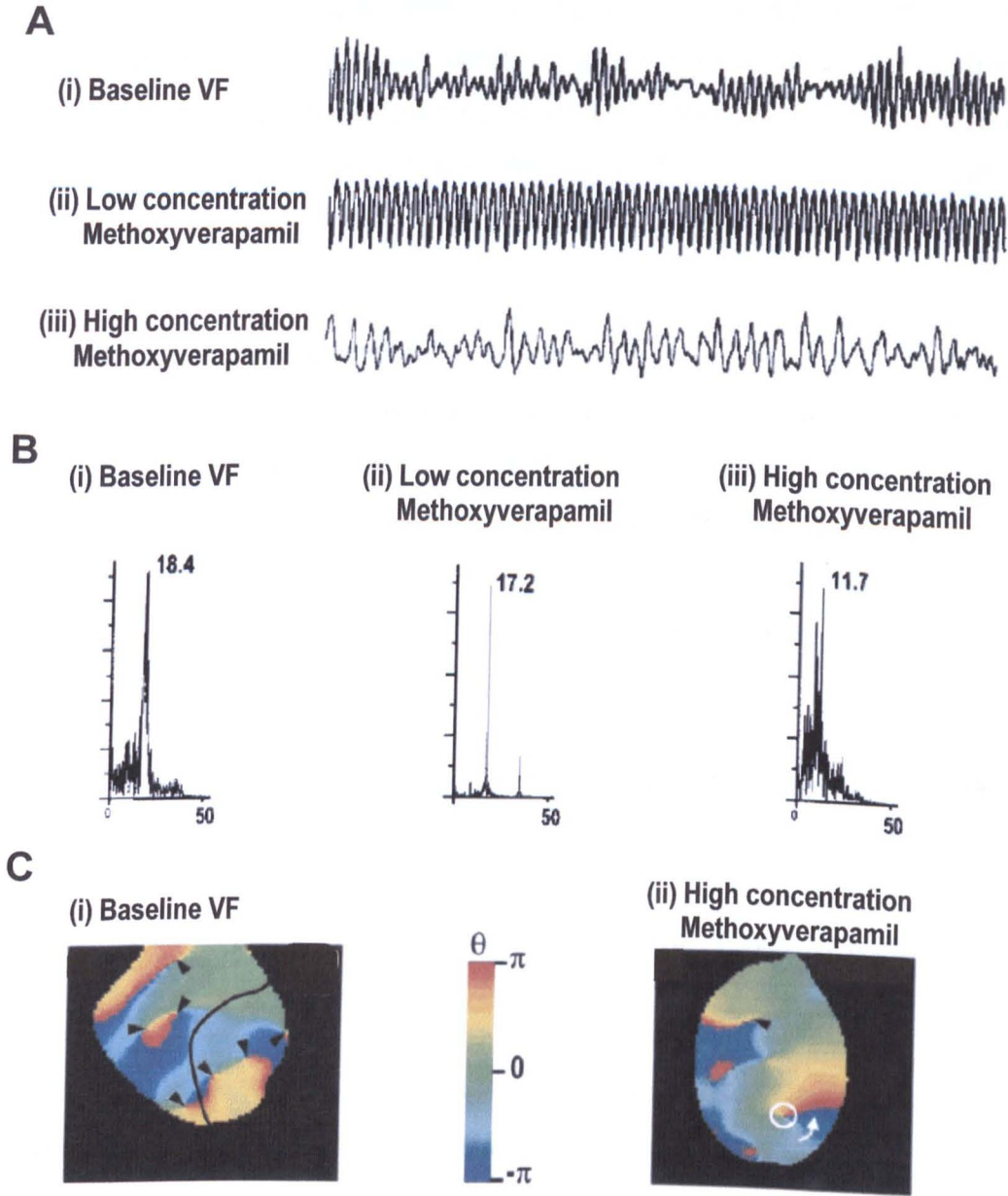


Figure 1.8 Two types of VF. Panel A: ECGs of (i) Baseline VF (type 1), (ii) VT under low concentration methoxyverapamil and (iii) Slow (type 2) VF in high concentration methoxyverapamil. Panel B: Power spectra of Panel A. This demonstrates slower DF in High concentration methoxyverapamil. Panel C: Phase maps of (i) Baseline VF – many points of singularity (White circle) with one wavebreak at area of slow conduction. (Adapted from (67)).

1.1.2.3 Progression of VF

1.1.2.3.1 Progression of Dominant Frequency

Under circumstances of continued coronary perfusion (i.e. cardiopulmonary bypass (71) or Langendorff-perfused isolated heart (46)), the frequency content of the ECG signal increases slightly after induction, then remains stable. When coronary perfusion is not supported, the frequency content rapidly declines (71, 72) irrespective of its aetiology (22). Intermediate levels of coronary perfusion give rise to lesser degrees of frequency decline (73). Therefore, the effectiveness of CPR and vasopressive agents to maintain coronary perfusion can be correlated to the DF or MF (30). The more complicated relationship between DF and defibrillation threshold (DFT) will be discussed later.

1.1.2.3.2 Metabolic consequences

The reduced myocardial blood flow associated with a VF arrest results in a collection of metabolic changes. Within 10 seconds, intracellular O_2 is virtually exhausted, forcing the cessation of aerobic metabolism, the depletion of high-energy phosphate compounds, the onset of anaerobic metabolism and the accumulation of metabolites (including lactic acid and CO_2) (74). This results in both intracellular and extracellular acidosis, and accumulation of extracellular K^+ .

The levels of acidic pH_{EC} in VF during ischaemia are not clear. Clinical and animal studies have examined plasma pH, rather than interstitial pH (75-78). In isolated ferret hearts the pH falls to 6.78 by 10 minutes during total ischaemia in sinus rhythm (79). Whereas measurement of interstitial pH in the in situ pig heart during VF supported by CPR showed the pH to fall to 6.38 at 11 minutes (80).

During ischaemia, there is an increase in passive K^+ efflux due to a) increased permeability of the cell membrane to anion and b) the developing intracellular acidosis (81). This results in a substantial rise in extracellular $[K^+]$, and depolarisation of the resting membrane potential (81, 82). As is the case with pH, the actual $[K^+]_{EC}$ during VF in ischaemia is not clear. Again clinical and animal studies have examined plasma $[K^+]$ rather than the interstitial $[K^+]$ (83). In the isolated guinea pig heart the $[K^+]_{EC}$ reached 11mM after 8 minutes of ischaemia in sinus rhythm, and 15mM after 15 minutes (81).

1.1.2.3 Possible role of transmembrane potential

Intracellular recordings during prolonged VF have demonstrated depolarisation of the resting membrane and alteration of AP morphology (84). The latter change was in keeping with I_{Na} inhibition, which occurs secondarily to membrane depolarisation. In this study, VF was induced by reperfusion after an ischaemic insult with prior baseline membrane potential measurement. During the first few minutes of VF, the membrane potential did not reach a stable diastolic level. Therefore the contribution of VF, as distinct from ischaemia, to membrane depolarisation was not ascertained.

Pharmacological inactivation of fast sodium channels, and thus inhibition of I_{Na} , results in slowing of the ECG DF (22, 85, 86). This suggests that membrane depolarisation, and secondary I_{Na} inhibition, could play a role in the DF decline in VF during ischaemia. Indeed, as illustrated in figure 1.6, optical mapping of VF during global ischaemia showed that the DF inversely correlated with (i) the rotational period of the epicardial spiral wave, and (ii) the dimensions of the central inactive core the wave rotated around (62). In fully perfused preparations, blockade of I_{Na} by tetrodotoxin resulted in slowing of DF and spiral wave rotation that was indistinguishable from that observed in global ischaemia (62).

The pattern of the electrophysiological changes that evolve with ischaemia can be mimicked by increasing methoxyverapamil concentrations as described above; ischaemia initially leads to APD shortening and flattening of APD restitution curve (87). This can promote spontaneous termination, which can also occur in patients with Brugada syndrome. Such patients, with structurally normal hearts, suffer repeated, non-sustained VF arrests (88, 89). To date, the genetic mutation responsible has only been identified in a minority of patients (c. 10%). All mutations identified have resulted in reduction of I_{Na} (90). Unfortunately, self-termination is not the case for the vast majority of VF arrests, which occur secondary to coronary artery disease or LV systolic dysfunction. Here, the underlying heterogeneity of the disease process negates the flattening of APD restitution. As VF continues, the progressing ischaemia is associated with reduced excitability, and there is transition into slow, type 2 VF (71).

1.1.2.4 Termination of VF

VF arrests have 2 possible outcomes; life or death. For the first to occur, a rhythm compatible with (and producing) contraction must be established, either spontaneously (an infrequent occurrence in conditions such as in Brugada syndrome (88, 89)), or by electrical

countershock with or without pharmacological assistance. If VF continues, it will eventually degenerate into asystole, where the myocardial electrical activity ceases, and death is almost inevitable (91).

1.2 Defibrillation by electric countershock

1.2.1 Mechanism of action

For over a century, it has been appreciated that electric shocks have the ability to terminate VF, as well as initiate it. The precise mechanism of defibrillation is not clearly understood. Over the past few decades conflicting theories, with supporting evidence, have been proposed by different investigators, using different experimental methods (for review see (92)). Principles that are generally accepted are: - (i) for defibrillation to be successful a shock must homogeneously depolarize a sufficient mass of myocardium to stop the fibrillation wavefronts (critical mass concept), and (ii) it must do so without launching new activations that re-initiate VF (93). Two main hypotheses exist for the source of such re-initiating activations; the "critical point re-entry" hypothesis (94, 95) and "virtual electrodes" hypothesis (96-98).

1.2.1.1 Critical mass concept

Since the beginning of the 20th century, it has been known that the ability to initiate and maintain a heart in VF is inversely related to its size (35, 99, 100). Indeed, studies investigating VF using the small-dimensioned rat heart often have to re-induce the arrhythmia, as self-termination is so commonplace (101). The prerequisite for a critical mass of excitable myocardium to sustain VF has been predicted by computer modelling (102) and demonstrated experimentally in dogs (103). Perfusing individual coronary arteries with potassium chloride solution (1mEq/ml) renders the subtending myocardium unexcitable. Simultaneous perfusion of the left anterior descending (LAD) and the left circumflex arteries reduces the mass of excitable myocardium below this critical mass threshold, so that VF is no longer sustained (103). Similarly, successful defibrillation needs only to prevent wavefront propagation within a critical mass. Thereafter the remaining excitable myocardium is too small to sustain VF.

1.2.1.2 "Critical Point re-entry" mechanism

During established VF, a countershock imposes an electric field on the myocytes that prolongs their refractory period, and hence prevents the wavefront propagation. The extent of refractory prolongation experienced by a myocyte is determined by (i) its location within the electric field and (ii) its excitation state at the point of shock application.

- (i) Depending on the electrode size and placement, certain areas of the ventricular myocardium will only experience low voltage changes in their membrane potential. After an unsuccessful countershock, activation occurs in such low potential areas (areas of critical local field strength), and result in VF being re-initiated (94, 104).
- (ii) Within the area of critical local field strength, the interval between the AP upstroke and the subsequent defibrillation shock (known as the coupling interval) also determines the probability of successful defibrillation (104). Normalised coupling intervals <40% of the mean fibrillation cycle length produce longer post-shock refractory periods, and are therefore more likely to result in successful defibrillation (105). Thus there is also a critical level of recovery.

The "critical point re-entry" mechanism hypothesises that after countershocks of insufficient strength re-entry will occur at the intersection of the critical local field strength and the critical level of recovery. A countershock of sufficient strength will produce a uniform prolongation of refractoriness throughout the ventricular myocardium, irrespective of the timing of the shock (104, 106, 107).

1.2.1.3 "Virtual Electrode" mechanism

Over the past decade, the validity of the "critical point re-entry" mechanism has been challenged. This hypothesis fails to explain all activation patterns that have been observed after an unsuccessful defibrillation. For instance, it cannot explain focal patterns of activation (108, 109), re-entry after a prolonged period of electrical quiescence (known as the isoelectric window) (109, 110) or re-entry in close proximity to the electrodes where the field strength is high (96). A hypothesis which can explain all these observations is the "Virtual Electrode" mechanism (for review see (111)).

The concept of the virtual electrode (VE) arose from bidomain modelling of cardiac tissue during extracellular unipolar stimulation (112). These simulations predicted that a single polarity electrode would simultaneously produce dog-bone shaped regions of depolarisation and hyperpolarisation as a result of the differential intracellular-to-extracellular conductivity. These predictions were verified experimentally, with depolarisation being attributed to the actions of a virtual cathode, whilst hyperpolarisation was induced by a virtual anode (Figure 1.9A) (113). Bipolar stimulation results in more complex patterns of virtual electrodes (114-116). As shown in figure 1.10, the virtual electrode pattern depends upon on the relative orientation of the dipole and the myocardial fibres.

For electrical field stimulation, theoretical (117) and experimental studies (118) resulted in virtual cathodes and anodes across the myocardium (Figure 1.11A). The position of these virtual electrodes was determined by the field configuration and the tissue structures. Within the virtual cathode, positive polarisation results in prolongation of activation and refractoriness (Figure 1.9B). In contrast, the negative polarisation of the virtual anode shortens the activation and the refractory period (Figure 1.9C). Where there is close spatial approximation of the virtual electrodes, the virtual cathode activation propagates to stimulate the now partially excitable virtual anode tissue. This stimulation is known as break-excitation (Figure 1.9D). The wave of break-excitation propagates slowly, as the virtual anode is not fully excitable. Therefore enough time elapses to allow full recovery of the virtual cathode region, which can now be re-excited. This leads to re-entry around a shock-induced phase singularity (Figure 1.11), and thus the re-initiation of VF (96, 98). Shock strengths that induce such phase-singularities are said to be within the heart's window of vulnerability. The highest shock strength that will induce such a phase singularity is known as the Upper Limit of Vulnerability (ULV) (119, 120).

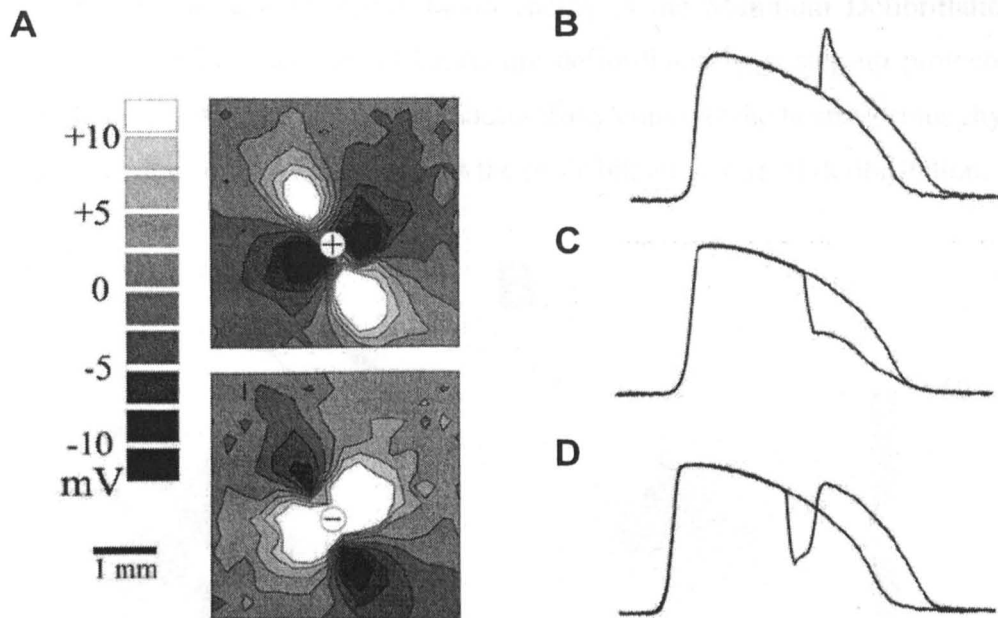


Figure 1.9 Virtual electrodes in unipolar stimulation. Panel A: Virtual electrode polarisation during anode (+) and cathode (-) stimulation. The change in polarity of the surrounding myocardium is represented in grey-scale, with virtual anodes in white and virtual cathodes in black. Note the dog-bone shape to the polarity. **Panel B:** Effect of virtual cathode stimulation on AP. There is positive polarisation, which results in prolongation of AP, repolarisation and thus the refractory period. **Panel C:** Effect of virtual anode stimulation on AP. The negative polarisation results in shortening of the AP, repolarisation and thus the refractory period. **Panel D:** Effect of virtual anode close to virtual cathode. The partially repolarised tissue can now be re-excited by the propagating activation from the virtual cathode. This results in re-entry and thus failure of defibrillation. (Adapted from (121)).

Under this hypothesis, defibrillation is successful when the shock is greater than the ULV. Here, the shock is of sufficient strength to restore full excitability to the myocardium underlying the virtual anode. The break-excitation now propagates rapidly, and returns to an unexcitable virtual cathode. At this point the break-excitation fails to propagate, and thus re-entry cannot occur.

1.2.2 Assessment of defibrillation energies

Owing to the chaotic nature of VF, identical experimental conditions can result in variable electrical activity at the point of defibrillation. This variable electrical activity results in variable defibrillation energies, and thus their assessment has a probabilistic component (122, 122). To allow for this, the defibrillation threshold (DFT) is defined as the energy that successfully defibrillates a certain percentage of VF episodes; e.g. the DFT₅₀ is the energy that successfully defibrillates 50% of VF episodes. Accurate determination of DFT₅₀ requires a complex protocol involving several short runs of VF (123). It is not possible to use this protocol in conjunction with long runs (~10 minutes) of VF without causing deterioration of the experimental preparation.

A simpler measurement of defibrillation energy is the Minimum Defibrillation Energy (MDE) (73). In this measurement hearts are defibrillated by a step-up protocol, and the MDE is determined as the energy that successfully converts the heart to sinus rhythm. This measurement does not take into account the probabilistic nature of defibrillation.

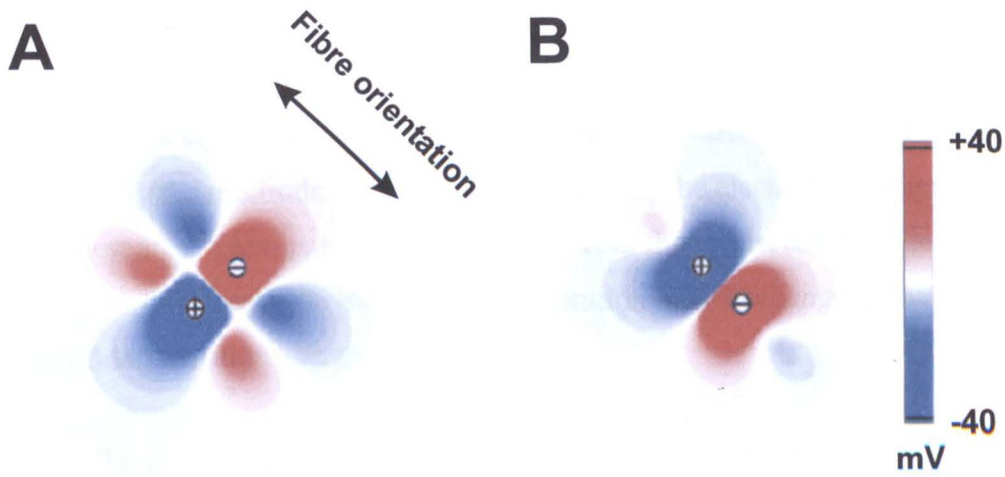


Figure 1.10 Virtual electrodes on bipolar stimulation. The pattern of virtual electrodes polarisation is dependent on the orientation of the dipole with respect to the myocardial fibres. Panel A: Dipole perpendicular to the longitudinal axis of the fibres produces an interweaving trefoil pattern. Panel B: Dipole parallel to the long axis of the fibres produce simpler patterns. (Adapted from (116)).

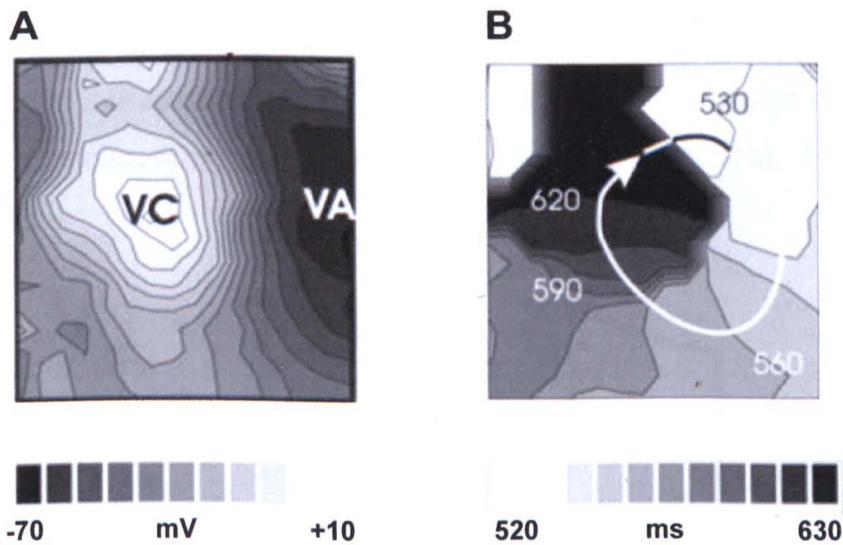


Figure 1.11 Shock-induced phase singularity. Panel A: Isopotential map after application of monophasic shock. A virtual electrode polarisation pattern is produced with a virtual cathode (VC) and virtual anode (VA) in close proximity. Panel B: Isochronal activation map of post shock activation. The break-excitation spreads from the virtual cathode to the virtual anode. As this propagation is slow full recovery of the virtual cathode has occurred and thus re-entry around a shock-induced phase singularity can occur. (Adapted from (121)).

1.2.3 Factors affecting successful defibrillation

Successful defibrillation is influenced by variables of the shock and the patient.

1.2.3.1 Countershock characteristics – electrode configuration and waveform

The ability of a countershock to polarise sufficient myocardium, with sufficient strength, is influenced by the electrode configuration. In general, the electrode configuration that gives the smallest area of low potential gradient results in the lowest defibrillation threshold (94). Throughout this thesis the electrode configuration was unchanged, and thus was not a source of defibrillation energy variation.

Historically, external defibrillators delivered monophasic impulses similar to that of figure 1.12A. Electronics required to produce such impulses are simpler than those required to make the impulse bidirectional (biphasic) (Figure 1.12B). However, monophasic countershocks require relatively high voltages to defibrillate successfully. On repeated application such voltages can damage the myocardium, and thus cause post resuscitation cardiac failure. Although extremely high voltage electric shocks have been shown to damage the myocardium (124), the shock voltages used clinically cause only transient, completely reversible dysfunction (125). Similarly, repeated low voltage shocks in the rat accentuated diastolic dysfunction (impaired myocardial relaxation), but not systolic dysfunction (94).

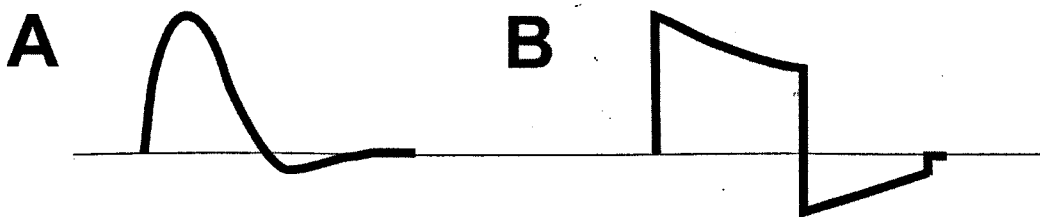


Figure 1.12 Defibrillator waveforms. Panel A: Monophasic waveform. Panel B: Biphasic waveform.

Mechanisms postulated to explain the greater effectiveness of the biphasic waveform are: -

(i) Critical point mechanism – As explained above, the "critical point re-entry" mechanism hypothesises that countershocks of insufficient strength will result in re-entry at the intersection of the critical level of recovery and the critical local field strength. In accordance with this theory, biphasic shocks should be more effective if they extend

refractoriness or increase field strength compared to equivalent strength monophasic shocks. Figure 1.13 shows the direct comparison of monophasic and biphasic waveforms of equal strengths on the action potential duration (APD). This shows that biphasic waveforms of lower voltage are able to produce equivalent APD prolongation to monophasic waveforms of higher voltages (126, 127). In terms of critical field strength, it has been suggested that a) electrical impedance is reduced during the second/reversed polarity phase – this aids current flow, and reduces the area below “critical field strength” (128) and b) the biphasic waveform is better able to stimulate the myocardium by effects on sodium channels (128). This second phenomenon may explain why biphasic waveforms are especially effective in prolonged VF (129). In early VF, cells are reactivated soon after their refractory period is over. In longer duration VF, the myocytes experience electrical diastole after the refractory period (post-repolarisation refractoriness) (130). In electrical diastole, cells must first be excited for the countershock to prolong their refractoriness. Biphasic waveforms achieve this more efficiently, as the first phase acts to excite the cells (127).

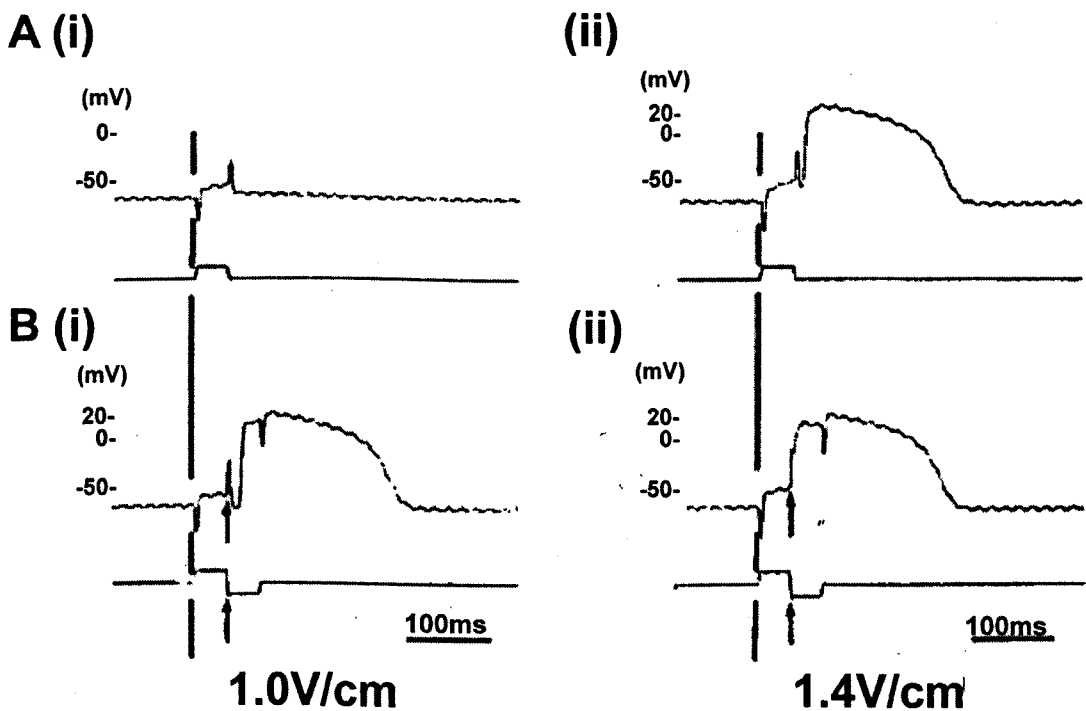


Figure 1.13 Transmembrane recordings from isolated myocytes. Panel A: Monophasic stimulation at voltages (i) just below and (ii) just above excitation threshold. Panel B: Biphasic stimulation at same voltages. (i) subthreshold voltage now triggers an action potential and (ii) suprathreshold voltage results in more prolonged APD. (Adapted from (127))

(ii) VE mechanism – this hypothesis more eloquently explains why monophasic shocks require greater energies than biphasic shocks. As explained in the VE hypothesis above, for monophasic shocks, successful defibrillation requires the shock to be greater than the

ULV, so that a phase-singularity is not produced. With biphasic shocks, the second part of the waveform reverses the first-phase polarisation. This removes the substrate of re-entry so that a phase singularity can no longer be produced (96).

1.2.3.2 Patient characteristics – arrest duration/ischaemia

As previously stated, the likelihood of successful defibrillation diminishes with time in out-of-hospital VF arrests. The influence of metabolic changes on the ability to defibrillate has been investigated in porcine models. However, these studies have not yielded consistent results. In one study, increased myocardial PCO₂, rather than acidosis, correlated with the haemodynamic efficacy of the resuscitation effort, and the consequent success of defibrillation (80). In another study, hypercarbia and hypoxia independently reduced the success of defibrillation (75). In a third, hyperkalaemia and ionised hypocalcaemia were associated with prolonged resuscitation efforts and unsuccessful defibrillation (83). None of these studies examined the underlying mechanism for the reduced defibrillation success. Nor did they relate the metabolic changes to VF frequency.

1.2.3.3 Paradox of relationship between DF and DFT

Both clinical studies and animal studies using in situ hearts, have correlated DF with defibrillation success, such that below a certain DF threshold, the likelihood of successful defibrillation is diminished (23, 30, 131). However, the relationship between DF and defibrillation threshold (DFT) is not a simple one. In the isolated Langendorff-perfused pig heart, reducing the perfusion rate not only reduced the DF, but also reduced the DFT compared to fully perfused controls (73). Barton et al. hypothesised that the lower DF reflected more synchronised and homogeneous electrical activity within the ischaemic myocardium. By reducing myocardial excitability and increasing refractoriness, ischaemia was proposed to enhance the electrical organisation. They predicted that this increased co-ordination facilitated defibrillation, and hence the reduced DFT. Similarly, the level of temporal coherence between orthogonal ECG recordings has been correlated to defibrillation success (132). Patwardhan et al. showed that higher levels of temporal coherence were associated with greater defibrillation success in dogs (132).

However, evidence to the contrary also exists. Chen's proposal of a slower, type 2 VF in ischaemia outlines that the reduced excitability produces wavebreak of the emerging post-shock wavefronts with consequent re-initiation of VF (68). Furthermore, a study in pigs demonstrated that more irregular ECGs in VF were associated with greater defibrillation

success (133). Therefore, the relationship between DF and DFT merits further characterisation.

1.3 Techniques for studying electrophysiology of VF

Through the decades, VF has been studied using different techniques in different models. Each of these methods has advantages and disadvantages, as summarised in table 1.1.

1.3.1 *Intact vs. isolated*

The major advantages of intact animals over isolated preparations are (i) they closely mimic human cardiac arrests and (ii) all of the hormonal influences are intact. The influence of autonomic stimulation in VF is complex. Sympathetic output appears to facilitate VF initiation by steepening the restitution kinetics (87) and increasing the dispersion of refractoriness (134, 135). In agreement with this beta-blockers are associated with a) spontaneous defibrillation during ischaemic-induced VF in isolated rabbit hearts (136) and b) reduced cardiac deaths from VF in the context of myocardial infarction in humans (137).

However, intact sympathetic innervation can complicate and confound the investigation of VF. Studies measuring VF intervals as a marker of refractory period have shown tremendous variation in the effect of sympathetic ganglion stimulation at different sites in different animals (135). Puzzlingly, sympathetic stimulation increased the dispersion of refractoriness in some hearts, yet decreased it in others. The influence of direct autonomic stimulation on dominant frequency of VF is as yet unknown. Standard processes to isolate the heart result in it being denervated. Although this denervation prevents the investigation of VF during autonomic activation, it minimizes inter-heart variation. Other advantages of the isolated heart preparation are (i) variables such as PO_2 , pH and $[K^+]_{EC}$ may be controlled individually and (ii) a wider range of observational techniques can be utilised (Table 1.1).

1.3.2 *Global ECG*

As the fluids of the body act as good electrical conductors, the electrical activity of the heart can be detected via electrodes on the body's surface. The electrical signal recorded between two surface electrodes is the extracellular algebraic summation of the action potentials (APs) of all the myocardial fibres of the heart (138). Figure 1.14 illustrates how

the various components of the surface ECG arise from the spread of activation and repolarisation throughout the heart. Owing to this global nature, the spatial resolution of the ECG is very low.

Method	Location	Can be used in vivo?	Maximum number of simultaneous recordings	Spatial resolution	Temporal resolution
Global ECG	-	Yes	1	low	High
Single cell microelectrode	Transmural on dissociation	No	1	cell	High
Floating microelectrode	Surface. Transmural on wedge preparation	No	~ 3	cell	High
MAP	Surface	Yes	~ 12	cm	High
Optical mapping	Superficial	No	100s – 1000s	$\mu\text{m} - \text{cm}$	High

Table 1.1 Summary of techniques for investigation of VF (adapted from (44)).

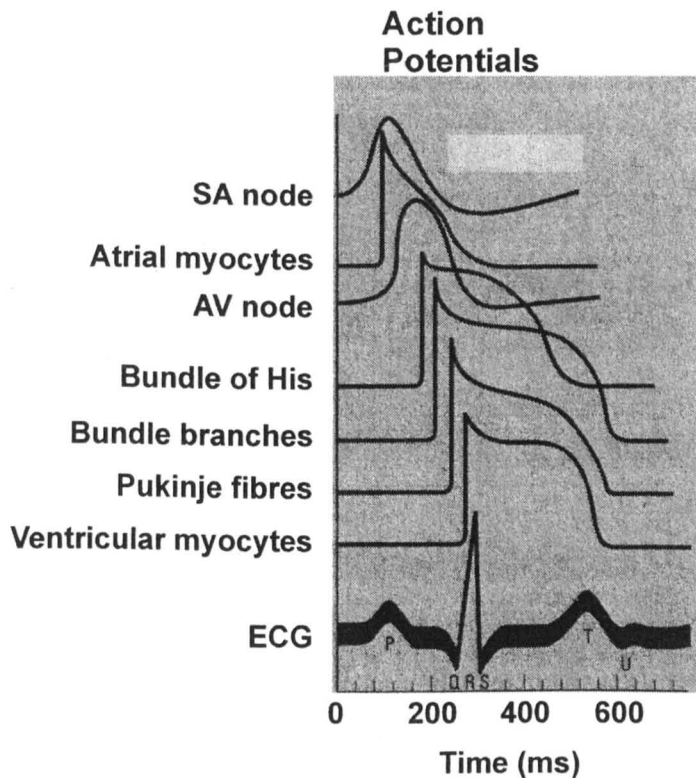


Figure 1.14 Origins of the ECG. The transmembrane AP for the SA node, the AV node, other parts of the heart's conducting system, atrial muscle and ventricular muscle are illustrated with reference to the surface ECG. The 'p' wave corresponds to the activation and repolarisation of the atrial myocytes. The QRS complex corresponds to the spread of activation across the ventricles. The ST segment occurs due to the electronegative summation of the ventricular AP plateaux, and the T wave results from the sequential repolarisation of the ventricular myocytes. (Adapted from (138)).

In clinical studies, the only method available to analyze VF is the surface ECG. Such recordings are non-invasive and are easily obtained; at cardiac arrests external defibrillators store the ECG recordings. However, these ECG recordings give a very general picture of the electrical activity of the heart, as a maximum of three leads, or axes of the heart, are recorded. Studies of intact animals, without thoracotomy to expose the heart, are subject to the same limitations.

In this thesis, a single lead global ECG was acquired from 2 electrodes mounted in the walls of the optical mapping chamber (Figure 2.2A). The time-course of the DF of this global ECG during VF was compared with previous clinical and animal studies.

1.3.3 Microelectrode

Glass microelectrodes impale a single cell. By comparing the intracellular potential to a reference extracellular electrode, the absolute membrane potential is measured. Such transmembrane recordings give a clearer appreciation of the cellular electrophysiological changes that occur during VF.

Traditional microelectrode techniques require a stable intracellular impalement to measure the membrane potential. Maintaining the microelectrode tip in the intracellular space can be difficult in multi-cellular preparations, and is impossible in the contracting whole heart. Therefore, traditional microelectrode techniques can only be performed on multi-cellular preparations that are unable support VF (cf. critical mass hypothesis). The technique of the floating microelectrode was adapted to allow epicardial transmembrane recordings from isolated whole hearts (81, 139) or in situ hearts (140). Rather than trying to maintain one stable intracellular impalement, the electrode is suspended from above (Figure 2.16) and allowed to make a series of repeated (or floating) impalements (141). The lack of stability of impalement limits the number of simultaneous measurements. Another limitation of this method is that only the epicardial surface of the isolated whole heart can be examined.

In this thesis, floating microelectrodes were used to assess the precise changes in LV epicardial transmembrane potential during VF.

1.3.4 Monophasic Action Potentials

In the early 1980s, Franz developed a contact electrode catheter that recorded Monophasic Action Potentials (MAPs) (142). Although the source of these signals is debated (143-145), Franz's hypothesis of their origin is still largely accepted (146).

The Franz contact electrode consists of 2 electrodes; one at the tip, in contact with the underlying tissue, and a second, placed more proximal on the catheter. As shown in figure 1.15, the pressure of the contact electrode causes fixed low-level depolarisation of the underlying tissue. Therefore, during diastole, there is a steady flow of current from the surrounding non-depolarised tissue to the low-level depolarised tissue underlying the electrode (Figure 1.15A). On activation, the surrounding tissue becomes more depolarised, and thus the current flow is reversed, producing the MAP upstroke and plateau (Figures 1.15B & C). As the surrounding tissue repolarises, the currents are again reversed to the original diastolic situation (Figure 1.15D).

Although unable to measure the actual membrane potential, MAPs have been shown to accurately reflect the repolarisation time-course of the transmembrane AP compared to adjacent glass microelectrodes (147). In contrast, the upstroke velocity of the MAP is slower than the transmembrane AP (146). This is due to the larger number of cells that MAP electrodes records from compared to glass microelectrodes. The number of cells that influence the transmembrane AP is determined by the space constant. Although the microelectrode impales a single cell, the resultant membrane potential is influenced by the electrical activity of the surrounding cells. The degree of electrical influence of a surrounding cell depends on its distance from the impaled cell. The influence decreases exponentially with distance and is described by the space constant. Typical space constants in the rabbit ventricle are 0.1 – 0.3mm (148). This equates to a 50% drop in the electrical potential influence at 200µm. In contrast, MAP electrodes have tip diameters of 1-2mm, and spheres of electrical influence beyond that. Precise space constants have not been determined for MAP electrodes, but spheres of influence are thought to be <5mm (146).

Advantages of MAP recordings are (i) non-reliance on stable impalement, (ii) a greater number of recordings are possible, which with increasing computer power allows surface maps to be constructed, and (iii) although contact electrodes are only influenced by the very surface layers of the epicardium (149), intramural needle electrodes can penetrate further (135). Disadvantages of MAP recordings are (i) the inability to record absolute potentials and (ii) the need to isolate the electrical apparatus during defibrillation (92)

therefore producing a short window of time during which electrical activity cannot be observed.

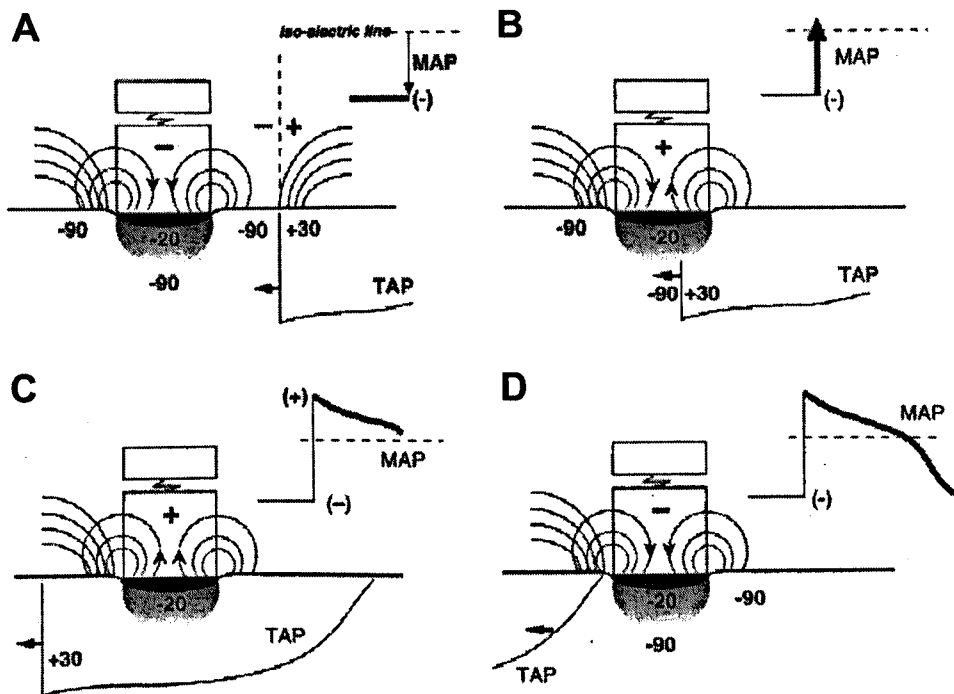


Figure 1.15 Hypothesis of genesis of MAP recording by contact electrode. Panel A: Late electrical diastole. The myocytes intracellular potential is -90mV . There is fixed depolarisation (grey shading) of the tissue underlying the contact electrode (black indentation). Thus a potential gradient exist between the normal surrounding tissue and the fixed depolarised tissue under the contact electrode. This results in an extracellular current flow from the normal tissue (circular lines with arrow). **Panel B:** Early electrical systole. The tissue under the electrode remains fixed. Depolarisation of the activation side tissue now reverses the current resulting in the MAP upstroke. **Panel C:** Mid systole. As the activation spreads all the surrounding tissue is now more depolarised than the reference area. This results in the MAP plateau. **Panel D:** Early diastole. As the activation wave recedes from the MAP the surrounding tissue returns to pre-activation potentials and the current reverts to that in A. (Adapted from (146), TAP = Transmembrane Action Potential).

In this thesis, MAP recordings were used to assess alterations in repolarisation and refractoriness simultaneously in the LV and RV. Repolarization and refractoriness cannot be measured directly during VF, therefore both parameters were assessed during epicardial pacing.

1.3.5 Optical mapping

Optical mapping allows the simultaneous recording of the electrical activity of hundreds to tens of thousands of sites on a cardiac surface (For review see (150, 151)). Hearts are first loaded with a voltage-sensitive fluorescent dye (such as RH237) that integrates into the myocyte membrane. After being excited by short wavelength light, the dye fluoresces at longer wavelengths. The spectral characteristics of this fluorescence are altered by the

membrane potential. Figure 1.16 shows how membrane depolarisation results in a shift of RH237's fluorescence spectrum to shorter wavelengths. This spectral shift affects the amplitude of the fluorescence as measured beyond a fixed long wavelength cut-off. Therefore membrane depolarisation results in a relative fall in fluorescence at longer wavelengths. On membrane repolarisation, the spectrum returns to its original characteristics, resulting in an increase in fluorescence back to pre-activation levels.

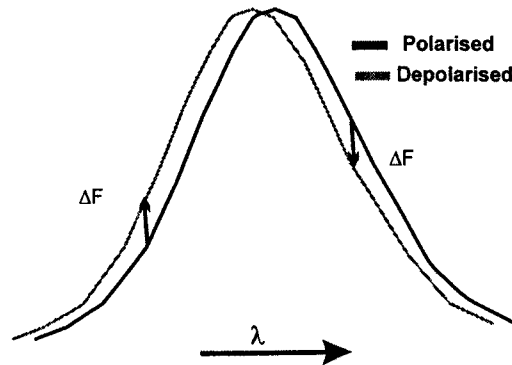


Figure 1.16 Diagram of voltage-sensitive spectral shift. Depolarisation produces a reduction in fluorescence at the red end of the spectrum e.g. RH237. (Adapted from (152)).

The nature of the optical action potential (AP) is different from the transmembrane AP recorded by a microelectrode. The optical AP reflects the activation of a group of cells that are defined by the photodiode size, the magnification and the depth of field. For the optical apparatus used in this thesis, this equated to a volume of $0.8 \times 0.8 \times 0.09\text{mm} \approx 0.056\text{mm}^2$ on the epicardial surface (Chapter 2.4). The surface cells have equal influence on the optical AP. The electrical influence from underlying cells is harder to define. As discussed above, the number of cells that influence the transmembrane AP is determined by the space constant with typical space constants in the rabbit ventricle is $0.1 - 0.3\text{mm}$ (148). This equates to 50% drop in electrical potential influence at $200\mu\text{m}$. Thus the number of cells influencing the optical AP is far greater than the number affecting the transmembrane AP as recorded by microelectrode.

For this reason, as shown in figure 1.17, the optical AP upslope is slower than the simultaneous transmembrane AP. Cells adjacent to each other do not activate simultaneously, but rather activate in rapid succession as the wave of excitation spreads. The extent of upstroke slowing depends on the number of cells influencing the membrane potential recording. In optical mapping the extent of this smearing is determined by the spatial resolution of the optical system. The spatial resolution is determined by a combination of the optical magnification, and the number of recording sites on the detector. The optical magnification is a limiting factor on the spatial resolution as

increasing magnification reduces signal quality (153). As shown in figure 1.18, fluorescent light is collected from fewer and fewer cells as the optical magnification is increased. Therefore, at higher magnifications optical signals have lower amplitudes, and are poorer quality as the signal-to-noise ratio falls (Figure 1.19).

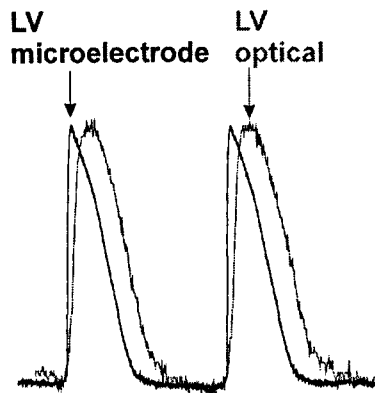


Figure 1.17 Comparison of microelectrode and optical upstroke. The raw data illustrated was recorded under control conditions whilst pacing at basic cycle length 180ms. The upstroke velocity of a LV optical signal (Chapter 7.3.2) is slower as it represents the summation of the activation of hundreds of thousands of cells from a volume of $\approx 0.056\text{mm}^2$. In comparison, the electrotonic influence on transmembrane recordings from a floating microelectrode (Chapter 9.3) is more limited.

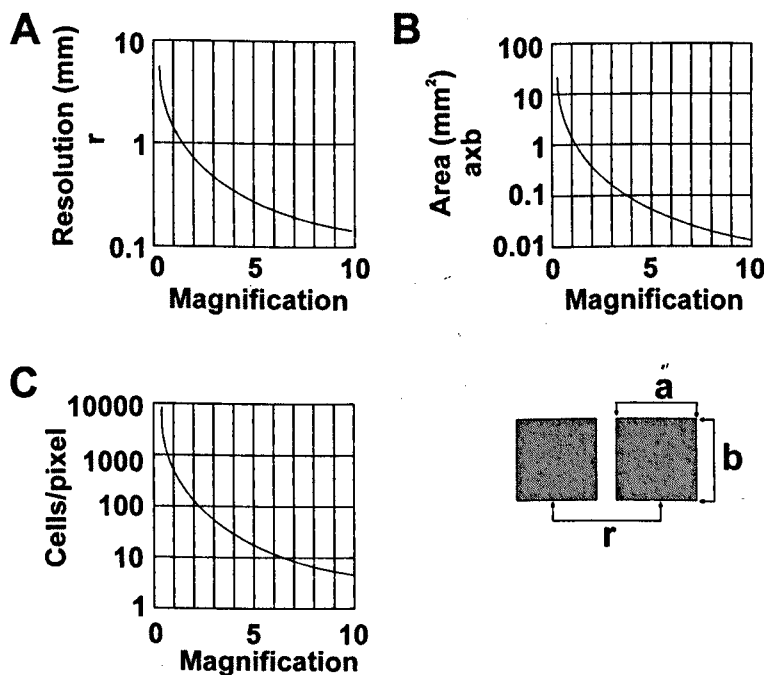


Figure 1.18 Influence of magnification in optical mapping. Panel A: Plot of magnification vs. spacial resolution – the spatial resolution, r , varies as inverse with the degree of optical magnification. Panel B: Plot of magnification vs. pixel area – the surface area of tissue imaged onto each photo element decreases with increasing optical magnification (pixel area = $a \times b$). Panel C: Plot of magnification vs. cells per pixel – the estimated number of cells that contribute to the signal focused onto any individual detector reduces with increasing magnification. (Adapted from (153)).

Movement during myocardial contraction alters the site that the detector is focused on, and therefore changes the signal fluorescence for reasons unrelated to the membrane potential (movement artefact). Although electro-mechanical uncoupling agents can be used to reduce or even eliminate movement, evidence is growing that they alter the electrophysiological properties that are being studied (139, 154, 155). Therefore in this thesis the use of electro-mechanical uncoupling agents was avoided where possible.

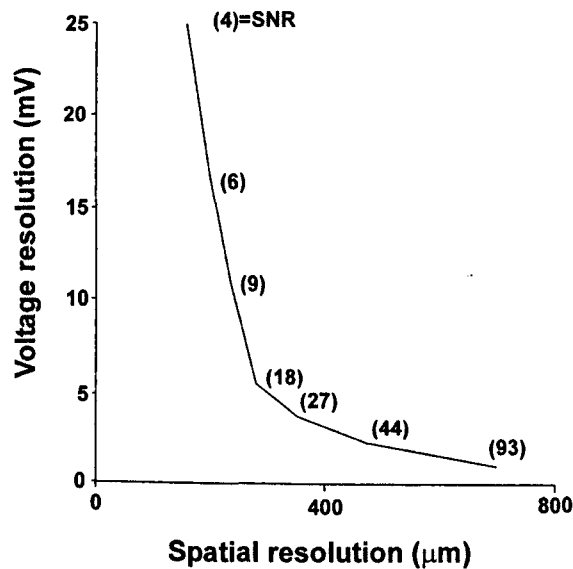


Figure 1.19 Voltage resolution and signal-to-noise ratio (SNR). Plotting voltage resolution vs. spatial resolution shows how the voltage resolution, and signal fidelity fall as the spatial resolution is increased (i.e. as the pixel area is decreased). This occurs because fewer cells are contributing to the optical action potential signal, whilst system noise and illumination remain constant. (Adapted from (153)).

Previously it was thought, that similar to contact electrodes, optical recordings originated from only the very surface layer of the epicardium. Evidence now shows that optical measurements may penetrate deeper. Using a transparent mapping array, Knisley et al. compared simultaneously the excitation intervals of optical and extracellular electrical recordings, and demonstrated that the differences between them could be attributed to deeper optical interrogation and the accompanying fibre rotation (149). This ‘depth of field’ effect is an additional complication, but its dependency on the optical properties of the set-up allows it to be quantified using standard optical equations (156). For the photodiode array (PDA) based optical set-up used in this thesis (Figure 2.4): -

$$\text{Depth of Field} = 1000\mu\text{m}/[(7 \times \text{NA} \times \text{magnification}) + \lambda_{\text{ex}}/2(\text{NA})^2]$$

$$= 1000/[(7 \times 1.4 \times 1.2) + 0.535/2 \times 1.4^2]$$

$$= 90 \mu\text{m}$$

$$(\text{NA} = \text{Numerical Aperture})$$

This depth of field is sufficiently shallow to exclude a major influence from deeper myocardial layers.

A major advantage of optical mapping is that the lack of electrical contact with the heart allows continuous recording during defibrillation (157).

1.4 Aims and hypothesis

The aims of this thesis were: -

- (i) To verify in the isolated rabbit heart the slowing of the ECG dominant frequency during VF under conditions of low-flow ischaemia.
- (ii) To investigate the spatiotemporal pattern of this electrical slowing using optical mapping.
- (iii) To investigate which components of ischaemia are responsible for the slowing of the ECG dominant frequency, and whether they produce the same spatiotemporal patterns as observed in VF during low-flow ischaemia.
- (iv) To assess which components of ischaemia reduce the likelihood of successful defibrillation by increasing the energies required to defibrillate.

The hypothesis at the outset was that a single component of ischaemia would be identified as being responsible for slowing the ECG dominant frequency, and that the same component would increase the energies required to successfully defibrillate VF.

2 Methods

2.1 Preparation for Langendorff perfusion

Male New Zealand White rabbits, weighing 2.5 – 3.0kg, were sacrificed by terminal anaesthesia using an intravenous cocktail of 0.5ml/kg Euthatal (sodium pentobarbitone 200 mg/kg, Rhône Mérieux) and 500 IU of heparin. The hearts were rapidly excised, transferred into chilled Tyrode's solution to transiently stop contractions, then mounted onto an aortic cannula and perfused retrogradely (Langendorff mode, Figure 2.1). The Tyrode's solution was composed of (units = mM) Na^+ 134.5, Mg^{2+} 1.0, K^+ 5.0, Ca^{2+} 1.9, Cl^- 101.8, SO_4^{2-} 1.0, H_2PO_4^- 0.7, HCO_3^- 20, acetate (CH_3COO^-) 20 and glucose ($\text{C}_6\text{H}_{12}\text{O}_6$) 50. This high glucose concentration prevented osmotic swelling with its incumbent electrophysiological changes (Prof. Guy Salama, Personal communication & (158)). The solution was filtered through a 5 μm filter (Whatman) prior to use. With the exception of acidic pH protocols, the solution pH was maintained at 7.4 by bubbling with a 95% O_2 /5% CO_2 gas mixture (BOC, UK). The solution perfusing, and surrounding the heart, was maintained at 37°C by a glass-column heat exchanger connected to a thermostat-controlled water bath (Figure 2.1). Using a Gilson Minipuls 3 peristaltic pump, the Langendorff perfusion was rate controlled rather than pressure controlled. A standard perfusion rate of 40ml/min was used in all but low-flow ischaemia experiments. A transducer connected to the aortic cannula monitored the perfusion pressure. Experimentation was discontinued when pressures rose above 70mmHg; typical starting pressures were approximately 45mmHg.

2.2 Pacing and ECG

Pacing was achieved by connecting the relevant electrodes to a Digitimer DS2 stimulator. This provided a constant voltage, square pulse of 2ms width. The timing of the pulse was computer controlled using locally developed software (Dr FL Burton, University of Glasgow). The pacing protocols for each experimental protocol are outlined in the relevant chapter.

In the optical experiments, global ECG signals were obtained using electrodes mounted within the chamber walls (Figure 2.2A). Signals from these electrodes were amplified by a MAP amplifier (custom built by Dr. Mark Watts, Glasgow Royal Infirmary), before being relayed to an oscilloscope (Nicolet Instrument Corporation, Wisconsin, USA.) to allow real-time viewing, and to the photodiode array (PDA). During optical experiments, the 4 corner channels of the PDA were reserved for recording the ECG and pacing stimuli

traces. In MAP and microelectrode experiments no ECG recordings were taken. In these experiments, pacing stimuli were recorded in a separate channel via the relevant amplifier.

2.3 VF induction

Experimentally VF can be induced in many ways, each with its advantages and disadvantages.

- (i) The most clinically relevant method of VF induction is through regional ischaemia/reperfusion. Regional ischaemia can be induced by external ligation of the Left Anterior Descending artery (LAD) (22). This method requires almost complete occlusion of the artery, which is technically difficult. Furthermore VF does not automatically follow the ischaemic challenge.
- (ii) The application of a low-voltage stimulus during the vulnerable period of repolarisation (i.e. the T wave) can induce VF by increasing repolarisation heterogeneity (159). This method requires the application of a strong enough stimulus at a precise time-point of the APD. Having 2 variables (amplitude and timing) reduces the reliability of this method, such that several attempts are often required to induce VF (160).
- (iii) A more reliable method of VF induction is the application of a high-voltage DC shock (160). However, this shock can cause damage to the heart, and secondarily to myocardial stunning, results in slowing of the VF frequencies immediately post induction (161), Dr F Burton, Personal Communications).
- (iv) VF induction by burst pacing does not damage the heart, or result in stunning. Therefore, this method of induction was preferred due to its lack of effect on VF frequencies (162) and lack of damage to the preparation. Compared to "Shock-on-T" induction (ii), burst pacing is more likely to induce VT (162). In such cases, VT was immediately detected on the ECG, and VF induced by a second burst-pacing salvo of 50Hz for 8s.

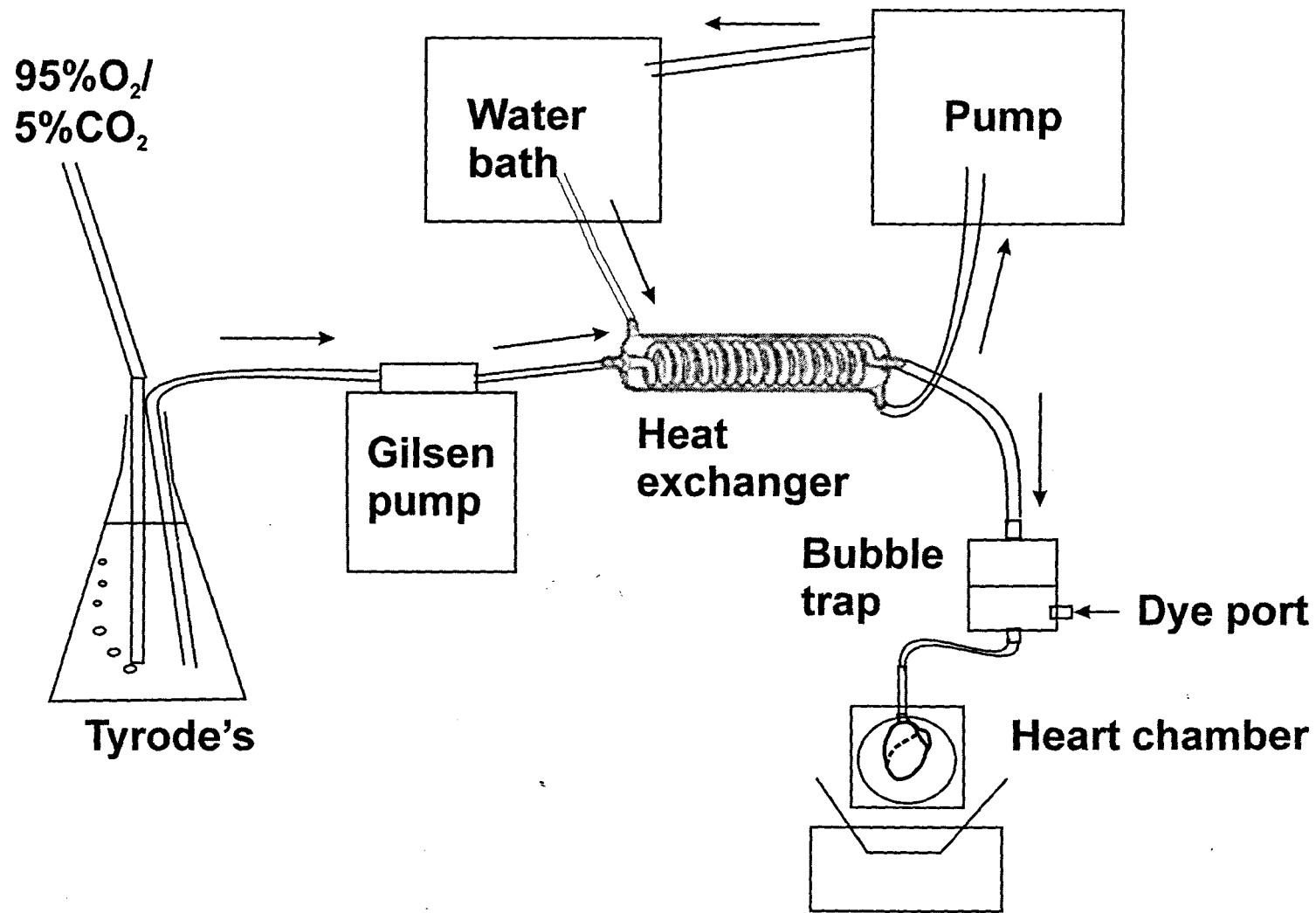


Figure 2.1 Langendorff perfusion apparatus

2.4 Defibrillation

Although VF can be defibrillated chemically (163, 164), electrical defibrillation is the standard practice in the clinical setting. In this thesis, hearts were defibrillated using an external cardiac defibrillator (Ventak ECD 2815, CPL, St Paul's, MN, USA). This defibrillator has a 140 μ F capacitor, 80% fixed tilt with 1st phase 60% of total duration. In this external defibrillator, the waveform duration is automatically adjusted to resistance load. The typical resistance of a rabbit heart was \sim 48 Ω , which gave rise to waveform duration of \sim 14ms. Shocks were delivered via custom-made stainless steel paddles (Figure 2.2A). The defibrillation paddles cradled the heart and reduced motion artefact. These paddles were fixed with respect to the front-plate and the area of optical interrogation. As the interrogation area was standardised using the left anterior descending artery (LAD) as a landmark, the paddle position on the heart was relatively constant. The orientation of initial electrode polarity was also kept constant.

2.5 Optical mapping

Epicardial membrane potentials from the anterior surface of the heart were acquired using an optical mapping array. Langendorff-perfused hearts were positioned into the custom-made Perspex chamber shown in figure 2.2. The heart's exterior surface was maintained at 37°C by allowing the coronary sinus effluent to fill the chamber. The contractile motion of the heart was reduced during optical recordings by (i) cradling it between the defibrillation electrodes and (ii) transiently applying gentle compression against the front-plate by sliding forward the back piston (Figure 2.2).

The hearts were loaded with a 100 μ l bolus of the voltage-sensitive, fluorescent dye RH237 (Molecular Probes) (Figure 2.3), dissolved in DMSO (1mg/ml). This bolus was administered into the coronary circulation by slow injection through the bubble trap "Dye port" (Figure 2.1). When RH237 is excited at 514.5nm, depolarisation by an action potential produces a fractional fluorescence decrease of approx. 2 – 6% (165). This highlights that a large component of the optical signal is due to background fluorescence (166). This background component was removed by software subtraction prior to data analysis.

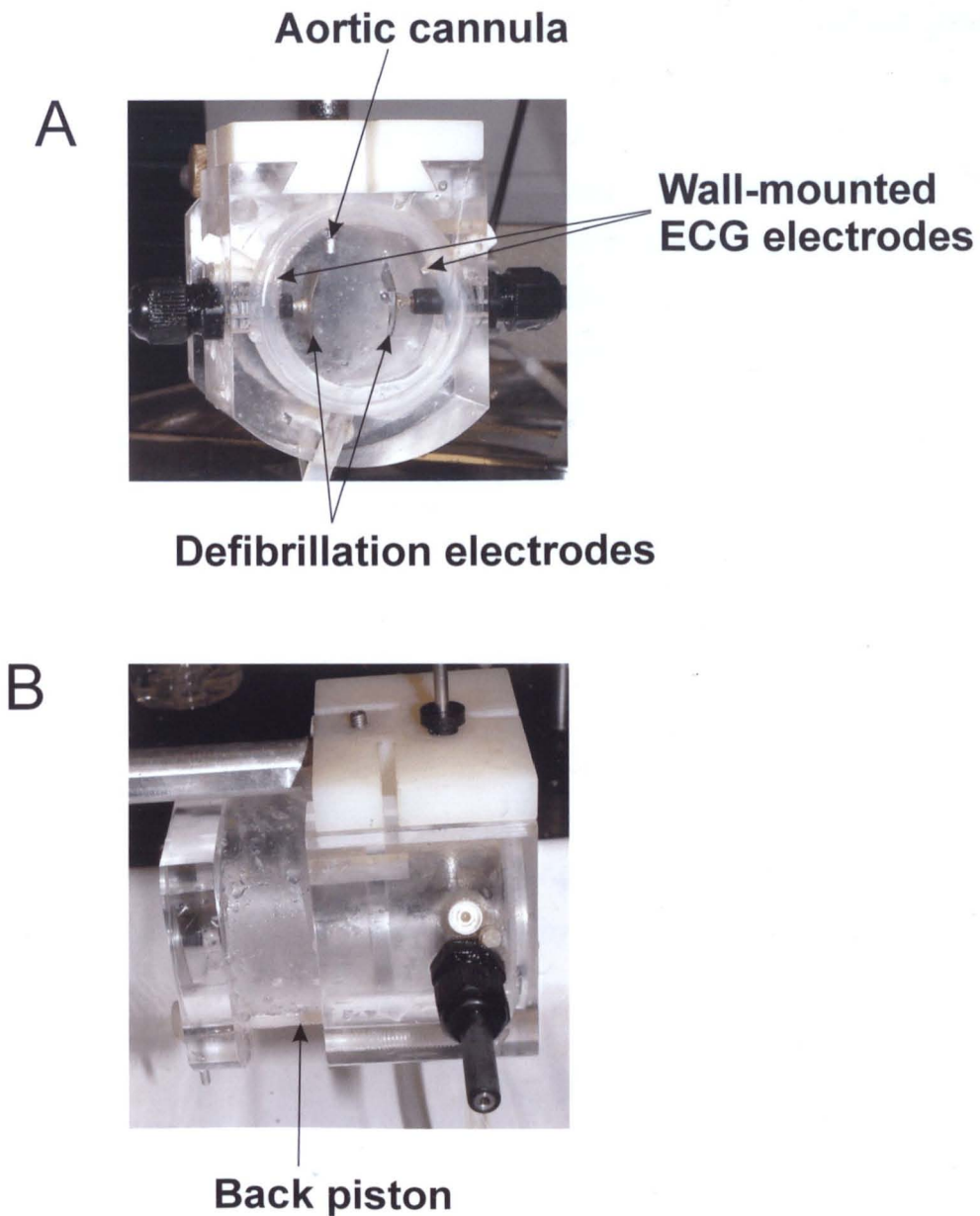


Figure 2.2 Photographs of the optical mapping chamber. Panel A: Photograph of the front elevation of Perspex chamber. This shows the defibrillation electrodes that cradled the heart, and the wall-mounted electrodes that record the ECG. Panel B: Photograph showing the side elevation. Sliding forward the back piston allowed transient compression of the heart against the frontplate.

Figure 2.4 illustrates how the anterior surface of the heart was illuminated with light from $4 \times 75\text{W}$ tungsten-halogen bulbs passing through $535 \pm 25\text{nm}$ interference filters (Comar Instruments) (Figure 2.4). Fluorescent light emitted from the epicardial surface was collected with a camera lens (Nikon 85mm, $f1:1.4$) and focused through a 695nm long-pass filter onto a 16×16 PDA (C4675-102, Hamamatsu Photonics). As the 4 corner channels were reserved for ECG and pacing signals, optical signals were acquired by 252 of 256 diodes. Each diode had a sensing area of $0.95\text{mm} \times 0.95\text{mm}$. The distance between the centres of adjacent diodes, or pitch, was 1.1mm . The magnification of the optical system was $\times 1.2$. Therefore each diode detected light from an epicardial area of

0.8mm × 0.8mm. Data was digitised at 1kHz, stored onto disk, and analysed offline using software written in IDL (Interactive Data Language, Research Systems Inc.). Photographic images of the epicardial area of interrogation were taken using a charged-coupled device (CCD). This CCD was perpendicular to the PDA, and at the same focal distance. The CCD and PDA were precisely aligned using a patterned black/white square print and a mirror. As the alignment was crucial for the correct identification of the RV/LV border, it was verified at the start of each experimental day. At the end of each experimental day, the location of the RV/LV boundary was confirmed by suture placement; the RV was incised and sutures inserted at the junction of the RV free wall and the inter-ventricular septum.

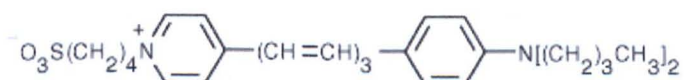


Figure 2.3 Chemical structure of RH237

A second critical element was the adjustment of the focal plane so that light was collected from the epicardial surface. This was achieved by adjusting the focus to give a sharp edge to the epicardial fat streaks on the heart's surface.

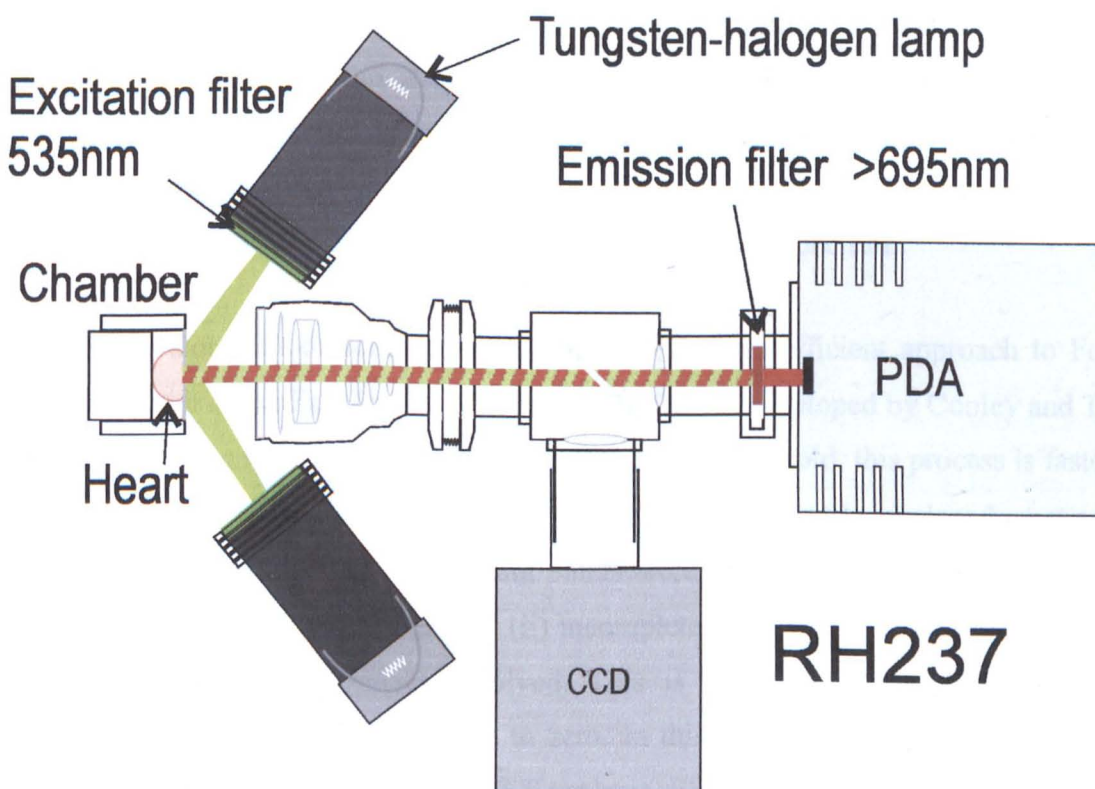


Figure 2.4 Diagram of the optical mapping set-up.

2.6 Analysis of VF

2.6.1 Frequency analysis of VF

Traditional spatiotemporal cardiac mapping involves (i) identification of the local activation time, usually taken as the time of dV/dt_{\max} of the AP upstroke (167), and (ii) subsequently plotting the spread of activation across the field of interest (48, 168). This creates a map of ever expanding contour lines (Isochronal mapping). Whilst ideal for analysing simple, repetitive rhythms, this method cannot be used to analysis the chaotic activity that occurs in VF. One approach to analysing complex rhythms like VF is to break the pattern into smaller constitutive parts, such as frequency (169). This can be accomplished using the mathematical tool of Fourier Transform, whose equation is outlined in figure 2.5.

$$s(t) = \frac{1}{\sqrt{2\pi}} \int_{-\infty}^{\infty} S(\omega) e^{i\omega t} d\omega$$

Figure 2.5 Fourier Transform equation

In 1807, Baron Fourier developed his mathematical formula to describe the temporal dispersion of heat around an iron anchor ring (170). The resulting Fourier Transform breaks down any time-based waveform into a series of sinusoidal waves, each with its own magnitude, frequency and phase. As shown in figure 2.6, plotting the amplitude of each sinusoidal wave against frequency creates a frequency power spectrum.

With the development of computers and software, a more efficient approach to Fourier analysis, known as the Fast Fourier Transform (FFT), was developed by Cooley and Tukey (171). By reducing the number of calculations more than 200 fold, this process is faster but at the cost of some data restrictions (172): - (i) The waveform to be analysed must consist of 2^n data points. In this thesis 4098 data points were used; 4s of 1kHz recordings (4000 points) extended by 98 zero-pad points. (ii) Incomplete sinusoidal cycles lead to inaccurate interpretation of the frequencies involved. This is prevented by applying a window weighting function that tapers the data to zero. In this thesis, the Hamming window was applied to all raw VF signals prior to FFT analysis. FFT power spectra were derived from ECG and optical pixel signals. From the VF optical data, the power spectra of the 252 pixels were summated to give a global power spectrum. This global power spectrum is

commonly known as the pseudoECG (psECG) (61, 173). The psECG reflects the average electrical activity of VF within the epicardial area examined.

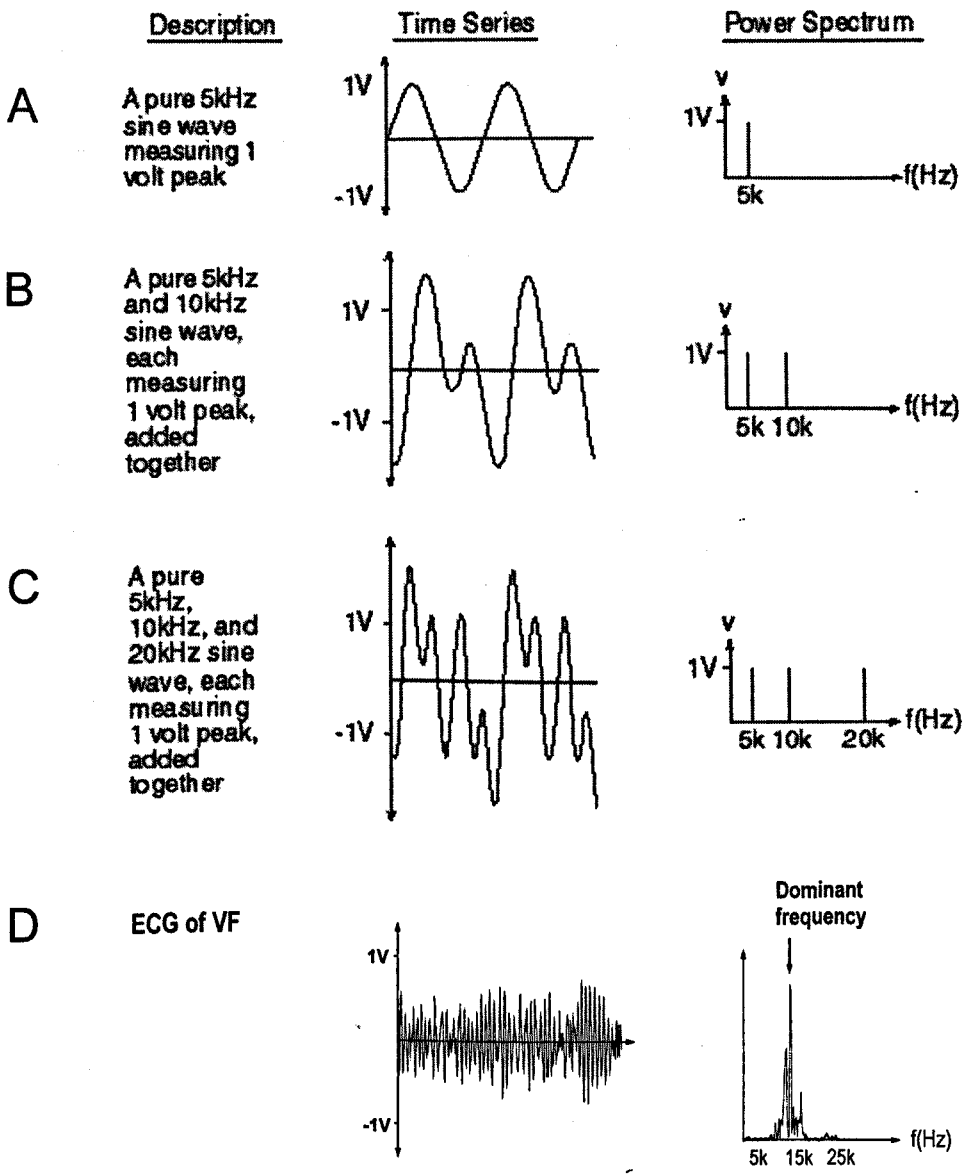


Figure 2.6 The Fourier Transform illustrated (adapted from (172)). Panel A: The signal and power spectrum are of a 5kHz pure tone. The single sine wave produces a power spectrum consisting of a single line. **Panel B:** The signal and power spectrum for combined pure tones of 5 and 10kHz at same amplitude and phase. The power spectrum of this wave has 2 lines of equal length. **Panel C:** the combination of fundamental (5kHz), first harmonic (10kHz) and second harmonic (20kHz) at equal amplitude and in phase give 3 lines of equal length on the power spectrum. **Panel D:** A typical ECG signal in VF produces a more complex power spectrum. However, there is a clear peak (or dominant) frequency.

From the FFT frequency power spectrum, statistical parameters can be derived and used to quantify the electrical activity of VF: - (i) Dominant Frequency (DF) – identified as the largest peak on the power spectrum, the DF is a measure of the predominant rate of activation. For the ECG, this reflects the predominant ventricular activation rate, whereas for optical signals, DF reflects the predominant activation rate within the confines of that pixel (174). As well as being equivalent to the ventricular fibrillation cycle length of

electrical mapping studies (4, 46, 135), the ECG-derived time-course of DF in VF has been well characterised in human and animal studies (21-24, 30). (ii) Median Frequency (MF) – The time-course of this measure of the average electrical activity has also been well characterised in human and animal VF studies (24-33).

For this thesis, both DF and MF were analysed in all the VF experiments. As the time-course and spatiotemporal patterns were identical in all conditions, only DF data is presented in this thesis.

2.6.2 Amplitude analysis in VF

During VF, the peak-to-peak amplitude of the ECG and optical signals was determined using locally developed software (Dr Francis Burton). This software first filtered the raw signal by polynomial subtraction, high pass (50Hz) and low pass (3Hz) filters. As shown in figure 2.7, the VF peaks were then identified as the points where dV/dt changed orientation (i.e. from +ve to -ve or vice versa). The difference in y value between 2 consecutive peaks was taken as the action potential amplitude.

2.6.3 Analysis of conduction velocity

2.6.3.1 Apparent conduction velocity in VF

In VF, the apparent conduction velocity was derived using software developed by Dr F. L. Burton (4, 46). This program first detects the activation front as dV/dt_{\max} in each pixel. These activation times are compared between adjacent pixels to establish wave direction. The wavefront velocity is calculated at the centre point of each 2×2 pixel squares. This process was repeated for all activations during the 4s datasets of VF. From these datasets, the mean and modal apparent CV was calculated.

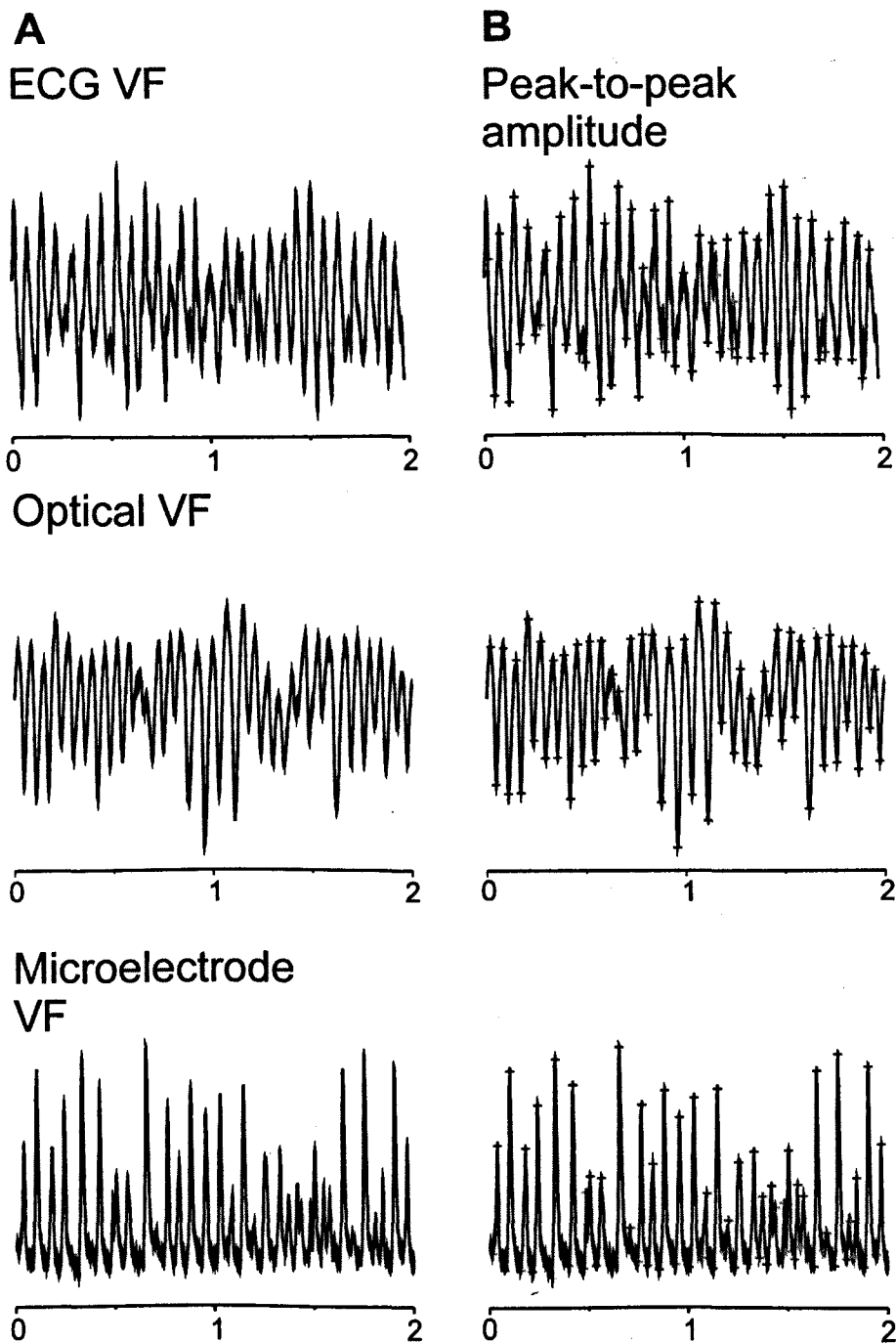


Figure 2.7 Illustration of peak identification in ECG, optical and microelectrode recordings. Panel A: illustrates the signals after filtering (polynomial subtraction, low and high pass). Panel B: shows peak identification as the change in direction of dV/dt . Amplitude was measured as the peak-to-peak excursion.

Figure 2.8 illustrates how in VF the patterns of wavefront propagation observed on the epicardial surface could result from simple linear conduction across epicardium or from more complex spiral waves in underlying intramural myocardium. Owing to the two-dimensional nature of optical mapping, it is impossible to determine the true direction of propagation in VF. For this reason, conduction velocity was also assessed during epicardial pacing.

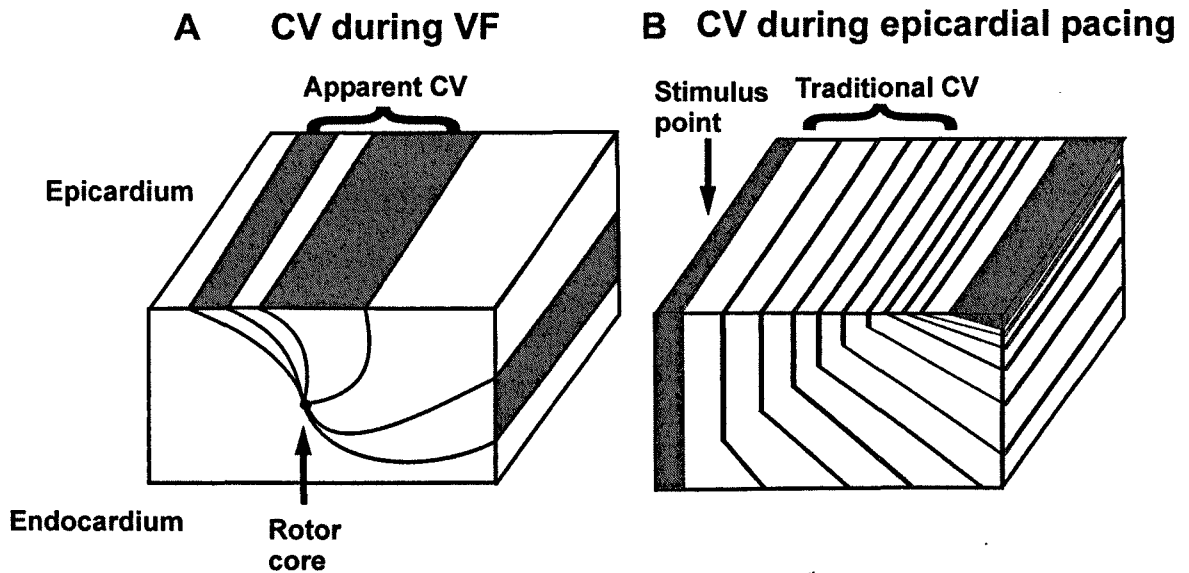


Figure 2.8 Illustration of the different possible pathways of epicardial activation. Panel A: In VF, epicardial activity is chaotic. The activation could originate from intramural rotors or multiple epicardial wavelets. Here a clock-wise rotating intramural rotor is illustrated. Currently it is not possible to differentiate the VF activation pathways from the optically mapped epicardial surface. Panel B: In epicardial pacing, the activation wavefront changes from epicardial to intramural propagation owing to the non-uniformity of intramural fibre orientation (175). This results in apparent acceleration of conduction. This diagrammatic representation shows how the epicardial CV changes with the direction of activation. Again the orientation of the underlying wavefront is indiscernible from the epicardial surface.

2.6.3.2 Conduction velocity from epicardial pacing

Normally conduction velocity (CV) is determined during epicardial pacing rather than during spontaneous activity, atrial pacing or endocardial pacing. Stimulating the epicardium directly allows epicardial conduction to be assessed without potential artefact from transmural conduction. A 1mm hole was drilled into the front-plate of the optical mapping chamber to allow epicardial stimulation with a bipolar platinum electrode. Bipolar stimulation was used in preference to unipolar to produce more reliable point of first activation.

In this thesis, the method for calculating epicardial CV was based on work by Bayly (176). (i) Activation times (time of dV/dt_{max}) were detected in each pixel using software developed in IDL (Interactive Data Language, Research Systems) by Dr Bum-Rak Choi (Pittsburgh, USA) (Figure 2.9A). (ii) From this activation matrix a series of polynomial curves were fitted to the epicardial activation times. (iii) From these curves two-dimensional velocity vectors were generated (176) (Figure 2.9B). Processes (ii) and (iii) were performed using software developed by Dr Francis Burton in MatLab 7.0 (The MathWorks Inc, Natick, MA.).

There are several potential pitfalls in using velocity vectors to generate a representative assessment of the epicardial CV: - (i) Stimulating the epicardium with a bipolar electrode does not produce a single activation point. Rather it produces complex patterns of virtual electrodes from which the activation spreads (114-116) (Figure 1.10). Therefore, the CV must be assessed beyond these virtual electrodes. (ii) Epicardial stimulation activates deeper structures that can result in faster conduction than the epicardium (purkinje fibres, intramural cusps (175)). This faster activation can breakthrough onto the yet unexcited epicardial surface (Figure 2.8B). Therefore, CV must be assessed within a certain perimeter to avoid contamination by intramural breakthrough conduction. (iii) Conduction does not spread uniformly across the myocardium. Rather there is anisotropy, with faster conduction along the length of the myocardial fibres (longitudinal CV) and slower CV perpendicular to this (transverse CV) (177). Therefore, the angle at which CV is assessed will also affect the value obtained. To avoid these pitfalls, and remove observer error, the CV was assessed by 3 different approaches: -

1. Radial – Figure 2.9 demonstrates the radial analysis of CV. The stimulation point was identified as the central point of activation (* in Figure 2.9A). This was confirmed as the bipolar electrode location through CCD imaging. From this stimulation point, the CV was assessed around a 5mm radius (Figure 2.9A). Plotting CV against the angle of incidence allowed determination of the peak CVs around the 5mm radius (Figure 2.9C). These were identified as the longitudinal CVs. Depending on the bipolar electrode location, the 5mm radius circle could cross the RV/LV boundary. Therefore the longitudinal CV was assessed along the activation axis travelling away from the septum. Transverse CVs were identified as the CVs perpendicular to the longitudinal axis. As neither of these axes crossed the ventricular boundary, the transverse CV was determined as the average of the two CVs perpendicular to the longitudinal CV. "

2. Linear – Figure 2.10 outlines the linear approach to CV determination. On the isochronal activation map a line was drawn from the stimulation point (*) through the most distant point on each isochrone in a direction away from the septum (Figure 2.10A). The CV, as derived from the incident velocity vectors, was plotted along the length of this line (Figure 2.10B(i)). Near to the bipolar stimulation point, the complex virtual electrodes produced prevent accurate determination of the velocity vectors. This leads to extremely variable and fast CV on the line-plot. At the distal regions edges of the line plot, intramural breakthrough again leads to artificially high and variable CV vectors. Between these points the plot had a low CV plateau which reflected the epicardial longitudinal CV. The longitudinal CV was taken along this plateau at a distance as close to 5mm from the

stimulus point as possible. Two lines were drawn perpendicular to this line (Figure 2.10A) and were used to assess the transverse CV in an identical manner (Figures 2.10 B (ii) & (iii)).

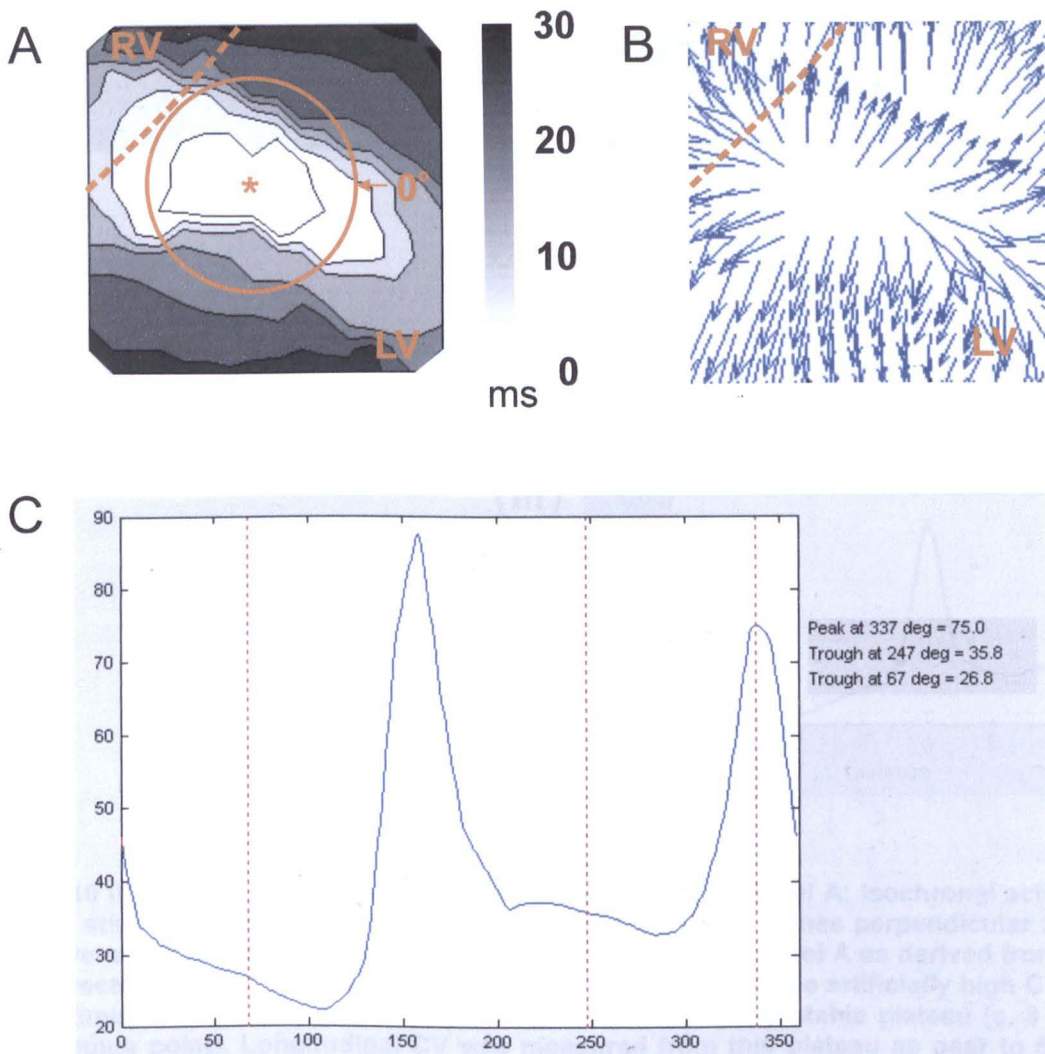


Figure 2.9 Illustrations of CV calculation from epicardial pacing and the radial approach to CV assessment. Panel A: Isochronal activation map with stimulation point (*) and circle of 5mm radius for radial CV assessment. The arrow indicates 0° on panel C. Panel B: Illustration of 2D velocity vectors derived from the activation times of Panel A as per (176, 176). Panel C: Plot of CV around the 5mm radius. 0° is indicated on panel A. The plot then works anticlockwise around the circle for a full revolution. The two peak CVs in this trace reflect the longitudinal velocities. The longitudinal CV was measured on activations travelling away from the RV/LV boundary (dotted red line at 337°). Transverse CV was calculated as the mean of the two CV values at the points perpendicular to the longitudinal CV (dotted red lines at 67° and 247°).

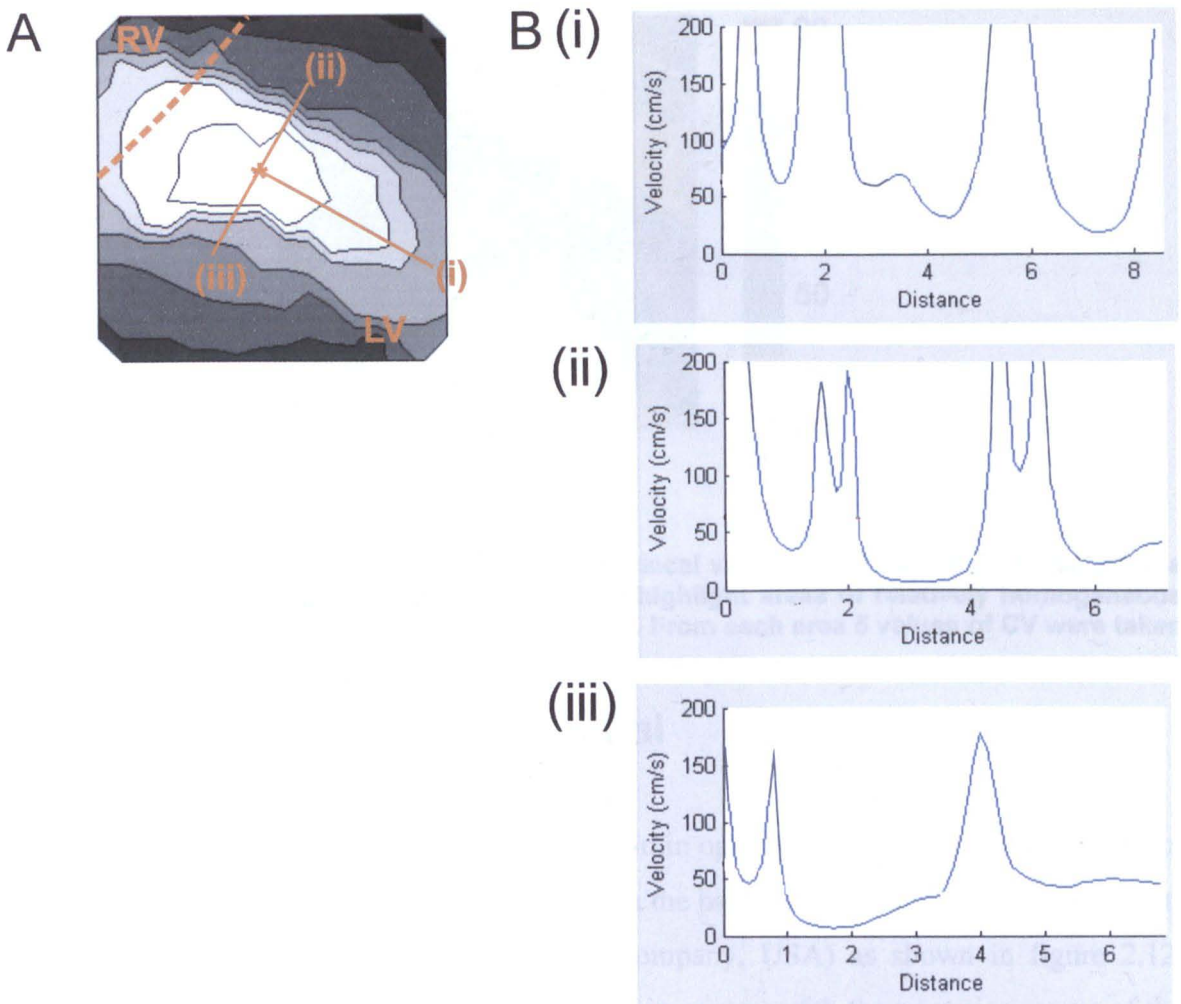


Figure 2.10 Illustration of linear approach to CV assessment. **Panel A:** Isochronal activation map with stimulation point (*), line for longitudinal CV (i), and 2 lines perpendicular (ii), (iii) for transverse CV. **Panel B:** Plots of velocity along the lines in panel A as derived from local velocity vectors (Figure 2.9B). (i) Longitudinal CV plot. Between the artificially high CV from pacing stimulus and intramural conduction there is a relatively stable plateau (c. 3 – 5cm from stimulus point). Longitudinal CV was measured from this plateau as near to 5cm as possible. (ii) & (iii) show the 2 linear velocity used to calculate transverse CV in an identical manner.

3. Point – Figure 2.11 displays the point CV approach to determining transverse CV. The local velocity vectors of figure 2.9B can be illustrated as a colour-coded map (Figure 2.11). This shows that there are 2 areas of more homogeneous CV along the same axes as the transverse CV. Five CV measurements were taken from each of the homogeneous areas, and the mean used as a further method to assess transverse CV.

Both radial and linear strategies were open to observer error in the selection of the stimulation point. In addition, the linear approach relied on the correct selection of the angle of incidence. Therefore the radial method produced more consistent longitudinal and transverse CV results, and was used in most situations.

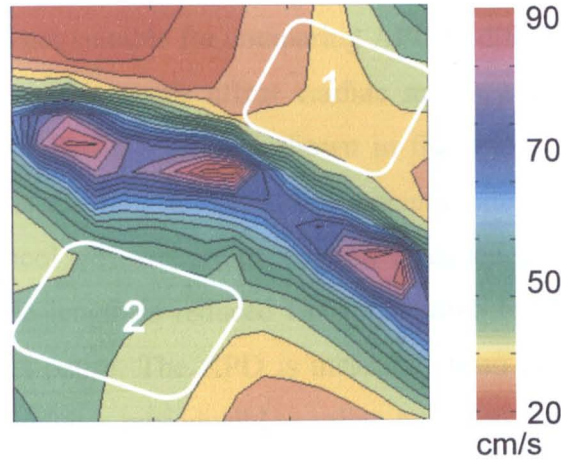


Figure 2.11 Point method for assessing CV. The local velocity vectors are represented in a colour-coded scale in this 2D maps. The boxes highlight areas of relatively homogeneous CV that are on the axes of transverse conduction. From each area 5 values of CV were taken and the average velocity calculated.

2.7 Monophasic action potential

The Langendorff-perfused hearts were placed within optical mapping Perspex chamber but in reversed antero-posterior orientation, and with the back-piston being replaced by a tight-fitting "Sylgard" silicone plastic disc (Dow Company, USA) as shown in figure 2.12. Through the 1mm hole in the "front-plate", now in contact with the posterior aspect of the heart, the RV was stimulated using a platinum bipolar electrode (Figure 2.12A). Two Franz contact electrodes were placed against the anterior surfaces of the LV and the RV respectively through tight punctures in the "Sylgard" disc (Figure 2.12B). Signals from the contact electrodes were amplified (custom built by Mark Watts, Glasgow Royal Infirmary), and subsequently digitalised at 1kHz (16bit) by a National Instruments data acquisition board (NI 6130E, National Instruments Inc., Tx, USA) within a PC. Signals were stored to disc for offline analysis.

2.7.1 MAP duration and restitution

APD restitution can be determined by 3 different methods: - (i) S_1S_2 protocol – a train of approx. 10 impulses at resting physiological cycle length, is followed by a single impulse at a shorter cycle length. This protocol is highly influenced by the cardiac memory of the physiological cycle length, and thus will not be influenced by the continuous adaptation to faster activations as occurs in VF (51, 178). (ii) Simulated VF – hearts are paced for 50 impulses with a randomly selected sequence of cycle lengths as observed in VF. At the end of the 50 impulses, a 300ms pause allows full repolarisation, so that APD can be measured.

This process is repeated 30 times to allow the plotting of a restitution curve (51) (Figure 2.13). This protocol is not suitable for comparing APD in different circumstances as a) the randomly selected pacing intervals affect cardiac memory differently, therefore giving variable APDs for a single DI as clearly shown in figure 2.13, and b) the time taken to perform the protocol is too long to assess the dynamic situation of low-flow ischaemia.

(iii) Steady state protocol – Hearts are paced with a sequence of 50 impulse salvos of set cycle length. The cycle length is reduced from one salvo to the next, and between each salvo there is a 500ms pause. The APD is measured from the last cycles at each cycle length. This protocol induces reproducible cardiac memory, and creates restitution slopes comparable to that of simulated VF (51). Therefore, in this thesis, steady state protocols were used to assess APD and restitution.

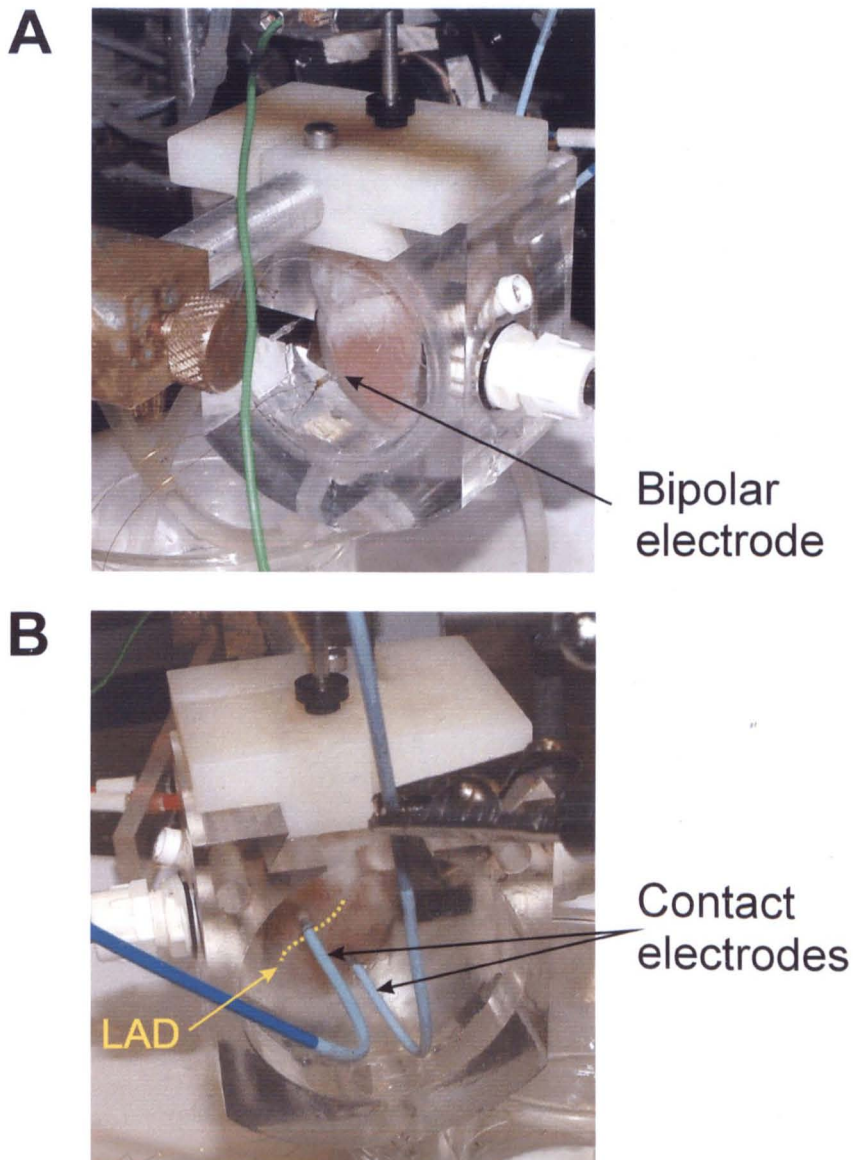


Figure 2.12 MAP recording. Panel A: Bipolar platinum electrode stimulating posterior aspect of RV. Panel B: Two Franz contact electrodes recording from the anterior aspect of the RV and LV. The LAD, indicated by yellow dotted line, guided the electrode placement.

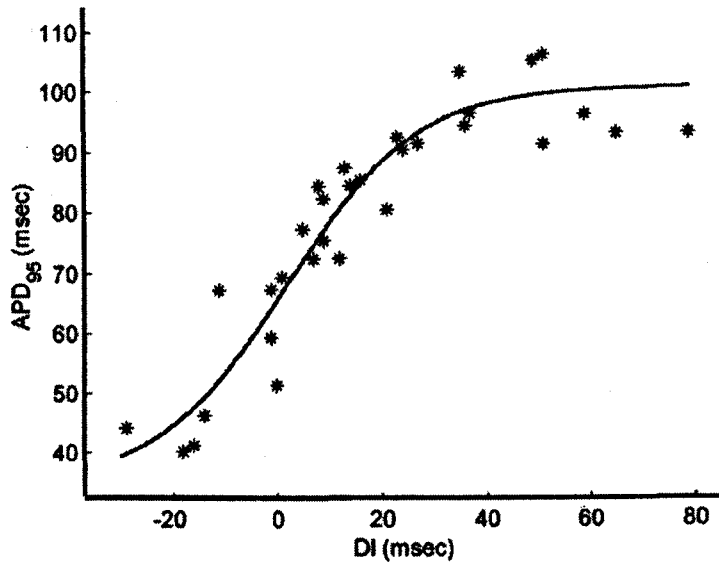


Figure 2.13 APD restitution as assessed by simulated VF. As the preceding DI is chosen randomly, the APD is variably affected by cardiac memory. This explains how a single DI can produce 2 different APD_{95} . (Adapted from (51, 51)).

APD was measured using locally developed software (Dr Francis Burton). The MAP upstroke was identified as the dV/dt_{max} and $MAPD_{50}$, $MAPD_{75}$ and $MAPD_{90}$ were calculated as shown in figure 2.14.

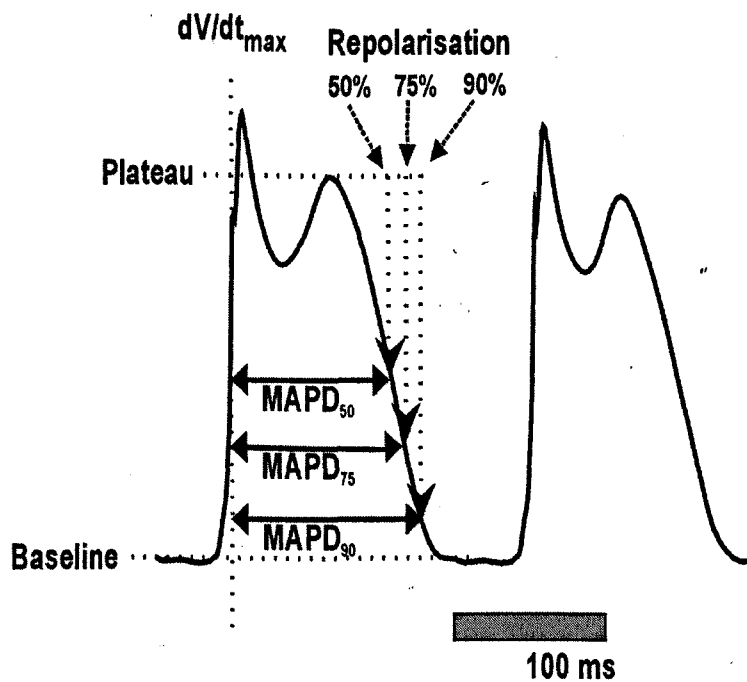


Figure 2.14 Assessment of MAPD. Activation point was identified as dV/dt_{max} . Repolarisation was assessed from MAP plateau with respect to Baseline. $MAPD_{50}$, $MAPD_{75}$ and $MAPD_{90}$ were measured as time from activation to 50%, 75% and 90% repolarisation.

2.7.2 Effective refractory period

Hearts were prepared as for MAP recording. To assess ERP, the ventricle was stimulated through one contact electrode, whilst recording capture through the other contact electrode (Figure 2.12B). Thus to assess LV ERP, stimuli were delivered through the electrode in contact with the LV, whilst the electrode in contact with the RV detected whether or not the stimulus had produced a propagating AP. The situation was reversed to assess RV ERP. The ERP was assessed using an S_1S_2 protocol, whereby the ERP was identified as the shortest S_2 interval that produced a propagating AP (Figure 2.15). All stimuli were delivered at twice the diastolic pacing threshold as assessed at basic cycle length (BCL) 300ms.

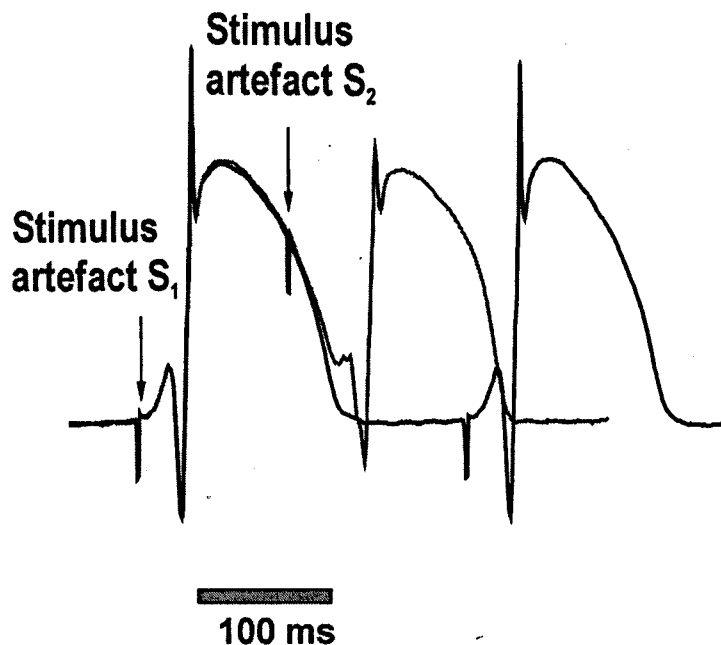


Figure 2.15 Illustration of S_1S_2 protocol to assess ERP. After 10 S_1 impulses at BCL = 300ms, a shorter S_2 was delivered. ERP was determined as the shortest S_2 to produce an action potential.

2.8 Floating microelectrode

Hearts were prepared for Langendorff perfusion, with the additional insertion of an intraventricular latex balloon within the LV. The balloons were placed whilst the heart was non-contractile in chilled Tyrode's solution. This ensured that no air entered into the coronary circulation. Balloons were inserted through a pulmonary vein, and then manoeuvred across the left atrium and mitral valve into the LV. Prior to microelectrode impalement the balloon was gently inflated to reduce contractile motion. Care was taken

not to over inflate the balloon and stretch the LV; the perfusion pressure was used as a guide to wall stretch.

Microelectrode experiments were performed within a Faraday cage. Hearts were placed within a chamber similar to that used for optical recording, but adapted for microelectrode impalement of the LV surface by boring a 0.5cm diameter hole in the Plexiglas front-plate. After placement of RV hook electrodes, the chamber was rotated by 90° to allow access to the anterior surface of the heart with vertical microelectrodes (Figure 2.16). Microelectrodes were pulled from borosilicate glass (WPI, Sarasota, FL) using a P-97 Flaming/Browning pipette puller (Sutter Instruments, Novato, CA). The microelectrodes were filled with 2M potassium chloride solution, before the tips were mounted onto silver chloride coated silver wire. The tips were secured in place, on the wire, by a drop of candle wax. The total resistance of the floating microelectrode was 20 – 25MΩ. Impalements of the LV epicardial surface were made under stereomicroscopic observation (Zeiss, Germany). Membrane potential signals were recorded via a Microprobe Model 750 (WPI, Sarasota, FL) with reference to a nearby silver chloride coated silver wire. Real-time signals were visualised both on oscilloscope (Nicolet Instrument Corporation, Wisconsin, USA), and on the computer monitor. Signals were digitalised at 1kHz (12bit) by a data acquisition board (DT2801 Data Translation Inc, MA, USA) and stored to disc. In 2 experiments, the raw analogue signals were recorded to VHS tape (VC-M23HM, Sharp electronic corp., NJ, USA) and digitised at 10kHz (12bit) through Digidata 1320 working with Clampex software (Axon Instruments Inc., CA, USA).

2.9 Statistical analysis

Throughout this thesis data are expressed as mean ± Standard Error of the Mean (SEM). Significance testing was performed using InStat3 (GraphPad Software Inc., USA). In VF, ANOVA was used to test the significance between VF protocols, and paired t-test was used to compare significancies between the ventricles of the same heart. Repeated ANOVA was used to assess changes in APD, ERP, dV/dt_{max} , pacing threshold and CV produced by low-flow ischaemia or hyperkalaemia, as these comparisons were made within the same heart under control and experimental condition.

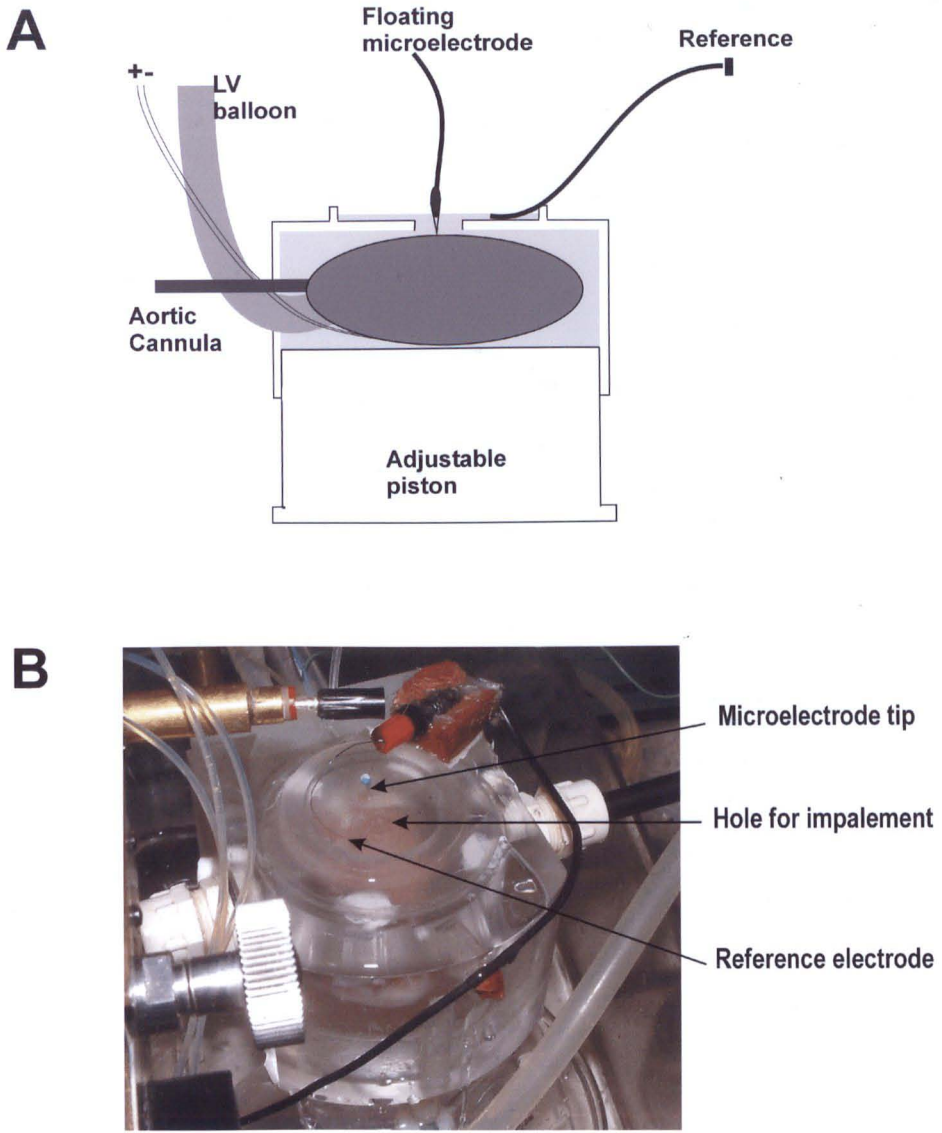


Figure 2.16 Microelectrode apparatus. Panel A: Illustration of microelectrode apparatus. Panel B: Photograph of heart within the chamber, and a microelectrode ready to impale.

3 VF frequency in ischaemia

3.1 Introduction

Previous work has shown that during VF, the changes of the ECG dominant frequency (DF) with time are determined by whether the heart is perfused or not. If the heart is fully perfused, the ECG DF is maintained (71, 73), whereas if the heart is not perfused, the ECG DF declines (22, 72, 73). The effect of intermediate levels of perfusion on ECG DF time-course has not been well characterised. *In situ* experiments have simply compared the ECG DF time-course in CPR supported animals to those with no CPR support (25). Similarly, isolated heart experiments have only examined a single low-flow perfusion rate along with full perfusion and no perfusion (73). Therefore, experiments were undertaken to observe the effect of intermediate perfusion on ECG DF time-course during VF in the isolated Langendorff-perfused rabbit heart.

In VF during full perfusion, spatiotemporal heterogeneity of the electrical activity has been described in the isolated guinea pig heart (63). In this study, optical mapping demonstrated that the LV DF increased with time, whilst RV DF remained unchanged. The purpose of the work described in this chapter was to determine the spatiotemporal organisation of VF during ischaemia. Prior to investigating the spatiotemporal organisation of VF during ischaemia using optical mapping, the model used in this thesis was validated by demonstrating identical heterogeneity during full perfusion to that reported in the literature (63).

3.2 Method

Animals were sacrificed and hearts Langendorff perfused as described in chapter 2.1. A pair of platinum hook electrodes was placed in the posterior aspect of the RV, well removed from the optical investigation area. After a period of stabilisation of approximately 20 minutes, hearts were loaded with 100 μ l RH237, and VF induced by burst pacing (50Hz for 8s). All hearts were perfused at 40ml/min for the first 60s of VF. During this interval, 4s epochs of ECG and optical recordings were taken every 30s. During control protocols, 40ml/min perfusion was maintained throughout. In experimental protocols, the perfusion rate was reduced at 60s to 10ml/min, 6ml/min, 4ml/min or 0ml/min. From 60s onwards, ECG recordings continued every 30s, whereas optical recordings were reduced to every 60s to prevent over-compression of the heart. After 600s, VF was terminated by defibrillation (Chapter 10). During experimental protocols, the epicardial temperature was maintained at 37°C by superfusing the chamber as follows.

Using the same water bath and Tyrode's solution, a second glass-column heat exchanger and Gilson pump continuously replenished the solution surrounding the heart via a port on the top-plate. To control for any confounding influence of degradation of the preparation, equal proportions of 1st and 2nd runs were performed for each protocol. It should also be noted that movement contaminated optical recordings in the initial experiments, and thus only the ECG data was analyzable. Chamber modifications removed this contaminant (Chapter 2.4).

As discussed fully in chapter 2.5.1, ECG and pixel signals were analysed in the frequency domain. FFT was used to create frequency power spectra, which allowed identification of the peak, or dominant frequency (DF), and the median frequency (MF). The power spectra of all 252 pixels were summated to create a global optical power spectrum, or pseudoECG (psECG) as it is commonly known (61, 173). Across the epicardial surface, during VF the spatiotemporal distribution of DF and MF was visualised by creating colour-coded maps. The colour scale of these maps, from blue-black (5Hz) through to pink-white (30Hz), represented the DF or MF in that pixel at that given time-point. As both DF and MF showed identical time-courses and spatiotemporal distributions, only DF results are presented.

A small series of non-perfused protocols was performed in hearts with chronic myocardial infarcts. Preparation and characteristics of this model are well described (179-181). In brief, adult male New Zealand White rabbits underwent a left thoracotomy under general anaesthesia. The marginal branch of the left circumflex coronary artery was ligated to produce an ischaemic area of 30 – 40 % of the LV. Animals were studied 8 weeks after coronary ligation.

3.2.1 Statistical analysis

Significance testing was performed using ANOVA of mean dominant frequency fractional change at 480s. P values are stated within the text.

Due to the variable location of the LV/RV boundary within the area of interrogation, mean ventricular frequencies were determined as the average DF from standardised squares of 3 × 3 pixels. Paired t-test was used for significance testing between ventricles of the same heart and ANOVA was used to make comparisons between protocols.

3.3 Results

3.3.1 ECG DF time-course with varied perfusion

As shown in figure 3.1, following VF induction the ECG DF increased during the 60s control period of all experiments. After 60s, in control protocols the ECG DF continued to increase, reaching a peak at 180 – 210s (fractional change = 1.36 ± 0.07 , $p < 0.001$ compared to baseline), before slightly slowing, and stabilising to values higher than those observed immediately post induction (fractional change = 1.23 ± 0.07 , $p < 0.05$ compared to baseline). In experimental protocols, perfusion rate reduction was associated with an immediate decrease in ECG DF. This ECG DF decline progressed until stabilising at a new slower DF steady state. This steady state was achieved by 480s (Figure 3.1). The initial rates of decline, and the steady state DF value, were dependent on the degree of perfusion reduction. The lower the perfusion rate, the quicker the ECG DF declined, and the lower the steady state value. Within this steady state period, all experimental ECG DFs were statistically different from control, but not from one other. Unperfused protocols were not included in this comparison, as none of the hearts remained in VF until the 480s analysis time-point.

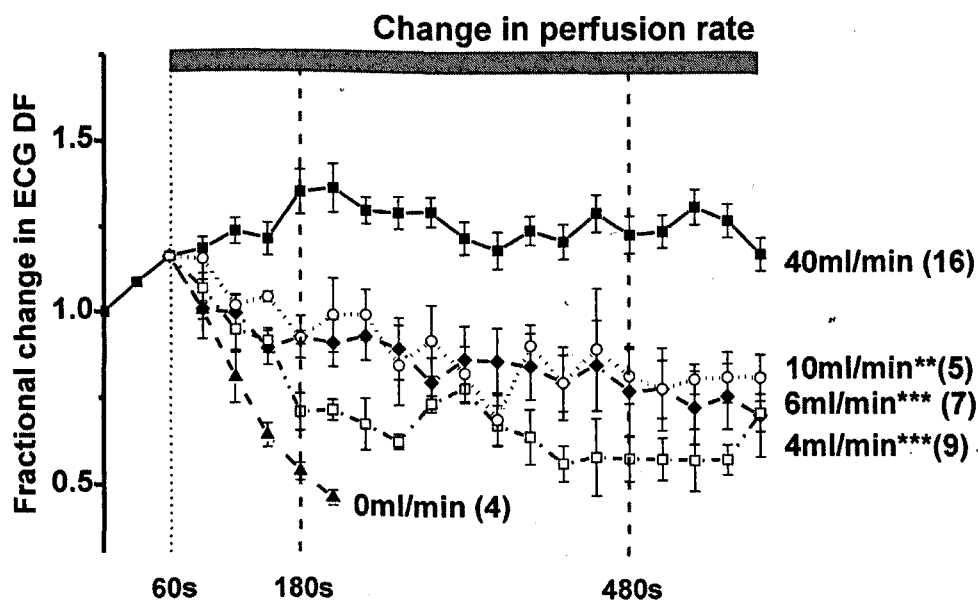


Figure 3.1 Time-course of ECG DF with varying perfusion rates as expressed by fractional change of starting DF. The mean starting DF was 13.2 ± 0.2 Hz. The number of protocols per perfusion rate is shown within parenthesis. During the first 60s, the DF of all preparations increased. During 40ml/min, this increase continued, reaching a peak at 180s, before slightly slowing and stabilising. On reduction of perfusion rate, the DF declined to reach a new steady state. The steady state value was dependant on the level of perfusion (** $p < 0.01$, *** $p < 0.001$ compared to 40ml/min fractional change at 480s).

On complete cessation of perfusion, VF spontaneously converted to a regular ventricular escape rhythm within 240s. During this total global ischaemia, the mean ECG DF immediately prior to conversion was $5.7 \pm 0.2\text{Hz}$. Commencing standard perfusion during this escape rhythm resulted in the return of sinus rhythm. During 4ml/min perfusion ($n = 9$), over 50% of protocols underwent such spontaneous conversion. During 6ml/min protocols, no such spontaneous conversion occurred. Thus 6ml/min was the lowest perfusion rate that consistently maintained VF for 600s in non-infarcted hearts.

Figure 3.2 shows that in the 8-week infarct model, complete cessation of perfusion was not associated with spontaneous conversion. In contrast, VF continued for 600s. In total global ischaemia, the ECG DF dropped to $4.3 \pm 0.4\text{Hz}$ in infarcted hearts. This was significantly lower than the ECG DF of $5.7 \pm 0.2\text{Hz}$ ($p < 0.05$) that occurred prior to conversion in non-infarcted hearts. In infarcted hearts, the optical signal amplitude from the infarcted tissue is greatly reduced (182). In her thesis, Walker compared the optical signal amplitude across the anterior surface of the infarcted heart. She showed that in the infarct zone the signal amplitude was at best only 30% of the amplitude of the optical signals from the non-infarcted tissue (182). This amplitude reduction increases the signal-to-noise ratio during VF, and therefore prevents reliable FFT interpretation from the infarct zone. The size of the infarct produced in this model is variable (181). In the four infarcted hearts used in this chapter the infarct was extensive. Thus there was insufficient non-infarcted LV tissue on the anterior heart surface to allow assessment of LV/RV heterogeneity.

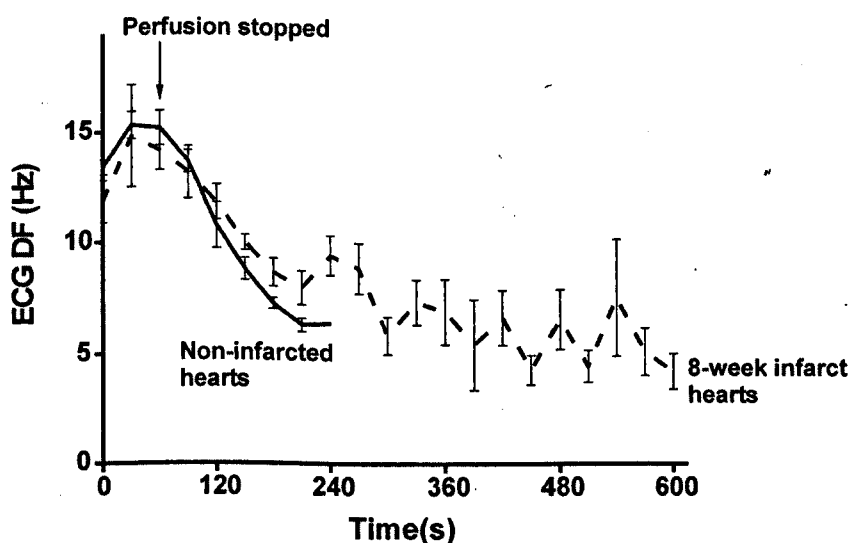


Figure 3.2 Time course of ECG DF in non-infarcted hearts ($n = 4$) and 8-week infarct model hearts ($n = 4$) during total global ischaemia. Spontaneous conversion occurred within 240s of perfusion cessation in stock hearts. The mean ECG DF immediately preceding conversion was $5.7 \pm 0.2\text{Hz}$. In contrast, in 8-week infarct model hearts, VF continued for 600s after perfusion cessation. The lowest mean ECG DF during this period was $4.3 \pm 0.4\text{Hz}$. This was significantly lower than the ECG DF at conversion in non-infarcted hearts ($p < 0.05$).

3.3.2 Optical measurements in VF during control and low-flow ischaemia

In VF, during control (40 ml/min) and low-flow ischaemia (6ml/min), the optical psECG DF displayed similar changes with time as observed in ECG recordings (Figure 3.3). However, the absolute DF values and fractional changes were slightly higher in the psECG compared to ECG in control, and consistently lower in psECG than ECG in low-flow ischaemia. This disparity is probably due to having a greater proportion of LV than RV within the flat anterior surface recording area (approx. 2:1) (see below). Better representation of the RV was impossible due to the curved nature of the epicardial surface.

As previously described for the ECG, there was an increase in psECG DF during the 60s control period immediately post VF induction. After 60s, in control experiments the psECG DF continued to increase to a peak at 280s (fractional change = 1.52 ± 0.14 , $p < 0.01$ compared to baseline), before stabilising at slightly lower values (fractional change = 1.27 ± 0.19 , $p = \text{NS}$ compared to 280s and baseline). In low-flow ischaemia, the reduction of flow to 6ml/min was associated with a steep decline in psECG DF. The psECG DF stabilised at a lower DF (fractional change = 0.50 ± 0.10 , $p < 0.001$ compared to baseline).

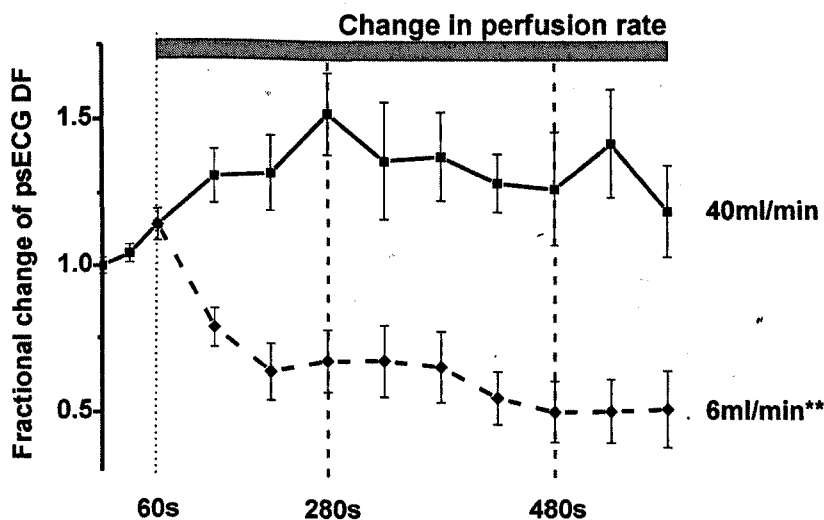


Figure 3.3 Time-course of psECG DF during control (40ml/min) and low-flow ischaemia (6ml/min), expressed as the fractional change of starting DF. The mean starting DF was $13.4 \pm 0.2\text{Hz}$, and 7 protocols were performed in each condition. During the first 60s, the psECG DF increased. In control experiments, this increase continued, reaching a peak at 280s, before slightly slowing and stabilising. In low-flow ischaemia, the psECG DF declined to a slower steady state DF (** $p < 0.001$ compared to control at 480s).

As clearly demonstrated in figure 3.4 and table 3.1, the spatial distribution of DF during VF was not homogeneous. DF heterogeneity developed in a progressive manner, and was well established by 480s. This corresponds to the steady state period observed in the ECG

and psECG DF time-courses. During control conditions, there was marked increase in the fractional DF of the LV to 1.62 ± 0.13 . This was significantly different from the RV ($p < 0.001$), where the fractional DF increased to 1.16 ± 0.04 . In VF during low-flow ischaemia, the DF changed in an opposite fashion (Figure 3.4 & Table 3.1). There was marked fractional DF reduction within the LV to 0.58 ± 0.08 . This was significantly different from the RV fractional DF ($p < 0.01$), which again remained unchanged at 0.94 ± 0.07 .

Dominant Frequency of VF (Hz)				
Site/Time	LV/0s	RV/0s	LV/480s	RV/480s
40ml/min (n = 7)	16.7 ± 1.4	13.4 ± 0.9	$26.1 \pm 1.9^{**}$	15.6 ± 1.3
6ml/min (n = 7)	15.2 ± 1.0	13.4 ± 0.9	$8.6 \pm 1.0^{**}$	12.3 ± 0.8

Table 3.1 Ventricular DF during control (40ml/min) and low-flow ischaemia (6ml/min). In both conditions LV DF changed significantly compared to starting frequencies (** $p < 0.01$). RV frequencies were unchanged.

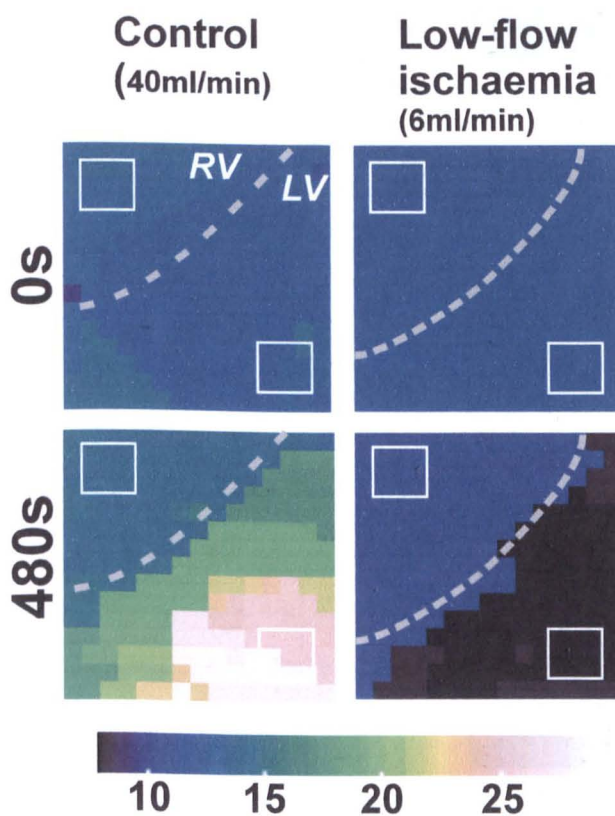


Figure 3.4 DF maps during VF in control (40ml/min) and low-flow ischaemic (6ml/min) conditions. The colour-coded maps display the DF in each pixel at the stated time-point. The dotted white line indicates the RV/LV boundary. The white squares indicate the standardised 3×3 regions from which the mean DF was derived. The maps demonstrate typical spatiotemporal organisation of DF at 0s and 480s during VF in control (40ml/min) and low-flow ischaemic (6ml/min) conditions. At 0s, all pixels displayed a similar DF of 12 – 14Hz. As VF progressed in control conditions, the LV DF increased. In contrast in VF during low-flow ischaemia the LV DF decreased. The RV DF remained relatively unchanged in both control and low-flow ischaemic conditions.

To verify the sharp transition of DF at the RV/LV boundary, and ensure no further heterogeneity more distant from the boundary, the LV and RV were optically mapped individually during control VF. In figure 3.5, the DF maps of the individual ventricles demonstrate that DF is relatively homogeneous within each ventricle. DF was compared between similarly spaced 3 x 3 pixel regions, but within the same ventricle (Figures 3.4 & 3.5). There was no significant difference in the fractional DF time-course between 2 regions within the same ventricle during control VF (LV, upper left 1.34 ± 0.07 , lower right 1.46 ± 0.1 ; RV, upper left 1.12 ± 0.07 , lower right 1.08 ± 0.01 , Figure 3.5). This indicates that the spatiotemporal heterogeneity of DF observed during VF in control and low-flow ischaemia occurs between the ventricles, and not within the LV or RV.

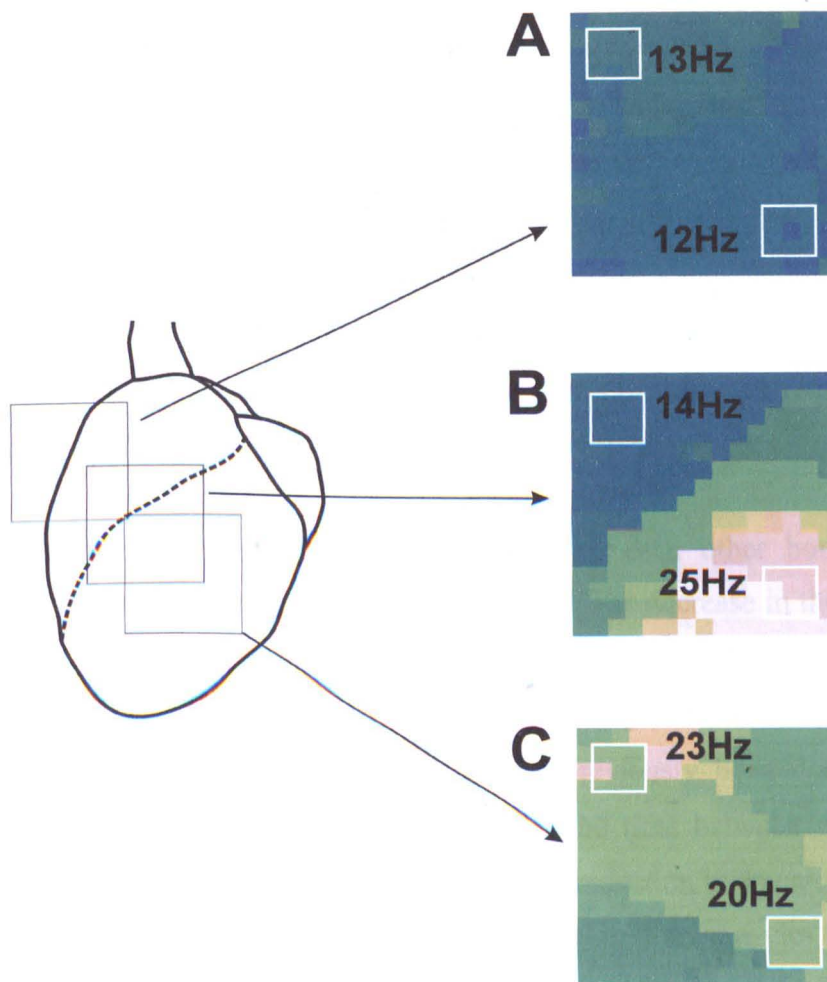


Figure 3.5 Investigation of the sharp transition of DF at the LV/RV boundary. Optical mapping was performed during control VF with the interrogation area placed in the LV or RV. The heart diagram illustrates the areas of interrogation with the arrows indicating the relevant DF map at 480s. The black dotted line indicates the RV/LV boundary, and the white squares the standardised 3 x 3 pixel regions used to derive the mean ventricular DF. Panel A: RV interrogation. Across the RV, the DF remained homogeneous at 12 – 13Hz. Panel B: Standard area of interrogation across the RV/LV boundary. This highlights the sharp transition in DF at the boundary. Panel C: LV interrogation. The DF was homogeneous across the LV at 20 – 25Hz. This confirms the sharp transition of DF at the RV/LV boundary, and the lack of further heterogeneity.

3.4 Discussion

3.4.1 Time-course of VF DF with varied perfusion

The dependence of the VF frequency time-course on myocardial perfusion is suggested by previous research in pigs (26, 28, 30). In these VF studies, CPR was combined with intravenous injections of saline, epinephrine or vasopressin, to produce varied degrees of peripheral vasoconstriction. More potent peripheral vasoconstriction diverted flow away from the peripheral circulation, thus giving better myocardial perfusion, and was associated with higher ECG MF. In the isolated Langendorff-perfused swine heart, the relationship between myocardial flow and VF frequency was confirmed (73). After an initial period where VF was not perfused, perfusion was commenced at either control flow rate or 10% of the control flow rate. At the end of non-perfusion period of VF, the ECG had a slow DF of 3.6 ± 1.4 Hz. On perfusing at the control rate, the ECG DF increased to 10.8 ± 1.1 Hz. However, commencing perfusion at 10% control rate the ECG DF only increased to 4.5 ± 1.1 Hz. The experiments in this chapter demonstrate that the relationship between myocardial perfusion and VF frequency holds for the Langendorff-perfused rabbit heart as well. These experiments show that lower myocardial perfusion rates produce more rapid declines in the ECG DF, and lower ECG DF at steady state.

The ECG and psECG DF time-courses were similar to each other both in control (40ml/min) and low-flow ischaemic (6ml/min) conditions. The decrease in the ECG DF in ischaemia reflects a reduction in global myocardial activation rate. In comparison, the decrease in the psECG DF reflects reduced activation in the epicardium alone. Reduced epicardial activation rates during ischaemic VF have previously been documented by electrical mapping (135). Here, as ischaemia evolved, the time between epicardial VF activations increased. Optical mapping has correlated this reduction in epicardial activation during ischaemic VF to slowing of the rotation of epicardial re-entrant cycles (62).

3.4.2 Spontaneous VF conversion in zero-flow ischaemia

The conversion of VF to a more regular rhythm during profound global ischaemia has previously been documented in rabbits (62, 72) and rats (101). Such spontaneous conversion is uncommon in larger animals, including humans. Theoretical explanations for this difference are (i) the need for a critical mass of myocardium to support VF and (ii) the different electrophysiological substrates of VF in clinical compared to experimental

settings. In the clinical setting, regional ischaemia and scarred infarcted tissue play a role in sustaining VF.

3.4.2.1 Critical Mass

For over a century it has been appreciated that large hearts sustain VF more readily than small hearts (99, 100). Garrey confirmed the need for a critical mass to maintain VF by sectioning ventricles from various animals (183). On shaving pieces of tissue from an already fibrillating ventricle, he noted that pieces less than 4cm^2 were unable to maintain VF. More recently, Zipes et al. demonstrated the same phenomenon in dog. Here the mass of excitable myocardium was reduced by bolusing 10ml of potassium chloride solution (1mEq/ml) down the relevant the coronary artery. Tissue perfused with this concentration of potassium chloride become depolarised, and thus are rendered unexcitable. Simultaneously perfusion of the left anterior descending (LAD) and the left circumflex arteries reduced the amount of excitable myocardium below the critical mass required for VF maintenance (103).

Computer modelling suggests that both "mother rotor" and "multiple wavelets" mechanisms of VF maintenance require a critical mass of excitable myocardium (102). For a "mother rotor" to be supported, the myocardium must be larger than its core size. In the case of multiple wavelets, an even greater mass is required for the break-up of the irregular wanderings of the numerous wavelets (102). During global ischaemia, the internal, non-excitable core of re-entrant cycles expands (Figure 1.6) (62). Thus the area required for each re-entrant cycle increases. Conversion occurs when the area required expands beyond the limits of the available tissue.

Although the heart failure model used this chapter is associated with increased ventricular size (wet heart weight infarct 13.0 ± 0.5 , sham 10.4 ± 0.3 from (180)), the increase is only 25%. If during global ischaemia, the re-entrant core enlargement occurred in a temporally linear fashion, one would predict that infarct hearts would spontaneously convert around 300s. Instead, there was no spontaneous conversion in infarcted hearts. Interpreting the ECG DF as an inverse marker for core enlargement (62), suggests that internal core expansion does not occur in a temporally linear fashion during total global ischaemia (Figure 3.2). However, comparing the reciprocals of ECG DF in a) non-infarct hearts prior to conversion ($1/5.7 = 0.18$) and b) the lowest DF in infarct hearts ($1/4.3 = 0.23$) indicates that the internal core enlarged approximately 36% more in infarcted hearts than non-infarcted hearts. This suggests that critical mass alone may not be the only factor

determining the lack of spontaneous conversion in 8-week infarct hearts in VF during total global ischaemia.

3.4.2.2 VF substrate

A second important factor in VF maintenance is the underlying electrophysiological substrate of the ventricle. Past research indicates roles for restitution and repolarisation heterogeneity in VF maintenance. Pharmacological interventions that flatten restitution curves, and thereby reduce heterogeneity, convert VF into VT (53, 54, 184). Ischaemia, with its similar effect on APD restitution curve (185), would also be expected to convert VF to VT as observed in non-infarcted hearts. Although ischaemic-driven flattening of APD restitution curve does not progress homogeneously throughout the heart (see Chapter 5 and (186)), this heterogeneity must not be sufficient to maintain wavebreak, and thus VF in the non-infarcted heart. Dispersion of repolarisation is increased in the 8-week infarct heart model as compared to the normal heart (187, 188). This could make the substrate sufficiently heterogeneous to maintain VF, even in the context of ischaemic flattening of restitution.

3.4.3 Spatiotemporal Organisation

Current literature describes 2 different patterns of spatiotemporal arrangement in perfused VF: - (i) apex-to-base distribution of DF (65, 189) and (ii) ventricular-based heterogeneity (63, 190).

3.4.3.1 Apex-to-base DF distribution

Using optical mapping in the guinea-pig heart, Choi et al. measured activation intervals and frequencies in perfused VF (65). They demonstrated that in apical region of the hearts, the APD was shorter, and was associated with shorter activation intervals and faster VF frequencies. In contrast, basally the APD was longer, and was associated with longer VF activation intervals and slower VF frequencies. The areas selected for this apex/base comparison were not specified in this paper. The area examined optically was on the anterior heart surface, and spanned the LV/RV border in a manner similar to this chapter (Figures 3.5B & 3.6A). This means that the apex area was predominantly LV, and the base predominantly RV. Indeed, the APD maps in this paper show the shortest APD (and thus presumably faster DF) to be in the LV, and the longest APD in the RV (Figure 3.6B). The paper goes on to perform circumferential VF mapping for a limited period, and localises

the slowest DF to posterior-RV. It is therefore possibility that any discrepancy between the findings of Choi et al. and this chapter are merely due to different definitions.

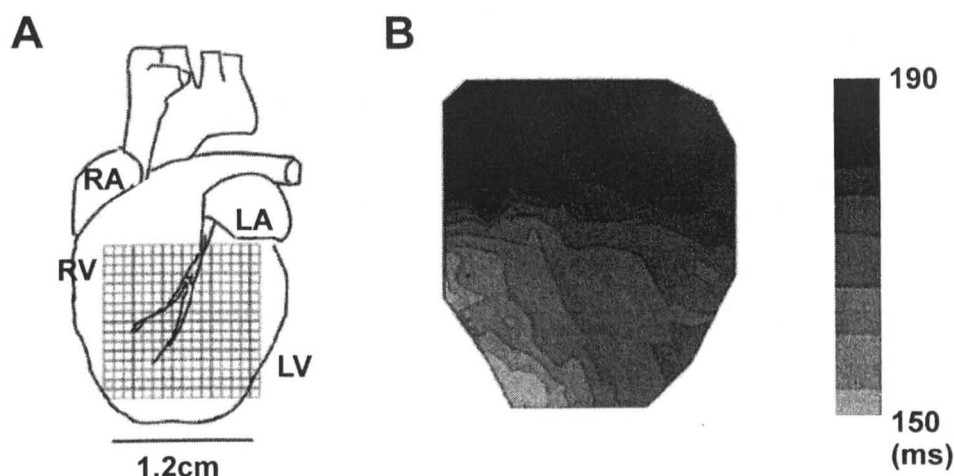


Figure 3.6 Apex-to-base repolarisation. Panel A: Area of interrogation on anterior surface of rabbit heart used by Choi et al. This area is identical to the standard region examined in this thesis (Figure 3.5B). **Panel B:** Isochronal map of APD across the anterior surface. The APD is shortest in the LV and longest in the RV. At the lower end of the septal zone interrogated there is a quick transition from short to long APD (Adapted from (65)).

A second paper that documents apex-to-base DF gradients uses Continuous Fourier Transform (CFT) to produce more precise DF maps (189). Using optical mapping in rabbits, Joel et al. studied the DF distribution generated by CFT compared to FFT. These higher definition maps show a gradient from apex-to-base in the LV, however, a sharp transition from LV to RV was still demonstrated. In this chapter, DF maps created using FFT showed no such gradient within either the LV or the RV, identifying instead a sharp transition between LV and RV DF.

3.4.3.2 Ventricular DF Heterogeneity

Ventricular heterogeneity in VF is well established (for review of this topic see (191)). Electrical mapping of VF shortly after induction revealed higher frequencies in the LV compared to the RV in both pig and dog (192, 193). Similarly in the guinea pig, optical mapping of VF during full perfusion demonstrated higher LV than RV frequencies, with a sharp transition between the 2 regions (63). Identical ventricular-based heterogeneity has been demonstrated in this chapter; LV frequencies dramatically increased in VF during full perfusion, whereas those of the RV were unchanged.

Investigating the underlying mechanism of this ventricular-based heterogeneity, Samie et al. demonstrated a larger outward background conductance in LV compared to RV myocytes (63). This larger outward conductance would be predicted to allow faster repolarisation, and thus the development of faster LV frequencies. Using low concentration barium chloride to selectively block I_{K1} , the enhanced outward background conductance has been attributed to the ventricular heterogeneity of Kir2.x expression (190). Here, Warren et al. demonstrated increased mRNA expression of Kir2.1 ($\times 1.97 \pm 0.45$) and Kir2.3 ($\times 1.47 \pm 0.08$) in LV compared to RV myocytes. They proceeded to demonstrate in the whole heart that I_{K1} blockade prevented the development of faster LV frequencies (190). While in single cells, I_{K1} blockade removed the differential magnitude of outward background current between the RV and LV myocytes (190).

A second mechanism proposed to underlie the spatiotemporal DF heterogeneity in fully perfused VF is the differential LV-to-RV response to osmotic swelling (158). In this study, the APD and DF distribution were assessed whilst perfusing isolated guinea-pig hearts with either iso-osmotic or hypotonic solutions. The iso-osmotic solution contained 5mM Glucose and 45mM Mannitol, whereas in the hypotonic solution, Mannitol was omitted. After 20 minutes of hypotonic perfusion, a sharp LV-to-RV transition was observed in (i) the APD during pacing, with a marked reduction in LV compared to RV APD and (ii) the epicardial DF during VF, with a marked increase in LV DF. During iso-osmolar perfusion a gradual apex-to-base gradient of APD and DF was observed, but with a definite LV-to-RV transition, albeit with a lower amplitude step. Choi et al. proposed that the source of this differential LV response to tonicity was the 27% greater expression of CIC-3 in LV compared to RV, as demonstrated by fluorescent antibody labelling. CIC-3 is one of several proteins responsible for producing $I_{CL,vol}$, a volume-regulated chloride current that become activated upon cell swelling (194). Activation of $I_{CL,vol}$ produces APD shortening and diastolic depolarisation, as its reversal potential (E_k) is -60 to -40mV (195, 196). Therefore, a greater relative magnitude of $I_{CL,vol}$ in the LV compared to the RV, would be expected to produce greater LV-to-RV APD shortening, and allow development of faster LV-to-RV DF. On blocking $I_{CL,vol}$ with 10 μ M indanyloxyacetic acid-94, Choi et al. demonstrated a reduction in the LV DF, however, the RV DF also decreased, and a sharp transition between LV/RV remained.

The activation of $I_{CL,vol}$ is unlikely to be an important factor in the heterogeneity demonstrated in this chapter as:- (i) the Tyrode's solution used contained 50mM Glucose, giving same tonicity as the iso-osmolar solution used by Choi et al. (Prof Guy Salama, Personal communication). (ii) The tonicity-induced alterations only developed after 20

minutes. It is possible that the increased metabolic demands of VF would result in greater cellular glucose extraction, thus rendering the solution hypotonic during VF. The DF heterogeneity in this chapter was fully established by 7 minutes, a time-point too early to be secondary to hypotonic alterations. (iii) Microelectrode impalement of the LV in VF during full perfusion with standard Tyrode's solution failed to demonstrate diastolic depolarisation (Chapter 9).

In this chapter, optical assessment of VF during low-flow ischaemia displays ventricular heterogeneity, where the LV DF markedly decreased, whilst the RV DF remained unaltered. Such maintenance of RV frequency in non-perfused VF has previously been implied (21, 22). Here, Carlisle et al. positioned a contact electrode onto the RV endocardial surface in dogs. Their results show that during globally ischaemic VF, the DF in the RV unipolar electrode was maintained, whilst the DF of the surface ECG decreased. A recent publication by Wu et al. describes an identical pattern of DF distribution to that demonstrated in this chapter, but in VF during global ischaemia rather than low-flow ischaemia (69).

The reduction in LV DF reflects decreased cellular activation rates in the LV compared to the RV during low-flow ischaemia. Theoretically, several electrophysiological mechanisms can produce a reduced activation rate, namely (i) prolongation in repolarisation (ii) prolongation of post-repolarisation refractoriness, (iii) reduced conduction velocity or (iv) raised activation threshold. A differential alteration of at least one of these electrophysiological mechanisms may account for the LV-to-RV DF heterogeneity during VF in low-flow ischaemia.

The differential LV-to-RV expression of Kir2.1 and Kir2.3 could underlie a heterogeneous electrophysiological response to low-flow ischaemia. However, LV-to-RV differences in the expression of other ion channels have been noted in a range of species (197, 198); these may also contribute to the ventricular differences in DF observed during VF.

Another possible explanation for any electrophysiological heterogeneity is differential perfusion of the LV compared to the RV. Studies in dogs (199) and rats (200) have shown differential control of vascular tone in the right and left coronary systems. In the dog, Quail demonstrated lesser degrees of vasodilatation in the left then right coronary systems by using increased aortic pressure to precipitate vasodilatation (199). It is thus possible that during low-flow ischaemia, there is a lesser degree of vasodilatation in the LV than the RV. One would expect such differential vasodilatation to result in more profound

ischaemia in the LV compared to the RV. Although this could account for the ventricular heterogeneity in low-flow ischaemia, it would not explain the similar pattern of DF distribution in total global ischaemia (69). Therefore, it is less likely that differential perfusion plays a predominant role

4 VF frequency & isolated ischaemic components

4.1 Introduction

It is clear that in VF, low-flow ischaemia produces a reduction in ECG and psECG DF. This decline in the global VF measurements is associated with a profound reduction in the LV DF. Ischaemia is a complex interaction of substrate depletions, metabolite accumulations and their sequelae. Although the outcome of prolonged ischaemic VF arrests is determined by such systemic sequelae as cytokine release and gut bacterial translocation, within the first 10 minutes the predominant influences are the local consequences of circulatory interruption: hypoxia, acidic pH_{EC} , raised $[K^+]_{EC}$ and energy substrate depletion (15). The influence of these individual ischaemic components on global and spatiotemporal DF progression during VF has not been clearly delineated. By altering the composition of the perfusing solution, it was possible to test the contribution of individual ischaemic components to the time-course of DF in low-flow ischaemia.

4.2 Methods

The protocols for VF induction, recordings and defibrillation were identical to those previously outlined in chapter 3.2. In all protocols, perfusion rate was maintained at 40ml/min. In control protocols, standard Tyrode's solution was perfused throughout. In experimental protocols, experimental solutions were introduced after 60s of VF. As shown by figure 4.1, there was a further 100s delay before this change reached 90% transition at the heart, due to the intervening tubing and bubble traps. The 90% transition time was determined through diluted black food colouring and spectrophotometry (Figure 4.1).

Standard Tyrode's solution was adapted to represent individual ischaemic components as discussed in chapter 1.2.3. All Douglas bags were prepared using a Penlon Gas Mixer (Abingdon, Berks) and solutions bubbled by Dymax 30 (Charles Austin pumps, Byfleet, Surrey). Experimental solutions were composed of: -

- Hypoxia – bubbling standard Tyrode's with 5% CO₂/95% N₂ Douglas bag mixture.
- Acidic pH_{EC} – pH 6.7 – bubbling standard Tyrode's with 20% CO₂/80% O₂ from a BOC mixed gas cylinder.
- pH 6.3 – bubbling standard Tyrode's with 20% CO₂/80% O₂ Douglas bag mixture.

Raised $[K^+]_{EC}$ – 8mM & 10mM

The isolated heart model employed relies on 50mM glucose to maintain osmotic pressure, and thereby reduce cellular swelling. Reduction of glucose to 20mM affected preparation integrity, and therefore data reliability. Introduction of Dextran 70 or albumin as osmotic substitutes did not improve preparation survival. Therefore further investigation into reduced energy substrate was abandoned. To control for any confounding influence of preparation degradation, equal proportions of 1st and 2nd runs were performed for each protocol.

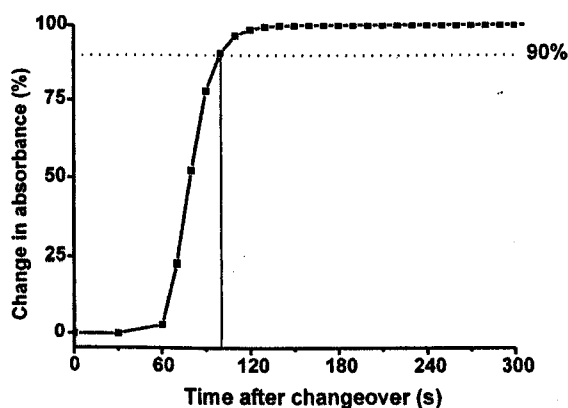


Figure 4.1 Solution transition time. This figure plots the change in the absorbance of aortic cannula effluent with time after switching clear solution to diluted black food-colouring solution. This demonstrates the delay in solution transition experienced by the heart.

As outlined in the chapter 2.5.2, ECG and pixel signals were analysed in the frequency domain using FFT. The frequency power spectra created allowed identification of the peak, or dominant frequency (DF), and the median frequency (MF). The power spectra of all 252 pixels were summated to create the global optical power spectrum, or psECG. Across the epicardial surface, the spatiotemporal arrangement of the DF and MF during VF was visualised by creating colour-coded maps. The colour scale of these maps represented the DF or MF in that pixel at that given time-point. As both DF and MF showed identical time-courses and spatiotemporal arrangements, only DF results are presented.

4.2.1 Statistical analysis

Significance testing was performed on the mean DF fractional changes at 480s using ANOVA. Due to the variable location of the LV/RV boundary within the area of interrogation, mean ventricular frequencies were determined as the average DF from standardised squares of 3×3 pixels (Figure 4.4). Paired t-test was used for significance

testing between ventricles of the same heart and ANOVA was used to make comparisons between protocols.

4.3 Results

4.3.1 Hypoxia

As shown in figure 4.2, the initial marked increase in ECG and psECG DF observed during VF in control conditions did not occur in VF during hypoxia. In control conditions, ECG DF peaked at 180 – 210s, with a fractional change of 1.31 ± 0.07 . For the same time-point, the ECG DF fractional change in hypoxic conditions was significantly different at 1.07 ± 0.02 ($p < 0.0001$). Similarly, in control conditions, the psECG DF fractional change reached a peak of 1.51 ± 0.14 at 240s, whilst the concurrent psECG DF fractional change in hypoxia was significantly lower at 1.08 ± 0.04 ($p < 0.0001$). Rather than a marked initial increase, there was a more gradual rise in the ECG and psECG DF during VF in hypoxic conditions. By the 480s assessment point, the ECG DF fractional change during hypoxia of 1.19 ± 0.12 was indistinguishable from the change of 1.23 ± 0.06 observed during control conditions (Figure 4.2(i)). Similarly, the psECG DF fractional change in hypoxia of 1.24 ± 0.10 was no different from the in control change of 1.26 ± 0.19 (Figure 4.2(ii)). In hypoxia, the ECG and psECG DF were significantly faster than frequencies observed in VF during low-flow ischaemia. In low-flow ischaemia, at the 480s assessment point, the ECG DF fractional change had dropped to 0.75 ± 0.13 ($p < 0.001$ compared to hypoxia, Figure 4.2(i)), whilst the psECG DF fractional change dropped to 0.50 ± 0.10 ($p < 0.01$ compared to hypoxia, Figure 4.2(ii)).

Assessment of the spatiotemporal VF organisation during hypoxia was hampered by the profound effect hypoxia had on signal amplitude (see Chapter 8). However, as shown in figure 4.4 and detailed in table 4.1, hypoxia had no significant effect on the DF spatiotemporal organisation compared to VF during control. By 480s, the RV DF fractional change had minimally increased to 1.18 ± 0.09 . This was not different from the RV DF fractional change in control conditions of 1.16 ± 0.04 . The LV DF fractional change markedly increased in hypoxia to 1.47 ± 0.23 at 480s. This was indistinguishable from LV DF fractional change increase of 1.62 ± 0.13 observed in control conditions, but was significantly different from the LV DF fractional change decrease of 0.58 ± 0.08 that occurred in VF during low-flow ischaemia ($p < 0.001$).

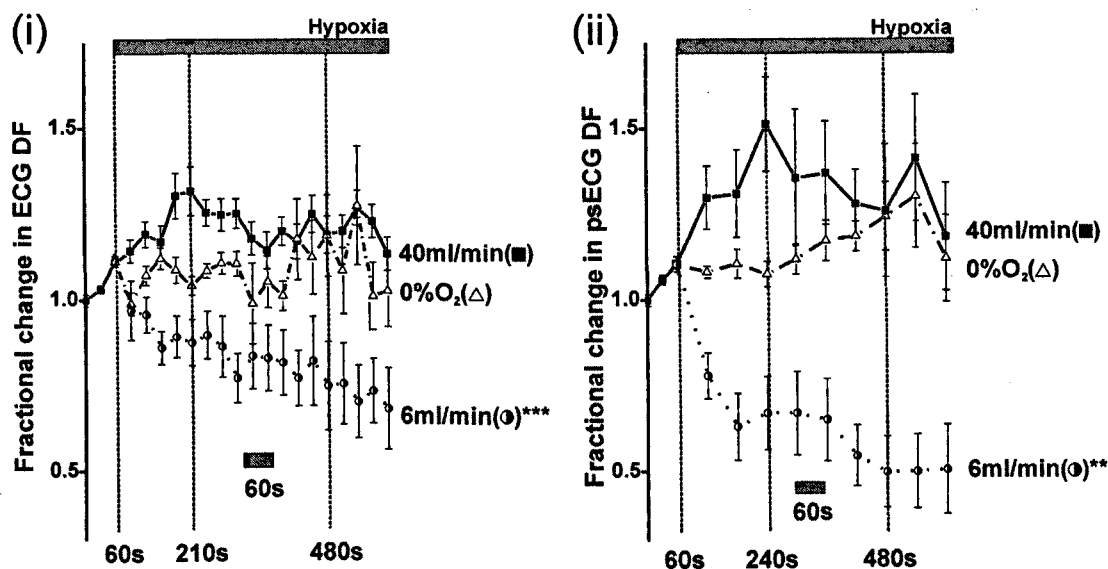


Figure 4.2 DF time-course during hypoxia compared to control (40ml/min) and low-flow ischaemia (6ml/min): - (i) ECG and (ii) psECG. At 480s, both global assessments showed no significant difference between DF in hypoxia compared to control. At 480s, both the ECG^{***} and psECG^{**} DFs were significantly faster than low-flow ischaemia (^{***} $p < 0.001$, ^{**} $p < 0.01$).

Dominant frequency of VF (Hz)				
Site/Time	LV/0s	RV/0s	LV/480s	RV/480s
40ml/min (n = 7)	16.7 ± 1.4	13.4 ± 0.9	26.1 ± 1.9 [§]	15.6 ± 1.3
Hypoxia (n = 5)	14.7 ± 1.0	12.4 ± 0.5	21.9 ± 1.0 [§]	14.7 ± 0.9
pH 6.7 (n = 7)	15.4 ± 1.3	13.5 ± 1.0	20.0 ± 1.2 [§]	17.8 ± 1.1
pH 6.3 (n = 4)	16.6 ± 1.0	12.6 ± 0.6	22.0 ± 2.4	16.7 ± 1.0
6ml/min (n = 7)	15.2 ± 1.0	13.4 ± 0.9	8.6 ± 1.0 [#]	12.3 ± 0.8
8mM K ⁺ (n = 5)	16.5 ± 1.9	13.0 ± 0.7	9.2 ± 1.0 [#]	12.5 ± 1.5
10mM K ⁺ (n = 4)	17.5 ± 1.5	14.7 ± 0.7	7.7 ± 1.4 [#]	7.7 ± 2.0 [~]

Table 4.1 Ventricular DF during VF in various individual ischaemic components compared to control and low-flow ischaemia. In hypoxia and pH 6.7, LV DF increased to levels indistinguishable from those in control conditions (40ml/min)[§], whereas raised [K]_{EC} produced LV DF lowering that was indistinguishable from low-flow ischaemia (6ml/min)[#]. In pH 6.3, LV DF was significantly lower than control ($p < 0.05$) but higher than low-flow ($p < 0.001$). RV DF was significantly reduced by 10mM [K]_{EC}[~] ($p < 0.001$). [#] and [§] mark LV DF that were not significantly different.

In summary, hypoxia did not reproduce the global or spatiotemporal DF alterations that were observed in VF during low-flow ischaemia.

4.3.2 Acidic pH_{EC}

In VF under acidic pH_{EC} conditions, the ECG and psECG DF demonstrated great variability in their early time-courses (Figure 4.3). All acidic pH_{EC} time-courses stabilised by the 480s assessment point. At 480s, in pH 6.7 the ECG DF fractional change rose by a factor of 1.19 ± 0.08 , and the psECG DF by 1.28 ± 0.06 . In pH 6.3, the ECG DF fractional change rose by a factor of 1.22 ± 0.04 , and the psECG by 1.30 ± 0.10 . These changes were

not significantly different from each other, or from those observed in the control pH 7.4, where ECG DF fractional change rose by 1.23 ± 0.06 , and psECG DF by 1.26 ± 0.19 . There was also no difference between the effects of acidic pH_{EC} and hypoxia on the global DF assessments during VF. In keeping with these findings, both severities of acidic pH_{EC} were associated with ECG and psECG DFs that were significantly higher than during low-flow ischaemia. In VF during low-flow ischaemia, the fractional change in ECG DF was 0.75 ± 0.13 ($p < 0.05$ compared to both levels acidic pH_{EC}), and the change in psECG DF was 0.50 ± 0.10 ($p < 0.001$ compared to pH 6.7, $p < 0.01$ compared pH 6.3).

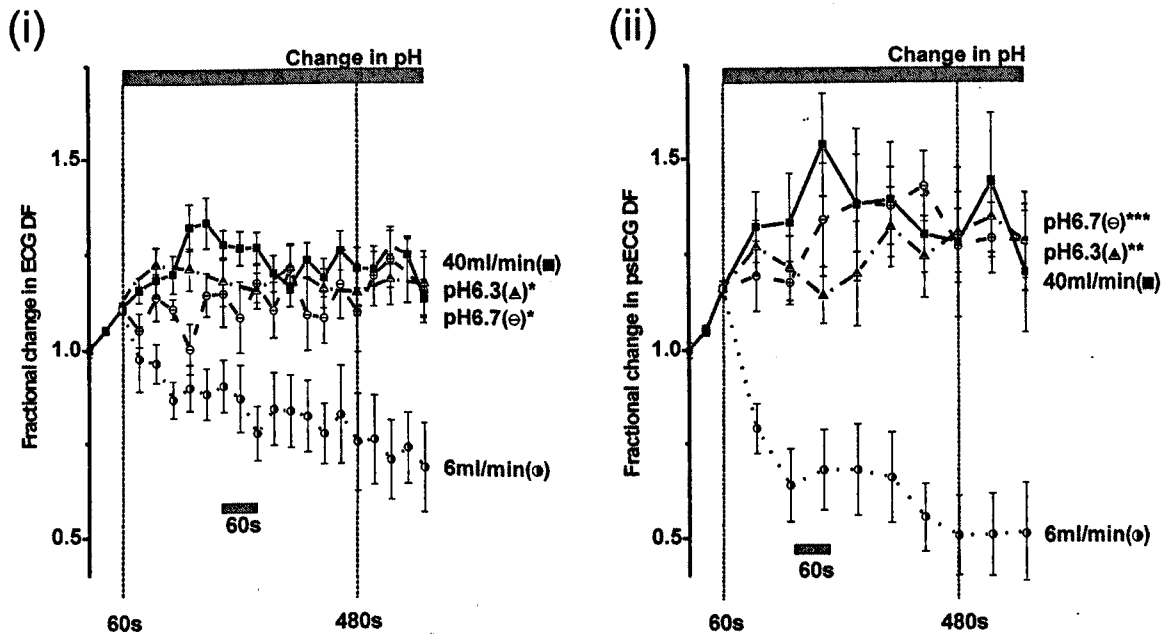


Figure 4.3 Time-courses of DF during VF with acidic pH_{EC} (pH 6.7 & pH 6.3) compared to control (pH 7.4, 40ml/min) and low-flow ischaemia (6ml/min): - (i) ECG DF – At 480s, neither pH 6.7 nor pH 6.3 were significantly altered the ECG DF compared control. Whereas at 480s, the ECG DF was significantly faster in both pH 6.7 and 6.3 than in low-flow ischaemia (* $p < 0.05$ compared to both levels of acidic pH_{EC}). (ii) psECG DF – Again at 480s neither acidic pH_{EC} significantly altered psECG DF compared to control. In both pH6.7^{***} and 6.3^{***} the psECG DF was significantly faster than in low-flow ischaemia (^{***} $p < 0.001$, $p < 0.01$).

In contrast to the global DF measurements, the spatiotemporal DF organisation during VF under acidic conditions was significantly different from both control and low-flow ischaemia (Figure 4.4, Table 4.1). Under acidic pH_{EC}, the LV DF tended to increase by a lesser degree than that observed in control (pH 7.4). In control, the LV DF fractional change increased to 1.62 ± 0.13 at 480s, whereas in pH 6.3, the LV DF fractional change increased to 1.32 ± 0.12 ($p < 0.05$). In pH 6.7, LV DF fractional change increase to 1.41 ± 0.07 was not significantly different from control. However these fractional changes were significantly different from the decrease in LV DF observed in low-flow ischaemia, where the LV DF decreased to 0.58 ± 0.08 ($p < 0.001$ compared to pH 6.7 & 6.3).

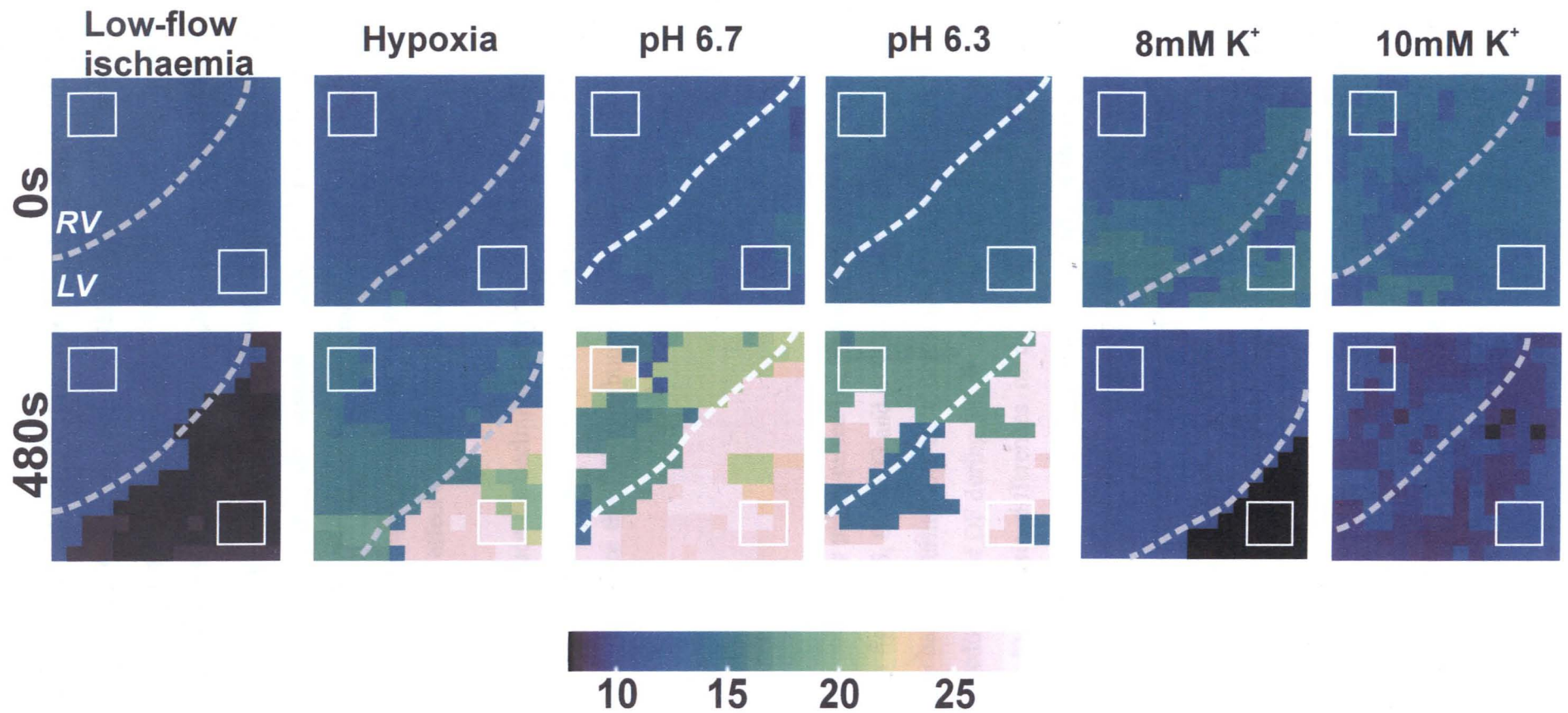


Figure 4.4 Typical DF maps during VF in low-flow ischaemia, raised $[K^+]_{EC}$, hypoxia and acidic pH_{EC} taken at 0s and 480s. Grey-dotted line illustrates RV/LV border and white squares the standardised 3×3 pixel areas used to derive mean ventricular DF. Colour scale represents DF in each pixel. Raised $[K^+]_{EC}$ reproduces changes of ischaemia whereas hypoxia and acidosis are more reminiscent of control conditions (Figure 3.4).

Also distinct from low-flow ischaemia and control, there was a tendency for RV DF to increase in acidic conditions (Figure 4.4, Table 4.1). At 480s, the RV DF remained unchanged in low-flow ischaemia with a fractional change of 0.94 ± 0.07 . In comparison, under acidic conditions the RV DF was significantly increased by a factor of 1.35 ± 0.06 in pH 6.7 ($p < 0.01$), and 1.33 ± 0.10 in pH 6.3 ($p < 0.05$). Although these RV DF increases under acidic pH_{EC} tended to be higher than the control change of 1.16 ± 0.04 , the difference did not reach significance. During acidic conditions, the LV DF tended to increase by more than the RV DF, but this difference was not significant (Table 4.1). Therefore acidic pH_{EC} had an equalising effect on the distribution of DF in VF.

In summary, acidic pH_{EC} did not reproduce the decline observed in global DF assessments in VF during low-flow ischaemia. Although acidic pH_{EC} affected the spatiotemporal organisation of VF, it did not reproduce the DF distribution observed during low-flow ischaemia.

4.3.3 Raised $[K^+]_{EC}$

In contrast to control, hypoxia and acidic pH_{EC} , raised $[K^+]_{EC}$ produced profound reduction of the ECG and psECG DF. In figure 4.5, the ECG and psECG DF in raised $[K^+]_{EC}$ clearly follow the corresponding DF changes during low-flow ischaemia. It should be noted that there was a time delay in the reduction of DF during VF in raised $[K^+]_{EC}$ compared to low-flow ischaemia. This relates to intrinsic differences in delay of application for each parameter. Reducing the perfusion to 6ml/min was immediately effective at the epicardial surface, whereas raising the solution $[K^+]_{EC}$ experienced the 90s transition delay as detailed in figure 4.1. By the 480s assessment point the ECG DF decreased fractionally to 0.76 ± 0.03 in 8mM $[K^+]_{EC}$, and 0.51 ± 0.09 in 10mM $[K^+]_{EC}$. These fractional changes could not be distinguished from that observed in low-flow ischaemia, where the ECG DF decreased to 0.75 ± 0.13 (Figure 4.5(i)). ECG DF fractional reductions in raised $[K^+]_{EC}$ were significantly different from:-

- (i) control conditions, where the DF increased by a factor of 1.23 ± 0.06 (vs. 8mM $[K^+]_{EC}$ $p < 0.01$, vs. 10mM $[K^+]_{EC}$ $p < 0.001$)

- (ii) hypoxia, where the DF increased by a factor of 1.19 ± 0.12 (vs. $8\text{mM } [K^+]_{EC}$ $p < 0.05$, vs. $10\text{mM } [K^+]_{EC}$ $p < 0.001$)
- (iii) pH 6.7, where ECG DF increased by a factor of 1.19 ± 0.08 (vs. $8\text{mM } [K^+]_{EC}$ $p < 0.05$, vs. $10\text{mM } [K^+]_{EC}$ $p < 0.001$)
- (iv) pH 6.3, where the ECG DF increased by a factor of 1.22 ± 0.04 (vs. $8\text{mM } [K^+]_{EC}$ $p < 0.05$, vs. $10\text{mM } [K^+]_{EC}$ $p < 0.001$).

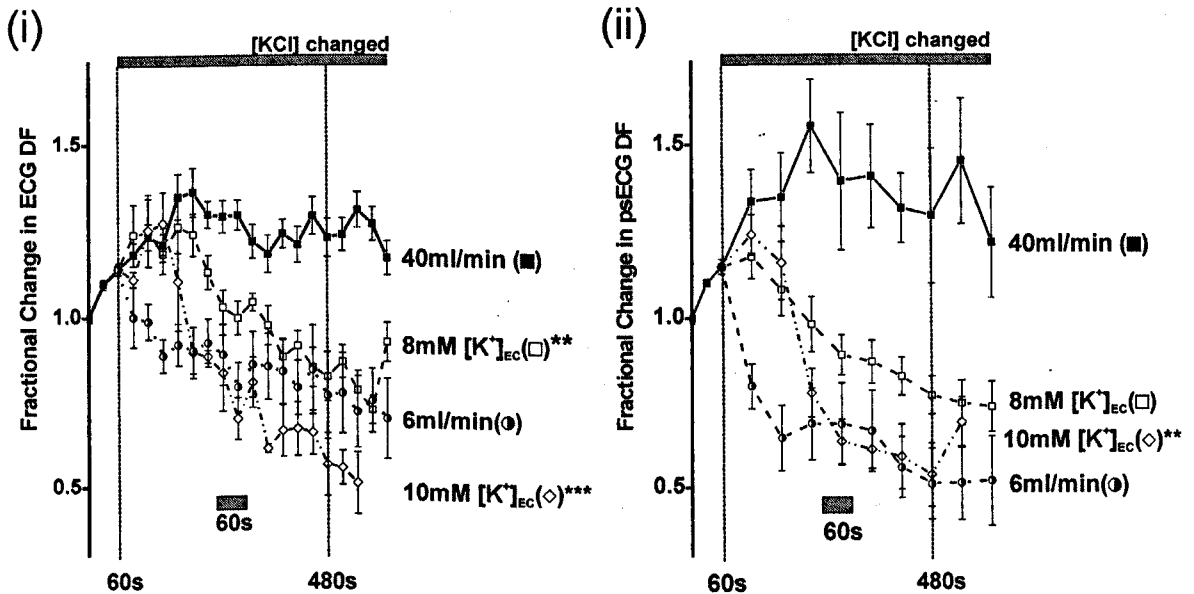


Figure 4.5 Time-course of ECG DF and psECG DF during VF in raised $[K^+]_{EC}$ (8mM and 10mM) compared to control (40ml/min) and low-flow ischaemia (6ml/min). (i) ECG DF – In both $8\text{mM } [K^+]_{EC}$ and $10\text{mM } [K^+]_{EC}$ the ECG DF was significantly reduced compared to control (** $p < 0.01$, *** $p < 0.001$). In contrast, the degree of ECG DF reduction could not be distinguished from that observed in VF during low-flow ischaemia. (ii) psECG DF – Although both 8mM and 10mM slowed the psECG DF compared to control, at 480s, only 10mM reached significance (** $p < 0.01$). The reduction of psECG DF produced by both $[K^+]_{EC}$ was indistinguishable from the psECG DF reduction that occurred during VF in low-flow ischaemia.

In raised $[K^+]_{EC}$, the psECG DF decreased fractionally to 0.73 ± 0.05 in $8\text{mM } [K^+]_{EC}$, and 0.50 ± 0.09 in $10\text{mM } [K^+]_{EC}$. These fractional changes were indistinguishable from each other, and from that observed in VF during low-flow ischaemia, where the psECG DF decreased to 0.50 ± 0.10 (Figure 4.5(i)). In $10\text{mM } [K^+]_{EC}$, psECG DF reduction was significantly different from control, where the DF fractional change increased to 1.26 ± 0.19 ($p < 0.001$). The psECG DF decrease in $10\text{mM } [K^+]_{EC}$ was also significantly different from (i) hypoxia, where the DF fractional change increased to 1.24 ± 0.10 ($p < 0.01$), (ii) pH 6.7, where psECG DF fractional change rose to 1.29 ± 0.10 ($p < 0.01$) and (iii) pH 6.3, where the psECG DF fractional change increased to 1.30 ± 0.10 ($p < 0.01$). In comparison,

the decrease in psECG DF in 8mM $[K^+]_{EC}$ was only significantly different from the increase observed during pH 6.3 ($p < 0.05$).

During perfusion with 10mM $[K^+]_{EC}$, all hearts spontaneously converted to a regular ventricular escape rhythm before 600s. Isolated protocols performed using higher KCl concentrations spontaneously converted at earlier time-points: 15mM $[K^+]_{EC}$ converted before 180s, while 12mM $[K^+]_{EC}$ converted at 300s.

The spatiotemporal organisation of VF in 8mM $[K^+]_{EC}$ was indistinguishable from that observed in 6ml/min low-flow ischaemia (Figure 4.4, Table 4.1). In 8mM $[K^+]_{EC}$, there was a marked fractional reduction in LV DF to 0.67 ± 0.04 . This was indistinguishable from the LV DF fractional reduction to 0.58 ± 0.08 observed during low-flow ischaemia. The RV DF was unchanged by perfusion 8mM $[K^+]_{EC}$ with a fractional change of 0.95 ± 0.03 at 480s. Again this was indistinguishable from the unchanging RV DF fractional change of 0.94 ± 0.07 observed in low-flow ischaemia. In 10mM $[K^+]_{EC}$, one protocol converted before 480s. Hearts still in VF at 480s in 10mM $[K^+]_{EC}$, showed equally marked DF slowing in the LV and RV. In the LV the DF fractional change of 0.46 ± 0.01 was indistinguishable from low-flow ischaemia, whereas in the RV, the DF fractional change was lowered to 0.53 ± 0.12 ($p < 0.01$ compared to RV fractional change in low-flow ischaemia).

At 480s, the fractional reduction in LV DF observed in 8mM $[K^+]_{EC}$ (0.67 ± 0.04) was significantly different from the fractional increase in LV DF observed under control conditions (1.62 ± 0.13 , $p < 0.001$). Similarly, the fractional reduction of LV DF produced by 10mM $[K^+]_{EC}$ (0.46 ± 0.01) was significantly different from control ($p < 0.001$).

In summary, perfusing VF with 8mM $[K^+]_{EC}$ solution reproduced the global and spatiotemporal DF alterations that were observed in VF during low-flow ischaemic conditions.

4.4 Discussion

This chapter demonstrates that the marked ECG and psECG DF reduction observed in VF during low-flow ischaemia is reproduced by raising $[K^+]_{EC}$, and not by imposing hypoxia or acidic pH_{EC} . Raising $[K^+]_{EC}$ to 8mM also reproduced the spatiotemporal DF

arrangement observed in low-flow ischaemia, with differential lowering of LV DF. Hypoxia and acidic pH_{EC} did not reproduce this spatiotemporal DF organisation.

4.4.1 Hypoxia

In VF during hypoxia, the global assessments of DF increased more gradually than in control. However, at steady state there was no significant difference between the two conditions. There was also no significant effect of hypoxia on VF spatiotemporal organisation compared to control conditions.

The first electrophysiological effects of hypoxia to develop is a profound and highly reproducible APD shortening (201-204). The exact cellular mechanism of this early APD shortening is unclear (205). Although the hypoxia-induced shortening can be blunted by increased glucose concentrations (206), and exaggerated by glycolytic inhibition (207), the ATP level only drops low enough to activate I_{KATP} after more prolonged periods of hypoxia than those examined in this chapter (208). The APD shortening associated with hypoxia would be predicted to increase the DF during VF. This was not observed.

Other electrophysiological adaptations to hypoxia, such as diastolic depolarisation, AP amplitude reduction and slowing of the upstroke velocity, are less consistently demonstrated in the literature. Most studies showed only minimal effects, or effects only after prolonged periods of hypoxia (202, 209, 210), whereas Morena et al. demonstrated profound, early changes (211). This variation appears to depend on the $[\text{K}^+]_{\text{EC}}$. In standard $[\text{K}^+]_{\text{EC}}$, diastolic potential and upstroke velocity are virtually unchanged by hypoxia (202-204, 209, 210). However in raised $[\text{K}^+]_{\text{EC}}$ hypoxia produced marked diastolic depolarisation, AP amplitude reduction and upstroke velocity slowing (203, 204). The relationship between hypoxia and $[\text{K}^+]_{\text{EC}}$ is bidirectional, with hypoxia producing a net efflux of K^+ (212). Thus, one may expect that more prominent changes were observed in experimental preparation that allowed K^+ accumulation, and that minimal changes would occur in preparations with continued perfusion. Therefore in the isolated Langendorff-perfused rabbit heart, one would predict only marginally greater K^+ accumulation in fully perfused, hypoxic VF than in control. This may explain the apparent lack of effect of hypoxia on DF demonstrated in this thesis.

4.4.2 Acidic pH_{EC}

Despite having virtually identical global DF assessments at steady state, the spatiotemporal DF organisation in VF under acidic pH_{EC} was significantly different from that observed in control. Compared to control conditions, there was a tendency for LV DF to be reduced, and RV DF to be increased. This qualitatively different effect of acidic pH_{EC} on the LV compared to the RV is difficult to explain.

Acidic pH has many effects on myocyte electrophysiology (213, 214) and on excitation-contraction coupling (215). Application of acidic pH produces a short-term reduction in calcium transient amplitude, which is then followed by increases to amplitudes greater than those observed at baseline (215). This adaptation of the Ca^{2+} transient to acidic pH is thought to result from complicated modulations of (i) L-type Ca channels, (ii) the ryanodine receptor (iii) the sarcoplasmic Ca^{2+} ATPase (SERCA) and (iv) the Na^+ - Ca^{2+} exchanger. It is possible that the profound effects of acidic pH on calcium dynamics influence voltage dynamics, and hence affects the DF in VF. At present, the interaction between voltage and calcium dynamics during VF is not well understood. Initial studies suggest that at VF induction, there is complete dissociation of voltage and calcium oscillations (216, 217).

Published data on the effect of acidic pH on electrophysiological properties are conflicting. For example, in one study, APD prolongation was more pronounced in respiratory than metabolic acidosis (220). In another study, there was marked APD prolongation in metabolic acidosis, but no prolongation in respiratory acidosis (218). Acidic-induced APD shortening has also been observed (219). It is possible that differential LV-to-RV APD alterations could underlie the effect of acidic pH on the spatiotemporal DF organisation in VF. For instance an LV APD prolongation and RV APD shortening could account for lowering of the LV DF whilst increasing the RV DF. To date there is no evidence of support this theory.

At the pH levels used in this chapter, acidosis has been shown to produce both diastolic depolarisation, and an associated reduction in the AP upstroke velocity (218, 220, 221). One would predict that diastolic depolarisation should bring the resting membrane potential closer to the AP activation threshold. However, acidosis also alters the voltage dependence of I_{Na} , such that the AP threshold shifts to more positive values. These pH dependent alterations do not occur in parallel, so that slight acidification decreases the gap between diastolic potential and AP threshold, whereas more profound acidification

increases the gap (213). If the LV and RV were to experience different degrees of metabolic stress during VF, then different levels of acidification could occur in the LV compared to the RV when both ventricles are being perfused at the same rate, with the same solution. If the LV experienced greater metabolic stress, this could result in more severe acidification of the LV compared to the RV. Such alterations could reduce the AP activation threshold in the RV, whilst increasing it in the LV, and thus explain the increased RV DF, and lowered LV DF compared to control. At present, there is no evidence of heterogeneity between the ventricles in the degree of metabolic stress experienced during VF.

Acidosis-induced diastolic depolarisation is thought to result from extracellular potassium accumulation (222). Such K^+ accumulation is thought to be secondary to I_{K1} inhibition. The relationship between I_{K1} and acidic pH is biphasic, with low-level acidification (pH 7.2 – 6.0) enhancing the current, whilst higher levels (pH 6.0 – 5.0) suppress it (219). In VF, the ongoing metabolic stress could produce acidification greater than that predicted by solution imposition alone. As described above, one could hypothesise that acidification would be more severe in the LV than the RV, with subsequent differential effects on I_{K1} . Indeed, acidic pH has also been shown to produce an initial hyperpolarisation prior to depolarisation in both respiratory (223) and metabolic acidosis (219). Another consideration is the possible ventricular heterogeneity of Kir2.x. The effect of such heterogeneity on such a complex relationship cannot be predicted.

As acidic pH did not reproduce spatiotemporal DF distribution of VF during low-flow ischaemia, investigation into these complex potential mechanisms was not pursued.

4.4.3 Raised $[K^+]_{EC}$

This chapter's demonstration of ECG DF slowing when $[K^+]_{EC}$ is raised is in keeping with research in the in situ canine heart (22). In this previous study, VF was induced by different methods, and the initial ECG DF recorded post induction. VF induction by intravenous potassium chloride infusion produced an initial ECG DF of 4.8 ± 0.8 Hz. This was significantly slower than the ECG DF on burst pacing induction of 9.9 ± 0.7 Hz. The study also suggested a less prominent effect of raised $[K^+]_{EC}$ on the RV. On VF induction by potassium chloride, an endocardial RV unipolar electrode displayed higher DFs immediately after initiation (8.3 ± 1.0 Hz) than the surface ECG (4.8 ± 0.8 Hz).

Similar results have been shown in the isolated guinea pig heart (224). Here Warren et al. induced VF by burst pacing, and perfused all preparation with 4mM $[K^+]_{EC}$ for the first 5 minutes. After 5 minutes, the perfusate $[K^+]$ was raised to 7mM or 10mM. On increasing the $[K^+]$ to 7mM, the LV DF fell from 21 ± 2 to 17 ± 3 Hz, whilst the RV DF rose from 13 ± 1 to 15 ± 1 . Switching from 4mM to 10mM resulted in maintenance of RV DF at 12 ± 1 , and reduction of LV DF from 16 ± 3 Hz to 14 ± 2 Hz. The results of Warren et al. are subtly different from those presenting in this chapter. Increasing $[K^+]$ to 8mM reduced the LV DF from ~ 16 Hz to ~ 9 Hz, whilst the RV DF remained unchanged at ~ 13 . On increasing $[K^+]$ to 10mM the both the LV and RV DF reduced to ~ 7.7 Hz. The subtle disparity of these could represent species differences, as different species demonstrate different cardiac repolarisation (for review of species repolarisation see (225)). Temporal differences may also explain the disparity; Warren et al. did not indicate the time of DF assessment (224). Biological variation, as suggested by the lack of similarity in LV DF in 4mM, may also have caused the disparity. More difficult to explain is why the different levels of increased $[K^+]$ concentrations had different effects on the DF heterogeneity in VF. As yet the cause for this remains unclear.

Warren et al. suggested that the LV-to-RV DF heterogeneity observed in raised $[K^+]_{EC}$ was a result of differential LV-to-RV expression of Kir2.x (224). Raising $[K^+]_{EC}$ is known to alter the conductivity of Kir2.x in a subtype-dependant manner. In raised $[K^+]_{EC}$, the outward current of Kir2.1 is increased, whilst the reversal potentials (E_k) of both Kir2.1 and Kir2.3 experience a rightward shift to less negative voltages (226). Such alterations in E_k result in diastolic depolarisation of the cell membrane in the presence of raised $[K^+]_{EC}$ (Chapter 9 & (202, 227)). Diastolic depolarisation is a classic consequence of ischaemia (140, 228), and has been directly linked to the local $[K^+]_{EC}$ (81). This highlights the key role of raised $[K^+]_{EC}$ in ischaemia, and suggests involvement of Kir2.x ventricular heterogeneity in the spatiotemporal organisation of ischaemic VF. With greater LV Kir2.x expression, one would predict that the diastolic depolarisation would be greater in the LV than the RV, assuming homogeneous ventricular milieu of all other channels. To date such preferential LV diastolic depolarisation has not been demonstrated.

Raised $[K]_{EC}$ will produce a rightward shift of E_k in all cardiac K^+ currents; namely I_{K_r} , I_{K_s} , $I_{K_{ATP}}$ and $I_{K_{to}}$. Heterogeneous expression of the channels responsible for these currents could also produce differential diastolic depolarisation. At present, there is a lack of research into the ventricular distribution of K^+ channels in the rabbit, including Kir channels. In dogs, $I_{K_{to}}$ and I_{K_s} are heterogeneous, with greater RV than LV current strength. Such heterogeneity should produce greater RV diastolic depolarisation in raised $[K^+]_{EC}$.

Also in dogs, I_{Kr} , I_{K1} and I_{KATP} have been shown to have equal LV-to-RV magnitude (229). Thus canine I_{K1} distribution is dissimilar to that observed in the guinea pig. Owing to such wide species variation, information about rabbit K^+ channel expression cannot be inferred from other species (review see (197)).

As with low-flow ischaemia, the isolated reduction in LV DF reflects decreased cellular activation rates in the LV compared to the RV in the presence of raised $[K^+]_{EC}$. Similarly, several electrophysiological mechanisms could be responsible for reducing the LV activation rate in this isolated fashion: - (i) differential LV-to-RV prolongation in repolarisation (ii) differential LV-to-RV prolongation of post-repolarisation refractoriness, (iii) differential LV-to-RV reduction in conduction velocity and (iv) differential LV-to-RV elevation of the AP activation threshold. These different mechanisms are explored in chapters 5 – 7.

5 Monophasic action potential duration and restitution in low-flow ischaemia & raised $[K^+]_{EC}$

5.1 Introduction

As previously demonstrated, in VF during low-flow ischaemia the ECG and psECG DF decreased with time (Chapter 3). This DF decline was reproduced by raising $[K^+]_{EC}$, and not by hypoxic or acidic conditions (Chapter 4). Optical mapping showed that the decrease in DF was heterogeneous, with a marked decrease in the LV DF, whilst the RV DF remained unchanged. This reduction in DF reflects decreased activation rates in the LV compared to the RV. Theoretically, several electrophysiological mechanisms can decrease activation rates: - (i) prolonged repolarisation; (ii) prolonged post-repolarisation refractoriness; (iii) raised activation threshold and (iv) reduced conduction velocity. This chapter documents the investigations into the first of these potential mechanisms, prolonged repolarisation. To account for the differential slowing of LV DF, but not RV DF, would require differential prolongation of repolarisation in the LV compared to the RV. Thus the LV APD would be longer than the RV APD. Although previous research documents APD shortening in ischaemia and raised $[K^+]_{EC}$ (230), a relative difference in LV-to-RV repolarisation time may still contribute to the differential LV DF slowing.

5.2 Methods

As described in chapter 2.7, Langendorff-perfused hearts were positioned in a chamber adapted to allow epicardial pacing of the posterior RV surface with a bipolar electrode. Simultaneous RV and LV MAPs were recorded using two Franz contact electrodes placed against the RV and LV anterior epicardial surfaces. As discussed in chapter 2.7, APD restitution can be assessed by several methods. In this chapter, the APD restitution was assessed using a steady state protocol, with the APD being measured from the last 5 activations of 50 paced beats salvos (51). The pacing stimulus strength was set at twice the diastolic threshold as assessed at a Basic Cycle Length (BCL) 300ms. Using this stimulus strength, salvos of BCL 250, 200, 175, and 150ms were applied. Beyond this, the BCL was decreased by 10ms until 130ms, and then by 5ms until loss of 1:1 capture. This protocol was performed in control conditions (5mM $[K^+]_{EC}$, 40ml/min perfusion rate) before the imposition of experimental conditions. Experimental conditions consisted of (i) flow rate reduction to 6ml/min (low-flow ischaemia) (n = 6), (ii) Tyrode's solution containing 8mM $[K^+]$ (n = 5) or (iii) Tyrode's containing 10mM $[K^+]$ (n = 4). The restitution protocol was repeated at 6 minutes (360s) and 10 minutes (600s) after the imposition of experimental conditions.

Using locally developed software, the activation point was identified as the maximal rate of depolarisation (dV/dt_{max}) on the MAP upstroke. $MAPD_{90}$ was calculated as time from the activation point to 90% repolarisation (Figure 5.1) (231). Restitution curves were plotted against BCL (51, 232) and Diastolic Interval (DI) (51, 52, 233). As the curves remained approximately parallel, comparisons between conditions and ventricles were made at BCL 300ms, 150ms and 125ms, and between the fractional changes of $MAPD_{90}$ at BCL 300ms. The significance was tested by repeated ANOVA.

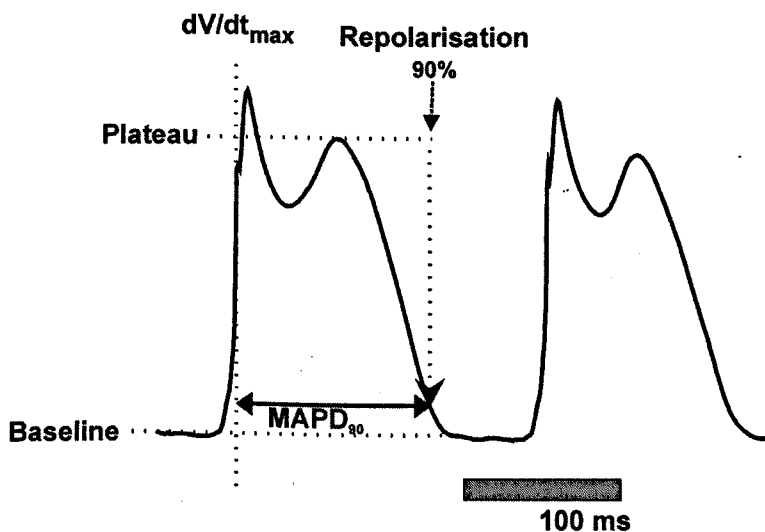


Figure 5.1 Assessment of $MAPD_{90}$. Activation point was identified as dV/dt_{max} . The percentage repolarisation was assessed from MAP plateau with respect to baseline. $MAPD_{90}$ was measured as the time from activation to 90% repolarisation.

5.3 Results

5.3.1 40ml/min vs. 6ml/min

Figure 5.2 demonstrates that pacing at BCL $<130ms$ produced alternate-beat APD variation in both ventricles under control conditions. This phenomenon, known as alternans, created zig-zagging of the curve at short DI in the plot of $MAPD_{90}$ vs. DI as seen in figures 5.3A(i) & B(i). Such zig-zagging can be eliminated by plotting scattergrams of APD vs. DI, and subsequently fitting to $y = y_0 + Ae^{(x-x_0)/t}$ using Origin (Originlab Corporation, MA, USA) (Figures 5.3A(ii) & B(ii)) (234).

At longer DIs, there was great variation between the hearts, such that RV $MAPD_{90}$ could be longer than LV $MAPD_{90}$ or shorter as in the experiments illustrated in figure 5.3. At shorter DIs, the curves overlapped in all experiments. Shorter DIs are more in keeping with the faster activation rates that occur in VF. The exact DIs produced by the pacing protocol

differed between experiments. Therefore the summary results from all 6 experiments were plotted against BCL (Figure 5.4A). This showed that in control conditions, the LV and RV APD restitution curves were not significantly different. In keeping with this, at BCL 300ms the LV MAPD₉₀ of 132 ± 3 ms was not different from the RV MAPD₉₀ of 133 ± 3 ms (Figure 5.5A), at BCL 150ms the LV MAPD₉₀ of 101 ± 4 ms was no different from the RV MAPD₉₀ of RV of 105 ± 4 ms (Figure 5.5B), and at BCL 125ms both LV and RV MAPD₉₀ were 89 ± 4 ms.

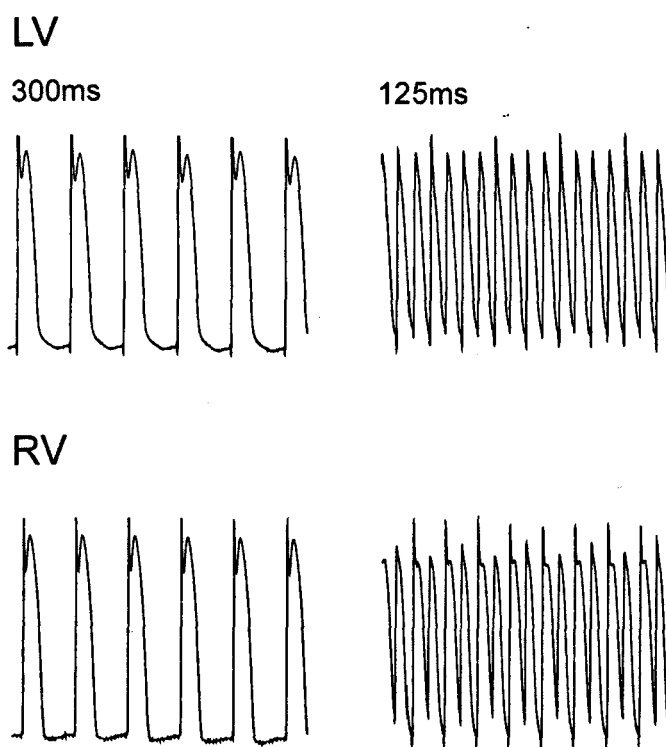


Figure 5.2 MAP recordings from the anterior epicardial surface of the LV and RV. Pacing at BCL <130ms resulted in alternate-beat APD variation (alternans) in both ventricles. Illustrated are recordings of RV & LV at BCL 300ms & 125ms.

After 6 minutes of low-flow ischaemia (6ml/min), the stimuli failed to capture 1:1 at BCL shorter than 150ms. In some experiments, the RV restitution curve shifted upwards to longer APD for a given DI, and the LV restitution curve to shift downwards to shorter APD for a given DI (Figure 5.3A). However, in other experiments both the LV and RV APD were prolonged, and in 1 of the 6 experiments was the LV APD was more prolonged than the RV (Figure 5.3B). With this considerable variation in the degree of shifting, the mean LV and RV restitution curves after 6 minutes of low-flow ischaemia were not significantly different from each other, and were not significantly different from control restitution curve (Figure 5.4A). In keeping with this, at BCL 300ms after 6 minutes of low-flow ischaemia, the LV MAPD₉₀ of 136 ± 11 ms was not significantly different from the

RV MAPD_{90} of $133 \pm 13\text{ms}$. As shown in figure 5.5A, neither of these MAPD_{90} were different from the control LV MAPD_{90} of $132 \pm 3\text{ms}$ or RV MAPD_{90} of $133 \pm 3\text{ms}$ at BCL 300ms. Similarly, figure 5.5B shows that at BCL 150ms there was no difference between the LV MAPD_{90} of $93 \pm 4\text{ms}$ and the RV MAPD_{90} of $95 \pm 10\text{ms}$ in low-flow ischaemia or with the control LV MAPD_{90} of $101 \pm 4\text{ms}$ and RV of $105 \pm 4\text{ms}$.

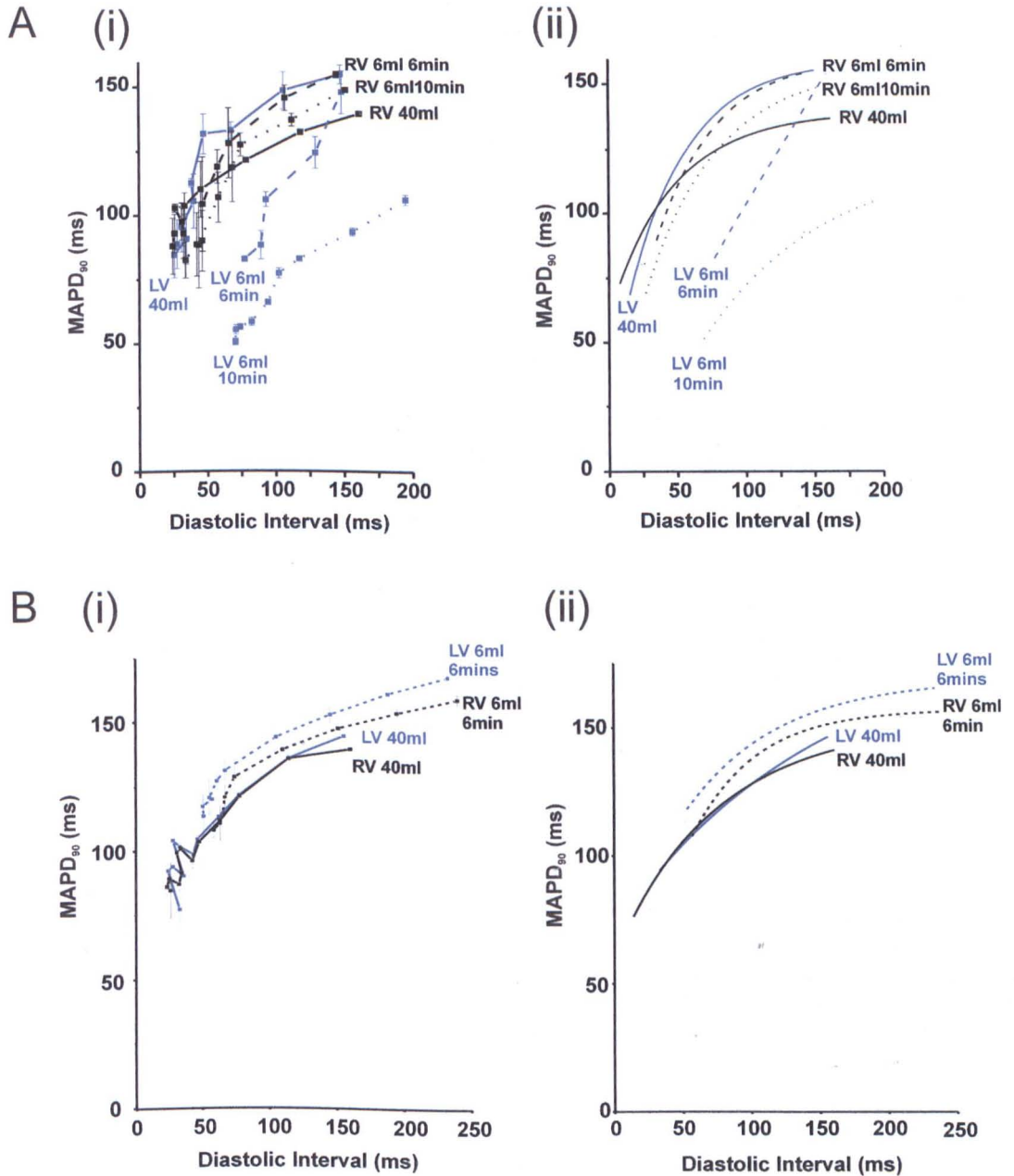


Figure 5.3 MAPD_{90} restitution curves during low-flow ischaemia. There was great variation between experiments. Panel A: Result from one experiment where RV APD prolonged in ischaemia and LV APD shortened (i) Mean MAPD_{90} of last 5 beats plotted against mean DI for those last 5 beats. This results in a zig-zag pattern at lower DI. (ii) 1st order exponential fits from scatter plots of the same experiment. Both plots show progressive reduction of LV MAPD_{90} with low-flow ischaemia. RV MAPD_{90} was prolonged especially at longer DI. Prolongation was longer at 6 minutes than 10 minutes in this experiment. Panel B: Experiment where both RV and LV were prolonged with LV more prolonged than RV. (i) Mean MAPD_{90} of last 5 beats. (ii) 1st order exponential fit of from scatter plots of the same experiment.

In the experiment illustrated in Figure 5.3A after 10 minutes of low-flow ischaemia, the RV restitution curve returned towards control values, whereas the LV curve shifted to even shorter values. This pattern was extremely variable between hearts. Thus plotting the mean LV and RV restitution produced overlapping curves (Figure 5.4A). Again in keeping with this at BCL 300ms, the LV MAPD₉₀ of 131 ± 10 ms was not different from the RV MAPD₉₀ of 136 ± 5 ms (Figure 5.5A), and at BCL 150ms the LV MAPD₉₀ of 94 ± 1 ms was not different from the RV MAPD₉₀ of 92 ± 10 ms (Figure 5.5B).

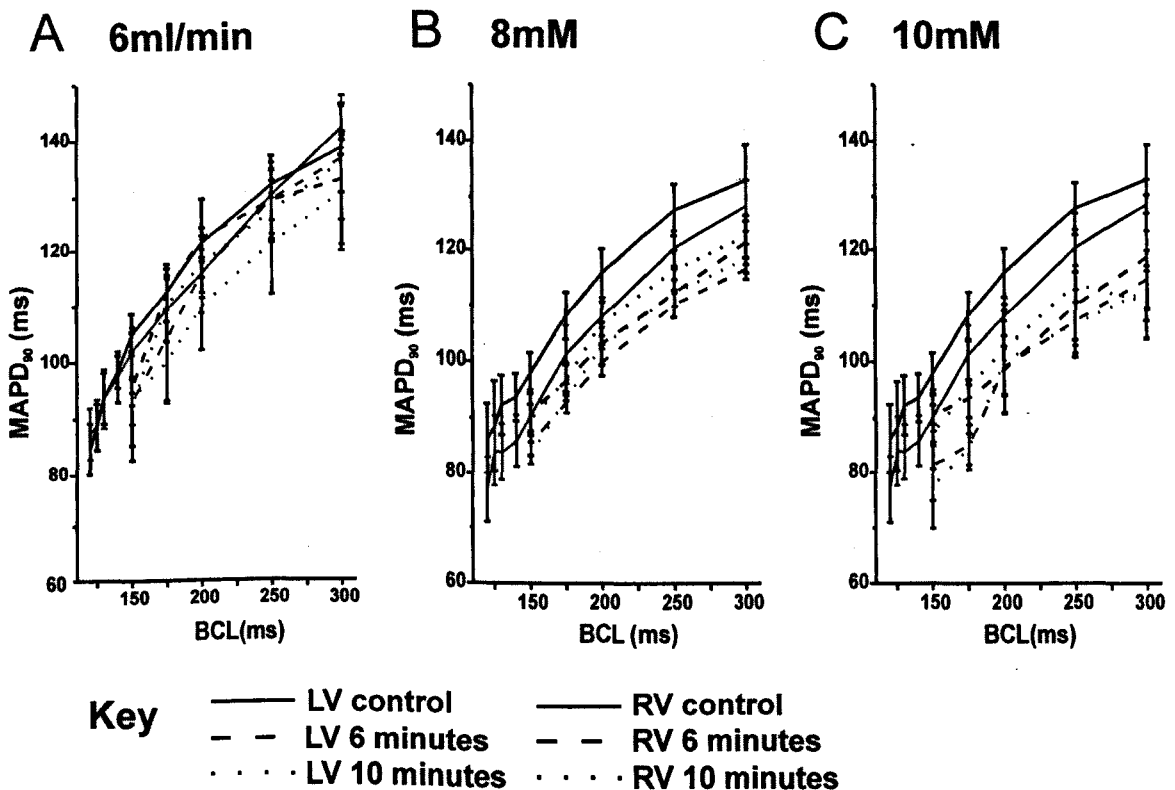


Figure 5.4 Mean MAPD₉₀ restitution plots. Panel A: MAPD₉₀ restitution in low-flow ischaemia (6ml/min) compared to control. Although there was progressive shortening of LV MAPD₉₀, this did not reach significance. Mean RV APD did not change. Panel B: MAPD₉₀ restitution in 8mM [K⁺] solution compared to control. Mean LV and RV APD progressively shortened to reach significant levels. Panel C: MAPD₉₀ restitution in 10mM [K⁺] solution compared to control. As with 8mM, 10mM [K⁺]_{EC} showed progressive and significant shortening in both ventricles.

The percentage changes in MAPD₉₀ were examined. This showed that after 10 minutes of low-flow ischaemia at BCL 300ms the LV MAPD₉₀ was unchanged at $90\% \pm 9\%$, and the RV MAPD₉₀ was unchanged at $100\% \pm 13\%$. At BCL 150ms both LV and RV MAPD₉₀ were unchanged at $97 \pm 6\%$. This suggests that differential prolongation of repolarisation in the LV compared to the RV was not the mechanism underlying reduced LV DF in low-flow ischaemia.

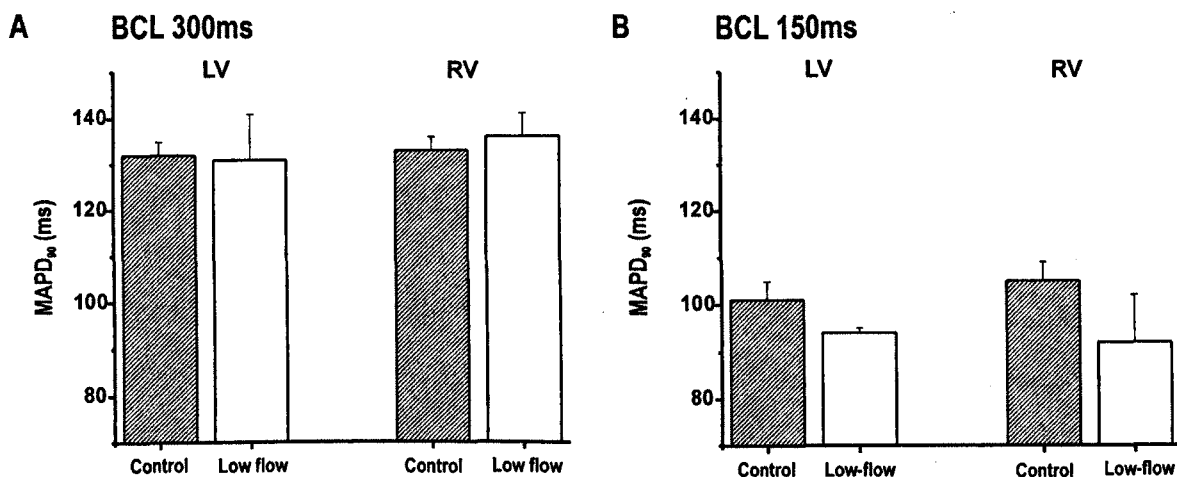


Figure 5.5 MAPD₉₀ in control (C) and low-flow ischaemia (6ml/min). Panel A: BCL 300ms – Neither the LV nor the RV MAPD₉₀ was significantly shortened by low-flow ischaemia (6ml/min). There was no significant difference between the RV and LV MAPD₉₀ in control or low-flow ischaemia. Panel B: BCL 150ms – Again neither the LV nor the RV MAPD₉₀ was significantly shortened by low-flow ischaemia (6ml/min), and there was no significant difference between the LV and RV MAPD₉₀ in either control or low-flow ischaemia.

5.3.2 5mM [K⁺]_{EC} vs. 8 & 10mM [K⁺]_{EC}

In both 8mM and 10mM [K⁺]_{EC} protocols, 1:1 capture could not be achieved with BCL <150ms. The restitution plots in figure 5.4 clearly show that MAPD₉₀ was shortened by raised [K⁺]_{EC} in a manner that was both time and concentration dependant. This shortening was only reached significance in 10mM [K⁺]_{EC} and after 10 minutes (Figure 5.6).

Looking at the results in more detail, after 6 minutes of perfusion with 8mM [K⁺] solution, the LV MAPD₉₀ was 117 ± 2ms at BCL 300ms, whilst the RV MAPD₉₀ was 121 ± 4ms. These were not significantly different from the respective baseline MAPD₉₀ in the LV of 128 ± 5ms, and RV of 133 ± 6ms. After 6 minutes of perfusion with 10mM [K⁺] solution, the LV MAPD₉₀ reduced to 115 ± 5ms as assessed at BCL 300ms, whereas the RV MAPD₉₀ decreased to 119 ± 11ms. Compared to respective baseline LV and RV MAPD₉₀, these were no significant changes. Assessing the MAPD₉₀ at BCL 150ms also gave no significant change in either level of raised [K⁺]_{EC} in either ventricle. In 8mM [K⁺]_{EC}, the LV MAPD₉₀ of 86 ± 2ms was not different from that in control conditions of 90 ± 2ms, and the RV MAPD₉₀ of 91 ± 4ms was unchanged from the control RV MAPD₉₀ of 98 ± 2ms. Similarly, in 10mM [K⁺]_{EC} the LV MAPD₉₀ of 81 ± 7ms and the RV MAPD₉₀ of 90 ± 2ms were unchanged compared to baseline.

After 10 minutes of perfusion with 8mM [K⁺] solution, the LV MAPD₉₀ was 118 ± 3ms at BCL 300ms, and the RV MAPD₉₀ was 122 ± 4ms. These ventricular MAPD₉₀ were not

significantly shortened compared to baseline values (Figure 5.6A). After 10 minutes of perfusing with 10mM $[K^+]_{EC}$ solution, the LV MAPD₉₀ had reduced to $113 \pm 3ms^*$ at BCL 300ms, whilst the RV MAPD₉₀ was $111 \pm 6ms^*$. Both of these ventricular MAPD₉₀ were significantly reduced compared to baseline (Figure 5.6A, * $p < 0.05$). Assessing the MAPD₉₀ at BCL 150ms also gave rise to significant changes in 10mM $[K^+]_{EC}$ but not in 8mM $[K^+]_{EC}$ (Figure 5.6B). In 8mM $[K^+]_{EC}$, the LV MAPD₉₀ of $84 \pm 1ms$ was not different from that in control conditions of $90 \pm 2ms$, and the RV MAPD₉₀ of $90 \pm 1ms$ was unchanged from the control RV MAPD₉₀ of $98 \pm 2ms$. In contrast, in 10mM $[K^+]_{EC}$ the LV MAPD₉₀ of $77 \pm 3ms^{**}$ and the RV MAPD₉₀ of $87 \pm 3ms^{**}$ were significantly shortened compared to baseline (** $p < 0.01$).

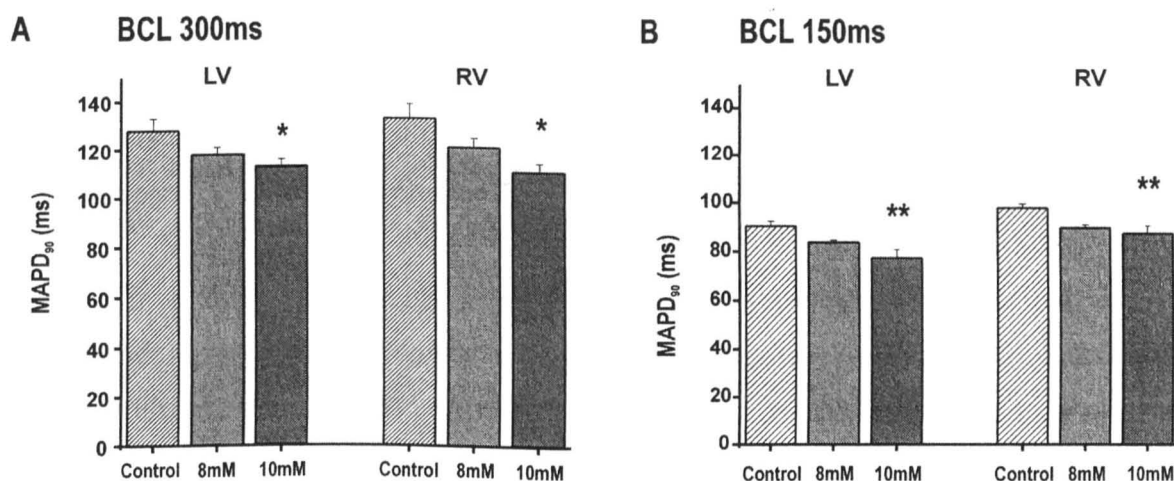


Figure 5.6 MAPD₉₀ in control (C), 8mM $[K^+]_{EC}$ and 10mM $[K^+]_{EC}$. Panel A: BCL 300ms – Compared to control (C), the LV and RV MAPD₉₀ were significantly shortened by 10mM $[K^+]_{EC}$ (* $p < 0.05$ compared to control) but not 8mM $[K^+]_{EC}$. In both 8mM and 10mM $[K^+]_{EC}$, there was no significant difference between the LV and RV MAPD₉₀. Panel B: BCL 150ms – Compared to control (C), LV and RV MAPD₉₀ were significantly shortened by 10mM $[K^+]_{EC}$ (** $p < 0.01$ compared to control) but not by 8mM $[K^+]_{EC}$. In 8mM $[K^+]_{EC}$ the LV and RV MAPD₉₀ were not significantly different from each other. Whereas in 10mM $[K^+]_{EC}$, the LV MAPD₉₀ was significantly shorter than the RV MAPD₉₀ ($p < 0.05$ LV vs. RV). This is not documented on the plot for clarity).

Although there was significant reduction of the MAPD₉₀ in both ventricles in 10mM $[K^+]_{EC}$, there was no significant difference in the concurrent RV-to-LV MAPD₉₀. There was also no difference in the relative change in MAPD₉₀ as experienced by each ventricle under raised $[K^+]_{EC}$ as shown by percentage change in MAPD₉₀ compared to baseline. After 10 minutes of perfusion in 10mM $[K^+]_{EC}$ solution, at BCL 300ms the LV MAPD₉₀ underwent a percentage reduction to $88 \pm 2\%$, which was not significantly different from the RV MAPD₉₀ percentage change of $83\% \pm 2\%$. Similarly at BCL 150ms, the LV MAPD₉₀ underwent a percentage reduction to $88 \pm 3\%$, which was not significantly different from the RV MAPD₉₀ percentage change of $93\% \pm 3\%$.

In summary, both the LV and RV MAPD₉₀ were significantly reduced after 10 minutes perfusion in 10mM [K⁺] solution. There was no difference in the percentage reduction experienced by each ventricle.

5.4 Discussion

In order to explain the differential LV-to-RV DF reduction in VF during low-flow ischaemia and raised [K⁺]_{EC}, repolarisation would have to be differentially prolonged in the LV compared to the RV. Thus the LV MAPD₉₀ would need to be differentially prolonged compared to the RV MAPD₉₀. This chapter demonstrated no significant reduction in LV or RV APD during low-flow ischaemic conditions. There was also no significant difference in the LV-to-RV APD during low-flow ischaemia. Although 10mM [K⁺] solution produced significant shortening of the APD, there was no difference in the degree of APD shortening between the LV and the RV. Nor was there any difference in the absolute values of the LV APD compared to the RV in either 8mM or 10mM [K⁺] solutions.

Previous investigations of MAPD dispersion during global ischaemia in the isolated rabbit heart showed differential alterations in the LV and RV restitution curves (186). Kurz et al. positioned 2 contact electrodes against the RV and LV epicardial surface in a manner similar to that used in this chapter. APD restitution was assessed by S₁S₂ protocol at baseline before the perfusion rate was reduced to 2.5ml/min, and APD restitution re-assessed after 2, 5 and 9 minutes. At baseline, there was no significant difference between the RV and LV APD. In response to global ischaemia, there was an initial APD prolongation, which was followed by APD shortening in both ventricles. The time-course of this APD alteration was different between the ventricles. In the LV, the APD prolongation lasted for 2 – 5 minutes, whereas in the RV the APD prolongation lasted 5 – 9 minutes. This produced divergent restitution curves, with LV APDs ~100ms longer than RV APDs after 5 minutes of ischaemia. At the DF assessment point of 480s used in this thesis this would mean that the RV APD would be prolonged compared to LV. This is opposite from the differential alteration required to explain LV DF slowing compared to RV.

In this chapter, the results from 1 experiment followed the same pattern as described by Kurz et al. (186). This is illustrated in figure 5.3A. Over the 6 experiments, the patterns of restitution altered in a highly variable fashion (Figure 5.3). Therefore, the mean of all 6 experiments showed no significant difference in APD restitution curves between the ventricles. One possible explanation for the discrepancy between the results of Kurz et al.

(186), and of this chapter, is the different perfusion rates used. In this chapter, the flow rate was reduced to 6ml/min, whereas Kurz et al. imposed more severe ischaemic conditions by reducing the flow to 2.5ml/min. One would predict that in the less severe ischaemic conditions of this chapter, the APD alterations would occur more gradually. Such a situation could produce a near unity of LV and RV APD; having reached its most prolonged values, the shortening LV APD could intersect with the prolonging RV APD at approximately the same value. Indeed, in 1 out of 6 experiments the LV APD was more prolonged than baseline and RV supporting this theory (Figure 5.3B).

There is no evidence in the literature for differential APD alterations of the LV compared to the RV in raised $[K^+]_{EC}$. The only evidence of any heterogeneity in the heart comes from single cell work. This showed that in raised $[K^+]_{EC}$ there was differential alteration of the APD dependent on the mural level within the LV (235). The subepicardial myocyte APD is more prolonged in 8.1mM $[K^+]_{EC}$ than the subendocardial myocyte.

In summary, differential alteration in repolarisation does not account for the slowing of the LV DF compared to the RV in VF as observed in both low-flow ischaemia and raised $[K^+]_{EC}$.

**6 Effective refractory period, pacing threshold
and dV/dt_{\max} in low-flow ischaemia and raised
 $[K^+]_{EC}$**

6.1 Introduction

Previous chapters have described how Dominant Frequency (DF) is reduced during VF in low-flow ischaemia and raised $[K^+]_{EC}$ in the ECG, the psECG and over the LV epicardial surface. In contrast, the RV DF was unchanged during VF in low-flow ischaemia and raised $[K^+]_{EC}$. Theoretically, several mechanisms could account for the reduction of DF in the LV but not the RV in low-flow ischaemia and raised $[K^+]_{EC}$. These mechanisms are (i) relative prolongation of LV repolarisation, (ii) relative prolongation of LV post-repolarisation refractoriness, (iii) relative elevation of the LV activation threshold and (iv) relative reduction of LV conduction velocity. Chapter 5 demonstrated that LV repolarisation is not prolonged compared to RV in either low-flow ischaemia, or raised $[K^+]_{EC}$. This chapter investigates the role of relative LV-to-RV changes of post-repolarisation refractoriness and activation thresholds in low-flow ischaemia and raised $[K^+]_{EC}$.

6.1.1 Prolongation of post-repolarisation refractoriness

In ischaemia, the Effective Refractory Period (ERP) extends beyond full repolarisation (236-238). This is known as post-repolarisation refractoriness. If during low-flow ischaemia and raised $[K^+]_{EC}$, there is differential prolongation of the LV post-repolarisation refractoriness compared to the RV, this may explain the differential LV DF slowing during VF in low-flow ischaemia and raised $[K^+]_{EC}$. Traditionally, the ERP is assessed by establishing the pacing threshold voltage at intervals well beyond post-repolarisation refractoriness, and then setting the pacing stimulus voltage at twice this threshold. The ERP is identified as the longest S_2 interval not to propagate during an S_1S_2 pacing protocol (239)

6.1.2 Raised threshold for activation

An action potential (AP) is triggered if the membrane potential depolarises above a certain potential or threshold. At this point, there is activation of the fast Na^+ current (I_{Na}), and an AP is propagated. In sinus rhythm and regular pacing, the peak systolic potential on activation is constant. This is not the case in VF. Figure 6.1 shows the considerable variation of the peak systolic potential that occurs during VF. If there were heterogeneity of the activation threshold potential throughout the myocardium, one would predict heterogenous activation rates. For instance, activations from an area where the potential

difference between the threshold and resting potentials is small may not cause sufficient depolarisation to trigger activations in a region where the potential difference is larger. Thus a relative increase in LV activation threshold, compared to the RV, could explain the differential lowering of the LV DF compared to the RV in low-flow ischaemia and raised $[K^+]_{EC}$. In this chapter, the pacing threshold was measured as a surrogate for AP activation threshold.

The activation threshold can be increased either by increasing the magnitude of the background outward current, or by reducing I_{Na} . The possibility of I_{Na} reduction was assessed by measuring the maximum MAP upstroke velocity (240). As discussed more fully in chapter 1.3.4, the upstroke of MAP recordings is influenced by more cells than in transmembrane recordings, and thus the upstroke velocities are slower. In the canine heart, the typical ventricular MAP upstroke velocity of 7V/s is much slower than the transmembrane upstroke velocities of 200-300V/s (146). Therefore changes in the MAP upstroke velocity give indirect assessments of I_{Na} .

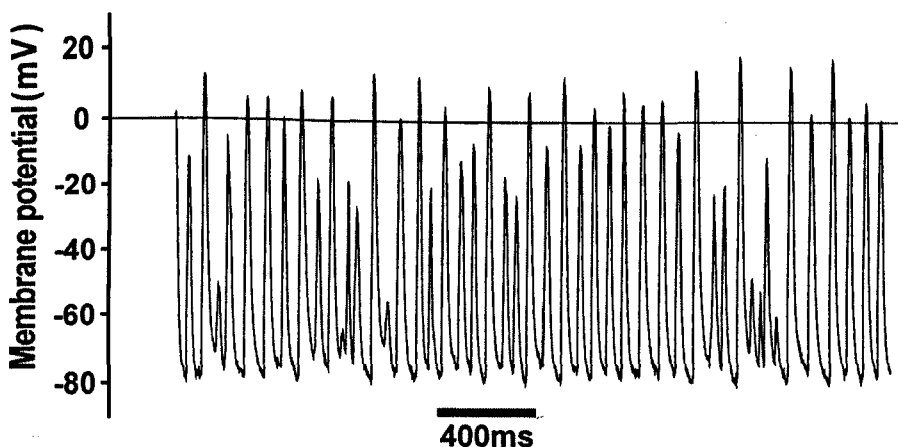


Figure 6.1 Transmembrane recordings during VF. There is considerable variation in the degree of systolic depolarisation between activations.

6.2 Methods

Hearts were prepared as per chapter 5. To assess the LV ERP, the heart was paced through the MAP electrode in contact with the LV, and any propagating activation detected via the MAP electrode in contact with the RV. To assess the RV ERP, the roles of pacing and detecting were reversed without repositioning the MAP electrodes. In each electrode, the pacing threshold was determined as the lowest voltage to capture 1:1 at BCL 300ms. The ERP was assessed by an S_1S_2 protocol using a 2ms duration stimulus set at twice the pacing threshold voltage. The S_1S_2 protocol consisted of eight beats at BCL 300ms (S_1), followed by a single stimulus at a shorter intervals (S_2) (Figure 6.2). The S_1S_2 interval was

initially set at 150ms, and was sequentially shortened by 5ms on subsequent stimuli trains. This step-wise reduction of S_1S_2 interval was continued until the S_2 activation failed to propagate to the detecting electrode. The S_1S_2 interval was now returned to the last interval that produced a propagating activation, and the step-wise reduction resumed using 2ms increments. The ERP was determined as the longest S_1S_2 interval to not to result in a propagating AP.

The pacing threshold and ERP were determined in control conditions (40ml/min, 5mM $[K^+]_{EC}$), and after 10 minutes (600s) of experimental conditions. Experimental conditions consisted of (i) low-flow ischaemia (6ml/min) ($n = 6$), (ii) Tyrode's solution with 8mM $[K^+]$ ($n = 5$) or (iii) Tyrode's solution with 10mM $[K^+]$ ($n = 5$). The maximum upstroke velocity (dV/dt_{max}) was measured during the BCL 300ms (S_1). The MAP amplitudes were calibrated according to the known voltage signals applied through the amplifier.

Comparisons were performed on the absolute data, and on fractional changes to reduce the influence of biological variation. Significance was tested using repeated measures ANOVA.

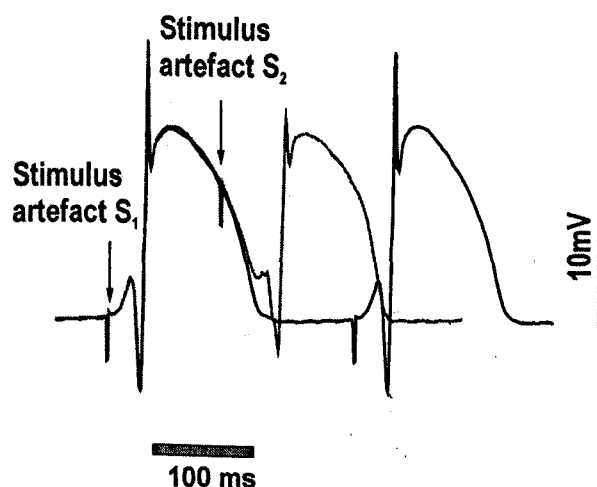


Figure 6.2 Illustration of S_1S_2 protocol to assess ERP. After ten S_1 stimuli, a shorter S_2 was delivered. ERP was determined as the shortest S_2 to produce a propagating action potential.

6.3 Results

6.3.1 Effective Refractory period (ERP)

As shown in figure 6.3, under control conditions the LV ERP of 123 ± 3 ms was not significantly different from the RV ERP of 119 ± 4 ms. In low-flow ischaemia, the LV ERP of 127 ± 7 ms was not significantly different from the RV ERP of 127 ± 8 ms. Neither the

LV ERP, nor the RV ERP was significantly different from baseline values. In 8mM $[K^+]$ solution, the LV ERP of 130 ± 4 ms was not significantly different from the RV ERP of 131 ± 6 ms (Figure 6.3). In 10mM $[K^+]$ solution, the LV ERP of 138 ± 6 ms was not significantly different to the RV ERP of 126 ± 4 ms. In 8mM and 10mM $[K^+]$ solutions neither the LV ERP, nor the RV ERP were significantly different from the respective baseline values.

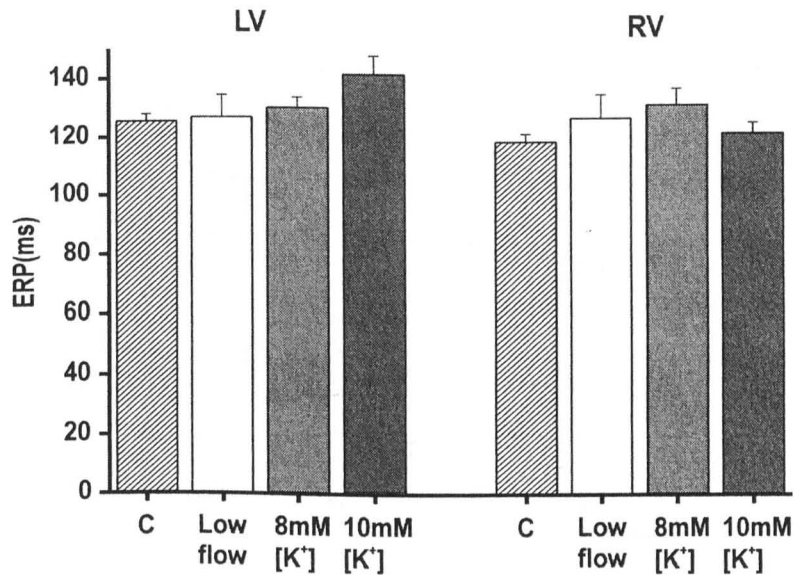


Figure 6.3 Plot of mean ERP in control (C), low-flow ischaemia, 8mM $[K^+]$ solution and 10mM $[K^+]$ solution. The ERP was not significantly different between the ventricles, and showed no significant change compared to control in low-flow ischaemia or raised $[K^+]_{EC}$. Comparing fractional change of LV and RV ERP in low-flow ischaemia and raised $[K^+]_{EC}$ showed no difference between the RV or LV.

To ensure that there was no relative change in ERP between the ventricles in response to low-flow ischaemia or raised $[K^+]_{EC}$, the ERP fractional change was calculated for each ventricle. In low-flow ischaemia, the fractional change in the LV ERP of 1.03 ± 0.06 was not significantly different from the RV ERP fractional change of 1.10 ± 0.06 . Similarly, in 8mM $[K^+]$ solution, the fractional change in LV ERP of 0.99 ± 0.03 was not significantly different from the RV fractional change of 1.11 ± 0.05 , and in 10mM $[K^+]$ solution, the LV ERP fractional change of 1.05 ± 0.02 was not different from the RV ERP fractional change of 1.03 ± 0.01 .

Using the $MAPD_{90}$ at BCL 150ms after 10 minutes of experimental conditions (Chapter 5.3) post-repolarisation refractoriness was calculated for each ventricle in each experiment. Both low-flow ischaemia and raised $[K^+]_{EC}$ produced significant post-repolarisation refractoriness. Figure 6.4 demonstrates that the post-repolarisation refractoriness was not significantly different between the LV and RV in low-flow ischaemia and 8mM $[K^+]$

solution. In low-flow ischaemia the post-repolarisation refractoriness in the LV of 38 ± 14 ms was not significantly different from that of the RV of 20 ± 2 ms. Similarly, in 8mM $[K^+]$ solution the post-repolarisation refractoriness in the LV of 43 ± 1 ms was not significantly different from the RV of 33 ± 4 ms. In contrast, in 10mM $[K^+]$ solution the LV the post-repolarisation refractoriness of 63 ± 3 ms was significantly longer than the 32 ± 5 ms in the RV (** $p < 0.01$). These results are in line with the changes in $MAPD_{90}$, where only 10mM $[K^+]$ solution produced differential shortening of the LV $MAPD_{90}$ compared to the RV.

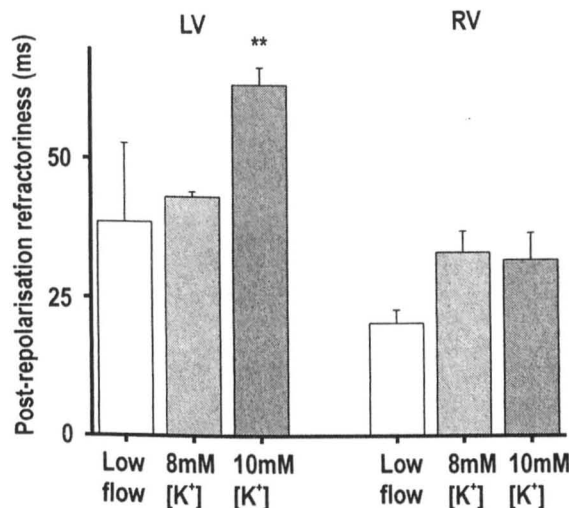


Figure 6.4 Post-repolarisation refractoriness. Post repolarisation refractoriness was calculated by subtracting the $MAPD_{90}$ at BCL 150 from the ERP. In low-flow ischaemia and 8mM $[K^+]$ solution the post-repolarisation refractoriness was not significantly different in the LV from the RV. In 10mM $[K^+]$ solution the LV post-repolarisation refractoriness was significantly longer than in the RV (** $p < 0.01$).

In summary, although low-flow ischaemia and raised $[K^+]_{EC}$ produced significant post-repolarisation refractoriness, only 10mM $[K^+]$ solution produced significantly longer post-repolarisation refractoriness in the LV compared to the RV. This was associated by significant shortening of the LV $MAPD_{90}$ compared to the RV. Thus there was no significant change in ERP in either ventricle in low-flow ischaemia or raised $[K^+]_{EC}$.

6.3.2 Activation threshold

Figure 6.5 shows how the pacing thresholds were increased heterogeneously by both low-flow ischaemia and raised $[K^+]_{EC}$ at BCL 300ms. In low-flow ischaemia, the LV pacing threshold increased by a factor of 3.5 ± 1.3 ($p < 0.05$) which was significantly different from the RV ($p < 0.05$) which only increased by 1.2 ± 0.1 . In 8mM $[K^+]$ solution, the LV pacing threshold increased by a factor of 2.6 ± 0.5 ($p < 0.01$) which was significantly different from

the RV pacing threshold ($p < 0.05$) that remained unchanged at 1.3 ± 0.3 . Similarly, 10mM $[K^+]_{EC}$ solution, the LV pacing threshold increased profoundly by a factor of 11.4 ± 8 , whilst the RV threshold only increased by a factor of 4 ± 2.2 . However, the great variation masked the detection of significant differences.

In summary, the LV pacing threshold was more markedly increased than the RV in low-flow ischaemia and raised $[K^+]_{EC}$. This differential change is in keeping with the lower LV DF compared to the RV DF in low-flow ischaemia and raised $[K^+]_{EC}$.

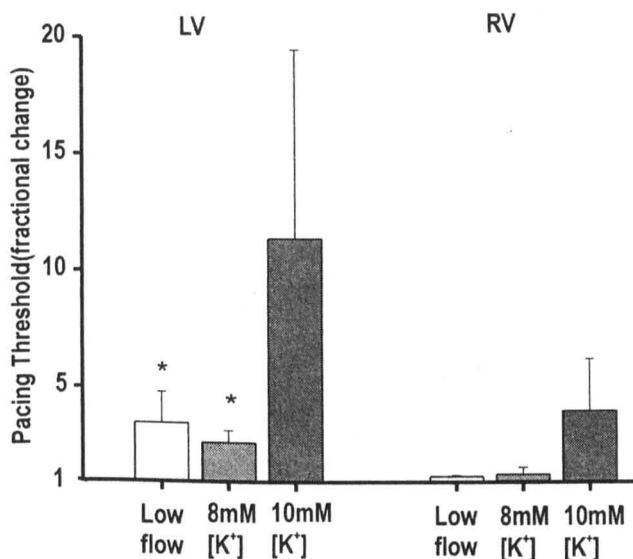


Figure 6.5 Fractional change of threshold voltage required to capture the respective ventricle at BCL 300ms. Thresholds were elevated in the LV during low-flow ischaemia* and 8mM $[K^+]_{EC}$ solution*, whereas the RV threshold remained unchanged (* $p < 0.05$; LV vs. RV fractional change). In 10mM $[K^+]_{EC}$ solution, the LV pacing threshold was increased compared to the RV but this did not reach significance.

6.3.3 Maximum Upstroke Velocity

The MAP amplitude was greater in the LV than the RV, such that at baseline the mean LV MAP amplitude was 15.3 ± 1.5 mV, whereas the mean RV MAP amplitude was 4.4 ± 0.4 mV. For this reason, LV dV/dt_{max} was approximately 3 times greater than RV. As shown in figure 6.6, at BCL 300ms, the maximum MAP upstroke velocity (dV/dt_{max}) was significantly reduced in the LV by both low-flow ischaemia and raised $[K^+]_{EC}$, whereas the RV dV/dt_{max} remained unchanged. In low-flow ischaemia, the LV dV/dt_{max} of 72 ± 24 mV/s was significantly reduced from baseline values of 147 ± 24 mV/s ($p < 0.001$). In comparison, in the RV the dV/dt_{max} of 72 ± 6 mV/s was unchanged from the baseline value of 93 ± 33 mV/s. Comparing the percentage changes in dV/dt_{max} , the LV was reduced to $44 \pm 10\%$ of baseline, whereas the RV was unchanged at RV $97 \pm 19\%$. The difference in these

percentage changes did not reach significance ($p = 0.06$). In 8mM $[K^+]$ solution, the LV dV/dt_{max} of 81 ± 21 mV/s was significantly reduced from baseline values of 218 ± 12 mV/s ($p < 0.001$). In comparison, in the RV the dV/dt_{max} of 27 ± 6 mV/s was unchanged from baseline of 36 ± 6 mV/s. Comparing the percentage change in dV/dt_{max} , the LV was reduced to $39 \pm 10\%$ of baseline, which was significantly different from the RV ($p < 0.05$) which remained unchanged at $90 \pm 22\%$. In 10mM $[K^+]$ solution, the LV dV/dt_{max} of 72 ± 21 mV/s was significantly reduced from baseline values of 218 ± 12 mV/s ($p < 0.001$). In comparison, in the RV the dV/dt_{max} of 24 ± 3 mV/s was unchanged from baseline of 27 ± 6 mV/s. Comparing the percentage change in dV/dt_{max} , the LV was reduced to $26 \pm 4\%$ of baseline, which was significantly different from the RV ($p < 0.05$), which remained unchanged at $87 \pm 31\%$.

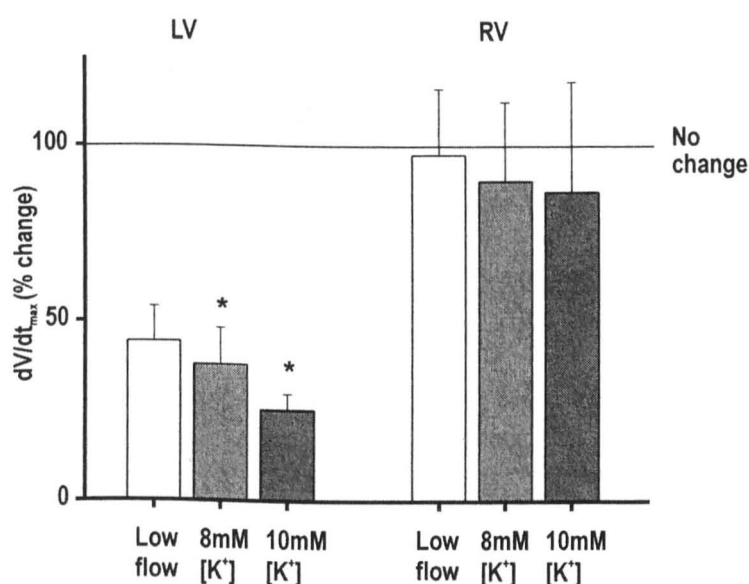


Figure 6.6 Percentage change in MAP upstroke velocity during low-flow ischaemia and perfusion with 8mM $[K^+]$ solution or 10mM $[K^+]$ solution. In low-ischaemia, the tendency for the LV dV/dt_{max} to be reduced compared to the unchanged RV dV/dt_{max} did not reach significance ($p = 0.06$). In both 8mM and 10mM $[K^+]$ solution the LV dV/dt_{max} percentage change was significantly different from that in the RV ($*p < 0.05$).

In summary, there was slowing of the LV MAP upstroke compared to the RV. This differential upstroke slowing was associated with a differential increase in LV pacing threshold, compared to the RV, in low-flow ischaemia and raised $[K^+]_{EC}$.

6.4 Discussion

This chapter examined the roles of post-repolarisation refractoriness and activation threshold in determining the spatiotemporal DF distribution during VF in low-flow ischaemia and raised $[K^+]_{EC}$. In low-flow ischaemia and raised $[K^+]_{EC}$, the relative LV DF

slowing could be explained by either (i) a differential prolongation of the LV post-repolarisation refractoriness or (ii) a differential increase in the LV activation thresholds.

6.4.1 Prolongation of post-repolarisation refractoriness

The results in chapter 5 showed no evidence of a differential prolongation of MAPD in LV compared to RV during low-flow ischaemia or raised $[K^+]_{EC}$. However, prolongation of ERP beyond full repolarisation (post-repolarisation refractoriness) remains a possible mechanism of the lower DF in the LV. Traditionally, ERP has been measured by first establishing the pacing threshold at intervals well beyond post-repolarisation refractoriness. Once established, the pacing stimulus strength is set at twice this threshold. The ERP is identified as the longest S_1S_2 interval not to capture during an S_1S_2 pacing protocol (239). Using such a protocol, this chapter demonstrated that the ERP did not change in either low-flow ischaemia or raised $[K^+]_{EC}$. Therefore, the differential LV-to-RV DF slowing in VF during ischaemia and raised $[K^+]_{EC}$ is not secondary to ERP changes. A similar lack of relationship between ERP and DF was demonstrated in canine atria (241). Here, Huang et al. observed that in atrial fibrillation (AF), the DF increased as the atria were dilated, whilst the ERP was unchanged.

Although the results of Huang et al. (241) and this chapter show no correlation between ERP and DF, a cautionary note must be made. The determination of ERP is highly dependent on the pacing stimulus voltage. Using stronger pacing voltages to assess the same state of post-repolarisation refractoriness will allow earlier myocardial capture, and thus will give shorter ERP measurements. If the same stimulus strength were used throughout the experiment, the interpretation of ERP alteration as distinct from changes in activation threshold becomes difficult. This difficulty of assessing and interpreting ERP in acute ischaemia due to the continuously changing diastolic thresholds is well known (134, 242). To this end previous studies have shown the ERP to increase (134, 242), decrease (242-244) or remain unchanged (244) during ischaemia dependent on whether the stimulus intensity used was static or a dynamic. As the aim of the experiments in this chapter was to study alterations of both ERP and activation threshold in low-flow ischaemia and raised $[K^+]_{EC}$, a set high stimulus voltage was not applied, but rather the diastolic threshold was assessed in each circumstance, and the standard of twice this threshold used to assess the ERP. With this in mind, there was no relative prolongation of LV ERP compared to the RV ERP. Thus post-repolarisation refractoriness cannot account for relative LV-to-RV DF slowing in VF during low-flow ischaemia and raised $[K^+]_{EC}$.

6.4.2 Raised threshold for activation

A differential increase in the LV activation threshold compared to the RV, could explain the lower LV DF in VF during low-flow ischaemia and raised $[K^+]_{EC}$. Differential elevation of the LV activation threshold means that greater current is needed to raise the membrane potential to threshold in the LV than the RV, and hence the safety margin for conduction is lower in the LV. With this lower safety margin for conduction activations will fail to propagate into the LV, and will therefore result in a lower LV DF. By measuring the pacing stimulus threshold as a surrogate for the activation threshold, this chapter demonstrated a relative increase in LV activation threshold compared to RV. This differential increase was observed in low-flow ischaemia and in raised $[K^+]_{EC}$. Similar elevations of the pacing voltage threshold have been observed by others during ischaemia (242, 245, 246) and in raised $[K^+]_{EC}$ (247).

Increases in the activation threshold suggest an altered balance between I_{Na} and the background potassium currents; either an increase in the background current or a decrease I_{Na} . The raised $[K^+]_{EC}$ that occurs in low-flow ischaemia, as well as when perfusing with 8mM or 10mM $[K^+]$ solutions, would tend to reduce background potassium currents, rather than increase them. As $[K^+]_{EC}$ increases, the intracellular-to-extracellular $[K^+]$ gradient is reduced. This reduces the background current's driving force. Therefore, the increase in the LV activation threshold in low-flow ischaemia and raised $[K^+]_{EC}$ is more likely to result from a reduction of I_{Na} than an increase in background current.

The change in the maximum MAP upstroke velocity provides complementary evidence for I_{Na} reduction in the LV. Although the relationship between maximum AP upstroke velocity and available sodium channels is not linear, the upstroke velocity gives a reasonable approximation of peak I_{Na} in conditions where non-sodium currents have minimal contribution (240). However, as ischaemia and raised $[K^+]_{EC}$ depolarise the cell membrane (81, 140, 202, 227), the slower $I_{Ca(L)}$ will start to contribute to the upstroke (240). Despite this, maximum upstroke velocity can still be examined as an indicator of I_{Na} . In low-flow ischaemia, and raised $[K^+]_{EC}$, the maximum MAP upstroke velocity was reduced in the LV but not the RV. Therefore, the elevated LV activation threshold was associated with reduced LV upstroke velocity.

The association between reduced I_{Na} magnitude, increased pacing threshold and reduced AP upstroke velocity has previously been demonstrated in non-cardiac tissues (248). Chen et al. showed a 42% reduction of Na^+ channel membrane density in the Na^+ channel $\beta 2$ -

subunit knockout mouse. The optic nerves of these mice had reduced I_{Na} , increased activation thresholds, and reduced AP upstroke velocity. Interestingly, the conduction velocity within these nerves was maintained.

The current literature also demonstrates that I_{Na} inhibition lowers the DF in VF (62). Here, Mandapati observed that low-level tetrodotoxin, a Na^+ channel blocker, reduced the DF by reducing the rotational rate of the VF re-entrant circuits. Mandapati et al. also observed that the relationship between the DF reduction and reduced rotational rate in the presence of tetrodotoxin was identical to that observed in total global ischaemia.

This chapter does not elucidate the mechanism of the proposed I_{Na} reduction during low-flow ischaemia and raised $[K^+]_{EC}$. As the inhibition has quick onset, and is immediately reversed, it is unlikely to be due to altered Na^+ channel density as in Chen et al. (248). The current literature documents depolarisation of diastolic membrane potential in ischaemia (140) and raised $[K^+]_{EC}$ (81). Such depolarisation reduces the Na^+ channel availability and increases activation threshold. Differential depolarisation of the LV diastolic potential compared to the RV could account for differential changes in the LV activation threshold, and thus the differential slowing of the LV DF in VF during ischaemia and raised $[K^+]_{EC}$.

The diastolic depolarisation of ischaemia and raised $[K^+]_{EC}$ occurs as the reversal potential (E_k) of K^+ channels undergo positive (rightwards) shift in the presence of increasing $[K^+]_{EC}$. One of the K^+ channels, Kir2.x also undergoes rightward shift of its E_k ischaemia and raised $[K^+]_{EC}$ (226). As the expression of Kir2.x, and the magnitude of the resultant I_{K1} current, are greater in the LV than the RV, one would predict that LV myocytes would experience greater diastolic depolarisation than RV myocytes in the same $[K^+]_{EC}$. Therefore differential LV-to-RV diastolic depolarisation is theoretically possible.

In summary, this chapter demonstrates differential elevation of the LV stimulation threshold compared to the RV in both low-flow ischaemia and raised $[K^+]_{EC}$. The associated differential reduction in LV dV/dt_{max} suggests that differential inhibition of I_{Na} in the LV compared to the RV may underlie this threshold elevation. It is theoretically possible that this differential I_{Na} inhibition is secondary to differential diastolic depolarisation as a result of the LV/RV heterogeneity of Kir2.x expression.

7 Alterations in conduction velocity

7.1 Introduction

Chapters 3 & 4 have described how the Dominant Frequency (DF) in the ECG, the psECG and by optical mapping of the LV is reduced during VF in low-flow ischaemia and raised $[K^+]_{EC}$. In contrast, the RV DF was unchanged during VF in low-flow ischaemia and raised $[K^+]_{EC}$. Theoretically, several mechanisms could account for the relative slowing of the LV DF in VF during low-flow ischaemia and raised $[K^+]_{EC}$. These mechanisms are (i) relative prolongation of LV repolarisation (Chapter 5), (ii) relative prolongation of LV post-repolarisation refractoriness (Chapter 6), (iii) relative elevation of the LV activation threshold (Chapter 6) and (iv) relative reduction of LV conduction velocity (CV). This chapter documents the investigations into CV heterogeneity in low-flow ischaemia and 8mM $[K^+]$ solution.

A relative slowing of the LV CV compared to the RV would slow the propagation of wavefronts from the RV into the LV. CV is altered by ischaemia (249) and raised $[K^+]_{EC}$ in a biphasic manner (218), (250). Early ischaemia is associated with minor elevations in $[K^+]_{EC}$, which increase CV. More prolonged ischaemia is associated with higher $[K^+]_{EC}$ that decrease CV. Therefore, differential slowing of the LV CV could be produced by either a relative decrease in the LV CV, or a relative increase in the RV CV.

In this chapter, CV was assessed during VF (apparent CV (46, 189)) and during epicardial pacing (traditional CV).

7.2 Methods

7.2.1 Apparent CV measurements in VF

Apparent CV was calculated from the VF data sets of chapters 3 & 4, using locally developed software (46). This software first identifies the activation times in each pixel as the point of dV/dt_{max} . The activation times of adjacent pixels were compared to determine the wavefront direction. Using the direction, and the activation times, the wavefront velocity was calculated at the junction of each group of 4 pixels. The process was repeated for all activation times during the 4s epochs of VF. From these data sets, the mean and modal apparent CV was calculated for each junction point. The results were plotted as colour-coded, two dimensional maps. Representative values for the LV and RV CV were derived from standardised squares, which were equivalent to those used to determine the

RV and LV DF in chapters 3 & 4. Similar patterns were observed for both the mean and the modal CV. As the mean CV showed less variability than modal CV, it alone is reported in this chapter, whilst acknowledging that modal CV is more in keeping with the "peak" nature of DF.

For the first 60s after VF induction, all hearts were perfused at the control rate of 40ml/min with standard Tyrode's solution. Experimental conditions were imposed from 60s onwards, and hearts were defibrillated at 600s. Comparisons were made between control and experimental conditions at 0s and 480s using ANOVA. The 480s time-point was representative of the steady state observed in DF, and was equivalent to 420s in experimental conditions.

7.2.2 Traditional measurements of CV

Hearts were Langendorff-perfused and mounted in the optical mapping chamber as per chapter 2.1. A 1mm diameter hole was drilled through the Plexiglass front-plate to allow the insertion of a bipolar platinum electrode. This electrode was used to pace the epicardium of the ventricles. The bipolar electrode was centralised within the optical recording area. Hearts were loaded with 100 μ l of 1mg/ml RH237. 3 μ M cytochalasin D was used to improve the precision of activation identification by reducing motion artefact. This concentration of cytochalasin D has been shown not to significantly affect CV in the rabbit heart (231). Hearts were perfused in Tyrode's solution containing 3 μ M cytochalasin D for 20 minutes. The perfusate was then switched back to standard Tyrode's solution. Both control and experimental protocols were performed during this "washout" phase. At the start of each CV protocol, the diastolic pacing threshold was assessed at BCL 300ms. Hearts were paced at twice this stimulus strength at BCL 250ms, 200ms and 150ms. Hearts were manipulated within the chamber to stimulate of each ventricle in turn. The CV protocol was performed in each ventricle during control conditions, before experimental conditions were applied. Experimental conditions consisted of either low-flow ischaemia (6ml/min, n = 4) or raised $[K^+]_{EC}$ (8mM, n = 4). After 6 minutes (360s) in experimental conditions, the CV protocol was repeated in each ventricle. Performing the CV protocol in both ventricles took c.60s, so that the protocol was completed by 420s. The short intrinsic delay of this experimental procedure resulted in one of the ventricles being exposed to experimental conditions for a marginally longer prior to CV assessment. To ensure this short intrinsic delay had no confounding effect on the CV data, the sequence of the LV-RV recordings was reversed in alternate experiments.

Offline, the activation time in each pixel was identified as the point of dV/dt_{\max} . Using software developed locally in MatLab (The MathWorks, Inc., MA, USA), these times were used to calculate the local conduction velocity (251). The conduction velocity can be artificially accelerated by intramural conduction or close pacing stimulus. Thus, to ensure the correct evaluation of conduction velocity, both transverse and longitudinal velocities were assessed using several different selection strategies. For full description and explanation of the different strategies see chapter 2.6. Briefly the strategies were: - (i) 5mm radial velocity (Figure 2.9) – the pacing site was identified as the central activation point on the isochronal activation map. CV was calculated at all points around a 5mm radius from the pacing site. The longitudinal CVs were identified as the 2 highest velocities around this circle. The transverse CV was measured on the circle at points perpendicular to the longitudinal CV. (ii) Linear velocity (Figure 2.10) – using isochronal activation maps, CV was calculated along a straight line. This line was drawn from the pacing site, through the fastest advancing point of the wavefront. The longitudinal CV was determined as the value of the "low plateau" velocity between the pacing artefact and the intramural breakaway conduction. Transverse CV was similarly assessed on perpendicular lines. (iii) Point velocity (Figure 2.11) – The CV was plotted across the epicardial surface as a colour-coded map. This shows 2 areas of homogeneous CV along the transverse CV axes. Five CV measurements were taken from each of the homogeneous areas, and the mean used as a further method to assess transverse CV. As all strategies gave similar results only the radial method data is reported.

Due to the variable location of epicardial stimulation point with respect to the septum/opposite ventricle, longitudinal velocity was assessed along the axis away from the septum. Transverse velocity was measured in both perpendicular axes then averaged. Comparisons between control and experimental conditions were made using repeated measures ANOVA.

7.3 Results

7.3.1 Apparent CV in VF

As shown in figure 7.1 & table 7.1, the apparent CV was homogeneous across the ventricles immediately after VF induction. As all protocols were commenced in control conditions, there were no differences in the baseline apparent CV. During VF in control conditions, the distribution of apparent CV remained homogeneous (Figure 7.1, Table 7.1).

At 480s, the mean percentage change of CV in the LV of $102 \pm 19\%$, was not significantly different from the percentage change of CV in the RV $117 \pm 19\%$.

As clear from figure 7.1, during VF in low-flow ischaemia the CV changed heterogeneously (Table 7.1). In low-flow ischaemia, the mean CV in the LV decreased profoundly to $64 \pm 7\%$ ($p < 0.01$). This was significantly different from the RV ($p < 0.05$) where the CV decreased non-significantly to $89 \pm 5\%$.

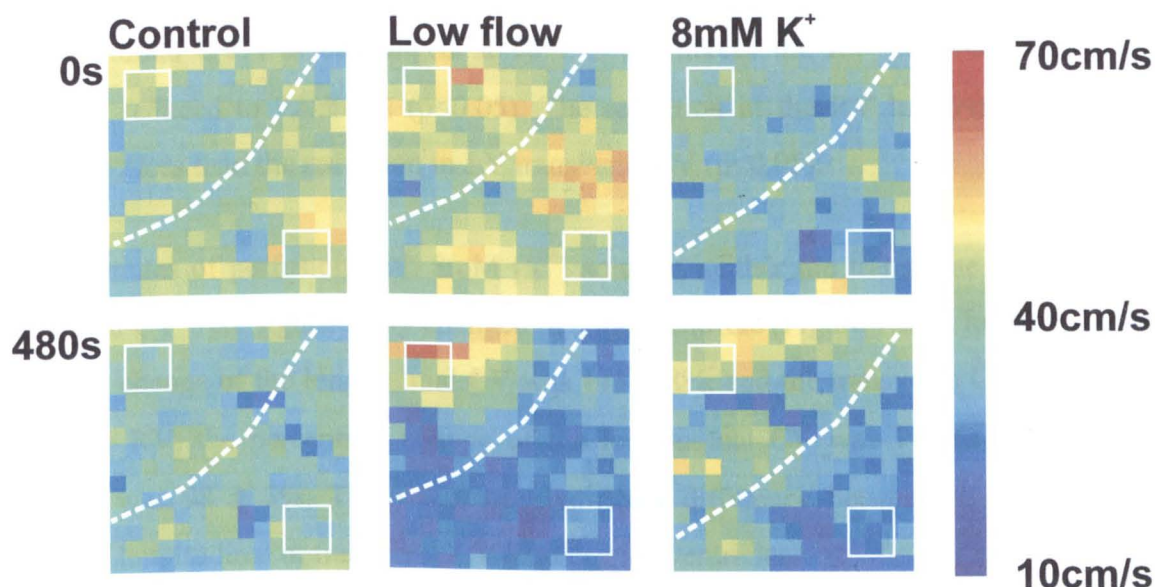


Figure 7.1 Apparent CV in VF. The colour-coded maps represent the CV at the junction of 4 pixels in the photodiode array. The maps represent typical CV maps at 0s and 480s in control, low-flow ischaemia and 8mM [K⁺] solution. The white dotted line delineates the LV/RV border, and the white squares indicate the regions used to derive the mean ventricular CV. At 0s, the CV was homogeneous across the ventricles in all protocols. At 480s, in control VF there was no significant change in either the LV or RV CV compared to 0s. At 480s in low-flow ischaemia, there was profound CV reduction in the LV compared to 0s. In the RV, CV remained unchanged. In 8mM [K⁺] solution, the LV CV was marginally reduced, whilst RV CV remained unchanged at 480s compared to 0s.

Apparent CV (cm/s)	Control (n = 7)	Low-flow (n = 7)	8mM [K ⁺] (n = 4)
LV 0s	36.5 ± 3.1	41.1 ± 3.0	35.1 ± 2.3
LV 480s	32.9 ± 3.1	$25.2 \pm 1.9^{**}$	$29.5 \pm 3.1^*$
RV 0s	34.6 ± 3.1	41.3 ± 2.4	35.9 ± 1.9
RV 480s	36.4 ± 0.6	36.7 ± 2.4	39.5 ± 2.1

Table 7.1 Mean apparent CV at 0s and 480s. During VF in control conditions the apparent CV remained unchanged. During low-flow ischaemia VF, the LV CV decreased (** $p < 0.01$ vs. baseline), whereas the RV CV was unaltered. During raised [K⁺]_{EC}, the LV CV was slightly reduced ($p < 0.05$ vs. baseline). Again the RV CV was unaltered.

During VF in 8mM [K⁺] solution, there was a tendency towards a difference in CV between the LV and RV (Figure 7.1, Table 7.1). Perfusing with 8mM [K⁺] solution caused

a marginal reduction of mean LV CV to $85 \pm 6\%$ ($p < 0.05$), whilst the RV remained unchanged at $112 \pm 9\%$. This difference was not significant ($\#p = 0.09$).

7.3.2 Traditional CV measurements

As clearly shown in figure 7.2A, there was a significant reduction in CV in the LV but not the RV after 6 minutes of low-flow ischaemia. The LV longitudinal CV fell to $69 \pm 8\%*$ and the LV transverse CV reduced to $70 \pm 1\%*$ ($*p < 0.05$ vs. baseline). In comparison, the RV longitudinal CV was unchanged at $98 \pm 2\%$, whereas the RV transverse CV was marginally reduced to $92 \pm 3\%$ ($p < 0.05$). The reduction in the RV transverse CV was significantly less than the reduction in LV transverse CV ($p < 0.05$).

After 6 minutes of perfusion with 8mM $[K^+]$ solution neither the transverse CV nor the longitudinal CV were significantly changed in either ventricle (Figure 7.2B). In the LV, the percentage change of the longitudinal CV was $113 \pm 8\%$, and the transverse CV was $99 \pm 5\%$. In the RV, the percentage change of the longitudinal CV was $117 \pm 7\%$ and the transverse was $98 \pm 5\%$. There was no significant difference between the percentage changes of longitudinal or transverse CV between the ventricles.

7.4 Discussion

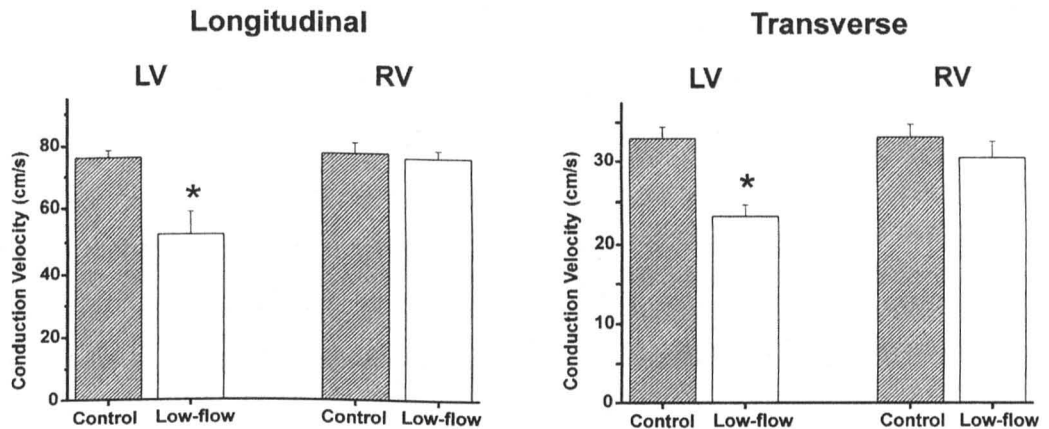
This aim of this chapter was to investigate the role of LV/RV heterogeneity of CV in producing the observed DF heterogeneity in low-flow ischaemia and raised $[K^+]_{EC}$. To do this, CV was assessed in VF (apparent CV) and during epicardial pacing (traditional CV). The CV values obtained in control during traditional CV measurements are in keeping with the current literature. Previous studies have measured the longitudinal CV in the rabbit as widely as 67 ± 4 cm/s (252) to 76 ± 11 cm/s (253). This chapter's mean LV longitudinal CV of 76 ± 3 cm/s lies within this range. The mean LV transverse CV of 33 ± 3 cm/s also compares well with previous measurements in rabbit of ~ 36 cm/s (252, 253).

The role of CV in VF is controversial. Theoretically, slowing of conduction has diametrically opposite effects on VF maintenance depending on whether the driving mechanism is “a mother rotor” or “multiple wavelets” (254). In their paper, Qu et al. predicted that conduction slowing will stabilise a mother rotor and therefore convert VF to VT. The same level of conduction slowing was predicted to reduce the rate of wavelet annihilation, thereby prolong VF duration.

7.4.1 Apparent CV and traditional CV discrepancy

Also controversial is the relationship between CV assessed in VF (apparent CV), and CV assessed during epicardial pacing (traditional CV). As explained fully in chapter 2.6, traditional measurements of CV limit the assessment to the epicardium, and allow assessment of conduction anisotropy that arises from myofibril orientation. In contrast, in VF the spiral waves drift chaotically across the myocardial fibres and myocardial layers. It is interesting that such chaotic pathways give rise to baseline CV in LV of 36.5 ± 3.1 , which is close to baseline transverse CV in the LV of 33 ± 3 cm/s. This suggests that conduction across the fibres rather than along them has more influence in VF.

A 6ml/min



B 8mM [K⁺]

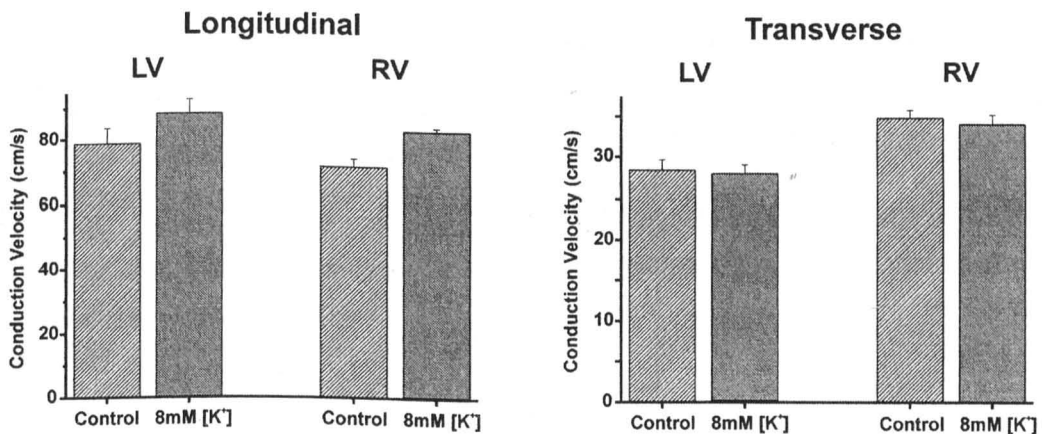


Figure 7.2 Bar plot of absolute traditional CV. Panel A: CV in low-flow ischaemia. Low-flow ischaemia decreased both longitudinal CV* and transverse CV* (* $p < 0.05$). Panel B: CV in 8mM [K⁺]_{EC}. In 8mM [K⁺]_{EC} neither the longitudinal CV nor the transverse CV were significantly altered, though there was a tendency for both to be increased.

Despite this similarity between apparent CV and transverse CV by traditional measurements, these CV assessments responded differently to perfusion with 8mM [K⁺] solution. The apparent CV in the LV was reduced in low-flow ischaemia, and 8mM [K⁺]

solution. The traditional CV in the LV was reduced in low-flow ischaemia, but was unaffected by 8mM $[K^+]$ solution.

One possible explanation for this disparity is the differences in the activation pathways between apparent and traditional CV (Figure 7.3). With epicardial pacing, the excitation travels outwards, through the epicardium, from the point of stimulation (Figure 7.3A). Beyond a certain distance, the epicardium starts to become activated from the underlying intramural myocardium (175). This produces artificially fast epicardial CV. This artefact can be avoided by measuring the CV closer to the activation point. In VF, the activations observed on the epicardial surface can arise from adjacent epicardium or from the underlying intramural myocardium (Figure 7.3B). Attempts to differentiate between these activation pathways from the optical action potential morphology has led to conflicting results (255-257). This, plus the ever-changing nature of the VF activations, means that at present it is not possible to determine the wavefront direction in VF. Therefore the apparent CV in VF could be influenced by electrophysiological changes of the underlying intramural myocardium, which would not influence the traditional CV. The intramural myocardium contains of a distinct population of cells known as "M cells". These M cells have unique electrophysiological properties (258, 259), and are effected differently from epicardial cells by drugs like quinidine (260). It is possible that these M cells undergo different electrophysiological adaptations to raised $[K^+]_{EC}$. However, there is no evidence in the current literature for such differential M cell responses to raised $[K^+]_{EC}$.

Another possible explanation for the disparity between the apparent and traditional CV is the different activation rates of VF and epicardial pacing. In VF, after 60 seconds the LV is activated at c.20Hz. This is equivalent to a BCL of 50s. Such short cycle lengths induce VF within seconds. Therefore it is not possible to assess traditional CV at activation rates equivalent to those experienced in VF. At higher activation rates, the Na channels do not fully recover (261). One would predict that this relative inhibition of I_{Na} would reduce the apparent CV compared to the traditional CV.

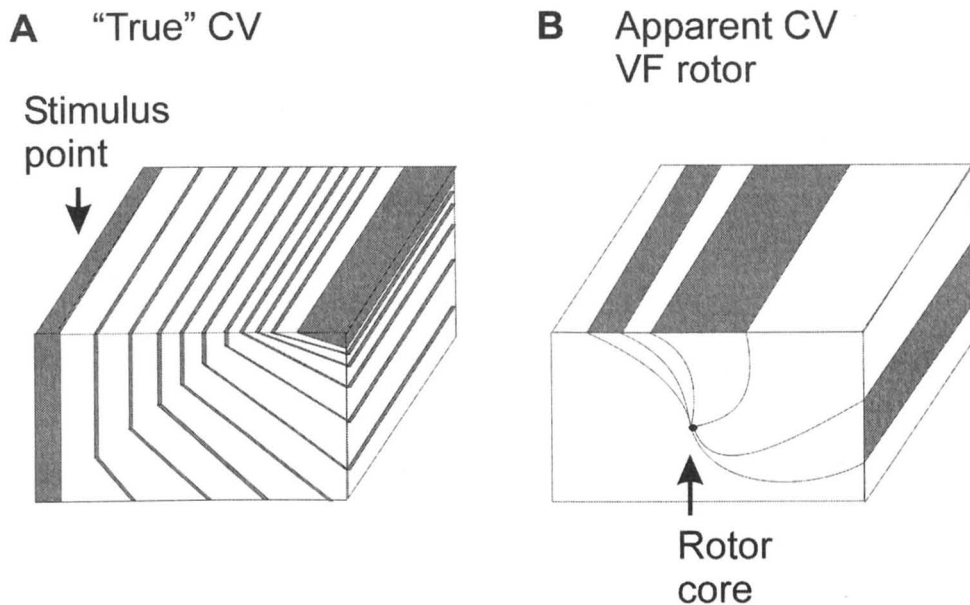


Figure 7.3 Illustration of different pathways of epicardial activation. **Panel A:** Traditional CV – the activation wavefront changes from epicardial to intramural source. As the orientation of the activation changes, the epicardial CV changes (175). From the epicardial surface, the orientation of the underlying wavefront is not easily indiscernible (255-257). **Panel B:** Apparent CV – In VF, epicardial activity is chaotic. The activation could originate from intramural rotors or multiple epicardial wavelets. Here an intramural rotor is illustrated. At present it is impossible to differentiate the activation pathway from optical mapping of the epicardial surface. If raised $[K^+]_{EC}$ affects intramural and epicardial conduction properties differently, this could explain the disparity between traditional and apparent CV.

7.4.2 Traditional CV

Previous research shows that as ischaemia evolves, CV is altered in a biphasic manner (for review see (249)). CV increases in the early stages of ischaemia. This increasing phase lasts for ~2 minutes, and is followed by a progressive decrease in CV. Therefore, at the 6 minute time-point used in this chapter, one would expect the CV to be reduced compared to baseline. Indeed, this chapter demonstrated reductions in the LV longitudinal CV and transverse CV, as assessed through epicardial pacing. However, in the RV, the longitudinal CV was unchanged after 6 minutes of low-flow ischaemia, and the transverse CV was only marginally reduced. This differential reduction of CV in the LV compared to the RV during low-flow ischaemia could explain the heterogeneous DF reduction in LV in VF during low-flow ischaemia. Although several studies have suggested a relationship between DF and CV (67, 70, 189, 262, 263), probably the most convincing study correlates the ECG DF to the rotation rate of the underlying epicardial re-entrant circuits (62). Here, Mandapati et al. showed that the evolving global ischaemia was associated with ECG DF reduction, and that this ECG DF reduction correlated with the decreasing rotational rate of optically imaged re-entrant circuits at that same time-point.

Whilst this chapter's results would support a causal role for CV heterogeneity in determining the DF heterogeneity in low-flow ischaemia, they do not support a role for CV heterogeneity underlying the identical pattern of DF heterogeneity in raised $[K^+]_{EC}$. Assessments of CV by epicardial pacing failed to demonstrate any significant change in CV in 8mM $[K^+]$ solution. If anything, during perfusion with 8mM $[K^+]$ solution, there was a tendency for the longitudinal and transverse CV to increase in both ventricles. Previous experimental and computer studies show a complex relationship between conduction velocity and $[K^+]_{EC}$ (218, 250). Elevating the $[K^+]_{EC}$ above 5mM results in progressive CV increases until a peak is reached at around 8 – 9mM. Elevating the $[K^+]_{EC}$ above this results in slowing of conduction. At c.12mM $[K^+]_{EC}$ the CV falls below baseline levels. Therefore, this chapter's demonstration of a trend towards increasing CV in 8mM $[K^+]_{EC}$ is in keeping with the current literature. Since the LV DF was significantly reduced in 8mM $[K^+]_{EC}$, CV reduction cannot be an underlying cause for DF reduction. This conclusion is supported by previous reports indicating a lack of correlation between CV and DF (241).

8 Changes in the amplitude of the VF signal with time

8.1 Introduction

In VF during low-flow ischaemia, the DF of the ECG and psECG decrease with time (Chapter 3). As previously discussed in chapter 1.1.1.4, both clinical (24, 29) and animal studies (30, 33) show that the decrease in ECG frequency is accompanied by a reduction in the amplitude of the ECG signal. In ischaemia during regular pacing, there is a reduction in amplitude of the action potential (AP) (140, 214, 228, 238, 264). This amplitude reduction is thought to result from multiple electrophysiological alterations in response to several metabolic components. The precise contributions of each of these are uncertain. However, it is possible that the fall in VF amplitude may arise from the same phenomenon.

The alterations in ECG amplitude in VF during full perfusion have not been evaluated. Therefore the contribution of VF itself to the amplitude decline is not known. Also unknown is whether the decrease in amplitude in non-perfused VF is homogeneous across the ventricles, or whether there is LV/RV heterogeneity, in a similar fashion to LV/RV heterogeneity of DF (Chapter 3). Finally, the contribution of hypoxia, acidic pH_{EC} and raised $[K^+]_{EC}$ to the amplitude decline in VF is not known.

This chapter investigates the time-course and spatiotemporal distribution of the amplitude changes in VF during full perfusion (control) and low-flow ischaemia (6ml/min perfusion). Having established this, the contribution of the principal ischaemic components to the amplitude changes and their spatiotemporal distribution will be investigated.

8.2 Methods

The amplitude of the ECG and optical signals during VF was measured using the data sets of chapter 3 & 4 as outlined in chapter 2.5.2. Briefly, locally developed software (Dr F. L. Burton) filtered the signal (polynomial subtraction, low (3Hz) and high pass (50Hz) filters), identified the peaks as points of changed dV/dt direction, and then calculated the peak-to-peak amplitude. The mean peak-to-peak amplitude was calculated for each ECG and optical recording during VF.

Owing to biological variation, the absolute ECG amplitude varied between preparations. For optical signals, this was further compounded by differential illumination within the recording field. At the centre of the optical field, the confluence of the 4 light sources led to greater intensity of illumination than at the periphery. To remove both biological and technical sources of variation, the VF amplitude was assessed by fractional change in the

individual preparations. Whilst it was possible to measure the ECG amplitude in sinus rhythm, it was not possible to measure the optical signal amplitude due to motion artefact. For consistency, the fractional changes in both ECG and optical amplitudes were calculated using the peak-to-peak VF amplitude immediately after induction as a baseline. Comparisons between experimental conditions were made using the mean fractional change over the 7 – 9 minute time interval and the single time-point of 480s. Significance testing with ANOVA showed identical significances for both the 7 – 9 minute time interval and the single 480s time-point. Therefore only the 7 – 9 minute time interval data are detailed to allow comparison with the microelectrode data (Chapter 9).

Owing to the variable location of the LV/RV boundaries within the area of interrogation, the amplitude change in each ventricle was derived from the same standardised 3×3 pixels as used to calculate mean ventricular DF in chapters 3 & 4. As the standardised LV and RV pixel squares were equidistant from the central point of illumination, differential photobleaching was assumed to be negligible. Significance between the ventricles was compared by paired t-test, whilst significances between different parameters were compared using ANOVA.

After initial loading, the fluorescent emission of voltage-sensitive dyes can be affected by variables other than the membrane potential. These variables include dye concentration (i.e. washout), dye internalisation to the inner leaflet of the cell membrane and dye photobleaching (156, 265). A progressive change in any of these variables could result in optical amplitude decline. To investigate the effect of these uncontrollable variables, the spontaneous degradation in the optical amplitude was investigated in non-VF preparations, using optical recordings were made by Dr N. Walker for the purpose of examining LV restitution. These long-term recordings were ideal for examining the change in signal amplitude with time. For this purpose signals were re-analysed in terms of amplitude changes with time. In these experiments, $3\mu\text{M}$ cytochalasin D was administered as per chapter 7.2, to reduce motion artefact. This allowed accurate measurement of AP amplitude during atrial pacing. As ventricular heterogeneity was not the focus of these protocols, the position of the LV/RV boundary was extremely variable and eccentric. This made selection of standardised 3×3 pixel squares in both ventricles impossible, and so the mean ventricular percentage amplitude changes cannot be reported.

8.3 Results

8.3.1 VF amplitude in control conditions

The induction of VF did not alter the ECG amplitude consistently. Compared to the amplitude in sinus rhythm, on VF induction individual preparations experienced either (i) an increase in ECG amplitude (as occurred in 21 of the 51 protocols, 41%), or (ii) a decrease in ECG amplitude (as occurred in the other 30 protocols, 59%). For all preparations the mean fractional change in ECG amplitude on inducing VF was 1.3 ± 0.2 (range 0.6 – 2.4), which was not significant. As VF continued, the ECG amplitude decreased (Figure 8.1A). Therefore, all changes were calculated as a fraction of initial VF amplitude, rather than a fraction of sinus rhythm amplitude.

As shown in figure 8.1A, in VF during control conditions (40ml/min, $n = 7$), the ECG amplitude fell over the first 4 minutes (240s). After 4 minutes the ECG amplitude did not change greatly, but rather approximated around a steady state value of ~55% of baseline. Comparing the changes of ECG amplitude with that of ECG DF showed reciprocal patterns (Figure 8.1C). In VF during full perfusion, the ECG DF increased to a peak at 3 minutes (210s), before slightly slowing to a steady state by 4 minutes (Chapter 3.3.1).

During VF in control conditions, the psECG amplitude declined more markedly than the ECG amplitude over the first 4 minutes to ~45% (Figure 8.1B). After 4 minutes, the psECG amplitude continued to decline, but at a slower rate. This slower decline was almost parallel to that observed in RA pacing (Figure 8.2).

Spatiotemporally, the reduction in optical amplitude was not homogeneous across the anterior surface of the heart (Figure 8.1D). Rather, there was a more profound amplitude reduction in the LV than the RV (Table 8.1). This LV/RV heterogeneity in amplitude reduction was not observed during regular atrial pacing. Figure 8.2A shows that during RA pacing ($n = 4$), the psECG amplitude declined in a more linear fashion. Using Origin 7.0 (OriginLab Corporation, MA, USA), the data was fitted to $y = mx + c$. Superimposing this best-fit line onto the psECG amplitude time-course during fully perfused VF, demonstrated a good fit for the slower amplitude reduction that occurred after 5 minutes. This suggests that the continued slow reduction in psECG amplitude is consistent with dye degradation. Indeed, correcting the psECG amplitude for dye degradation resulted in identical fractional changes to those in the ECG amplitude (Figure 8.2B). During RA pacing, the fractional

reduction in optical signal amplitude was homogeneous across the area of interrogation (Figure 8.2C). This suggests that signal degeneration occurs in a homogeneous fashion within the ventricles.

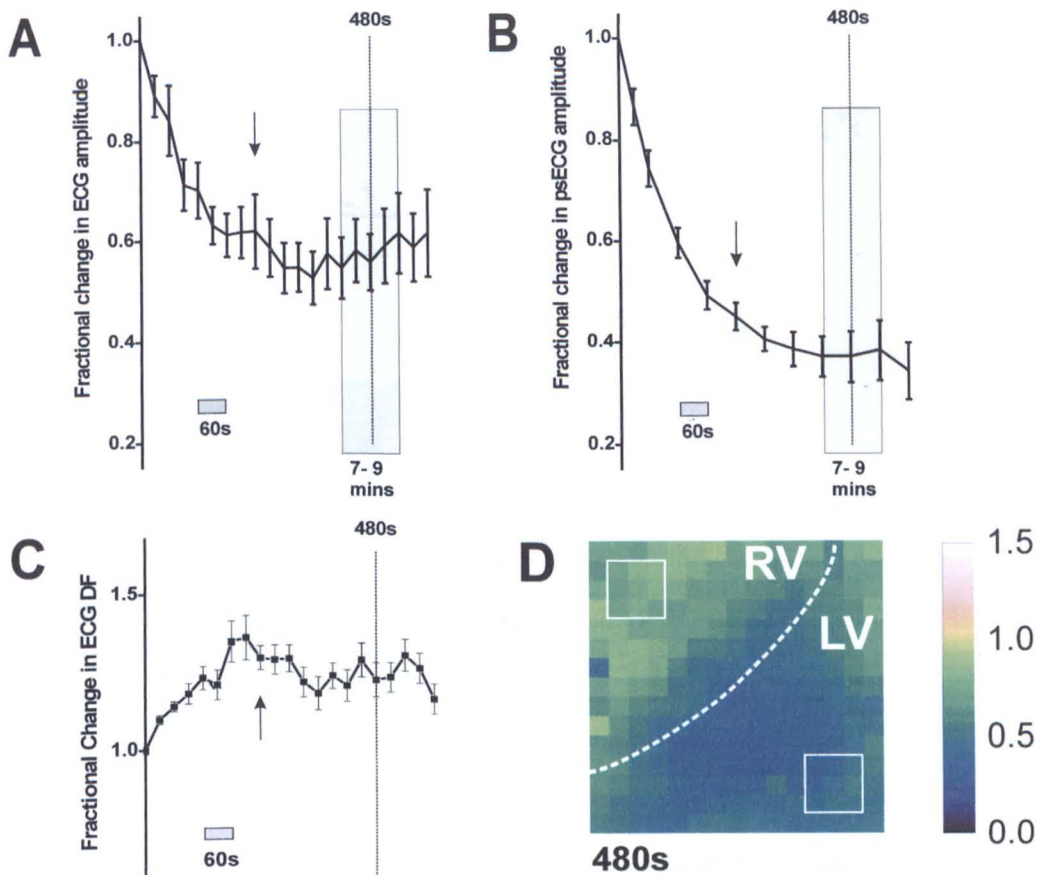


Figure 8.1 Amplitude and DF changes during VF under control conditions (n = 7). Panel A: Plot of changes in ECG amplitude with time. The mean fractional change in ECG amplitude was calculated using ECG amplitude immediately after VF induction as baseline. The ECG amplitude decreased for the first 4 minutes (arrow = 240s). After this the ECG amplitude stabilised at a level of ~55%. Panel B: Plot of change in psECG amplitude with time. Again there was an initial period of marked amplitude reduction over the first 4 minutes (arrow). By this point the psECG amplitude had reduced to ~45%. After this the psECG amplitude continued to decrease but at a slower rate. This continued amplitude reduction could be explained by dye degradation (Figure 8.2). Panel C: Plot of changes in ECG DF with time. The rapid decrease in amplitude coincided with the initial increase in DF (arrow = 240s). After this both amplitude and DF stabilised. Panel D: Colour map of the fractional change in amplitude in each pixel at 480s. The optical signal amplitude has decreased more markedly in the LV than in the RV (dotted white line = LV/RV boundary, white squares = standardised areas for determining mean ventricular fractional changes).

Amplitude (%)	Control	Low flow	0% PO ₂	pH6.7	pH6.3	8mM K ⁺	10mM K ⁺
LV	33±5**	32±3	27±6***	45±8	20±6***	60±15	86±13
RV	63±8**	49±9	59±11***	56±5	55±4***	100±15	91±16

Table 8.1 Percentage change in VF amplitude in LV and RV. In control, pH 6.3 and 0%PO₂, the LV amplitude experienced more profound amplitude reductions than the RV (**p<0.01, ***p<0.001). Experimental protocol results for fractional change in optical amplitude in the LV can be divided into 2 groups: - (i) LV amplitude reduction that was equivalent to control – pH 6.7, pH 6.3, low-flow ischaemia and 0% PO₂, and (ii) LV amplitude reduction that was less than control – raised [K⁺]_{EC}. This only reached significance in 10mM (p<0.05). The fractional change of amplitude in the RV was similar in all protocols.

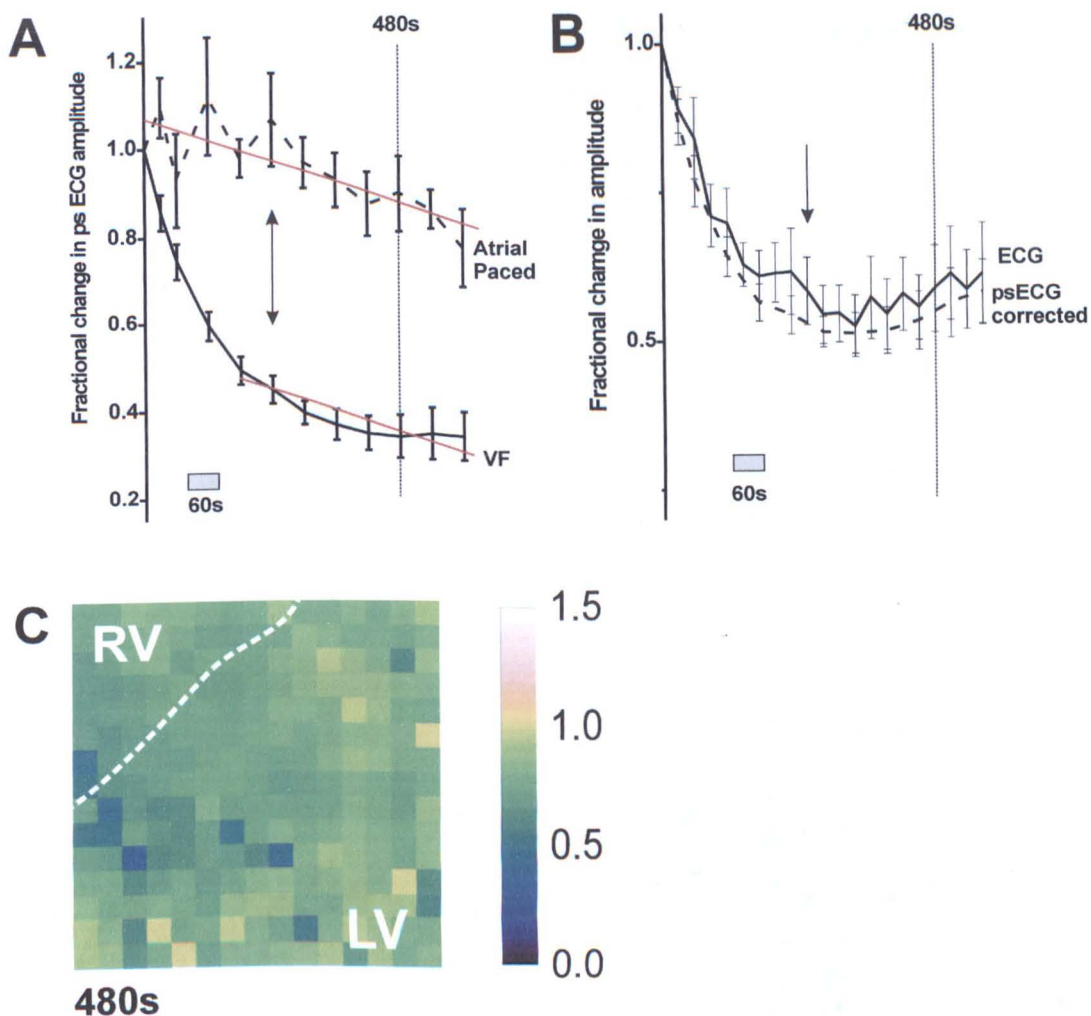


Figure 8.2 Effects of dye degradation on optical signal amplitude. Panel A: Plot of change in ps ECG amplitude with time during atrial pacing and during VF in control conditions. In RA paced hearts, the ps ECG amplitude decreased in a more linear fashion. This amplitude reduction is probably due to a combination of dye washout, internalisation and photobleaching. The superimposed red line is the best linear fit ($y = mx + c$) as determined by Origin 7.0. In VF, the ps ECG amplitude decreased rapidly until 240s (arrow), and then decreased more slowly. This secondary phase of amplitude decline runs almost parallel to the best-fit line of the amplitude changes during right atrial pacing. Panel B: Plot of amplitude changes in ECG and corrected ps ECG. The ps ECG was corrected for dye degradation using the linear fit equation from panel A. The changes in ECG and corrected ps ECG amplitude overlap. This suggests that the secondary decline in the ps ECG is due to dye degradation. Panel C: Colour map of the fractional change in amplitude during RA pacing after 480s. In RA pacing, the optical signal amplitude was only marginally reduced. This optical amplitude reduction occurs homogeneously across the area of interrogation.

8.3.2 VF amplitude in low-flow ischaemia

In figure 8.3, the ECG and ps ECG show similar patterns of amplitude change in VF during the low-flow ischaemia. On reducing the flow rate to 6ml/min, there was an immediate increase in the ECG and ps ECG amplitude that reached a peak at 120s. This amplitude increase coincided with an initial decline in ECG DF (Figure 8.3C). Optical mapping at this 120s time-point showed an increase in the LV amplitude (Figure 8.3D).

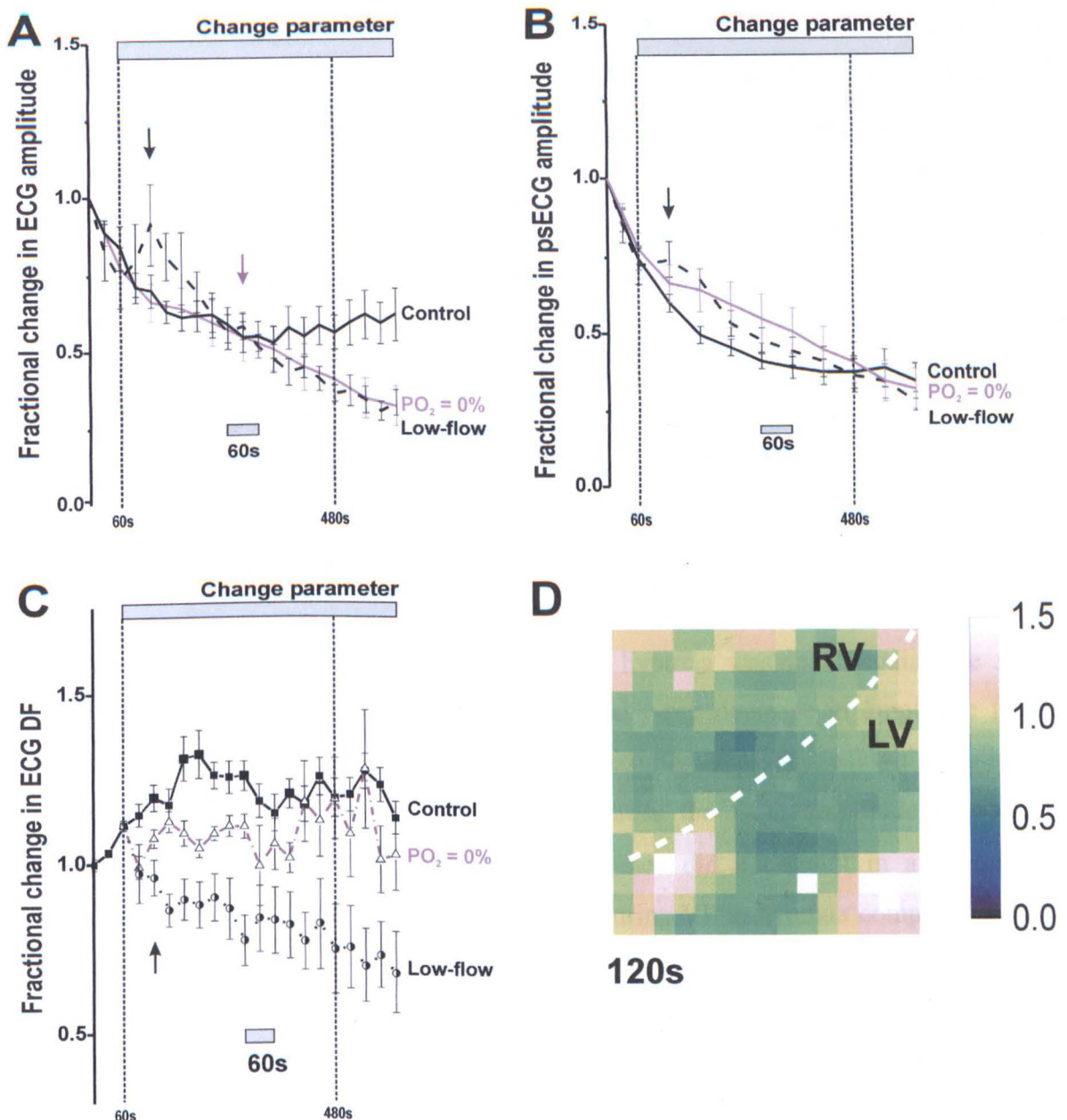


Figure 8.3 Amplitude changes during VF in low-flow ischaemia ($n = 7$) and hypoxia ($n = 6$). Panel A: Changes in ECG amplitude with time. In low-flow, the ECG amplitude increased until 120s (black arrow). After this, the amplitude steadily declined. Although the amplitude reduction tended to be greater than control, this was not statistically significant over the 7 – 9 minute assessment interval. During hypoxia, the ECG amplitude declined in a manner indistinguishable from control until 4 minutes (magenta arrow = 280s). After this the ECG amplitude continued to decrease but did not become significantly different from control amplitude change. Panel B: Changes in psECG amplitude with time. With the exception of the initial amplitude increase immediately on flow reduction, the psECG amplitude changed in a similar manner in both hypoxia and low-flow ischaemia, and was indistinguishable from psECG amplitude changes in control conditions. Panel C: Changes in ECG DF with time. The transient increase in ECG and psECG amplitude from 60 – 120s coincided with a marked decrease in DF (arrow). Panel D: The colour-coded map displays the fractional change in optical VF amplitude in each pixel. This map illustrates the typical findings at 120s during low-flow ischaemia (black arrow in panels A – C). This shows that the LV amplitude was increased compared to the baseline optical amplitude taken immediately after VF induction (white dotted line = LV/RV boundary).

After the peak at 120s, the ECG and psECG amplitudes decreased in a near linear fashion until the protocol end at 600s (Figures 8.3A & B). Although after 120s in low-flow

ischaemia the ECG amplitude continued to decline, over the assessment interval of 7 – 9 minutes the mean fractional change in ECG amplitude in VF during low-flow ischaemia of 0.38 ± 0.04 was not significantly different from that in control conditions of 0.57 ± 0.06 . The psECG amplitude declined steadily in a manner that is indistinguishable from the control. Over the 7 – 9 minute period, the mean fractional change in psECG amplitude of 0.35 ± 0.04 was not significantly different from that in control of 0.37 ± 0.04 .

In low-flow ischaemia, the spatiotemporal distribution of the fractional amplitude change at 480s was also not significantly different from control, although there was a tendency for a greater reduction in RV optical amplitude (Figure 8.4 (i), Table 8.1).

8.3.3 VF amplitude in hypoxia

The initial progression of ECG VF amplitude in hypoxia was indistinguishable from control (Figure 8.3A). In both, there was an initial rapid decrease in amplitude for 4 minutes. After this the curves diverged, as hypoxia was associated with continued reduction of ECG amplitude to 0.47 ± 0.11 , whereas the ECG amplitude in control conditions stabilised to 0.57 ± 0.06 . This divergence did not result in a significant difference between the ECG amplitude reductions during VF in hypoxia compared to that during control.

The psECG amplitude in VF during hypoxia showed no divergence from the amplitude changes of VF during control conditions (figure 8.3B). Over 7 – 9 minutes the psECG amplitude in hypoxia fell to 0.4 ± 0.07 compared to the control psECG amplitude reduction of 0.37 ± 0.04 .

The spatiotemporal distribution of the amplitude change during hypoxia was indistinguishable from control with a similar degree of LV and RV amplitude reduction (Table 8.1, Figure 8.4(i)).

8.3.4 VF amplitude in acidic pH_{EC}

As is clear from figure 8.5, in VF during acidic pH_{EC} there was great variability in the ECG amplitude changes. However, over the 7 – 9 minute assessment period, the ECG amplitudes stabilised at 0.71 ± 0.1 in pH 6.7 and 0.55 ± 0.08 in pH 6.3. Neither of these

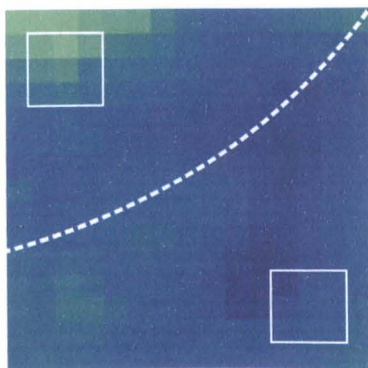
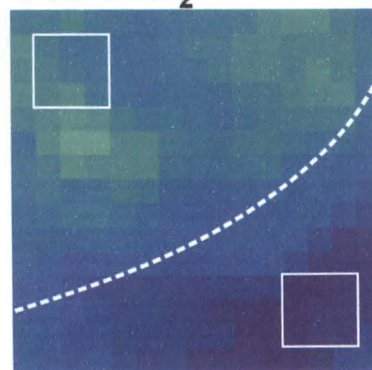
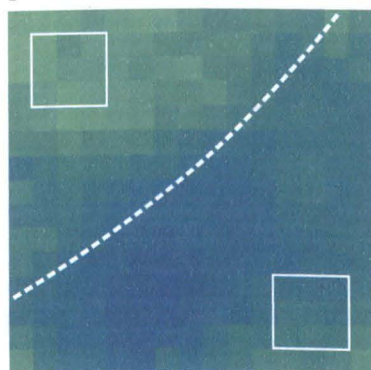
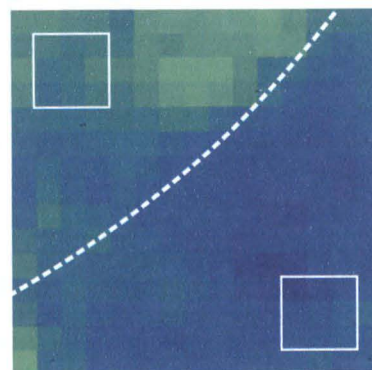
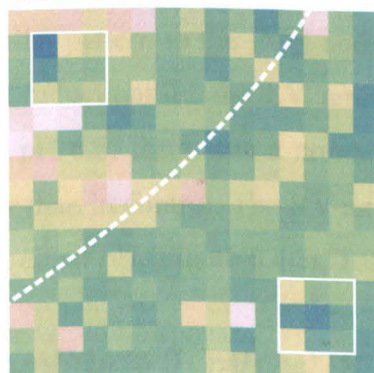
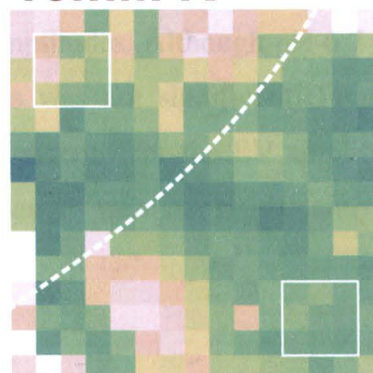
(i) Low-flow**0% PO₂****pH 6.7****pH 6.3****(ii) 8mM K⁺****10mM K⁺**

Figure 8.4 Colour-coded maps of fractional change in optical signal amplitude during VF. These maps show typical spatiotemporal distribution of amplitude change during VF at 480s. The changes are expressed as a fraction of the corresponding site's amplitude immediately after VF onset. The arrangements fall into 2 groups compared to control VF (Figure 8.1C): - (i) Similar or slightly greater reduction in VF amplitude compared to control VF (Figure 8.1C): - (i) Similar or slightly greater reduction in VF amplitude – low-flow, hypoxia and acidic pH_{EC}. (ii) Lesser reduction in VF amplitude with no significant change in LV or RV amplitude – raised [K⁺]_{EC}. (White dotted lines = LV/RV boundary, white squares = standardised areas to determine ventricular optical amplitude).

The psECG amplitude showed less variability in VF during acidic pH_{EC}. Although the psECG amplitude fell less in pH6.7 to 0.54 ± 0.06 , this was not significantly different

from the control reduction of 0.37 ± 0.04 (Figure 8.5). For pH 6.3, the psECG amplitude decline to 0.4 ± 0.04 was also indistinguishable from that of control.

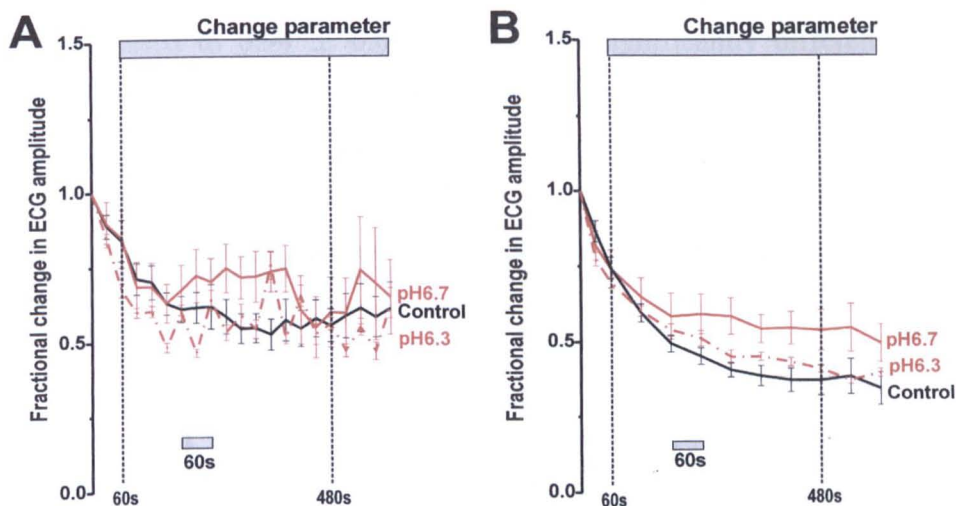


Figure 8.5 ECG and psECG amplitude during VF in acidic pH_{EC} . Panel A: Changes in ECG amplitude with time – Although highly variable, neither pH 6.7 ($n = 8$) nor pH 6.7 ($n = 7$) altered the amplitude reduction compared to control. Panel B: Changes in psECG amplitude with time – again the amplitude reduction at both pH levels was not significantly different from control.

Looking at the spatiotemporal distribution of the amplitude changes, the LV amplitude followed a similar pattern to the ECG and psECG amplitudes. Although pH 6.7 tended to produce lesser reductions in the LV amplitude, this was not significant (Figure 8.4(i), Table 8.1). At pH 6.3, there was a non-significant tendency for the LV amplitude to be reduced greater than in control. The RV amplitude changes were not significantly different from control at either pH (Figure 8.4(i), Table 8.1).

8.3.5 VF amplitude in raised $[K^+]_{EC}$

During VF in raised $[K^+]_{EC}$, the ECG amplitude initially decreased to a trough of 0.77 ± 0.09 in 8mM $[K^+]_{EC}$ and 0.49 ± 0.04 in 10mM $[K^+]_{EC}$ at 210s (Figure 8.6A). This was not significantly different from the fractional change of 0.62 ± 0.05 in control conditions at the same time-point. Similarly, the psECG amplitude decreased to a trough of 0.67 ± 0.08 in 8mM $[K^+]_{EC}$ and 0.60 ± 0.04 in 10mM $[K^+]_{EC}$ at 180s (Figure 8.6B). Again neither of these reductions were significantly different from the fractional psECG amplitude change in control conditions of 0.49 ± 0.03 . After the respective troughs, there was a steady increase in ECG and psECG amplitude in both raised $[K^+]$ solutions. In 8mM $[K^+]$ solution, the ECG amplitude had increased to 1.05 ± 0.13 at 7 – 9 minutes. This was significantly different from the control ECG fractional change of 0.57 ± 0.06 (** $p < 0.01$).

The psECG amplitude increased to 0.78 ± 0.09 in 8mM $[K^+]_{EC}$ solution compared to the change in control of 0.37 ± 0.04 ($***p < 0.001$). In 10mM $[K^+]_{EC}$ solution, the ECG amplitude increased to 0.87 ± 0.15 , which was not significantly from control. However, the psECG increased to 0.94 ± 0.09 that was significantly different from control ($***p < 0.001$). Neither the ECG nor the psECG amplitude changes were significantly different in 8mM $[K^+]_{EC}$ solution compared to 10mM $[K^+]_{EC}$ solution.

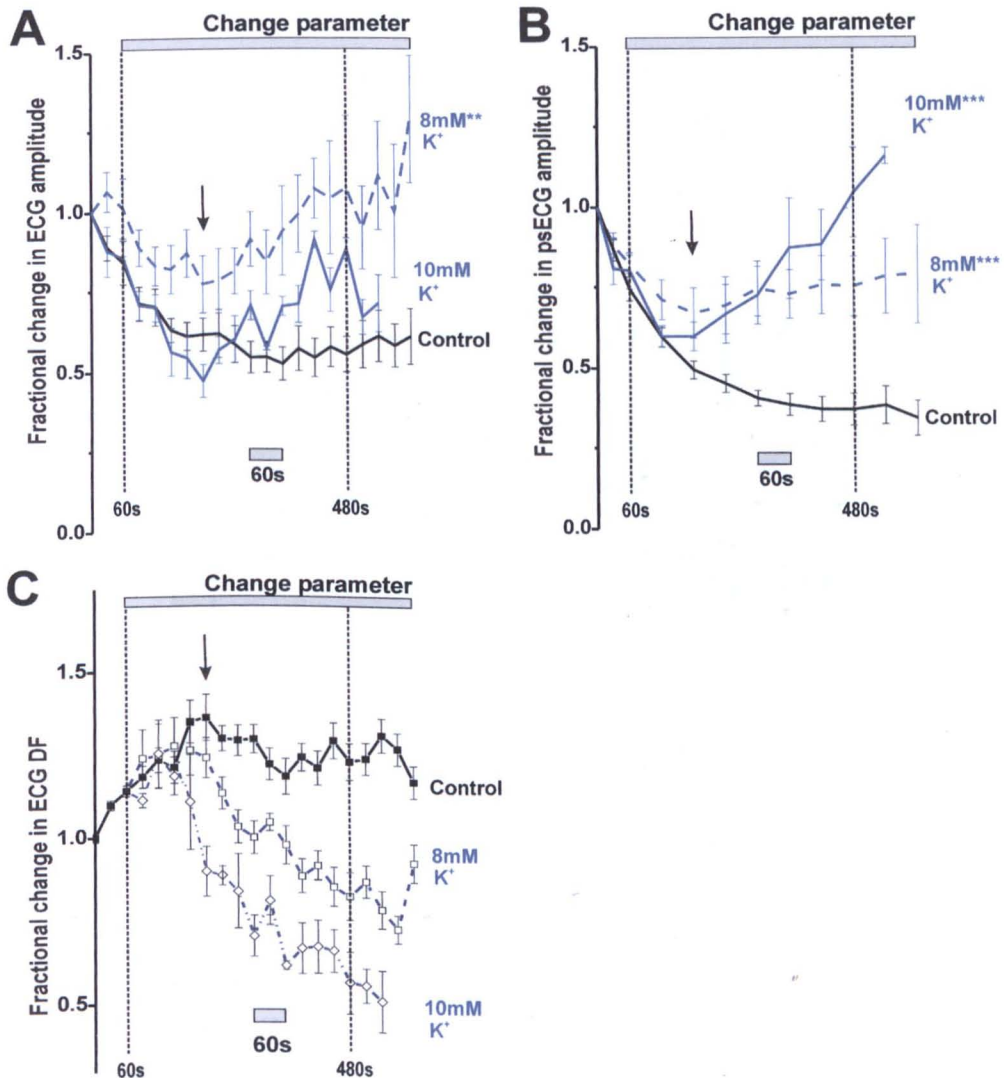


Figure 8.6 ECG and psECG amplitude during VF in 8mM ($n = 6$) and 10mM ($n = 5$) $[K^+]_{EC}$ solutions. **Panel A:** Changes in ECG amplitude with time – in raised $[K^+]_{EC}$ the ECG amplitude decreased until 210s (arrow). After 210s, the ECG amplitude increased in both 8mM^{**} and 10mM $[K^+]_{EC}$ ($**p < 0.01$). **Panel B:** Changes in psECG amplitude with time – Similar patterns of amplitude change was observed in psECG as ECG. An initial decrease in amplitude to 180s (arrow), was followed by steady increases in both 8mM^{***} and 10mM^{***} $[K^+]_{EC}$ ($***p < 0.001$). **Panel C:** Changes in ECG DF with time – In raised $[K^+]_{EC}$ the period of VF amplitude decline was associated with increasing DF (till arrow). The rising amplitude thereafter was associated with decreasing DF.

The amplitude changes were almost reciprocal to the fractional changes in ECG DF in raised $[K^+]_{EC}$. The initial fall in amplitude was associated with the initial increase in DF (Figure 8.6C). The following increase in amplitude was associated with decreasing DF.

In raised $[K^+]_{EC}$, the spatiotemporal amplitude alterations were also different from those observed during VF in control conditions (Table 8.1, Figure 8.4(ii)). At 480s, the RV amplitude was maintained in both raised $[K^+]_{EC}$ protocols. At 480s in 10mM $[K^+]_{EC}$, the LV amplitude had decreased to a lesser extent than in control ($p < 0.05$) or in 8mM $[K^+]_{EC}$ ($p < 0.001$) (Table 8.1).

The spot analysis at 480s does not give a full impression of the spatiotemporal changes of optical amplitude that occurred during VF in raised $[K^+]_{EC}$. Looking at the fractional change maps each minute reveals that the RV amplitude was essentially unchanged throughout the 8mM and 10mM $[K^+]_{EC}$ protocols (Figure 8.7), whereas the LV amplitude declined until 240s (Figure 8.7B), before increasing (Figure 8.7C). This progression is similar to that observed in the psECG amplitude (Figure 8.6B).

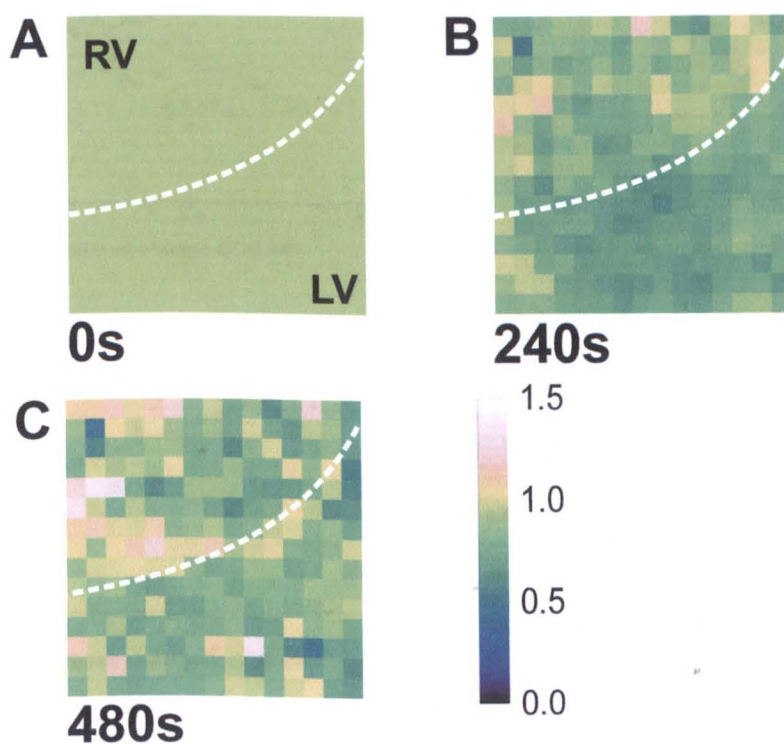


Figure 8.7 Spatiotemporal progression of amplitude during VF in 8mM $[K^+]_{EC}$ solution. Panel A: 0s – As the amplitude changes were normalised to the amplitude at 0s, this colour map is uniform = 1. Panel B: - 240s – the LV amplitude has reduced, whereas the RV remains largely unchanged. Panel C: - 480s – the LV amplitude has increased compared to 240s (panel B). Again the RV amplitude was largely unchanged.

8.3.6 Relationship between amplitude and DF

The above results suggest that during VF, an inverse relationship exists between the amplitude changes and the changes in DF. For example, in control, hypoxia and acidic pH_{EC} , the increasing DF was associated with decreasing ECG and psECG amplitudes. Whereas in raised $[K^+]_{EC}$, and transiently in low-flow ischaemia, the decreasing DF was

associated with an increase in VF amplitude. To investigate this relationship further, the ECG and psECG fractional amplitude changes and fractional DF changes were plotted as scattergrams, and fitted with $y = mx + c$ using Origin 7.0 (Figure 8.8). For control, hypoxia, acidic pH_{EC} and raised $[K^+]_{EC}$, the individual scattergrams displayed negative correlations between the fractional changes in VF amplitude and DF (data not shown). Combining these protocols into a single scattergram for ECG (Figure 8.8A) and psECG (Figure 8.8B) confirmed the inverse relationship. The more complex temporal changes that occur during VF amplitude in low-flow ischaemia did not correlate negatively with VF DF (Figures 8.8C & D).

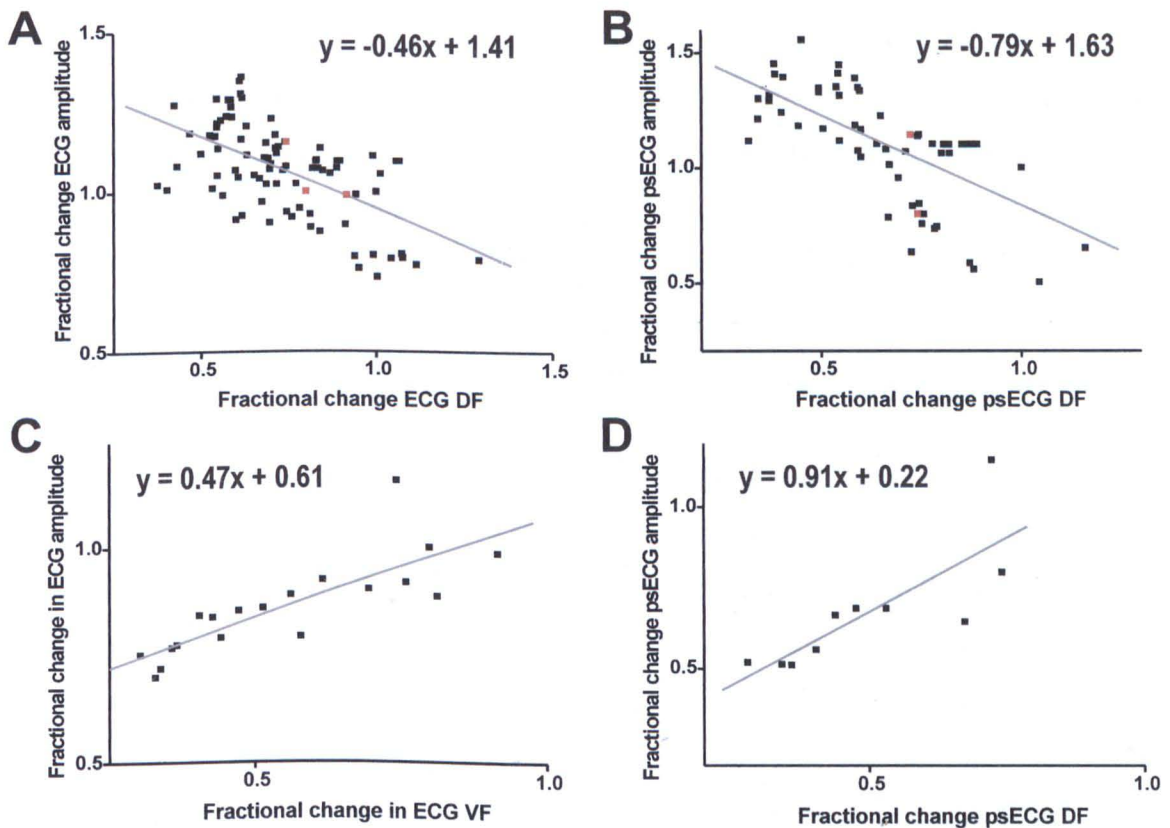


Figure 8.8 Scattergrams of fractional change in VF amplitude against fractional change in VF DF. Panel A: ECG – Scattergram of the fractional change of ECG amplitude against the fractional change of ECG DF during control, hypoxia, acidic pH_{EC} , raised $[K^+]_{EC}$ and selected points during low-flow ischaemia (■ = low-flow 60 – 120s only). This shows an inverse relationship between fractional changes in amplitude and DF during VF. Panel B: psECG – the similarly created scattergram for psECG also demonstrates an inverse relationship between amplitude and frequency (■ low-flow ischaemia). Panel C: ECG in low-flow ischaemia. This scattergram of the fractional change in ECG amplitude vs. fractional change in ECG DF in VF during low-flow ischaemia contains data of all time-points. The more complex temporal changes in VF amplitude that occurs during low-flow ischaemia results in a direct relationship between amplitude and frequency. Panel D: psECG in low-flow ischaemia demonstrates a similar direct relationship to the ECG (Panel C).

8.4 Discussion

The aim of this chapter was to study the global and spatiotemporal changes in VF amplitude with time during full perfusion and low-flow ischaemia, and to examine the contribution of hypoxia, acidic pH_{EC} and raised $[\text{K}^+]_{\text{EC}}$ to these changes.

8.4.1 VF amplitude in control conditions

In VF during fully perfused control conditions, the amplitude of the ECG decreased in a non-linear fashion. An initial period of rapid amplitude reduction was followed by stabilisation at ~55% (Figure 8.1A). The ECG gives a global assessment of the electrical activity of the heart, and as such a reduction in its amplitude could represent (i) a homogeneous decrease in the amplitude of the electrical activations across the heart, (ii) heterogeneous changes or (iii) no real decrease in the amplitude of the electrical activations, but rather an increase in electrical disorganisation, as is known to occur in fully perfused VF (266). With increased disorganisation, the local electrical vectors will increasingly oppose each other, and will therefore reduce the electrical amplitude measured at a global level.

The reduced electrical co-ordination of VF compared to sinus explains the immediate reduction in the ECG amplitude on VF induction that occurred in 59% of experiments. Less clear is the reason for the increase in ECG amplitude at induction that occurred in the other 41% of experiments. In sinus rhythm, hearts were compressed in an attempt to eliminate motion artefact from the optical signals (Chapter 2.4). In the hypo-contractile state of VF lesser degrees of compression were required to do this. The greater compression required in sinus rhythm was produced by greater displacement of the chamber's back piston (Figure 2.2), and resulted in a physical movement of the heart relative to the fixed wall-mounted ECG electrodes. This tended to move the heart out of the line of the fixed electrodes, and so may explain an artificial increase in ECG amplitude on VF induction, as lesser degrees of compression kept the heart more in-line with the fixed ECG electrodes.

Although the psECG is also a global measure of electrical activity, its amplitude change is derived from the amplitude changes recorded in each of the 252 photodiodes. Each photodiode records the electrical activity from a small epicardial area (0.8 mm × 0.8 mm). Therefore, vector alignment does not influence the amplitude of the optical signals in VF. As the psECG amplitude decreased in a similar non-linear manner as the ECG amplitude, this would suggest that the decrease in the electrical activation amplitude was real (Figures

8.1A & B). Although there were differences between the ECG and psECG amplitude changes, with the psECG experiencing a more profound initial amplitude reduction, and continuous slower amplitude decline, these differences could be accounted for by dye degradation (Figure 8.2).

Optically mapping VF during control conditions revealed that the reduction in activation amplitude was heterogeneous with more profound amplitude reduction in the LV than the RV (Figure 8.1C). The ventricular nature of this heterogeneity in amplitude reduction is reminiscent of the LV/RV heterogeneity in DF, where in control conditions the LV DF increased, whilst the RV DF remained unchanged (Chapter 3). The proposed mechanism of DF heterogeneity (Chapter 3.4.3) may also explain the LV/RV heterogeneity in VF amplitude changes. The greater LV-to-RV expression of Kir2.x results in a greater magnitude of I_{K1} within the LV, allowing faster frequencies to develop (63, 190). This greater magnitude of I_{K1} will oppose I_{Na} to a greater extent. If the I_{Na} magnitude is the same in both ventricles, the greater I_{K1} magnitude in the LV will result in lower levels of depolarisation on activation in the LV compared to the RV (i.e. a lower systolic depolarisation). To date there is no evidence to support this hypothesis.

Another possible mechanism for the LV/RV heterogeneity in amplitude changes is differential perfusion of the LV compared to the RV. Studies in dogs (199) and rats (200) have shown differences in the control of the vascular tone in the right and left coronary arteries. In the dog, Quail et al. demonstrated lesser degrees of vasodilatation in the left then the right coronary arteries in response to increased aortic pressure (199). During VF in control conditions, the perfusion rate was maintained at 40ml/min. However, the aortic pressure tended to increase from ~40mmHg in sinus rhythm to ~50mmHg immediately after VF induction (as these values were not recorded, no further analysis is possible). Therefore, during VF in control conditions, one would predict lesser vasodilatation of the LV vascular bed. Such lesser vasodilatation could produce a relative ischaemia in the LV compared to the RV.

In VF, the rapid activation rates lead to enhanced energy consumption (267, 268). In the presence of localised ischaemia, this enhanced energy consumption could outstrip energy production, and result in the loss of maintenance of membrane ionic gradients. Under such circumstances, the resting (diastolic) membrane potential becomes depolarised (81, 140). Such diastolic depolarisation could reduce the optical amplitude by (i) reducing the excursion to AP plateau and (ii) by reducing the number of active Na channels, and thus the magnitude of I_{Na} (269).

Optical mapping detects relative changes in fluorescence, and therefore indicates relative changes in membrane potential. The absolute membrane potential cannot be inferred. Therefore, it is impossible to distinguish by optical mapping between amplitude reductions secondary to diastolic depolarisation from reductions due to reduced systolic depolarisation. Such differentiation requires measurement of the absolute transmembrane potential, as can be achieved with floating microelectrodes (Chapter 9).

8.4.2 VF amplitude in low-flow ischaemia

As outlined in this chapter's introduction, both clinical (19, 24, 29) and animal studies (30, 33) have shown a reduction in ECG amplitude during VF when cardiac perfusion is not maintained. Similarly, this chapter demonstrates a reduction of ECG and psECG amplitude in VF during low-flow ischaemia. However, on reducing the perfusion rate, the ECG, psECG and LV optical amplitude transiently increased (Figure 8.3). Two possible explanations for this initial increase in amplitude are: -

- (i) Hyperpolarisation – as discussed more fully in section 8.4.4 below, low levels of intracellular acidosis hyperpolarise the resting membrane potential (219). Such hyperpolarisation should increase the amplitude of VF activations, as tended to occur in pH 6.7 (Figures 8.4 & 8.5, Table 8.1). In no-flow ischaemia, the myocardial pH decreases in an exponential fashion with time (270). Thus any hyperpolarisation will be transient, as the pH falls to levels that depolarise the resting membrane potential (219).
- (ii) Increased electrical co-ordination – in global ischaemia, VF becomes more co-ordinated (36, 62, 271, 272). Such co-ordination could give rise to an apparent increase in amplitude. This increased co-ordination could have been caused by raised $[K^+]_{EC}$, which will be discussed more fully in section 8.4.5.

Following this transient increase, the ECG, psECG and LV amplitudes declined steadily (Figure 8.3). However, each of these amplitude reductions differed in their relationship to the relative VF amplitude changes in control conditions. For instance, in control conditions the ECG amplitude stabilised at 4 minutes, where the ECG amplitude in low-flow continued to decrease. This is in keeping with the continuous reduction of AP amplitude that occurs in ischaemia during regular pacing (140, 214, 228, 238, 264). More difficult to explain is the equivocal effect of low-flow ischaemia on the amplitude reduction of the psECG and LV optical signals compared to control. One possible explanation is the effect of the signal-to-noise ratio on lower amplitude optical signals. In optical mapping, the

signal-to-noise ratio depends on many factors from magnification (see Chapter 1.3.5) to dye degradation (150). In a given optical system, the signal-to-noise ratio is fairly stable over time, experiencing only a slow exponential decline with a time constant in the order of 75 minutes (273). Even with a stable signal-to-noise ratio, the artefacts are greater in lower amplitude than higher amplitude signals. In VF, the amplitude of the optical signal markedly decreased, with psECG amplitude falling to <45% after 5 mins. At such low levels of absolute change in fluorescence, the greater effect of signal noise could obscure any true difference in psECG and LV amplitude in low-flow ischaemia compared to control.

8.4.3 VF amplitude in hypoxia

Although solutions were changed after 60s of VF, the 90% transition did not occur at the heart until 180s (Figure 4.1). At this point, in contrast to VF in low-flow ischaemia, there was no initial increase in ECG or psECG amplitude on lowering the PO_2 . Instead, during hypoxia there is a steady decline in both the ECG and psECG amplitudes (Figure 8.3). Possible explanations for this difference are: - (i) lack of hyperpolarisation – unlike acidosis, reductions of the intracellular PO_2 are not associated with a transient hyperpolarisation phase (202, 204, 211), or (ii) lack of increased organisation – as shown in figure 4.2, neither the ECG nor psECG DF changed dramatically on application of hypoxia. This would suggest that in hypoxia, VF remained rapid and disorganised.

As with VF in low-flow ischaemia, during hypoxic VF the ECG amplitude did not stabilise, but continued to decline. Also similar to low-flow ischaemia, the psECG and LV amplitude reductions in VF during hypoxia were indistinguishable from control. Again the greater influence of noise on the lower amplitude signals could be obscuring further amplitude reductions.

As discussed in chapter 4.4.3, previous research into the effects of hypoxia on the resting membrane potential and AP amplitude have shown variable results. The major source of this variation appears to relate to each study's method of perfusing their preparation, and the inherent effect on K^+ accumulation and $[K^+]_{EC}$, rather than the level of PO_2 . For example, in continuously superfused cellular preparations, K^+ could not accumulate and the diastolic potential and AP amplitude remained virtually unchanged during an hour of hypoxia (202). Similarly, in Langendorff-perfused whole heart (204) and papillary muscle preparations (203, 214) at 5mM $[K^+]_{EC}$, after 10 minutes of hypoxia the diastolic membrane potential depolarised by <2mV, and the AP amplitude remained virtually

unchanged. In contrast, in regional hypoxia in Langendorff-perfused pig hearts Morena et al. documented $\sim 10\text{mV}$ diastolic depolarisation, and moderate amplitude reduction for any given $[\text{K}^+]_{\text{EC}}$ (211).

So in fully perfused, hypoxic VF in the Langendorff-perfused rabbit heart, one would expect only a marginal increase in $[\text{K}^+]_{\text{EC}}$ compared to control. It is uncertain if such small increases in $[\text{K}^+]_{\text{EC}}$ would be sufficient to partially depolarise the membrane, and therefore reduce the VF amplitude. This could not be investigated by floating microelectrode, as preparations were continuously superfused in this apparatus and the bathing solution was open to the room environment (Chapter 9).

8.4.4 VF amplitude in acidic pH_{EC}

As with dominant frequency (Chapter 4.4.2), the relationship between VF amplitude change and extracellular pH is complex. In this chapter, there was a trend for both ECG and psECG amplitude to be conserved during perfusion at pH 6.7 in compared to VF in control conditions. No such trend was observed at pH 6.3. A similar pattern was observed for the LV optical amplitude; at pH 6.7, the LV amplitude tended to be decreased by a lesser extent than control, whereas at pH 6.3 the LV amplitude reduction tended to be greater. Neither of these changes reached significance.

As outlined in chapter 4.4.2, individual studies have shown acidic pH_{EC} to depolarise the resting (diastolic) membrane potential over a range of pHs from 6.0 – 6.7 (218, 220, 221, 274). Such depolarisation would reduce the amplitude of the VF activations. In contrast, Sato et al. demonstrated a small hyperpolarisation of the diastolic potential at $\text{pH} > 6.0$, and depolarisation at $\text{pH} < 6.0$ (219). Hyperpolarisation should increase the amplitude of the VF activations, and therefore may account for the non-significant increases in the ECG, psECG and LV amplitudes in pH 6.7 in this chapter. Depolarisation of the diastolic potential in acidic pH_{EC} is thought to result from extracellular K^+ accumulation secondary to inhibition of I_{K1} by acidosis (222). The relationship between I_{K1} and pH is biphasic (219). Low levels of acidification (pH 7.2 – 6.0) enhance the current, whereas higher levels (pH 6.0 – 5.0) inhibit it (219). Thus low levels of acidification would be expected to hyperpolarise the diastolic potential, and higher levels depolarise it. In VF, the ongoing metabolic stress could produce greater acidification than that predicted by solution imposition alone. Hence it is possible that the pH 6.7 solutions could enhance I_{K1} , hyperpolarise the diastolic membrane potential, and thus conserve the VF amplitude. Whereas pH 6.3 solutions could inhibit I_{K1} , depolarise the diastolic potential, and thus

equal or enhance the amplitude reduction. Therefore, as with frequency, I_{K1} could explain the complex, but subtle effects of acidic pH_{EC} on the activation amplitude in VF.

As discussed in section 1.2.3, the reduction of pH_{EC} during VF in low-flow ischaemia is not clear from the current literature. Complete ischaemia in sinus rhythm can reduce the intracellular pH to 6.78 at 10 minutes (79), whereas in VF supported by CPR, that at best gives perfusion at 25% of the normal flow (17), the pH_{EC} dropped to 6.38 at 11 minutes (80). Therefore, it is conceivable that the pH fell to 6.3 during low-flow ischaemia, where perfusion was 10% of control flow rate. This would suggest that acidic pH_{EC} , as well as hypoxia, is contributing to the decline in VF amplitude in low-flow ischaemia. As before, this could not be investigated by floating microelectrode, as preparations were continuously superfused and the bathing solution was open to the room environment (Chapter 9).

8.4.5 VF amplitude in raised $[K^+]_{EC}$

As discussed above, the 90% changeover in solutions did not occur at the heart until 180s (Figure 4.1). ECG, psECG and LV amplitudes decreased progressively until ~180s in VF during raised $[K^+]_{EC}$. After ~180s, the ECG, psECG and LV amplitudes increased (Figures 8.6 & 8.7). This amplitude augmentation runs contrary to the theoretical expectations as explained below.

In theory, raising the $[K^+]_{EC}$ from 5.5mM to 11mM will depolarise the resting membrane potential from -82mV to -64mV. Experimental data confirms this membrane depolarisation; using microelectrodes in whole heart (81, 214) and cellular (202) preparations, raising $[K^+]_{EC}$ to 11mM depolarised the membrane by around 26mV. In these studies, as the resting (diastolic) membrane potential became less negative, the AP amplitude was reduced (81, 202). Thus one would predict that raising $[K^+]_{EC}$ during VF would depolarise the diastolic potential and reduce the activation amplitude.

The observed increase in VF amplitude coincided with a reduction in ECG, psECG and LV DF. This suggests that as the frequency of the activations decreased, the electrical activity in VF became more organised, and hence the amplitude of the global measurements increased as the local electrical vectors reinforced each other. Such increased organisation need not be associated with an actual increase in amplitude at the cellular level. Such dissociation between cellular and global amplitudes could explain the apparent contradictory findings of increased activation amplitude in VF during raised $[K^+]_{EC}$. The

lack of an increase in action potential (AP) amplitude at the cellular level was confirmed by recording the absolute membrane potential in VF during raised $[K^+]_{EC}$ using floating microelectrodes (Chapter 9.3).

8.4.6 Relationship between frequency, organisation and amplitude

In all VF protocols, including low-flow ischaemia from 60 – 120s, the ECG and psECG amplitudes were inversely related to the relative DF (Figure 8.8). So as the ECG and psECG DF increased, the VF amplitude declined, whereas a decrease in DF was associated with an amplitude increase.

As explained above, in control conditions VF becomes more disorganised with time (266). Therefore the constituting electrical vectors of the ECG should increasingly oppose each other, and reduce the global electrical amplitude of the VF activations. This vector explanation cannot account for the reduction of amplitude of the psECG. The LV/RV heterogeneity of the amplitude decline would also suggest a true reduction in cellular AP amplitude, which was confirmed by microelectrode (Chapter 9.3). One would predict a similar finding during VF in hypoxia and acidic pH_{EC} . Unfortunately this could not be verified by microelectrode as the solution bathing the region of epicardial impalement was open to the air.

Previous studies have shown AP amplitude to decrease in low-flow ischaemia (140, 228, 238, 264) and raised $[K^+]_{EC}$ (81, 202, 214). The investigations in this chapter showed an initial or persistent increase in ECG and psECG amplitude during VF in low-flow ischaemia and raised $[K^+]_{EC}$. Once again, a possible explanation for the increase VF amplitude on the ECG is increased co-ordination of the electrical activity, allowing local electrical vectors to reinforce, rather than oppose each other. Indeed, increased co-ordination of electrical activity in VF during ischaemia is well documented (36, 62, 271, 272).

A similar concept may explain the observed increase in psECG and LV optical AP amplitude during VF in low-flow ischaemia and raised $[K^+]_{EC}$. In optical mapping, the signal from a single pixel represents the summation of the activity of the hundreds of cells (153). For this reason, the upstroke of the optical AP is slower than that of a glass microelectrode AP in the same area (153) (Figure 1.16). In VF, as the DF falls, the activation wave progresses across the myocardium more slowly (70, 263, 275). Thus

within a pixel, a greater number of the cells will reach peak activation and peak fluorescence at the same time. This more synchronised activity will produce an increase in fluorescence amplitude, which may not be associated with a true increase in cellular electrical amplitude. Indeed microelectrode impalement failed to show an increase in amplitude at the cellular level during VF in raised $[K^+]_{EC}$ (Chapter 9.3).

8.4.7 Conclusion

During VF in control conditions there was a reduction in the activation amplitude, which probably reflects a decline in membrane excursion at the cellular level. This amplitude reduction is probably enhanced by low-flow ischaemia as suggested by the ECG, but not in the more noise-sensitive psECG. Both hypoxia and pH 6.3 also tended to enhance the ECG amplitude reduction compared to control. Although raised $[K^+]_{EC}$ increased the activation amplitude during VF, this could be due to enhanced synchronisation. Thus a combination of hypoxia and acidosis, and even raised $[K^+]_{EC}$, are probably involved in the amplitude reduction of VF during low-flow ischaemia.

9 Membrane potential during VF

9.1 Introduction

The experimental results from chapters 3 – 8 have suggested a series of questions concerning the electrophysiology of VF. These questions were: -

(i) In VF during control conditions, the ECG, psECG and LV optical AP amplitude decreased with time (Chapter 8). The reduced activation amplitude could be due to depolarisation of the diastolic membrane potential, reduction in the systolic potential, or a combination of both. Transmembrane recording of the membrane potential during VF in control conditions will help elucidate the relative contributions of changes in the diastolic and systolic potential.

(ii) During VF in low-flow ischaemia and raised $[K^+]_{EC}$, there was either a transient or persistent increase in the ECG, psECG and LV optical AP amplitude (Chapter 8). Theoretically, neither of these conditions should increase the activation amplitude during VF. Therefore the amplitude increase could be artificial and due to increased alignment of the local electrical vectors as the electrical activity becomes more co-ordinated. Transmembrane recordings of the membrane potential during VF in low-flow ischaemia and raised $[K^+]_{EC}$ will detect whether or not a real increase in the AP amplitude occurs at the cellular level.

(iii) During VF in low-flow ischaemia (Chapter 3) and raised $[K^+]_{EC}$ (Chapter 4), the LV dominant frequency (DF) slowed, whilst the RV DF remained unchanged. This LV/RV DF heterogeneity was shown to be associated with differential elevation in the LV activation threshold compared to the RV (Chapters 5 – 7). The hypothesis was raised that the increase in activation threshold resulted from depolarisation of the diastolic membrane potential leading to a partial inhibition of I_{Na} . Transmembrane recordings of the membrane potential will show if the diastolic membrane potential depolarises during VF in low-flow ischaemia and raised $[K^+]_{EC}$.

To address these issues the absolute membrane potential was measured by floating microelectrode during VF in control conditions, low-flow ischaemia and raised $[K^+]_{EC}$.

9.2 Methods

Hearts were prepared as per chapter 2.8. Briefly, hearts were Langendorff-perfused, had an LV balloon inserted, and then were placed in a chamber adapted for microelectrode

impalement of the LV surface. These adaptations included boring a 0.5cm diameter hole in the Plexiglas front-plate, and adding a 2nd supporting column to allow the chamber to be held horizontally as well as vertically. Borosilicate glass microelectrodes were filled with 2M KCl and the tips mounted onto silver chloride-coated silver wire to give a total resistance of 20 – 25M Ω . Signals were recording via a dual microprobe Model 750 amplifier (WPI, Sarasota, FL), before being stored digitally at either 1 or 10 kHz. The electrical apparatus was calibrated at the start of each day.

Prior to VF induction, the baseline transmembrane potential was recorded during RV pacing at BCL 180ms. Typical baseline signals are shown in figure 9.1A. Hearts were burst paced into VF, and fresh impalements were achieved approximately every 30s. Figure 9.1B shows a typical transmembrane recording during VF. For 60s the heart was perfused in standard Tyrode's solution at 40ml/min in all protocols. After 60s, perfusion in standard Tyrode's solution at 40ml/min was maintained in control protocols. In experimental protocols either the perfusion rate was decreased to 6ml/min (low-flow ischaemia) or the solution $[K^+]$ was increased to 8mM. After approximately 600s in VF, hearts were defibrillated by intra-aortic injections of 2M $[KCl]$ solution.

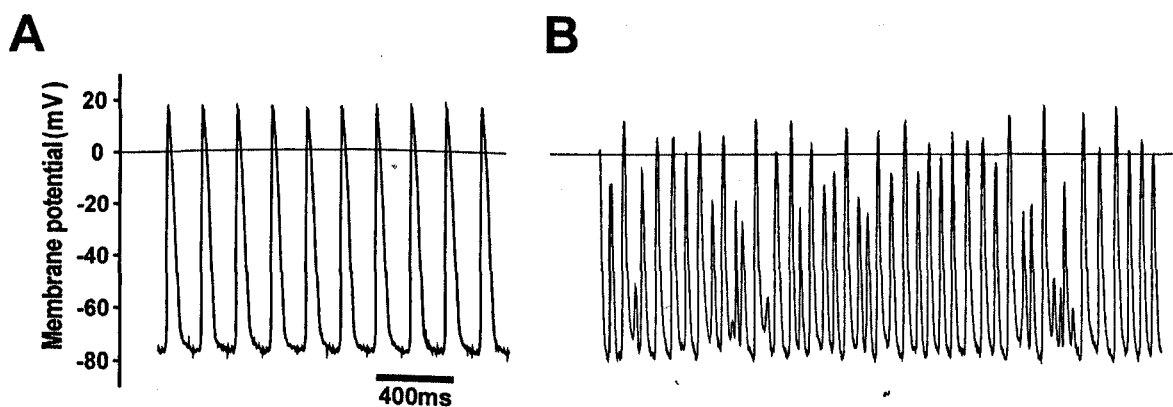


Figure 9.1 Sample microelectrode recordings. Panel A: LV impalement during baseline pacing at BCL = 180ms. Panel B: LV impalement during VF.

Signals were analyzed offline for amplitude and frequency changes using FFT (Chapter 2.5). Signals were converted to absolute membrane potentials using that day's calibration curve. Peaks were identified in Origin (Originlab corporation, USA), and the mean diastolic and systolic membrane potential calculated for each impalement. As the precise time of impalement could not be strictly controlled, values were collated into time bins and expressed for the time period in a horizontal step-wise graph. As with ECG and psECG amplitude, significant changes in membrane potential were assessed over the 7 – 9 minutes time interval. Systolic and diastolic potentials at 7 – 9 minutes were compared using the

paired t-test to baseline membrane potentials during control pacing (BCL 180s) in same heart. Comparisons between protocols were performed by repeated ANOVA.

Using dyes and spectrophotometry, the 90% transition time for washing in different $[K^+]$ in this set-up was estimated (Figure 9.2). The electrophysiology set-up used for floating microelectrode work had a larger dead space than the optical system, hence the transition between solutions was not as swift, and 90% transition was achieved after 220s. Therefore, the 90% transition time for $[K^+]$ was after 280s of VF.

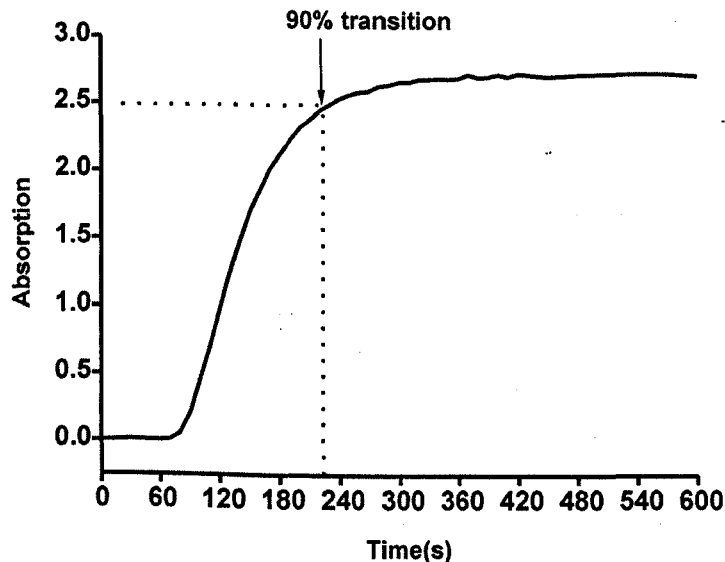


Figure 9.2 Transition time to wash in different $[K^+]$ solutions in the microelectrode set-up. This was assessed using dyes and absorption spectrophotometry.

9.3 Results

As shown in figure 9.3, during VF in control perfusion, low flow ischaemia and 8mM $[K^+]_{EC}$, the changes in DF with time from transmembrane recordings of the LV epicardial surface were similar to the DF changes of the psECG. In 8mM $[K^+]_{EC}$, the later decrease in DF recorded from microelectrode as compared to psECG can be explained by the greater delay till 90% solution transition of 280s in microelectrode compared to 150s for optical mapping.

During VF in control conditions, the diastolic membrane potential at 7 – 9 minutes of $-65 \pm 3mV$ was not significantly different from the diastolic potential during baseline pacing of $-72 \pm 4mV$ (Figures 9.4 & 9.7). In contrast, as shown in figure 9.4, the maximum systolic membrane potential sharply decreased on VF induction, and continued to decline throughout the period of VF. By the 7 – 9 minutes assessment point, the maximum systolic

potential had reduced to $-24 \pm 5\text{mV}$, which was significantly lower than the maximum systolic potential at baseline of $18 \pm 3\text{mV}$ ($p < 0.0001$, Figure 9.7). Compared to baseline pacing, the peak-to-peak amplitude at 7 – 9 minutes was significantly reduced to $47 \pm 6\%$ ($p < 0.001$). However, using the peak-to-peak amplitude on VF induction as baseline, the AP amplitude reduction was only to 86%. Approximately 15 minutes after defibrillation, the amplitude was re-assessed at BCL 180ms. This showed full recovery of amplitude (Figure 9.4).

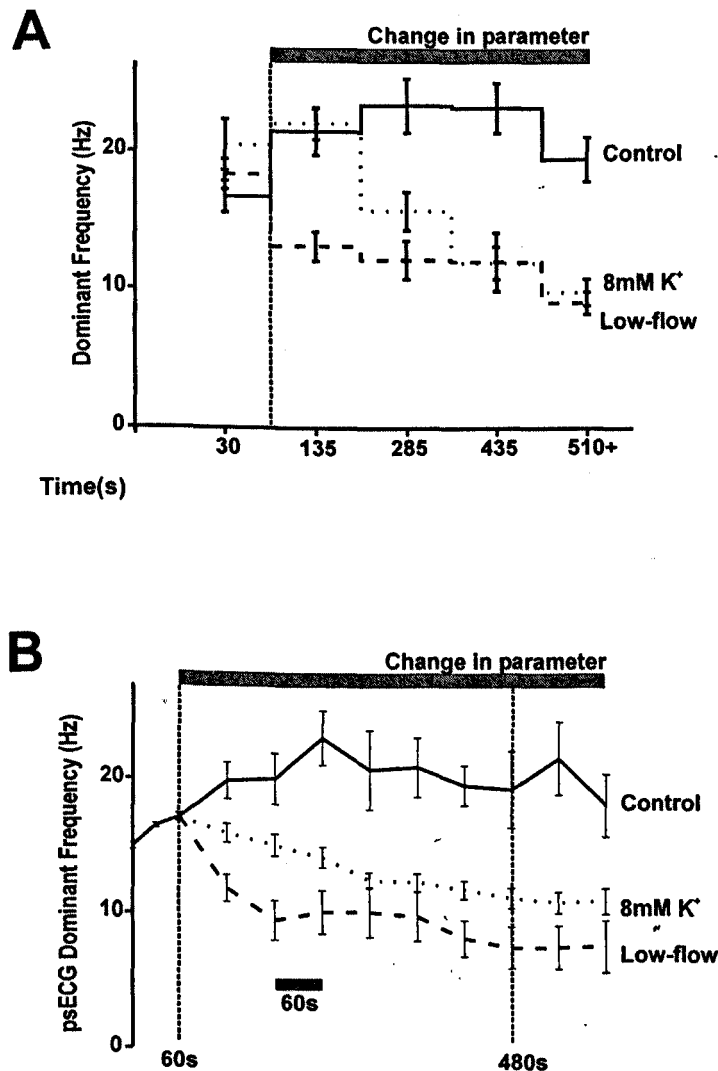


Figure 9.3 Dominant frequency during control, low-flow ischaemia and 8mM $[\text{K}^+]_{\text{EC}}$. Panel A: Microelectrode DF. As with psECG there was (i) an increasing DF in control VF, (ii) a decreasing DF in low-flow ischaemia and (iii) a decrease after an initial delay with 8mM $[\text{K}^+]_{\text{EC}}$. Panel B: psECG DF. The progression patterns are similar to those observed by microelectrode. The notable exception is the more immediate decrease in DF in 8mM $[\text{K}^+]_{\text{EC}}$. This is due to the shorter time to reach 90% solution transition in the optical apparatus.

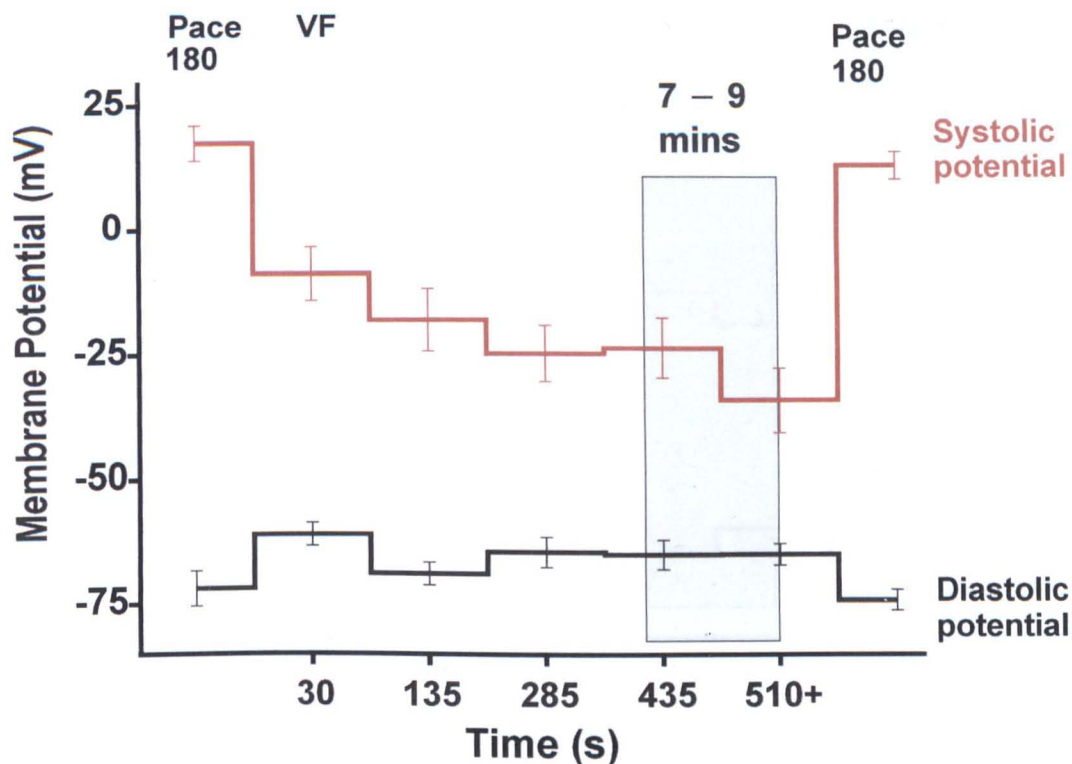


Figure 9.4 Membrane Potential during baseline pacing at BCL 180ms (Pace 180) and VF in control conditions. Immediately after VF induction, there was a decrease in amplitude mainly due to a more negative maximum systolic potential. The systolic potential continued to become more negative with time. In contrast, the diastolic potential remained unchanged. Post VF, the systolic potential recovered to pre-VF levels after ~15 minutes. The grey square indicates the 7 – 9 minutes time interval used for statistical comparisons.

In VF during low-flow ischaemia the maximum systolic potential dropped to the more negative value of $-19 \pm 8\text{mV}$ immediately after VF induction (Figure 9.5). After this the maximum systolic potential stabilised. By the 7 – 9 minutes assessment point the maximum systolic potential of $-10 \pm 8\text{mV}$ was significantly different from that during baseline pacing of $13 \pm 4\text{mV}$ ($p < 0.05$). The diastolic potential of $-68 \pm 3\text{mV}$ was not significantly different from the baseline pacing potential of $-76 \pm 2\text{mV}$. Compared to baseline pacing, the VF peak-to-peak amplitude was significantly reduced to $66 \pm 12\%$ at 7 – 9 minutes ($p < 0.05$). Thus there was no evidence of peak-to-peak amplitude increase during low-flow ischaemia. Again, the peak-to-peak amplitude during pacing at BCL 180 returned to the pre-VF level after ~15mins.

In VF during low-flow ischaemia, neither the maximum systolic nor the diastolic potential was significantly different from VF under control conditions at 7 – 9 minutes (Figures 9.5 & 9.7).

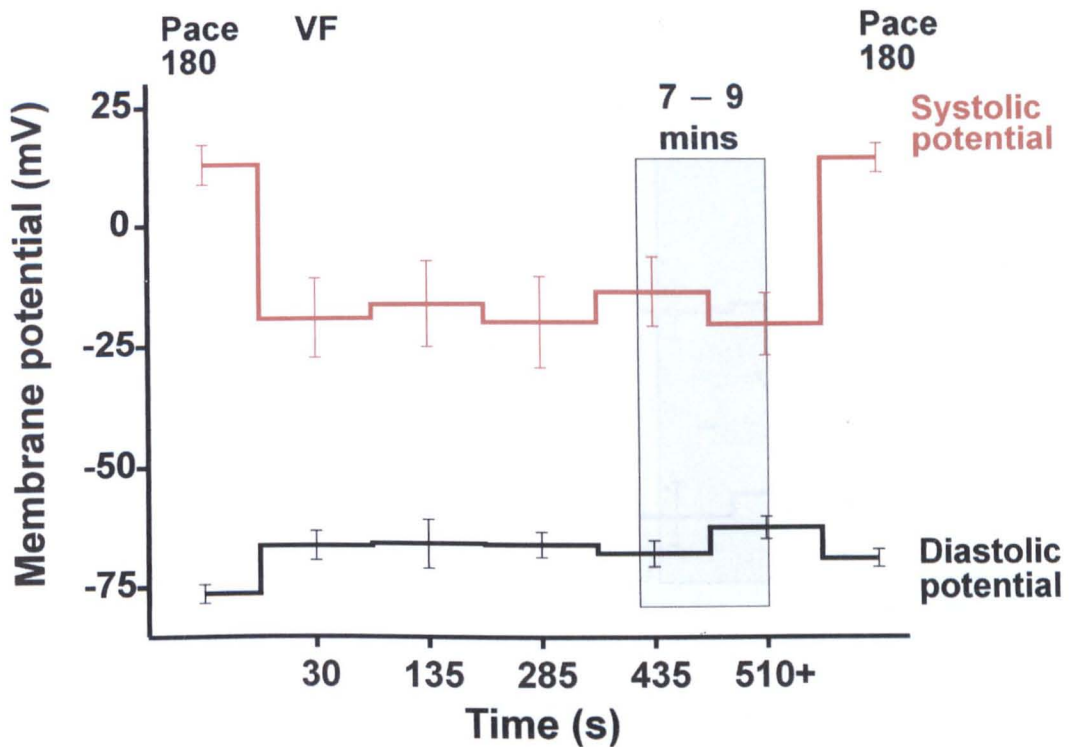


Figure 9.5 Membrane Potential during baseline pacing in control conditions (Pace 180) and during VF in low-flow ischaemia. Immediately after VF induction, the maximum systolic potential became more negative. The diastolic potential remained unchanged. After 15 minutes recovery time, the systolic potential returned to baseline values.

During VF in $8\text{mM } [\text{K}^+]_{\text{EC}}$, the maximum systolic potential dropped to the more negative value of $-24 \pm 5\text{mV}$ on VF induction (Figure 9.6). However, as figure 9.6 demonstrates, both the maximum systolic and the diastolic membrane potential gradually depolarised as VF continued in $8\text{mM } [\text{K}^+]_{\text{EC}}$ solution. By 7 – 9 minutes, the maximum systolic potential of $-14 \pm 4\text{mV}$ was significantly different from that during baseline pacing of $4\text{mV} \pm 4$ ($p < 0.05$). By 7 – 9 minutes the diastolic potential had depolarised to $-55 \pm 8\text{mV}$ in $8\text{mM } [\text{K}^+]_{\text{EC}}$. This was significantly depolarised compared to the baseline resting membrane potential during pacing of $-80 \pm 5\text{mV}$ ($p < 0.05$). Although the absolute diastolic potential of $-55 \pm 8\text{mV}$ during VF in $8\text{mM } [\text{K}^+]_{\text{EC}}$ solution was not significantly different from that of the absolute diastolic potential of $-65 \pm 3\text{mV}$ during VF in control conditions, the relative change in the diastolic potential of $\sim 25\text{mV}$ compared to $\sim 7\text{mV}$ in control was significantly different ($p < 0.001$, Figure 9.7).

Compared to baseline pacing, the peak-to-peak VF amplitude at 7 – 9 minutes was significantly reduced to $49 \pm 6\%$ ($p < 0.001$). Comparing the peak-to-peak amplitude at 7 – 9 minutes to the peak-to-peak amplitude immediately after VF induction, the amplitude was reduced to only 93%. There was no evidence of any increase in AP amplitude during VF in raised $[\text{K}^+]_{\text{EC}}$.

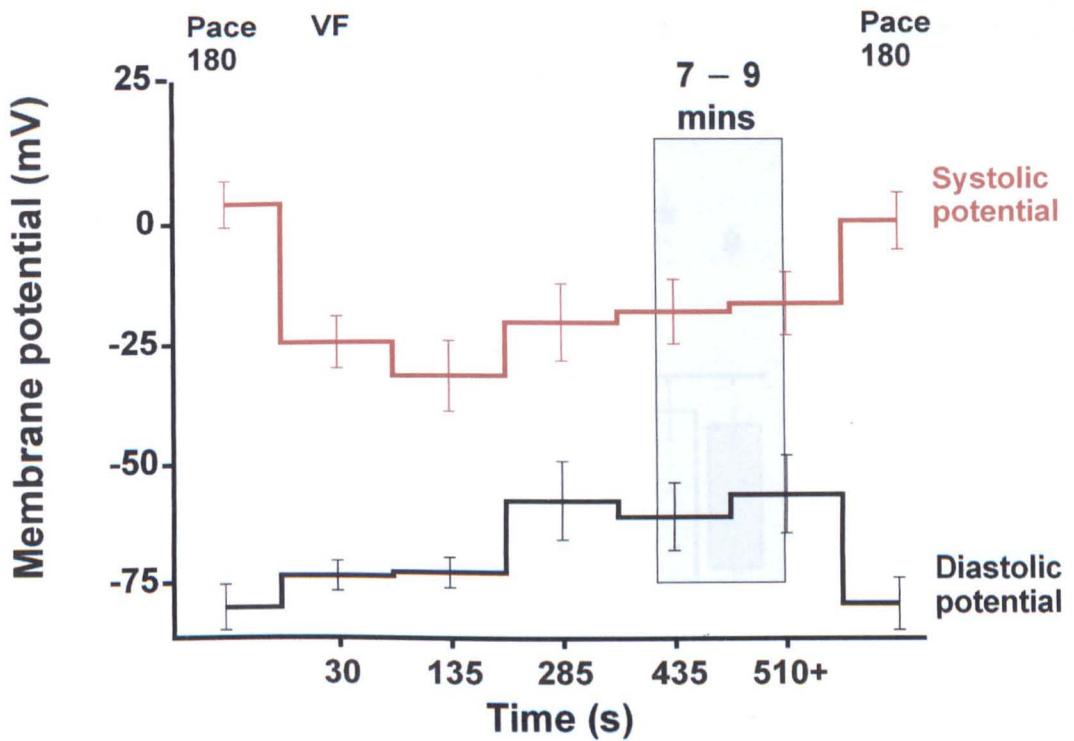


Figure 9.6 Membrane potential during baseline pacing in control conditions (Pace 180) and during VF in 8mM $[K^+]_{EC}$ solution. Immediately on VF induction there was a drop in the maximum systolic potential to more negative values, while the diastolic potential remained unchanged. On increasing $[K^+]_{EC}$ the diastolic potential depolarised. There was a tendency for systolic potential to depolarise in raised $[K^+]_{EC}$. At no point did the peak-to-peak transmembrane potential show an increase in VF amplitude.

In summary, there was significant reduction in the transmembrane peak-to-peak AP amplitude during VF in low-flow ischaemia, raised $[K^+]_{EC}$ and control conditions, as shown in figure 9.7. The amplitude reductions were due to variable combinations of depolarisation of the diastolic membrane potential and more negative maximum systolic membrane potentials. In control conditions, the amplitude reduction was primarily due to the more negative maximum systolic potentials. In 8mM $[K^+]_{EC}$, depolarisation of the diastolic membrane potential was more important. VF in low-flow ischaemia showed the smallest amplitude change and both processes appeared to be of equal importance.

9.4 Discussion

The aim of this chapter was to answer three specific questions by intracellular recordings: -
 (i) Is the amplitude reduction in control VF due to depolarisation of the resting (diastolic) membrane potential or reduction in the maximum systolic potential? (ii) Is the apparent amplitude increase in VF in low-flow ischaemia and raised $[K^+]_{EC}$ due to a real increase in the AP amplitude at the cellular level or is it a phenomenon of increased electrical coordination? (iii) Does the resting membrane potential depolarise in VF during low-flow

ischaemia and raised $[K^+]_{EC}$, and thus support the hypothesis of increased activation threshold due to partial inhibition of I_{Na} secondary to diastolic membrane depolarisation?

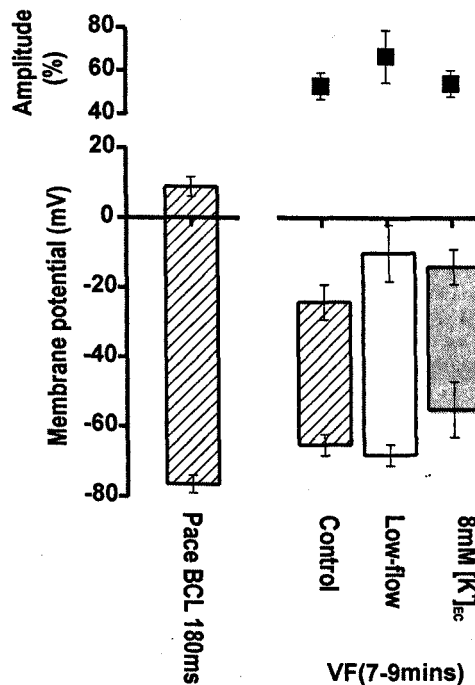


Figure 9.7 Plot of mean membrane potential and amplitude change at 7 – 9 minutes with respect to baseline pacing at BCL 180s. In control conditions, there was a dramatic reduction in the maximum systolic potential during VF. The maximum systolic potential was also reduced in low-flow ischaemia and raised $[K^+]_{EC}$, but not to the same extent. In raised $[K^+]_{EC}$, diastolic depolarisation was observed. In all protocols there was a significant reduction in amplitude compared to baseline pacing.

9.4.1 Reduced systolic depolarisation in VF during control conditions

Transmembrane recordings during VF in control conditions confirmed that a reduction in AP amplitude occurs, and showed this to be due to reduced systolic depolarisation rather than to diastolic depolarisation. The reduction in LV AP amplitude to 86% recorded during VF was less than the reduction to 33% measured optically. Correcting the LV optical data for dye degradation results in a lesser reduction of VF amplitude in the LV to 54%; this is in the same order as the reduction in ECG amplitude to 55%. So although there was a reduction in activation amplitude at the cellular level, this cannot explain all the amplitude reduction of ECG and optical recordings. In the ECG, this discrepancy may arise from increasing global disorganisation during VF (266).

The same explanation may also explain the discrepancy with the optical recordings. As explained fully in chapter 1.3.5, optical signals are influenced by a greater number of cells than transmembrane recordings from microelectrode impalement. This is why the upstroke

velocity of optical AP is slower than the corresponding microelectrode AP as shown in figure 1.16. As the AP propagates across the $\sim 1\text{mm}^2$ of epicardium recorded by the photodiode, there is a delay in the activation time of each cell. During regular pacing in control conditions, the average of the transverse and longitudinal velocity was $\sim 50\text{cm/s}$ (chapter 7.3.2). This creates an approximate 2ms spread of activation times across the pixel area (Figure 9.8A). This spread of activation acts to reduce the upstroke velocity. However, due to the AP plateau, the amplitude is not reduced. In contrast, in VF the apparent conduction velocity in control conditions of $\sim 35\text{cm/s}$ creates a greater spread of activation times across the pixel of 3.5ms (Figure 9.8B). This, combined with the change in activation morphology, would be predicted to result in a reduction in amplitude compared to microelectrode recordings. So theoretically, a change in the local synchrony of activation could also affect the optical amplitude.

9.4.2 No amplitude increase in low-flow ischaemia or raised $[\text{K}^+]_{\text{EC}}$

In contrast to the amplitude of the ECG, psECG and optical signals in the LV pixels (Chapter 8.3), transmembrane recordings did not demonstrate a transient or persistent increase in the activation amplitude in VF during low-flow ischaemia or raised $[\text{K}^+]_{\text{EC}}$. This is in keeping with previous research (81, 140), and supports the hypothesis outlined in chapter 8.4.6, that the increased ECG, psECG and LV optical signal amplitudes were due to increased electrical co-ordination of the myocytes at slower activation frequencies.

9.4.3 Diastolic depolarisation in raised $[\text{K}^+]_{\text{EC}}$

In keeping with previous research (81), this chapter demonstrated significant depolarisation of the diastolic membrane potential during VF in raised $[\text{K}^+]_{\text{EC}}$. This supports the hypothesis that the relative elevation of the LV activation threshold in raised $[\text{K}^+]_{\text{EC}}$ is due to partial inhibition of I_{Na} through depolarisation of the diastolic membrane potential. The presence of differential diastolic depolarisation in the LV compared to the RV in raised $[\text{K}^+]_{\text{EC}}$ was not examined because of technical constraints. Clearly, demonstration of differential LV/RV diastolic depolarisation would support the hypothesis more strongly. Potential ways to address this deficit are discussed in chapter 11.4.1.

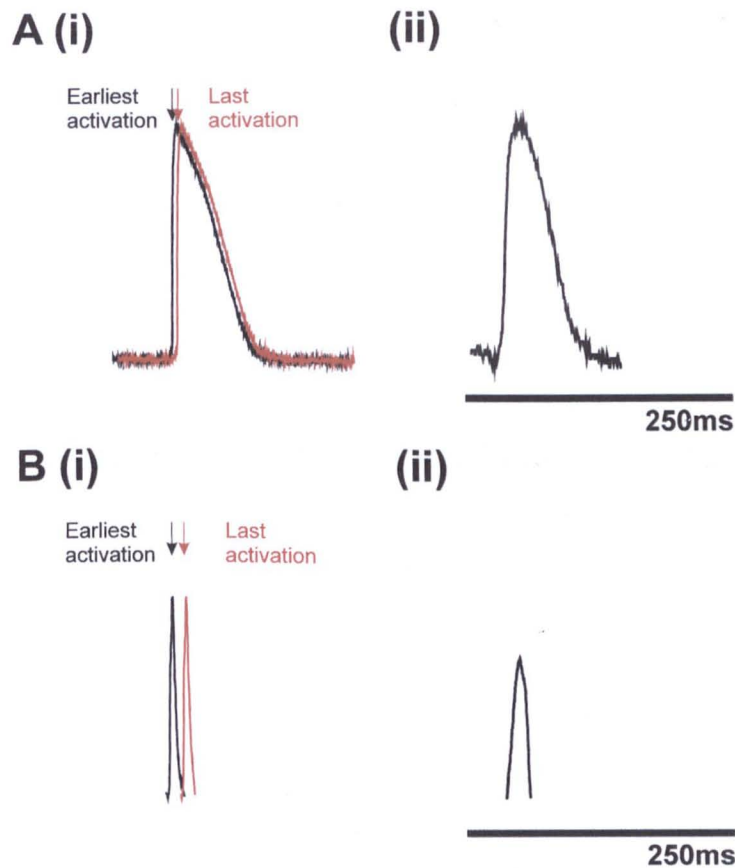


Figure 9.8 Illustration of earliest and latest activation within a single pixel in regular pacing and VF. Panel A: During regular pacing. (i) Transmembrane AP – assuming a CV of 50cm/s across the $\sim 1\text{mm}^2$ pixel, the maximal delay between the first and last activation would be approximately 2ms. This delay is illustrated here. One can appreciate how such a delay will result in slowing of the optical AP upstroke as shown in (ii), but will have minimal effect on amplitude as the signals largely overlap. Panel B: During VF. (i) Transmembrane AP – the reduced CV of $\sim 35\text{cm/s}$ has increased the maximal delay to $\sim 3.5\text{ms}$. This increased delay, with the changed activation morphology, now allows little overlapping of the earliest and latest activation. This could explain the greater reduction of signal amplitude recorded optically, as shown in (ii).

The lack of significant depolarisation in low-flow ischaemia is not in agreement with previous studies (140), and may be due to technical issues. For example, there was constant superfusion of the impalement surface to allow electrical continuity with the ground reference electrode. This superfusion probably washed away the cellular K^+ efflux, thereby preventing significant K^+ accumulation and consequent depolarisation. Without this superfusion, K^+ would be predicted to accumulate and so depolarise the diastolic potential. Such depolarisation would be expected to inactivate I_{Na} , reduced AP upstroke velocity and raise the AP activation threshold. As superfusion does not prevent the accumulation of K^+ within the deeper myocardium layers, these tissues will undergo diastolic depolarisation, and thereby result in the reduced LV DF that was observed on microelectrode impalement of VF during low-flow ischaemia.

10 Minimum defibrillation energies

10.1 Introduction

As outlined in sections 1.1.1.4 & 1.2.2.3, over the last couple of decades it has been well established that longer duration out-of-hospital arrests are associated with lower frequency content of the ECG, and diminished defibrillation success (6, 23, 32, 33, 276, 277). More recently, animal and clinical studies have shown that CPR prior to defibrillation attempts increased the ECG Dominant Frequency (DF) (24, 278, 279), and improved defibrillation success (9, 12, 13, 280-282). This suggests that ischaemia increases the energy required to defibrillate successfully, known as the defibrillation threshold (DFT), and that partial reversal of ischaemia by CPR reduces the DFT.

Paradoxically, experimental assessments of DFT, rather than rates of defibrillation success, have not demonstrated an increase in DFT under ischaemic conditions. In VF during low-flow ischaemia, the DFT was not increased in rabbits (283), and the related parameter of the Minimum Defibrillation Energy (MDE) was reduced in swine (73). Supporting these experimental results, computer modelling has predicted a fall in the upper limit of vulnerability (ULV) in global ischaemia (284, 285). As explained in chapter 1.2.3, the ULV of a preparation is the highest shock strength that induces VF. The close inter-relationship between the ULV and DFT is well established (120, 286, 287).

In this thesis, hearts were defibrillated after 600s of VF. This chapter reports the defibrillation energies required to terminate VF in the protocols outlined in chapters 3 & 4. Thus this chapter documents the energies required to successfully defibrillate VF during control, low-flow ischaemia, acidic pH_{EC} , hypoxia and raised $[K^+]_{EC}$ conditions, and in the unperfused 8-week infarct model hearts. As discussed more fully in chapter 1.2.2, owing to the probabilistic nature of defibrillation (122), accurate DFT determination requires several short runs of VF defibrillated by an up-down protocol (123). Such lengthy processes cannot be performed in longer periods of VF. Therefore in this thesis, the more straightforward estimate of MDE was determined (73).

10.2 Methods

Hearts were prepared as per chapters 3 & 4, and defibrillated as outlined in chapter 2.4. After 600s, hearts were defibrillated using an external cardiac defibrillator (Ventak ECD 2815, CPL, St Paul's, MN, USA) delivering shocks via custom-made stainless steel paddles that are shown in diagrammatic form in figure 10.1, and in photographic form in

figure 2.2A. The orientation of the electrode polarity was kept constant, and as the defibrillation paddles cradled the heart to reduce motion artefact, the distance from the epicardial surface was constant. The paddles were fixed with respect to the frontplate and the area of optical interrogation (Figure 10.1). As the interrogation area was standardised using the left anterior descending artery (LAD) on the anterior surface as a landmark, the paddle position on the heart was relatively constant.

As detailed in table 10.1, only certain energies could be administered by the Ventak ECD defibrillator. The defibrillator setting indicated the level of potential energy the capacitor was charged to. As capacitors always leak prior to discharge, the energy delivered across the heart was never 100% of the potential energy. The actual voltage applied by a certain charge depends on the resistance in the system. The resistance of the apparatus was fixed for all experiments, and therefore the resistance of the heart was the only variable. The degree of variation in heart resistance was negligible (heart resistance = $48 \pm 0.5\Omega$). The defibrillator measured the system resistance, and calculated the peak voltage and energy supplied.

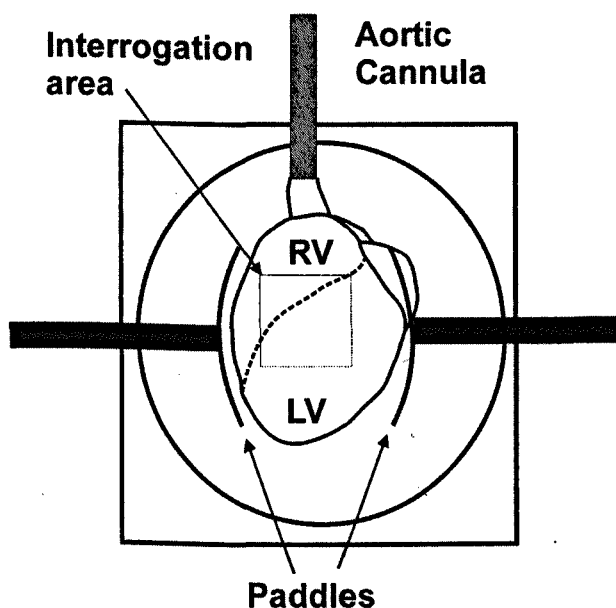


Figure 10.1 Diagram of the defibrillation set-up. The paddles were fixed in 2 dimensions, with only be moved towards or away from the heart possible. As in all experiments the area of interrogation was standardised to the LV/RV border using the LAD as a landmark, the position of the paddles with respect to the heart was also consistent.

The first shock administered was at the lowest defibrillator setting of 0.1J. Inbuilt programming prevented administration of biphasic shocks at 0.1J. If defibrillation failed, the shock strength was repeatedly increased to the next defibrillator energy setting until defibrillation was successful. The maximum shock strength applied was 5J (Table 10.1). This terminal shock strength was chosen as shocks >5J were (i) virtually never successful

and (ii) when they were successful, they were associated with a permanent increase in the perfusion pressure of >80 mmHg. Such perfusion pressures indicated a level of preparation degradation that was incompatible with further experimentation (chapter 2.1). The strength of shock that successfully defibrillates the heart by such a step-up protocol is known as the MDE (73). To control for any confounding influence of preparation degradation, equal proportions of 1st and 2nd runs were performed for each protocol.

Energy setting (J)	Mean voltage \pm SD (V)	Mean energy \pm SD (J)	Waveform
0.1	38 \pm 1.5	0.098 \pm 0.004	Monophasic
0.3	61 \pm 1.8	0.298 \pm 0.006	Biphasic
0.5	79 \pm 2.9	0.477 \pm 0.008	Biphasic
0.8	99 \pm 3.9	0.759 \pm 0.013	Biphasic
1.0	111 \pm 3.8	0.960 \pm 0.015	Biphasic
2.0	155 \pm 4.7	1.895 \pm 0.039	Biphasic
3.0	189 \pm 7.9	2.836 \pm 0.055	Biphasic
4.0	217 \pm 6.9	3.778 \pm 0.061	Biphasic
5.0	244 \pm 7.	4.705 \pm 0.092	Biphasic

Table 10.1 Energy settings of Ventak ECD and the corresponding voltage, energy and waveform delivered.

Heterogeneity of repolarisation and refractoriness is thought to play a role in defibrillation outcome (275). In the chaotic activity of VF, with multiple wandering wavelets, it can be assumed that cells become activated as soon as their effective refractory period is complete. Using this assumption, electrical mapping studies of VF assessed epicardial refractoriness through the time intervals between VF activations (4, 46, 134, 135). Through these VF intervals (VFIs), the dispersion of refractoriness was assessed by their coefficient of variance. The DF of a pixel represents the predominant VFI in that pixel during the optical recording. Therefore in an attempt to assess the dispersion of refractoriness during VF, the coefficient of variance of the optical DFs was calculated. For each time interval the standard deviation for the DF of the 252 individual optical signals was multiplied by 100, and then divided by the mean. The fractional change of the coefficient of variance was determined at 480s using the coefficient of variance immediately after VF induction as baseline.

10.3 Results

10.3.1 *Minimum defibrillation energy (MDE)*

As shown in Figure 10.2, the mean MDE required to defibrillate VF in low-flow ischaemia of 93 \pm 24V was not significantly different from that required in control conditions of 73 \pm

9V. Similarly, the MDE in 8mM $[K^+]$ solution of $56 \pm 3V$ was not significantly different compared to control (Figure 10.2). VF in 10mM $[K^+]$ solution spontaneously converted to a regular ventricular escape rhythm before 600s.

In VF during 0% PO_2 and acidic pH_{EC} , significantly stronger shocks were required to defibrillate VF compared to control and 8mM $[K^+]_{EC}$. In 0% PO_2 the MDE was $148 \pm 21V$ (** $p < 0.01$ vs. control and 8mM $[K^+]_{EC}$), and in pH 6.7 the MDE was $177 \pm 26V$ (** $p < 0.001$ vs. control and 8mM $[K^+]_{EC}$)(Figure 10.2).

In both pH 6.3 and unperfused 8-week infarct protocols, all hearts remained in VF after 5J shocks. In these protocols, application of shocks $>1J$ produced prolonged periods of asystole, after which the first electrical activity was VF. Successful defibrillation in these protocols required a combination of intra-aortic bolus injection of 2M $[KCl]$ solution and 5J shocks.

10.3.2 DF and MDE

To examine the relationship between MDE and the electrical activity, the MDE was plotted against the psECG DF immediately prior to defibrillation. It was not possible to calculate the concurrent ECG DF as the amplifier was disconnected during defibrillation. As shown in figure 10.3, there was no correlation between the MDE and the psECG DF.

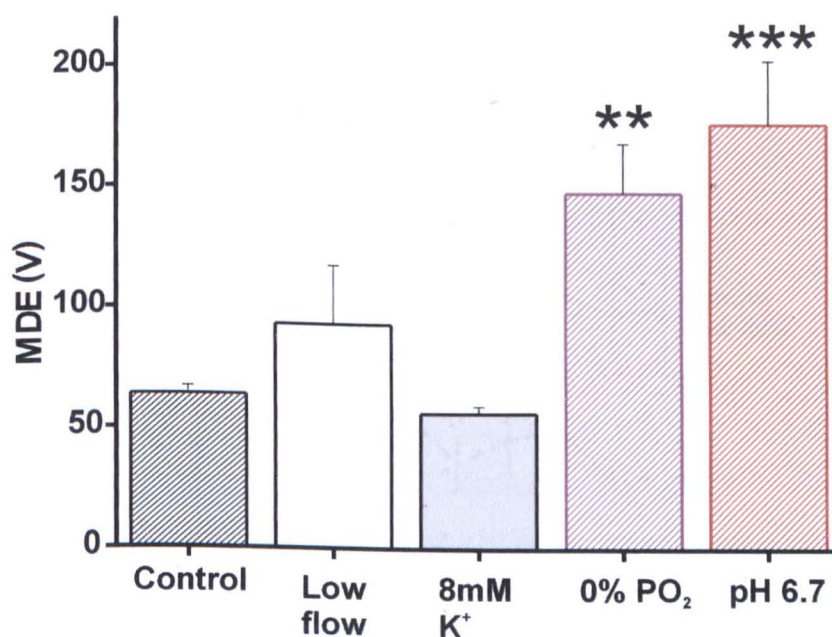


Figure 10.2 Plot of mean MDE \pm SE. The MDE was significantly raised by pH 6.7 and 0% PO_2 when compared to control (** $p < 0.01$, *** $p < 0.001$).

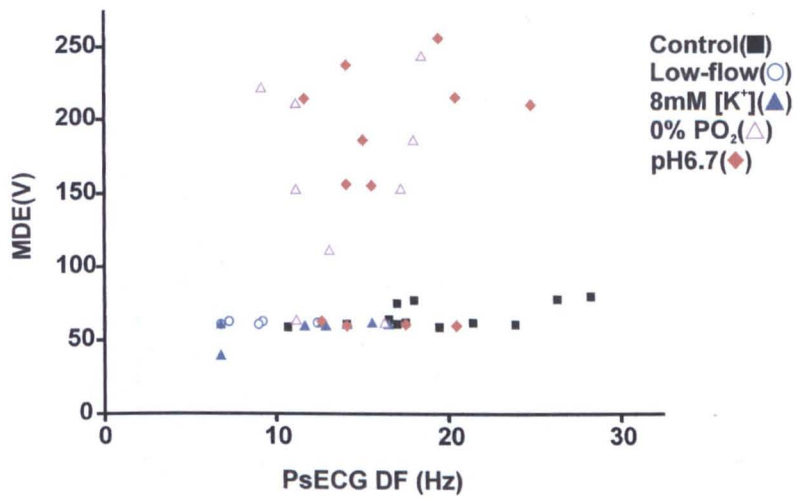


Figure 10.3 Scattergram of psECG DF vs. MDE. The DF of the psECG was calculated immediately prior to defibrillation. Plotting psECG DF against the MDE determined at the same time shows no linear correlation.

10.3.3 Coefficient of variance

The coefficient of variance of the optical dominant frequency was calculated for each time interval. The coefficient of variance was not significantly different between the protocols immediately after VF induction (data not shown). As VF progressed, the coefficient tended to increase with time in all protocols except acidic pH_{EC}, where it tended to remain constant. For clarity, in figure 10.4 only the data from control, low-flow ischaemia and pH 6.7 conditions are plotted for the full time-course. There was no significant change in coefficient of variance as assessed by absolute values or by the fractional change in each heart (Figure 10.5).

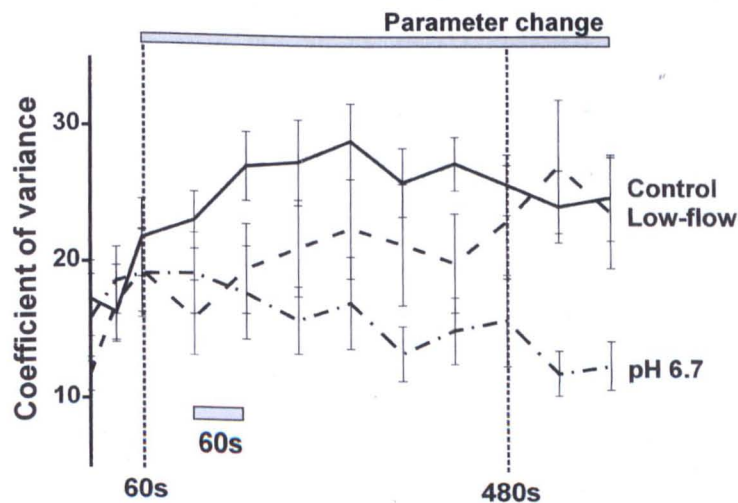


Figure 10.4 The coefficient of variance of the optical DF. The coefficient of variance was calculated for the DF of all 252 optical signals. Although there was a tendency for the coefficient to increase in control and low-flow, and to decrease in pH 6.7, there was no significant difference as assessed at 480s.

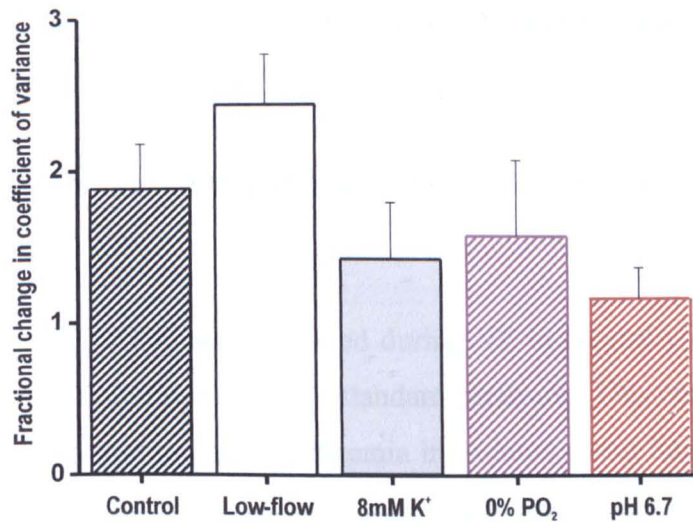


Figure 10.5 Mean fractional change in coefficient of variance. The coefficient of variance of the DF of the 252 optical signals was calculated for 0s and 480s. For each protocol the fractional change from 0s to 480s was calculated. There was no significant difference in the fractional change in coefficient of variance between any of the protocols.

10.4 Discussion

In this chapter, the mean MDE was not significantly altered by low-flow ischaemia or 8mM [K⁺] solution compared to control. Instead, the MDE was significantly elevated by hypoxia and acidic pH_{EC}.

10.4.1 MDE in low-flow ischaemia

Successful defibrillation requires a shock to homogeneously depolarize a sufficient mass of myocardium to stop the fibrillation wavefronts without launching new activation waves. Thus defibrillation fails because the shock that terminates fibrillation also reinitiates fibrillation. Several different mechanisms leading to the reinitiation of VF have been proposed; from critical point re-entry (94, 104), through virtual electrodes (96) to Delayed After Depolarisations (DADs) (288). Along with the uncertainty surrounding the mechanism of defibrillation failure, there are equally conflicting views on the impact of ischaemia on DFT. To date, most investigators have concentrated on the effects of regional ischaemia on DFT. Different research groups have shown that occlusion of the LAD artery could increase DFT (289, 290), decrease DFT (291), or to have no effect on DFT (292), (293) such that even the size of the ischaemic area had no significant effect on DFT (294). In the small number of studies that examined the effect of global ischaemia on DFT, there was an equal range of findings. In the isolated swine heart, Barton et al. documented a decrease in MDE in prolonged low-flow ischaemia (73). In contrast, Cheng et al. demonstrated a wider window of vulnerability to shock-induced arrhythmia in isolated

rabbit hearts suggestive of a raised DFT (295). However, Behrens et al. found that global ischaemia had no effect on DFT (283).

10.4.1.1 Evidence for unchanged defibrillation energies in global ischaemia

In this chapter, equivalent MDE were attained during VF in control conditions and low-flow ischaemia with the flow rate at 15% of standard perfusion. This compares well to the only previous study of global low-flow ischaemia in isolated rabbit hearts (283). Behrens et al. found that the energy required to defibrillate control conditions of $271 \pm 33\text{V}$ was not different from the energy of $268 \pm 42\text{V}$ that was required when the flow rate was reduced to 20%. The absolute energies required to defibrillate in both conditions were much higher than those documented in this chapter (control = $73 \pm 9\text{V}$, low-flow ischaemia = $93 \pm 24\text{V}$). The higher absolute energy values in Behrens et al. are probably due to a combination of differences in (i) protocols, (ii) electrode arrangements and (iii) biphasic waveform characteristics.

(i) Behrens et al. measured the DFT_{50} by an up-down protocol. The hearts were made ischaemic for 10 – 15 minutes before several short periods of 5 – 10s of VF were induced and defibrillated. Due to the longer period of 600s of VF in ischaemia used in this thesis, such an up-down protocol could not be performed. Rather, the MDE was determined.

(ii) Behrens et al. used parallel circular electrodes that were held 6cm apart and perpendicular to the long axis of the heart. Although the resistance was not stated, one would expect such an electrode arrangement to have higher resistances than the cradling electrodes applied in this thesis.

(iii) Factors affecting the efficacy of biphasic waveforms are numerous and complex (for full summary see (296)). These factors include waveform duration and shape (297, 298), tilt (299) and capacitor size (300). The Medtronic defibrillator used by Behrens et al. had a smaller $120\mu\text{F}$ capacitor compared to the $140\mu\text{F}$ capacitor of the ECD used in this chapter. This smaller capacitor gave a waveform duration of 5ms compared to the 14ms waveform duration in this current study.

10.4.1.2 Evidence for decreased defibrillation energies in global ischaemia

Using isolated pig hearts, Barton et al. observed that lower energies were required to defibrillate VF during perfusion at 10% standard rate compared to perfusion at standard rate (73). Barton et al. also observed that the ECG DF decreased during VF in low-flow ischaemia. They hypothesised that the slower ECG DF in low-flow ischaemia represented more organised myocardial electrical activity, and that this more organised activity could be defibrillated more easily, hence the reduction in MDE. Three computer simulations support this hypothesis.

The first of these simulations used the bidomain model of human atrial tissue (301). Here, Plank et al. calculated that higher energies would be required to defibrillate increasing levels of fibrillation complexity. By increasing the spatial heterogeneity of the acetylcholine dependant potassium channel they controlled the degree of wavebreak of a single spiral rotor. As the degree of wavebreak increased, the energy predicted to terminate the arrhythmia also increased.

The second simulation supporting the hypothesis of an inverse relationship between electrical complexity and the defibrillation energy was performed using the Auckland model of canine ventricles (302). Here, Hillebrenner et al. predicted that multiple scroll waves would require higher energies to be successfully defibrillated than a single scroll wave.

The third supporting simulation examined the effect of complete global ischaemia on the ability to induce arrhythmia in the bidomain model of the canine ventricle (284). Here, Rodriguez et al. predicted the lowering of the ULV in total global ischaemia compared to control conditions. As previously explained, the ULV and DFT are known to be intimately related (120, 286, 287). Thus predicting a lowering in ULV also implies a lowering of the DFT (284).

The observations and simulations of reduced defibrillation energy were derived from larger hearts compared to those used in this thesis or in Behrens et al. It is therefore possible that the reduced defibrillation energies are an indirect feature of the greater myocardial mass. For instance, although Barton et al. (73) and Behrens et al. (283) both increased shock strength by 50V increments, the greater resistance of the larger swine heart of 84Ω would reduce the concurrent increase in current and power associated with this voltage increase.

As discussed more fully later, in this chapter, there was no correlation between the rate of electrical activity and MDE (Figure 10.3).

10.4.1.3 Evidence for increased defibrillation energies in global ischaemia

There is no direct assessment of DFT or MDE that demonstrates an increase in global ischaemia. However such a result could be implied from the optical mapping study by Cheng et al. using isolated rabbit hearts immobilised by BDM (295). Here Cheng et al. demonstrated an increase in the dispersion of repolarisation times, 20 minutes after the perfusion rate was reduced to 25%. Concurrent with this increased dispersion, they demonstrated an increased window of vulnerability to shock-induced arrhythmia. This means during low-flow ischaemia VF could be induced by a monophasic countershock at more points of the AP than in control. The resultant VF spontaneously defibrillated in all control protocols, whereas defibrillation shocks were required to convert VF in ischaemic conditions. The applicability of this study to this chapter is difficult as: - (i) the percentage flow reduction was much lower in this thesis, (ii) the duration of ischaemia was twice as long as that used in this thesis and (iii) the use of BDM can in itself increase the window of vulnerability as subsequently demonstrated by the same group (155).

10.4.2 MDE in hypoxia

During hypoxia, increased energies were required to defibrillate VF compared to control conditions. To date only a few studies have investigated the effects of hypoxia on the required defibrillation energy. Of these studies, one canine study showed that hypoxia lowered the DFT from $83 \pm 49\text{J}$ in control to $58 \pm 28\text{J}$ ($p < 0.01$) (294), whereas another canine study showed no effect of hypoxia on DFT (303). These studies were performed on in situ hearts with CPR support during VF. Thus any hypoxia-induced K^+ efflux would partially accumulate (214), reduce the potassium equilibrium potential, depolarise the diastolic membrane potential, and therefore lower the defibrillation threshold (304). In the Langendorff-perfused rabbit heart extracellular K^+ would not be expected to accumulate. Indeed, the lack of difference in hypoxia compared to control in either the VF frequency (Chapter 4) or VF amplitude (Chapter 8) supports this prediction.

In the absence of K^+ accumulation, it is difficult to predict the effect of hypoxia on defibrillation energies. Some effects of hypoxia would tend to increase the required energy, whereas other effects would tend to decrease it. In the Langendorff-perfused guinea pig

heart, Salama et al. showed an increase in the regional dispersion of repolarisation during hypoxia and hypothermia (305). The association of increased dispersion of repolarisation with increased defibrillation energies is well documented (295, 306, 307). In contrast, hypoxia has been shown to abolish DADs (308), which have been proposed as a source of VF reinitiation (288). By abolishing these spontaneous calcium releases, hypoxia could reduce the tendency for reinitiation of VF, and thus increase than chance of successful defibrillation.

10.4.3 MDE in acidic pH_{EC}

Acidic pH_{EC} increased the energies required to defibrillate VF compared to control conditions. As with hypoxia, previous research into the effects of acidic pH_{EC} on required defibrillation energy is limited and conflicting. Kerber et al. failed to show any change in DFT with either respiratory or metabolic acidosis (309). However, they only reduced the arterial pH to 7.25. In contrast, a Chicago research group repeatedly demonstrated the need for more countershocks and greater total defibrillation energy in hypercarbic acidosis (310-312). The arterial pH was reduced to pH 6.7 in all these studies. In this chapter, pH 6.7 increased the MDE from $73 \pm 9V$ to $177 \pm 26V$ ($p < 0.001$), and during pH 6.3, VF was resistant to defibrillation with shocks as high as 250V. In pH 6.3, shock strengths $>110V$ produced an isoelectric window longer than 20s. One would normally expect such a prolonged isoelectric window to be associated with successful defibrillation. However, in pH 6.3, the first activation after this window was VF.

Acidic pH is well recognised for its arrhythmogenicity (for review see (213)). As well as affecting the resting membrane potential, APD and activation threshold (discussed fully in chapter 4.4.2), acidic pH can precipitate arrhythmias through (i) the triggered activity of EADs (313-315) and DADs (221, 308, 316), (ii) producing re-entrant susceptible substrates such as calcium (Ca^{2+}) alternans (317, 318), (iii) CV slowing (218, 319) and (iv) increased gap junction resistance (320-322). Several of these mechanisms have been associated with defibrillation failure.

10.4.3.1 DAD and acidic pH

DADs consist of transient diastolic depolarisations of the membrane that occur secondary to spontaneous release of Ca^{2+} from the sarcoplasmic reticulum (SR) (323), and are often associated with calcium overload of the SR (324). By reducing the Ca^{2+} load, and thus suppressing DADs, amiodarone can chemically defibrillate VF (325). Similarly,

defibrillation shocks that significantly reduce the SR Ca^{2+} load tend to be successful, whereas those that fail to reduce the SR Ca^{2+} load often fail to defibrillate (326). This has led to the hypothesis that in unsuccessful defibrillation, VF is reinitiated by DADs from the Ca^{2+} overloaded SR. Evidence to support this comes from optical mapping of near-DFT strength shocks (327). In this study, VF was shown to be reinitiated by focal activity after complete repolarisation. Subsequent experiments by the same group demonstrated improved defibrillation success and reduced DFT with the DAD inhibitor, flunarizine (288). Acidic pH has been shown to increase the frequency and amplitude of DADs (221, 308). Thus one would predict that acidic pH should have the reverse effect to flunarizine, and therefore should reduce the success of defibrillation and increase DFT.

10.4.3.2 Re-entry substrate and acidosis

Re-entry is another important mechanism for reinitiating VF after unsuccessful defibrillation (109). In order to sustain re-entry a tissue must provide (i) functional conduction block and (ii) large enough functional circuit to allow adequate repolarisation and re-activation (for review see (38)).

i) Functional conduction block – The first of these requirements may arise from alternans. By slowing Ca^{2+} recycling in the SR, acidic pH can produce both mechanical and Ca^{2+} alternans (317), which in turn can lead to alternans of the APD (328, 329). APD alternans can cause conduction block if the voltage oscillations are spatiotemporally out of phase; that is that adjacent areas having short and long APD on the same activation (330, 331). The inherent instability of such discordant alternans leads to functional conduction block, and thus re-entry (332). However, this does not take into account the voltage/ Ca^{2+} interaction. To date, the role of the voltage/ Ca^{2+} interaction in alternans has only been proposed by computer modelling (333). In this study, two contrasting voltage/ Ca^{2+} interactions were proposed: - (a) Negative voltage/ Ca^{2+} interaction – as shown in figure 10.6, the greater amplitude Ca^{2+} transient predominantly inactivates L-type Ca^{2+} channel resulting in a shortened APD. (ii) Positive voltage/ Ca^{2+} interaction – here the larger Ca^{2+} transient predominantly affects Na^+ - Ca^{2+} exchanger to prolong the APD (Figure 10.5). Positive interactions will tend to amplify changes in the system. Such a system is predicted to be less stable and more arrhythmogenic. It has yet to be established which type of voltage/ Ca^{2+} interaction prevails in acidic pH.

(ii) Functional circuit – By slowing wave propagation, acidic pH allows re-entry to become established in smaller circuits. In acidic pH, AP propagation is slowed by a combination of I_{Na} inhibition (334) and increased gap junction resistance (320-322).

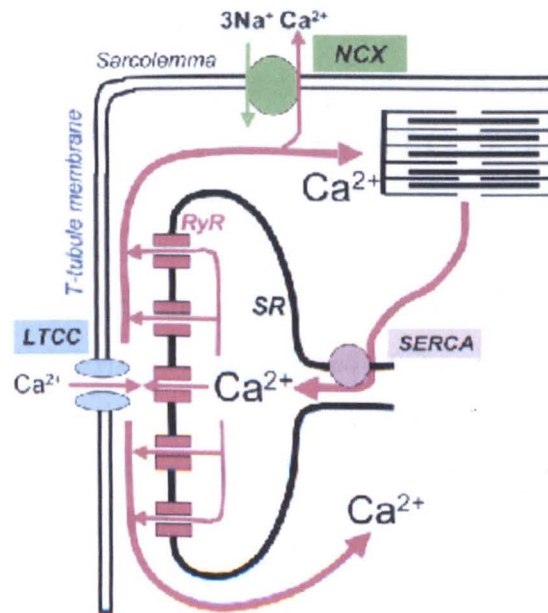


Figure 10.6 Voltage- Ca^{2+} interactions. A small amount of calcium enters the myocyte via the L-Type Ca^{2+} Channel (LTCC). This activates Ca^{2+} -Induced Calcium-Release (CICR) from the SR via the Ryanodine receptor (RyR). On relaxation, the released Ca^{2+} is either sequestered back into the SR via the Sarcoplasmic-Endoplasmic Reticulum Ca^{2+} ATPase (SERCA) or extruded out of the cell by Na^{+} - Ca^{2+} exchanger (NCX) with a reciprocal influx of Na^{+} . The released Ca^{2+} stops the Ca^{2+} influx by negative feedback on both LTCC and RyR. In negative voltage/ Ca^{2+} interaction, the feedback inhibition of LTCC is greater than the influx of Na^{+} , so that a larger Ca^{2+} transient is associated with a shorter APD. In positive voltage/ Ca^{2+} interaction, the Na^{+} influx via NCX predominates thus prolonging the APD (Adapted from (335)).

So in summary, despite conflicting evidence for the effect of acidic pH on defibrillation energy requirements, the electrophysiological effects of acidosis support an increase in energy requirements. This is in keeping with the increased MDE produced by pH 6.7 and the defibrillation resistance of pH 6.3 demonstrated in this chapter.

10.4.4 MDE in raised $[K^{+}]_{EC}$

Although there was no significant change of MDE in 8mM $[K^{+}]$ solution compared to control and low-flow ischaemia, there was a tendency towards reduction. Higher $[K^{+}]$ solutions resulted in spontaneous defibrillation to a regular ventricular escape rhythm before 600s. This suggests that the MDE was actually reduced and was not detected due to technical restraints. As outlined in section 10.2, the ECD could only deliver biphasic shocks $>60V$. Thus it was not possible to detect MDE below 60V. As the MDE for VF in

control conditions was $64 \pm 2V$, a significant reduction of MDE by raised $[K^+]_{EC}$ compared to control was impossible to detect. Previous clinical experience would support this conclusion. Prior to the invention of electrical defibrillators, chemical VF defibrillation was developed (163), and used in cardiac surgery (164). Indeed, this technique was been re-evaluated for use after coronary artery bypass surgery to prevent mechanical damage of the newly grafted vessels by the intra-thoracic defibrillator paddles (336). Previous animal research has also shown that raised $[K^+]_{EC}$ lowers DFT (304). In this canine study, cardiac perfusion was maintained by cardiopulmonary bypass, and the $[K^+]_{EC}$ raised by potassium chloride infusion. Babbs et al. demonstrated that the percentage reduction of DFT was linearly related to $\log[K^+]_{EC}$ and the potassium equilibrium potential (E_K). This linear relationship supported their hypothesis that raised $[K^+]_{EC}$ would reduce DFT by bringing the diastolic membrane potential nearer to the cellular firing threshold of -50 to $-60mV$. Indeed, when the diastolic membrane potential was raised above the firing threshold to $-46mV$ by $16mM [K^+]_{EC}$, Babbs et al. observed spontaneous defibrillation.

The inverse relationship between $[K^+]_{EC}$ and DFT only applies to global increases in $[K^+]_{EC}$. Regional increases in $[K^+]_{EC}$ increases the DFT (306). This was hypothesised to arise from the increased heterogeneity of various electrophysiology parameters such as repolarisation, refractoriness and conduction velocity.

10.4.5 MDE in infarcted hearts during zero-flow ischaemia

In zero-flow ischaemia, non-infarcted hearts spontaneously defibrillated from VF within 240s (Chapter 3.3.1). In comparison, 8-week infarct hearts remained in VF for 600s, and were resistant to defibrillation. As with acidic pH_{EC} , shocks $>1J$ produced long isoelectric gaps after which the first activation was VF. Two phenomena may contribute to this defibrillation resistance: - (i) electrophysiological consequences of border zone and scar tissue and (ii) increased heterogeneity secondary to cardiac failure.

10.4.5.1 Electrophysiological consequences of scar tissue

An important risk factor for sudden cardiac death from VF is the presence of an infarct scar (337). The myocardium at the interface of normal and scar tissue, which is commonly known as the border zone, undergoes extensive remodelling (for review see (338)). Border zone remodelling involves fibroblast infiltration, disruption of the myofibril structure, and changes in the patterns of connexion expression (339-341). This border zone exhibits slower epicardial conduction velocities compared to the surrounding normal and infarcted

tissue (182), and has been linked to arrhythmogenesis in both dogs (342) and rabbits (343). Through electrical mapping, Peters et al. localised re-entrant circuits of VT to the border zone in 4-day infarct canine hearts (342). A similar localisation of shock-induced arrhythmias was demonstrated in 4-week infarct rabbit hearts with optical mapping (343). In this study, Li et al. demonstrated a higher ULV in infarcted compared to normal hearts, thus implying an increase in DFT. They also found that shock-induced VF was most commonly initiated by a break-excitation wavefront that originated within the border zone. Although such break-excitations can reinitiate VF after failed defibrillation, they do not explain this chapter's findings of re-excitation after prolonged isoelectric windows (295).

10.4.5.2 Electrophysiological heterogeneity in cardiac failure

Distinct from the border zone, non-infarcted myocardium also undergoes remodelling (for review see (344)). As they adapt to the relative increase in workload, the non-infarcted ventricular myocytes hypertrophy (345, 346), with the degree of hypertrophy dependent on the extent of the infarct (347). The electrophysiological properties in these hypertrophied, non-infarct myocytes are changed, with increased CV (252), prolonged APD (348) and altered Ca^{2+} transients (179). The evidence is conflicting as to whether or not these adaptations increase the electrophysiological heterogeneity across the heart. For example, in the rat the difference in APD and Ca^{2+} transients between myocytes from the RV free wall and septum was reduced post infarction (349). In the rabbit however, the APD and Ca^{2+} transients were shortened in subendocardial myocytes, but prolonged in subepicardial and M-type myocytes (179). Also in the rabbit, Ng et al. used a combination of MAPs and the calcium sensitive dye Indo-1 to show increased dispersion of APD and Ca^{2+} transient duration across the non-infarcted epicardial surface of 8-week infarct hearts compared to equivalent regions in control hearts (180, 188).

Increased epicardial APD dispersion is also a feature of non-infarct related heart failure. In canine tachycardia-induced cardiomyopathy, Pak et al. demonstrated increased repolarisation heterogeneity, and an increased incidence of malignant arrhythmias (350). In this model the DFT was also increased (351, 352). This suggests that the increase in defibrillation energies is not only due to the electrical consequences of the infarct.

10.4.5.3 Cardiac dilation and defibrillation energy

The 8-week rabbit infarct model has an increased LV end-diastolic diameter (179-181). In theory, this increased cardiac volume associated with cardiac failure should affect the

minimum field strength for a given shock. The inverse square law dictates that the electric field intensity falls as square of the distance from the electrode increases. Indeed in cardiac tissue, the field strength does fall with distance (353) and cardiac dilatation increases DFT (354, 355). However, the long isoelectric window observed in the infarcted hearts after shocks $>1J$, suggests that the field strength was sufficient to inactivate all electrical activity including the area of minimum field strength. So although cardiac dilatation could explain an increase in defibrillation energy, it does not explain the immediate reinitiation of VF.

10.4.6 Lack of relationship between DF and MDE

As discussed above, previous studies have suggested a correlation between the complexity of the electrical activity and the required defibrillation energy (73, 284, 301, 302). In contrast, clinical studies have shown that the slower electrical activity of more prolonged out-of-hospital arrests are associated with less successful defibrillation (6, 23, 32, 33, 276, 277), and that partial restoration of perfusion increased the ECG DF (24, 278, 279) and improved defibrillation success (9, 12, 13, 280-282).

In this thesis, there was no correlation between the VF electrical activity as measured by the psECG DF immediately prior to defibrillation and the MDE. Indeed, the ischaemic components which increased MDE compared to control, namely hypoxia and acidic pH_{EC}, did not change the ECG, psECG or LV optical DF compared to control (Chapter 4.3, Figure 10.7). In contrast, low-flow ischaemia and raised $[K^+]_{EC}$ markedly slowed the ECG, psECG and LV optical DF, had no significant effect on the MDE.

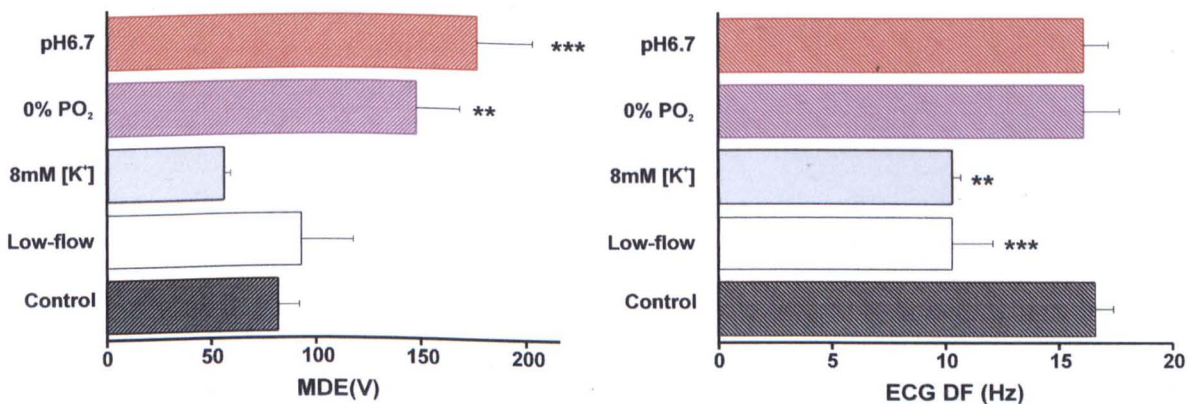


Figure 10.7 Bar charts of MDE and ECG DF. Panel A: MDE is significantly raised by pH 6.7 (***) $p < 0.001$ vs. control) and 0% PO₂ (** $p < 0.01$ vs. control) but unaffected by low-flow ischaemia or 8mM [K⁺] solution. Panel B: In contrast, the ECG DF was significantly reduced by low-flow ischaemia (***) $p < 0.001$ vs. control) and 8mM [K⁺] solution (** $p < 0.01$ vs. control) but unaffected by pH 6.7 or 0% PO₂.

The lack of correlation between DF and MDE is not surprising. As discussed above the success or failure of a shock is influenced by far more factors than the electrical coordination at the point of defibrillation. Factors such as trigger potential (288), heterogeneity of refractoriness and conductivity all have roles to play in defibrillation failure (356). Thus relating MDE to DF is too simplistic.

10.4.7 *Coefficient of variation as measure of dispersion of repolarisation*

A key concept in defibrillation is the heterogeneity of repolarisation and refractoriness prior to defibrillation. Computer modelling has predicted that more complex electrical activity at the point of defibrillation will require greater shock strength to terminate the arrhythmia (301, 302). Previous studies have used the coefficient of variance of the ventricular fibrillation interval to assess the dispersion of refractoriness during VF (4, 46, 135). By measuring the interval between VF activations, this method assumes that in VF, a cell will be activated as soon as its ERP is completed. Under the same principle, the DF should represent the predominant refractoriness within the 0.8×0.8 mm epicardial surface the photodiode recorded from (Chapter 2.4). In an attempt to quantify the heterogeneity of the electrical activity in VF, the coefficient of variance for the optical DFs was calculated. This failed to show any significant change in electrical heterogeneity either between, or within protocols.

11 Synopsis

The main aim of this thesis was to identify the contributions of the principal metabolic components of ischaemia to the slowing of the electrical activity in VF, and to establish whether the same components were responsible for increasing the energy required for successful defibrillation. These investigations were performed on the isolated Langendorff-perfused rabbit heart using a combination of optical mapping, MAP electrodes and floating microelectrodes. The main findings of this thesis were: -

- (i) That there was LV/RV heterogeneity in DF during VF in low-flow ischaemia, and that this pattern was most closely reproduced by raised $[K^+]_{EC}$, rather than hypoxia or acidic pH_{EC} .
- (ii) That the electrophysiological mechanism underlying this ventricular heterogeneity was most probably a differential increase in the activation threshold in the LV compared to the RV.
- (iii) That there was LV/RV heterogeneity in activation amplitude in VF.
- (iv) That the ischaemic components that led to an increase in the required defibrillation energy did not slow the electrical activity in VF.

11.1 Spatiotemporal heterogeneity in dominant frequency

Previous research in VF has shown that the temporal changes in ECG frequency are dependant on the level of myocardial perfusion (30, 73). Similar dependence of the ECG DF on perfusion rate in the isolated rabbit heart was demonstrated in chapter 3. On reducing the perfusion rate, the DF declined to a steady state value. The rate of ECG DF decline, and the steady state value achieved depended on the perfusion rate (Figure 3.1). Perfusion at 6ml/min was designated as low-flow ischaemia, as this was the lowest perfusion rate to reliably maintain VF for 600s. Examining the spatiotemporal distribution of the electrical activity, optical mapping revealed LV/RV heterogeneity in the DF, when the ECG DF was at steady state (480s). During control conditions, the LV DF increased with time and was also increased compared to the contemporaneous RV DF (Figure 3.4). In low-flow ischaemia, the LV DF decreased with time, whilst again the RV DF remained unchanged.

On imposing individual metabolic components of ischaemia during VF, the ECG and psECG DF were not significantly altered by hypoxia or acidic pH_{EC} compared to control

(Figures 4.2 & 4.3). In contrast, during VF in raised $[K^+]_{EC}$, the ECG and psECG showed a declining DF pattern that was indistinguishable from that of low-flow ischaemia (Figure 4.5). Looking at the spatiotemporal DF organisation in VF, the DF pattern in hypoxia was indistinguishable from control (Figure 4.4), and the DF pattern in raised $[K^+]_{EC}$ was indistinguishable from low-flow ischaemia. The DF pattern in acidic pH_{EC} was different from both control and low-flow ischaemia, with the LV DF increasing to a lesser extent than in control conditions, and the RV DF now also increasing.

Thus raising $[K^+]_{EC}$ best reproduced the global and spatiotemporal frequency changes observed in VF during low-flow ischaemia.

11.2 Electrophysiological mechanism of dominant frequency heterogeneity

Four theoretical mechanisms were identified as potential sources of the spatiotemporal DF heterogeneity in VF during low-flow ischaemia and raised $[K^+]_{EC}$: (i) differential prolongation of LV repolarisation; (ii) differential prolongation of LV post-repolarisation refractoriness; (iii) differential reduction in LV conduction velocity and (iv) differentially increase in LV activation threshold.

11.2.1 (i) Prolongation of repolarisation

Repolarisation and refractoriness are interlinked phenomena. Only when the membrane is starting to repolarize from the action potential plateau does it start to gain the excitability of the relative refractory period. By prolonging the plateau phase, the absolute refractory period (ARP) is prolonged. In VF, it has been argued that a ventricular myocyte will be activated as soon as it is capable (4, 46, 357). Thus, by extending the ARP, the activation rate and the dominant frequency (DF) would be reduced. To explain the DF reduction in the LV, but not the RV, a differential prolongation of the LV APD would be required. Simultaneous measurements of LV and RV $MAPD_{90}$ in control conditions showed no baseline differences. In low-flow ischaemia, neither the LV nor the RV $MAPD_{90}$ were significantly altered. The tendency for the LV APD to be shorter than the RV APD in low-flow ischaemia would be more in keeping with higher DF in the LV than the RV. In raised $[K^+]_{EC}$, both RV and LV $MAPD_{90}$ were significantly shortened, but to similar degrees. Thus differential prolonged repolarisation cannot explain the LV/RV heterogeneity of DF during VF in low-flow ischaemic or raised $[K^+]_{EC}$ conditions.

11.2.2 (ii) Prolonged of post-repolarisation refractoriness

In ischaemia, the ARP extends beyond AP plateau, and even full repolarisation (236, 237). This post-repolarisation refractoriness can be assessed by measuring the effective refractory period (ERP). If post-repolarisation refractoriness was differentially longer in the LV than the RV, this could explain its lower DF during low-flow ischaemia and raised $[K^+]_{EC}$. As discussed fully in chapter 6.4.1, the assessment of refractoriness in ischemia is difficult. Traditionally, ERP has been assessed by establishing the pacing threshold at intervals well beyond possible post-repolarisation refractoriness, setting the pacing stimulus at twice this voltage then, using an S_1S_2 protocol, identifying the ERP as the point of non-capture (239). Using this protocol, the baseline LV and RV ERP were not significantly different in control conditions (Figure 6.3), and were not significantly changed in either ventricle during low-flow ischaemia or raised $[K^+]_{EC}$. This result indicates that differential prolongation of the LV post-repolarisation refractoriness also cannot account for the LV/RV heterogeneity of DF during VF in low-flow ischaemic or raised $[K^+]_{EC}$ conditions.

11.3 (iii) Reduced conduction velocity

The role of conduction velocity (CV) in VF is controversial. Computer modelling predicts opposite effects of conduction slowing on VF maintenance depending on whether the underlying mechanism is a “mother rotor” or “multiple wavelets” (254). On one hand conduction slowing will stabilise a mother rotor and convert VF to VT, whereas on the other hand slowed conduction will reduce the rate of wavelet annihilation and thereby prolong VF duration. Ischaemia alters CV in a temporally biphasic fashion. After onset of ischaemia, the CV increases for ~120s before progressively decreasing (205). In VF, the 480s assessment point represents 420s in the experimental condition. Therefore at 480s in VF during low-flow ischaemia, the CV should be reduced. After 420s of low-flow ischaemia, both longitudinal and transverse CVs were reduced by ~30% in the LV. However, in the RV, longitudinal CV was maintained, and transverse CV reduced to lesser degrees (~7%) (Figure 7.2). This differential effect may be the basis for the reduced DF in LV in low-flow ischaemia. However, in raised $[K^+]_{EC}$ there was no change in CV, and therefore CV reduction cannot be a necessity for the DF to be reduced in VF.

11.3.1 (iv) *Raised activation threshold*

An action potential is triggered if the resting membrane potential depolarises above a certain threshold voltage and sufficient Na^+ current (I_{Na}) is activated to rapidly depolarise the membrane. This threshold voltage can be increased either by increasing the magnitude of the background outward current, or by reducing I_{Na} . In VF, the AP amplitude is highly variable. It is therefore conceivable that low amplitude activations from an area with a low activation threshold will not trigger activity in an adjacent region with a high activation threshold. For this reason, a differential increase in LV activation threshold could reduce the LV DF.

During low-flow ischaemia and raised $[\text{K}^+]_{\text{EC}}$ the activation threshold was increased in the LV compared to the RV (Figure 6.4). Previous research has documented raised activation thresholds in ischaemia (242, 242, 245, 246) and in raised $[\text{K}^+]_{\text{EC}}$ (247). This increased LV activation threshold was associated with a slower MAP upstroke velocity in the LV compared to the RV, suggesting a reduction in the available Na^+ channels or an increase in the background K^+ currents (Figure 6.5). The association between reduced magnitude of I_{Na} , increased pacing threshold and reduced AP upstroke has previously been demonstrated in neural tissues (248).

During VF in 8mM $[\text{K}^+]$ solution, there was a significant depolarisation of the diastolic membrane potential (Figure 9.6). In contrast, the expected diastolic depolarisation in VF during low-flow ischaemia was not demonstrated (Figure 9.5). This lack of diastolic depolarisation may well result from the superfusion of the epicardial surface. This superfusion may have prevented any accumulation of the ischaemic-related K^+ efflux, and thereby prevented any depolarisation secondary to increased $[\text{K}^+]_{\text{EC}}$. As superfusion cannot prevent the accumulation of K^+ within the deeper myocardium layers, these tissues will undergo diastolic depolarisation. Such depolarisation will inactivate I_{Na} , reduce AP upstroke velocity, increase the activation threshold, and thereby reduce LV DF as was observed on microelectrode impalement of VF during low-flow ischaemia (Figure 9.3).

Bringing this evidence together has led to the unifying theory that the LV DF slowing in VF during low-flow ischaemia and raised $[\text{K}^+]_{\text{EC}}$ is due to LV diastolic membrane depolarisation. This LV diastolic depolarisation causes partial inactivation of the I_{Na} , and thereby increases the LV activation threshold. In support of this theory, inhibition of I_{Na} has been shown to reduce ECG DF in VF (62). In this study, Mandapati et al. observed that when hearts in VF were perfused with the Na channel inhibitor, tetrodotoxin, the rotational

rate of re-entrant circuits was reduced and the internal core of the re-entrant circuits was enlarged. These changes were identical to those they observed in VF during ischaemia.

11.3.1.1 Mechanism of ventricular heterogeneity – role of I_{K1} ?

The ventricular nature of VF heterogeneity is not a new concept. Shortly after VF induction the electrical activity is more complex in the LV than the RV (358), with higher frequencies developing in the LV compared to the RV (192, 193). Optical mapping has demonstrated that the transition between the 2 regions is sharp (63). In this thesis similar sharp transitions were observed in all VF protocols. As discussed in 3.4.3.2, Warren et al. proposed the LV/RV heterogeneity in VF during control conditions was due to the differential expression of Kir2.1 and Kir2.3 in LV myocytes compared to RV myocytes (190). This differential Kir2.x expression may also account for the differences in the LV and RV DF in VF during low-flow ischaemia and raised $[K^+]_{EC}$.

In raised $[K^+]_{EC}$, the reversal potentials (E_k) of both Kir2.1 and Kir2.3 experience a rightward shift to less negative voltages (226). Such alterations in E_k result in diastolic depolarisation of the cell membrane when $[K^+]_{EC}$ is raised (202, 227). The greater LV Kir2.x expression would be predicted to cause greater diastolic depolarisation in the LV than the RV. A greater diastolic depolarisation in the LV would lead to greater I_{Na} inhibition, and therefore greater increases in the activation threshold in the LV than the RV.

11.4 Amplitude changes in VF

Both clinical (19, 24, 29) and animal (30, 33) studies have demonstrated that the activation amplitude of the ECG diminishes with time in non-perfused VF. In comparison there is no literature detailing amplitude changes in perfused VF.

11.4.1 Control conditions

Under control conditions, the VF ECG amplitude rapidly decreased over the first 4 minutes, then stabilised at ~55% of the initial VF amplitude. This pattern closely mirrored the ECG DF frequency changes, where the DF increased over the first 3 minutes, before slightly slowing and stabilising at values greater than those immediately post VF induction. As the ECG is a global assessment of electrical activity, 2 possible processes could result in this frequency/amplitude relationship: - (i) the faster electrical activity could be more

dyssynchronous. In this scenario, local electrical vectors would increasingly oppose each other, and therefore reduce the global amplitude recorded; (ii) increasingly faster activations could start to impinge on the Na^+ channel recovery. This would result in lower numbers of Na^+ channels opening, a lower I_{Na} magnitude, and thus lower activation amplitude (maximum systolic potential).

In optical mapping, each photodiode records the electrical activity from an epicardial area of less than 1mm^2 . Therefore the VF amplitude reduction to $\sim 45\%$ of baseline observed in the psECG suggests a cellular amplitude reduction rather than a co-ordination phenomenon. Optical mapping also revealed a more pronounced reduction of LV than RV amplitude with the LV amplitude reducing to $\sim 33\%$ of baseline. Transmembrane recordings from the LV epicardial surface confirmed an absolute reduction in the AP amplitude during VF in control conditions but only to 86% of baseline amplitude. So the LV amplitude reduction in VF was probably due to a combination of reduced electrical co-ordination and reduced I_{Na} magnitude.

11.4.2 Low-flow ischaemia, hypoxia and acidic pH_{EC}

On flow reduction there was a transient increase in ECG, psECG and LV optical AP amplitude, which corresponded to the initial dramatic decline in VF DF. From this point onwards the ECG, psECG and LV optical AP amplitudes were indistinguishable from control conditions. The amplitude changes in hypoxic and acidotic conditions were also indistinguishable from control.

11.4.3 Raised $[\text{K}^+]_{\text{EC}}$

Exposure of VF to raised $[\text{K}^+]_{\text{EC}}$ decreased the ECG, psECG and LV DF. These DF decreases were accompanied by increases in the corresponding amplitudes. When this data was plotted alongside the DF and amplitude results from VF in control, hypoxic and acidic conditions, they all followed the same correlation, perhaps suggesting a similar mechanism of amplitude alteration. Transmembrane recordings of VF during raised $[\text{K}^+]_{\text{EC}}$ demonstrated that the reduction of DF was associated with depolarisation of both the diastolic and maximum systolic membrane potentials. There was however no increase in the peak-to-peak amplitude of the membrane potential oscillations in VF during raised $[\text{K}^+]_{\text{EC}}$. Instead the tendency was for the peak-to-peak amplitude to be reduced.

Although each photodiode records from a small epicardial area ($<1\text{mm}^2$), and is therefore less influenced by the macroscopic VF organisation than the ECG, each photodiode is still affected by the activity of hundreds of myocytes. In VF, where there is no AP plateau, the peak-to-peak amplitude of the optical signal will be affected by the degree of intercellular electrical co-ordination, and thus the number of cells contributing to the signal. As the dominant frequency slows, the activation wave rotates around its spiral core more slowly (62). This allows greater degrees of intracellular electrical co-ordination to produce an artificial increase in the optical amplitude in VF during raised $[\text{K}^+]_{\text{EC}}$.

11.5 Minimum defibrillation energy

In order to successfully defibrillate VF a shock must (i) depolarise sufficient myocardium to disrupt the propagation of the fibrillation wavefronts and (ii) not produce new excitations that re-initiate VF (92). The mechanism of re-initiation is still unclear. This thesis examined the effect of low-flow ischaemia and its principal metabolic components on the minimum defibrillation energy (MDE) required to terminate VF. Whilst low-flow ischaemia (6ml/min) and raised $[\text{K}^+]_{\text{EC}}$ (8mM) had no significant effect on MDE compared to control, lower perfusion rates and higher $[\text{K}^+]$ concentrations spontaneously converted VF in under 600s. This suggests that a true reduction in MDE by low-flow ischaemia and 8mM $[\text{K}^+]_{\text{EC}}$ was not detected due to technical issues such as the defibrillator programming prevented application of biphasic shocks $<60\text{V}$. In general, previous research supports the reduction of defibrillation energies in low-flow ischaemia (73, 284, 302) and raised $[\text{K}^+]_{\text{EC}}$ (304).

Spontaneous conversion did not occur in the 8-week infarct heart failure model, even on complete cessation of perfusion. In these protocols shocks $>110\text{V}$ completely abolished the electrical activity for over a minute. After this prolonged isoelectric window, the first activation degenerated into VF. This phenomenon probably results from a combination of the electrical consequences of scar tissue (182, 343) and the increased dispersion of refractoriness that occurs in heart failure of any origin (350-352).

Decreasing the extracellular pH to 6.7 was associated with an increase in MDE. The well-known arrhythmogenic properties of acidic pH are discussed in 10.4.3. Such arrhythmogenic properties may account for the defibrillation resistance in pH 6.3, where despite prolonged iso-electric windows, the first activation degenerated into VF.

During hypoxia, VF required more energy to be defibrillated successfully. The limited amount of previous literature shows hypoxia both increasing and decreasing the required defibrillation energy. Theoretical predictions of hypoxia's effect on defibrillation energies are difficult as hypoxia increases repolarisation heterogeneity (suggesting an increase in energy required) (305), and inhibits DADs (suggesting a decrease) (308).

11.6 Future work

11.6.1 *Diastolic depolarisation*

The data in this study suggests that the spatiotemporal DF heterogeneity in VF during low-flow ischaemia and raised $[K^+]_{EC}$ results from the differential elevation of the LV activation threshold compared to the RV, and that this occurs secondary to differential diastolic depolarisation of the LV compared to the RV in these conditions. The differential increase in the LV activation threshold in raised $[K^+]_{EC}$ was shown to be associated with diastolic depolarisation in the LV epicardium. However it was not shown that the LV underwent greater diastolic depolarisation than RV. Therefore an area of future work would be to study the effect of raised $[K^+]_{EC}$ on the resting membrane potential in single cells isolated from the RV or LV.

11.6.2 *Heterogeneity of I_{K1} in rabbit*

This thesis also hypothesises that the differential elevation of the LV activation threshold, and the resultant spatiotemporal DF heterogeneity in VF during low-flow ischaemia and raised $[K^+]_{EC}$, could be secondary to a differential ventricular magnitude of I_{K1} . In low-flow ischaemia and raised $[K^+]_{EC}$, the extracellular accumulation of K^+ results in a rightward shift of the I_{K1} reversal potential (226), and thus depolarises the resting membrane potential. If this current has greater magnitude in LV than RV, then differential depolarisation of the resting membrane potential should occur. This hypothesis gains credence from work in guinea pigs (63, 190, 224) which demonstrated a greater magnitude of I_{K1} in LV compared to RV myocytes (63), and that this I_{K1} heterogeneity was the result of increased expression of Kir2.x in the LV compared to the RV (190). This greater degree of background current produced faster LV repolarisation, and thus allowed the development of higher DF in the LV compared the RV. Inhibiting I_{K1} with BaCl abolished this ventricular DF heterogeneity (190).

At present there is no evidence to either support or refute ventricular heterogeneity of $I_{K1}/Kir2.x$ in the rabbit. The distribution of I_{K1} magnitude has wide species variation; where the guinea pig has almost double the magnitude of I_{K1} in LV compared to the RV myocytes (63, 190), the dog has equal magnitudes of I_{K1} in both ventricles (229). Therefore the ventricular heterogeneity of I_{K1} needs to be confirmed in the rabbit. This could be done through a combination of (i) patch-clamp experiments on isolated LV and RV myocytes, (ii) Using BaCl in whole heart preparations to assess its effect on the frequency heterogeneity, (iii) in situ hybridisation of Kir2.x (approaches have been made towards Prof. Mark Boyett for potential collaborations).

11.6.3 Voltage - calcium interactions during VF in low-flow ischaemia

The importance of voltage-calcium interactions in VF induction is increasingly being recognised (for review see (359)). Theoretically (360) and experimentally (361) spontaneous calcium release has been linked to the first wavebreak event that initiates VF. On top of this, evidence is emerging that positive voltage-calcium alternans is important in creating dynamic instability that may also precipitate VF (333, 335). The role of calcium in VF maintenance is supported indirectly by studies showing (i) conversion of VF to VT by blockade of L-type calcium channels (66, 362, 363) and (ii) the association of failed defibrillation with non-reversal of intracellular calcium overload (326). In contrast simultaneous recordings of voltage and calcium during perfused VF show a lack of any relationship between the 2 signals immediately after VF induction (216, 217). As yet the role of calcium in VF during ischaemia has not been examined. It is possible that during the slower voltage oscillations that occur in low-flow ischaemia and raised $[K^+]_{EC}$ that voltage and calcium oscillations could become re-associated. This phenomenon could be examined in the VF model used in this thesis by imaging the calcium transient simultaneously with the membrane potential via a second photodiode array, a dichroic mirror and co-loading with Rhod 2AM (48).

11.7 Clinical Relevance

11.7.1 Reversal of hypoxia and acidosis

This thesis demonstrated that the minimum defibrillation energy required to successfully defibrillate prolonged episodes of VF was increased by hypoxia and acidosis. This would

suggest that directed reversal of these factors could enhance defibrillation success. More rapid reversal of hypoxia in the prolonged arrest scenario could be achieved by prioritising intubation, and ventilating with 100% O₂ along with the initial CPR (75), rather than mouth-to-mouth ventilation which maximally provides 17% O₂ (18). Such procedures would entail paramedic intubation, and require a high degree of training to ensure proper ET tube insertion (364).

The reversal of acidosis with buffering agent has previously been attempted with variable success (365-367). This probably relates to the fact that in ischaemia, the acidosis is primarily an intracellular lactic acidosis, which buffers are less able to reverse (367). Therefore, establishing perfusion and maximising oxygenation are more likely to reverse this acidosis (17, 77).

11.7.2 *Antero-posterior vs. Antero-lateral paddle position*

This thesis demonstrated that in VF during low-flow ischaemia the electrical activity was faster in the RV than the LV. This suggests that the RV acts as a primary driving force in VF during low-flow ischaemia, and that adequate coverage of the RV by the electrical field is a prerequisite for successful defibrillation. In human anatomy, the RV falls more within the electrical field of antero-posterior (AP) positioned paddles than those placed in the antero-lateral (AL) position. The superior efficacy of AP over AL electrode placement in atrial fibrillation conversion has been shown in some studies (368-372) but not others (373, 374). Another consideration is the aetiology of clinical VF; in this thesis VF was induced by burst pacing, whereas most clinical arrests occur in the context of ischaemia/reperfusion of myocardial infarction (5). Here the higher activity of the RV may be irrelevant; 8-week infarct rabbit hearts were resistance to defibrillation even after prolonged abolition of all electrical activity.

12 Appendix

Heterogeneity of ventricular fibrillation dominant frequency during global ischemia in isolated rabbit hearts

J Caldwell*, FL Burton, GL Smith‡ and SM Cobbe*

Institute of Biomedical and Life Sciences, University of Glasgow, UK.

*Division of Cardiovascular & Medical Sciences, Faculty of Medicine, University of Glasgow, UK.

‡*Corresponding author:*

Godfrey L. Smith

West Medical Building

University of Glasgow

Glasgow G128QQ

UK

Abstract

Introduction: Studies of ventricular fibrillation (VF) show that the dominant frequency (DF) of the ECG decreases as ischemia develops. The aim of this study was to examine the spatiotemporal organisation of the electrical activity associated with VF under ischaemic conditions.

Methods and Results: Isolated rabbit hearts were Langendorff-perfused at 40ml/min with Tyrode's solution and loaded with RH237. Anterior epicardial optical action potentials were recorded with a photodiode array (252 sites, 15×15mm). After 60s of VF (induced by burst pacing), global ischemia was produced by low flow (6ml/min), or the solution changed to impose hypoxia (95% N₂/5% CO₂), acidic pH_o (6.7, 80% O₂/20% CO₂) or raised [K⁺]_o (8mM). DF of the optical signals was determined at each site. Conduction velocity (CV), action potential duration (APD₉₀), effective refractory period (ERP), activation threshold, dV/dt_{max} and membrane potential were measured in separate experiments during regular ventricular pacing. During VF, ischemia decreased the DF in the left ventricle (LV) (58±6%, p<0.001 cf. baseline) but not the RV (93±5%). Raised [K⁺]_o reproduced this pattern (LV DF: 67±12%, p<0.001; RV DF: 95±9%). LV DF did not decrease in hypoxia or acidic pH_o. During ventricular pacing, ischemia decreased CV in the LV but not the RV. Raised [K⁺]_o did not change CV in LV or RV. Ischemia and raised [K⁺]_o both shortened APD₉₀. ERP was

not significantly altered, but LV activation threshold was increased by both ischemia and raised $[K^+]_o$, and was associated with decreased dV/dt_{max} , and diastolic depolarisation.

Conclusions: These results suggest that during VF decreased ECG DF in global ischemia is largely due to elevated $[K^+]_o$ affecting LV, rather than RV electrophysiology. Possible explanations for the reduced LV DF are diastolic depolarisation, reduced dV/dt_{max} and increased activation threshold. These parameters are unchanged in the RV during ischemia.

Key words: Optical mapping, ischemia, ventricular fibrillation.

Introduction

In ventricular fibrillation (VF), the electrical activity of the ventricles is uncoordinated, resulting in loss of cardiac output and death unless corrective measures are undertaken¹. VF is the major cause of sudden death, with an estimated annual European death rate of 123,000². Regardless of the underlying mechanism of the electrical activity associated with VF ("mother rotor"³ or "multiple wavelet"⁴), the result is high frequency deflections (3-5 Hz in humans) of the ECG⁵. This signal is thought to reflect oscillations of the ventricular membrane potential^{6,7,8}. The frequency of these oscillations is not uniform across the heart; higher frequencies are observed in the left ventricle (LV) than the right (RV)^{9,10}.

Experimentally, myocardial perfusion can be maintained during VF. Under these circumstances, ECG frequency remains relatively constant¹¹. In contrast, when the heart was not perfused, ECG frequency decreases⁶ and the intervals between epicardial activations increase¹². This suggests that during VF, ischemia influences the electrical properties of the myocardium such that the rate of activation is reduced. The underlying cellular mechanism of this phenomenon is unknown. Recent work suggests that this ischemic frequency slowing occurs heterogeneously across the ventricles¹³, the VF frequency being reduced more in the LV than the RV. The electrophysiological mechanism underlying this RV-LV heterogeneity is unclear. The primary metabolic consequences of ischemia are hypoxia, acidic pH and raised extracellular potassium. The aim of this study was to determine which of these components of ischemia are responsible for the differential reduction in frequency between the LV and the RV.

Methods

Langendorff perfusion

The investigation conforms to the *Guide for the Care and Use of Laboratory Animals* published by the US National Institutes of Health (NIH Publication No. 85-23, revised 1996). Adult male New Zealand White rabbits (weight 3-3.5 Kg) were sacrificed by intravenous injection of 0.5 ml/kg Euthatal (sodium pentobarbitone 200 mg/kg, Rhône Mérieux) with 500 IU of heparin. The hearts were rapidly excised and perfused in Langendorff mode with Tyrode's solution at 37°C (composition (mM): Na 134.5, Mg 1.0, K 5.0, Ca 1.9, Cl 101.8, SO₄ 1.0, H₂PO₄ 0.7, HCO₃ 20, acetate 20 and glucose 50) pH 7.4 (95% O₂ /5% O₂). Hearts were perfused at constant rate (40ml/min) using a Gilson Minipuls 3 peristaltic pump. Perfusion pressure was

monitored with a transducer in the aortic cannula.

Optical mapping

The heart was placed in a custom-made Plexiglas chamber (Figure 1). The chamber allowed control of bathing solution temperature, and recording of global ECG via wall-fixed electrodes. The heart was loaded with 100 μ L of the voltage sensitive dye RH237 (Molecular Probes), dissolved in DMSO (1mg/ml). Light at 535 ± 25 nm (interference filter, Comar Instruments Ltd, UK) from four 75W tungsten-halogen lamps illuminated the anterior surface of the heart (see online Figure 1). Light emitted from the heart was collected using a camera lens (Nikon 85mm, NA 1.4), passed through a 695nm long-pass filter, and the image focused on a 16×16 photodiode array (C4675-102, Hamamatsu Photonics UK Ltd). Each diode had a sensing area of $0.95\text{mm}\times 0.95\text{mm}$ with a pitch (distance from centre to centre) of 1.1 mm. The image of the anterior region of the heart was focused on the array at $\times 1.2$ magnification, each diode detected light from a $0.8\text{mm}\times 0.8\text{mm}$ area of epicardium and therefore the full array recorded from a $15\times 15\text{mm}$ area. (Figure 1A). Digitised data samples were stored on disk and analyzed using software written in IDL (Interactive Data Language, Research Systems Inc.).

Studies during Ventricular Fibrillation

VF protocol and analysis

VF was induced by burst pacing (50Hz stimulation for 8s) via platinum hook electrodes placed in the RV. All hearts were perfused with normal Tyrode's solution at 40ml/min for the first minute of VF. During control protocols, 40ml/min perfusion was maintained. In experimental protocols, either the perfusion rate (global ischemia - 6 ml/min) or solution composition was altered at 60s. ECG and optical recordings were taken for 4s periods. ECG was recorded every 30 seconds and optical measurements every minute.

The peak (dominant) frequency (DF) was identified from power spectra of ECG and optical signals. Summing the power spectra from all 256 pixels gave a global or pseudoECG (psECG) power spectrum (Figure 1 B-D). The progressive changes in psECG DF were similar to ECG DF, so only the ECG DF is shown (Figure 2). Plots of psECG DF are shown in the online supplemental data (Online Figure 2). To assess ventricular heterogeneity the mean DF from a 3×3 pixel area in both LV and RV was calculated. The position of the RV-LV border was confirmed by dissection at the end of the experiment.

Epicardial membrane potential measurements using a floating microelectrode

Hearts were prepared as above, but without dye loading and with the additional insertion of an LV balloon to reduce motion. The hearts were placed in a chamber similar to that used for optical recording but adapted for microelectrode impalement of the LV surface by boring a 5mm diameter hole in the Plexiglas front-plate. The chamber was turned 90° to allow access to the surface of the heart with vertical microelectrodes. These were pulled from borosilicate glass (WPI, Sarasota, FL) using a P-97 Flaming/Browning pipette puller (Sutter Instruments, Novato, CA) and filled with 2M KCl before the tips were mounted onto silver chloride

coated silver wire (total resistance 20-25M Ω). Impalements were made into the epicardial LV surface and the membrane potential signals were recorded via Microprobe Model 750 (WPI, Sarasota, FL). Transmembrane recordings were taken during RV pacing with a basic cycle length (BCL) of 180ms, and during VF. Signals were also analyzed in the frequency domain as above.

Components of ischemia

In order to study the effects of individual components of ischemia on electrophysiological changes during VF, standard Tyrode's solution was adapted according to previous studies^{14,15,16}. Acidic pH_o of 6.7 was produced by bubbling with 20% CO₂/80% O₂¹⁴; hypoxia was produced by bubbling with 5% CO₂/95% N₂ mixture¹⁵; hyperkalemia was produced using 8mM or 10mM [K⁺]_o¹⁶.

Studies during ventricular pacing

Conduction velocity protocol

Hearts were prepared for optical voltage mapping as above, and the LV or RV was paced on the epicardial surface via bipolar stimulating electrodes. The hearts were paced at BCL 250ms, and the activation pattern of the LV and the RV under control conditions were recorded. To assist immobilization, hearts were perfused with 3 μ M cytochalasin D for 20 minutes before measurements were made. At this concentration, cytochalasin D has been shown in this preparation not to affect conduction velocity¹⁷. Activation times were recorded at 6-7 minutes of either global ischemia (6ml/min) or raised [K⁺]_o (8mM).

Activation time was determined as the time of maximum upstroke (dV/dt max) of the optical signal¹⁸. Using locally developed software written in MATLAB (The MathWorks, Inc., MA, USA), these times were used to calculate local conduction velocity (For details see online Figure 3).

Refractory period measurements

Monophasic action potentials (MAPs) were recorded using Franz contact catheters (Ag-AgCl electrode, 2mm diameter, Boston Scientific/EP Technologies, San Jose, CA, USA) placed against the LV and RV epicardial surface. LV and RV MAPs were recorded simultaneously. Using a distant RV epicardial bipolar stimulating electrode, steady-state restitution protocols¹⁹ were performed after 6 and 10 minutes of either 6ml/min low-flow global ischemia or perfusion with 8mM [K⁺]_o. ERP was assessed by stimulating at twice diastolic threshold voltage through one contact electrode whilst recording MAPs at the other. The S₁S₂ protocol used consisted of 8 beats at BCL 300ms (S₁) followed by shorter test stimulus (S₂). The initial S₂ interval of 150ms, was reduced by 2ms until capture no longer occurred (Figure 6A). Threshold voltages were also recorded.

Statistical analysis

Data are expressed as mean \pm SEM. Significance testing with ANOVA, paired t-test or Wilcoxon matched

pairs were performed using InStat3 (GraphPad Software Inc., USA). For ECG and psECG progression data at 480s were compared.

Results

Simultaneous ECG and Optical signals in VF

Figure 1A(i) shows a Langendorff-perfused rabbit heart in the optical mapping chamber. The superimposed grid represents the area of the myocardium recorded by the photodiode array (16×16 elements). The anterior descending coronary artery that approximately delineates the RV-LV border is clearly visible. The two white squares are two 3×3 pixel squares placed in the RV and LV regions. Panel A (ii) is a typical record of 256 optical action potentials recorded from the epicardial surface. Panel B is a typical ECG recording from an isolated heart in sinus rhythm (i) and VF (ii). Panel C shows a typical optical signal from an LV pixel in sinus rhythm (i) and VF (ii). Panel C (i) and (ii) shows records from a pixel situated in the RV region of the array. The VF activation rate is clearly higher in the LV than the RV. ECG and optical power spectra are shown in Figure 1D. This shows the dominant frequency of the optical signals recorded from the LV region is higher when compared with signals from the RV region and with the ECG.

Effects of perfusion rate on the dominant frequency

Typically, the DF of the ECG shortly after induction was 12-13Hz. This value changed with time, depending on the experimental condition. The evolution of DF under control conditions (40ml/min perfusion) is shown in Figure 2A. Expressed relative to the DF at time zero, the ECG DF increased to a peak value over the initial 180s ($136\pm 7\%$, $p<0.001$), before decreasing, and stabilizing at values higher than those observed at VF induction ($123\pm 7\%$, $p<0.05$). On reduction of the rate of perfusion, the ECG DF rapidly decreased and stabilized at a lower DF value by 420s. The rate of decline, and the final steady-state value, depended on the perfusion rate such that DF declined more quickly at lower perfusion rates and reached a lower steady-state value (Figure 2A). Similar time courses were observed for median frequency values of the ECG (results not shown). On complete cessation of perfusion, DF rapidly decreased but the VF converted to a more regular rhythm within 240s in all hearts. Restoring perfusion resulted in spontaneous conversion to sinus rhythm. During perfusion at 4ml/min, 5 out of 9 hearts underwent spontaneous conversion. VF was maintained for periods longer than 720s during perfusion at 6ml/min and did not spontaneously convert to sinus rhythm. Optical psECG recordings showed similar DF changes to those observed with the ECG (Online Figure 2A).

LV-RV differences in VF dominant frequency.

The geometry of the heart prevents simultaneous recording of the optical signals from the entire epicardial surface of the LV and RV with a single camera. Therefore a region of the heart was chosen that spanned the LV-RV border on the anterior surface of the heart. From the optical map of this area, two standardized 3×3mm regions in the LV and RV were examined. To ensure that the difference observed from these two regions was representative of each ventricle, measurements of DF were made whilst imaging an area fully within the LV or the RV (Online Figure 4). The DF maps indicate that the values of DF are homogeneous

over individual ventricles. Comparing the DF of two standardized 3×3mm regions within one ventricle (region 1 and 2) showed no significant differences. The mean DF during normal perfusion VF increased to 134±7% in region 1 of the LV and to 146±10% in region 2. In the RV, the mean DF increased to 112±7% in region 1, and 108±1% in region 2. These data suggest that the optical signals from an area spanning the LV-RV border represent the activity in both ventricles.

Measurements from the area spanning the LV-RV border indicate that the spatial distribution of VF dominant frequency was not homogeneous (Figure 3 & Table 1). DF increased in the LV during standard perfusion, whereas in the RV DF was only marginally increased (LV vs. baseline, 162±13%, $p<0.001$; RV vs. baseline, 116±4%, $p=NS$; LV vs. RV $p<0.001$). This LV-RV dispersion developed progressively over 480s in all hearts. In contrast, during low-flow global ischemia at 6 ml/min, there was a marked reduction of LV DF, but no significant change in the RV (LV, 58±8%, $p<0.001$; RV, 94±7%, $p=NS$; LV vs. RV $p<0.01$).

Effect of acidic pH_o

Perfusion with Tyrode's at pH 6.7 inhibited the initial increase in ECG DF (Figure 2B) and psECG DF (online Figure 2B). Instead there was a more gradual increase in DF to steady state values, which were not significantly different from control.

Perfusion with acidic solution altered the spatial distribution of the DF values (Figure 3, Table 1). At 480s, the LV DF increased to a lesser extent than that observed with normal Tyrode's (pH 7.4, 162±13%; pH 6.7, 141±7%, $p<0.01$). Whereas the RV DF increased to values significantly higher than control (pH 7.4, 116±4%; pH 6.7, 135±6%; $p<0.01$). These changes produced an absolute DF value in the LV (~20Hz) after 480s that was not significantly different from that in the RV (~18Hz, Figure 3 and Table 1). In separate experiments, the effects of higher PCO₂ (lower pH) were examined. Perfusion with 50% CO₂ (pH 6.3) had similar effects to those seen at 20% CO₂ (pH 6.7) (results not shown).

Effect of hypoxia

The global measures of frequency (i.e. ECG and psECG) showed that DF in hypoxia was not significantly different from control at 480s (Figure 2C, online Figure 2C). The spatial heterogeneity was also indistinguishable from control (Figure 3 and Table 1).

Effect of elevated [K⁺]_o

Raised [K⁺]_o had a profound effect on ECG DF and psECG DF (Figure 2D, online Figure 2D). The time course and extent of the changes in DF were similar in 8mM and 10mM [K⁺]_o, but spontaneous conversion occurred in 75% of experiments using 10mM [K⁺]_o, and 20% using 8mM. In the presence of raised [K⁺]_o the spatial characteristics of VF were indistinguishable to those observed in 6ml/min global ischemia; DF was decreased more in the LV than RV (LV 67±4%, $p<0.001$; RV 95±3%, $p<0.001$; LV vs. RV $p<0.001$; Figure 3, Table 1).

Epicardial transmembrane potential in VF

Figure 4A(i) shows a typical transmembrane potential recorded with a floating microelectrode on the LV epicardial surface of a Langendorff-perfused rabbit heart. Figure 4A(ii) shows the transmembrane potential recording from the same area after VF induction. The averaged signals of membrane potential from the epicardial surface of the LV revealed a similar DF progression to those of ECG and psECG under control conditions, low-flow ischemia and 8mM $[K^+]_o$ (Figure 4B). Under control conditions, the diastolic membrane potential during VF was not significantly different from pre-VF values (BCL 180ms, -72 ± 4 mV; VF, -65 ± 3 mV). In contrast, the maximum systolic membrane potential decreased in VF (BCL 180ms, 18 ± 4 mV; VF, -24 ± 5 mV, $p < 0.01$). Systolic and diastolic membrane potentials during low-flow ischemia were not significantly different from control. Perfusion with 8mM $[K^+]_o$ during VF depolarized the diastolic membrane potential (BCL 180ms, -80 ± 5 mV; VF, -55 ± 8 mV; $p < 0.05$).

Electrical properties of the myocardium during ventricular pacing

Both low-flow global ischemia and raised $[K^+]_o$ reduced VF frequency in the LV. Potential mechanisms include changes in: (i) conduction velocity, (ii) refractory period or (iii) excitability of the ventricular myocardium. Conduction velocity cannot be measured accurately during VF in the intact LV, owing to the unknown contribution of transmural versus trans-epicardial activation. The refractory period and excitability also cannot be measured directly during VF. We therefore undertook further experiments during regular ventricular pacing to investigate whether low-flow ischemia or elevated $[K^+]_o$ induced changes in conduction velocity, repolarization, refractoriness or excitability of sufficient magnitude to account for the observed changes in DF in the LV and RV.

Conduction velocity

After 6-7 min of low-flow global ischemia there was a significant reduction of both longitudinal and transverse velocity in the LV (longitudinal $69 \pm 8\%$, $p < 0.05$, transverse $70 \pm 1\%$, $p < 0.05$, $n = 4$; Figure 5). The RV longitudinal velocity was unchanged ($98 \pm 2\%$), but the transverse velocity was reduced by a small amount ($92 \pm 3\%$, $p < 0.05$). The reduction in the transverse velocity was significantly less in the RV than the LV ($p < 0.05$).

After 6-7 min perfusion with 8mM $[K^+]_o$ neither LV nor RV conduction velocities were significantly changed, though there was a tendency for all velocities to increase ($n = 4$, Figure 5).

Action potential duration, refractory period and excitability measurements

The observed interventricular differences in DF may be due to a difference in repolarization and/or refractoriness of the myocardium. Prolongation of the LV APD or ERP relative to the RV could explain the slower DF observed in the LV. $MAPD_{90}$ and ERP were assessed during low-flow ischemia or elevated $[K^+]_o$, as outlined in the Methods. Under control conditions, LV and RV $MAPD_{90}$ were not significantly different (Figure 6B). In low-flow ischemia, $MAPD_{90}$ tended to shorten in LV and lengthen in the RV, but these

alterations were not significant. Elevated $[K^+]_o$ caused both LV and RV MAPD₉₀ to decrease significantly compared to control values ($p < 0.01$) (Figure 6.B). The percentage change was not significantly different between the ventricles (LV $93 \pm 3\%$, RV $92 \pm 1\%$).

As the mean data show (Figure 6C), there was no significant difference between LV and RV ERP in control conditions. Neither low-flow ischemia nor elevated $[K^+]_o$ had a significant effect on LV or RV ERP as assessed at the standard pacing threshold (diastolic threshold $\times 2$). However, the voltage threshold for pacing the LV was increased by both low-flow ischemia and elevated $[K^+]_o$. This effect was not evident when stimulating the RV (Figure 6D). This differential effect occurred both for low-flow global ischemia (LV, $\times 3.5 \pm 1.3$; RV, $\times 1.2 \pm 0.5$; $p < 0.05$) and elevated extracellular $[K^+]$ (LV, $\times 2.6 \pm 0.5$; RV, $\times 1.3 \pm 0.3$; $p < 0.05$). One of the causes of an elevation of threshold could be inactivation of Na^+ channels responsible for phase 0 of the action potential. Consistent with this explanation was the differential reduction of the maximum upstroke velocity (dV/dt_{max}) of the MAP recording in the LV but not the RV (Figure 6E), in both low-flow ischemia (LV, $44 \pm 10\%$, $p < 0.05$; RV, $97 \pm 19\%$) and elevated $[K^+]_o$ (LV, $39 \pm 10\%$, $p < 0.05$; RV, $90 \pm 22\%$).

Discussion

This study shows that the reduction in the dominant frequency (DF) of the ECG during low-flow global ischemia is due to reduced DF in the LV but not the RV. The reduced DF is reproduced by raising $[K^+]_o$ and not by the reduction of PO_2 or extracellular pH.

The reduction in dominant frequency of the ECG reflects decreased activation rates of the myocardium as indicated by the optical and microelectrode recordings. Theoretically, several mechanisms could be responsible for the decrease the frequency of activation: (i) reduced conduction velocity; (ii) prolongation of the action potential; (iii) prolongation of post-repolarization refractoriness; (iv) raised voltage threshold for activation.

Reduced conduction velocity

The role of conduction velocity (CV) in VF is controversial. Theoretically, slowing of conduction has diametrically opposite effects on VF maintenance depending on whether the driving mechanism is a "mother rotor" or "multiple wavelets"²⁰. Conduction slowing stabilizes the mother rotor and converts VF to VT, whereas slowed conduction reduces the rate of wavelet annihilation thereby prolonging VF duration²⁰. The biphasic nature of ischemia-induced alterations in CV is well documented (for review see²¹). Initially after the onset of ischemia, CV increases (~ 2 minutes) and then decreases again. Thus at 6-7 mins (the time point used in this study), conduction velocity would be expected to be lower. In the ventricular pacing experiments, both longitudinal and transverse velocity were reduced in the LV by $\sim 30\%$. In the RV, longitudinal velocity was maintained and transverse velocity reduced to a much lesser degree ($\sim 7\%$). Therefore, this differential effect may be the basis for the reduced DF in LV in low-flow global ischemia. However, no change in CV was observed in elevated $[K]_o$ despite the decreased DF observed in the LV. This is in keeping with previous observations that CV slowing in ischemia was not solely due to $[K]_o$ accumulation²², and shows that a reduction in CV is not a prerequisite for reduced DF in VF.

Previous experimental and modeling studies show a complex relationship between conduction velocity and $[K^+]_o$ ^{23,24}. Elevation above 5mM results in increasing velocities to a peak at around 8-9mM. At concentrations above ~8mM conduction velocity decreases, at $[K^+]_o$ of ~12mM, velocity falls below control values²³. Since DF slowed at these $[K^+]_o$ values, a mechanism other than reduced CV would appear to be responsible. Such a lack of correlation between CV and DF has been demonstrated in atrial tissue²⁵.

Prolongation of repolarization

Repolarization and refractoriness are interlinked phenomena. By prolonging the plateau phase, the effective refractory period (ERP) is also prolonged. In VF, it has been argued that a ventricular myocyte is reactivated as soon as it is excitable²⁶. Therefore, extending the ERP would reduce the activation rate and the dominant frequency (DF). To explain a DF reduction in the LV, but not the RV, a differential prolongation of the APD would be required. We did not consider it feasible to measure APD during VF, because of the variation in morphology and diastolic potential (Figure 4). Measurements of APD using MAP recordings during ventricular pacing showed that on average there were no differences in APD between LV and RV. Furthermore, APD did not change significantly during low-flow global ischemia. Thus prolonged repolarization and therefore ERP cannot be used to explain reduction of DF in LV under low-flow conditions. Furthermore, elevated $[K^+]_o$ mimicked the change in DF in both LV and RV but did not prolong the APD; instead elevated $[K^+]_o$ reduced APD equally in both LV and RV by ~10%.

Prolongation of post-repolarization refractoriness

In ischemia, the ERP may extend beyond full repolarization^{27,28,29}. If post-repolarization refractory period was differentially longer in the LV, this could explain its lower DF during low-flow ischemia and raised $[K^+]_o$. As discussed by Opthof et al. the assessment of refractoriness in ischemia is difficult¹². Traditionally, ERP has been assessed by establishing the pacing threshold at intervals well beyond possible post-repolarization refractoriness, setting the pacing stimulus at twice this voltage then, using an S₁S₂ protocol, identifying the ERP as the point of non-capture³⁰. Using this protocol failed to reveal any significant change in ERP in either LV or RV (Figure 6C). This is consistent with the reported lack of relationship between ERP and DF in canine atria²⁵ and indicates that prolonged ERP cannot account for the decreased DF in low-flow global ischemia.

Raised threshold for activation

An increase in LV threshold for activation could reduce DF by increasing the time between repetitive activation of the myocardium. The threshold voltage can be increased either by increasing the magnitude of the background outward current or by reducing sodium current (I_{Na}).

In this study we observed a differential increase in LV threshold voltage, as represented by the increased pacing threshold during low-flow global ischemia and elevated $[K^+]_o$. Such raised voltage thresholds have been observed by others, both during ischemia^{31,32,33} and in the context of elevated $[K^+]_o$ ³⁴. In the MAP experiments described in the current study, slower MAP upstroke was associated with this higher stimulation threshold, suggesting a reduction in the available Na⁺ channels or increased background K⁺ currents. The

association between reduced magnitude of I_{Na} , increased pacing threshold and reduced AP upstroke has been demonstrated in other tissues³⁵. Interestingly, these changes had no effect on conduction velocity. A similar dissociation between the degree of activation of I_{Na} and CV has not been shown directly in cardiac tissue. However, previous studies have shown a lack of correlation between maximum AP upstroke velocity and conduction velocity^{25,23}.

Past research recording transmembrane potentials during ischemia⁸ and raised $[K^+]_o$ ¹⁶ showed depolarization of diastolic membrane potential. In the present study in VF there was a significant depolarization of the diastolic membrane potential when perfusing with increased $[K^+]_o$. Our lack of demonstration of significant changes in diastolic potential in low-flow ischemia could be due to perfusion with normal Tyrode's solution in the volume adjacent to the epicardial surface. This may have limited the increase in $[K^+]_o$ in the epicardium during low-flow global ischemia, thereby preventing significant depolarization. As superfusion would not prevent the accumulation of K^+ in the deeper myocardial layers, diastolic depolarization should occur within these tissues during ischemia. Such depolarization would be expected to inactivate I_{Na} , reduce AP upstroke velocity, and thereby result in the observed slowing of dominant frequency.

Thus we hypothesize that global ischemia and raised $[K^+]_o$ cause diastolic membrane depolarization, which causes partial inactivation of the I_{Na} , and thereby increases the activation threshold voltage. In support of this hypothesis, inhibition of I_{Na} caused a reduction in DF³⁶. This study showed that perfusing hearts with low concentrations of tetrodotoxin caused reduced rotational rate of re-entrant circuits and enlargement of their internal core, in a manner identical to that observed in non-perfused hearts.

Mechanism of ventricular heterogeneity - role of IK_1 ?

Ventricular heterogeneity of VF is not a new concept. Higher frequencies develop in the LV compared to the RV shortly after VF induction¹⁰. Optical mapping has demonstrated a sharp transition between the 2 regions⁹. Similar sharp transitions have been observed in low-flow global ischemia and elevated $[K^+]_o$ in the present study. In a previous publication, the source of this heterogeneity was thought to be the differential expression of Kir2.1 and Kir2.3 in LV myocytes compared to RV myocytes³⁷. The differential expression of Kir2.1 and Kir2.3 may also be the basis of the differences between LV and RV reported in this study. However, differences in the expression of other ion channels between LV and RV have been noted in a variety of species^{38,39}; these too may contribute to the differences in the DF observed in perfused and low-flow global ischemia.

Conclusion

During VF in low-flow global ischemic conditions there is decrease in the dominant frequency of VF in the LV. This study shows for the first time that raised $[K^+]_o$, and not low PO_2 or acidic pH_o alone, are responsible for this effect. This study also demonstrated that the insensitivity of the RV to raised $[K^+]_o$ was the basis for the observed DF heterogeneity in previous research. The underlying electrophysiological mechanism is unknown, but the data suggests that raised activation threshold in the LV, and not the RV, is the cause. This indicates that intrinsic electrophysiological differences between the LV and RV may be responsible for dramatic differences in the VF dominant frequency during low-flow ischemia.

Aknowledgements

Dr. Caldwell is a British Heart Foundation Clinical PhD Fellow. The authors would like to acknowledge guidance by Prof. Guy Salama on the use 50mM glucose to avoid confounding hypotonic effects.

References

1. Genesis of cardiac arrhythmias: Electrophysiological considerations: Braunwald E, Zipes DP, Libby P, eds: *Heart Disease: a textbook of cardiovascular medicine*. Philadelphia: W.B. Saunders, 2005, pp, 803-861.
2. Atwood C, Eisenberg MS, Herlitz J, Thomas RD: Incidence of EMS-treated out-of-hospital cardiac arrest in Europe. *Resuscitation* 2005; 67:75-80.
3. Chen J, Mandapati R, Berenfeld O, Skanes, AC, Jalife J: High-frequency periodic sources underlie ventricular fibrillation in the isolated rabbit heart. *Circ Res* 2000; 86:86-93.
4. Choi BR, Nho W, Liu T, Salama G: Life span of ventricular fibrillation frequencies. *Circ Res* 2002; 91:339-345.
5. Strohmeier HU, Eftestol T, Sunde K, Wenzel V, Mair M, Ulmer H, Lindner KH, Steen PA: The predictive value of ventricular fibrillation electrocardiogram signal frequency and amplitude variables in patients with out-of-hospital cardiac arrest. *Anesthesia & Analgesia* 2001; 93:1428-1433.
6. Carlisle EJ, Allen JD, Kernohan WG, Anderson J, Adgey AA: Fourier analysis of ventricular fibrillation of varied aetiology. *Eur Heart J* 1990; 11:173-181.
7. Akiyama T: Intracellular recording of in situ ventricular cells during ventricular fibrillation. *Am J Physiol Heart Circ Physiol* 1981; 240:H465-H471.
8. Czarnecka M, Lewartowski B, Prokopczuk A: Intracellular recording from the in situ working dog heart in physiological conditions and during acute ischemia and fibrillation. *Acta Physiol Pol* 1973; 24:331-337.
9. Samie FH, Berenfeld O, Anumonwo J, Mironov SF, Udassi S, Beaumont J, Taffet S, Pertsov AM, Jalife J: Rectification of the Background Potassium Current: A Determinant of Rotor Dynamics in Ventricular Fibrillation. *Circ Res* 2001; 89:1216-1223.
10. Newton JC, Smith WM, Ideker RE: Estimated Global Transmural Distribution of Activation Rate and Conduction Block During Porcine and Canine Ventricular Fibrillation. *Circ Res* 2004; 94:836-842.

11. Martin G, Cosin J, Such M, Hernandez A, Llamas P: Relation between power spectrum time course during ventricular fibrillation and electromechanical dissociation. Effects of coronary perfusion and nifedipine. *Eur Heart J* 1986; 7:560-569.
12. Opthof T, Coronel R, Vermeulen JT, Verberne HJ, van Capelle FJ, Janse M J: Dispersion of refractoriness in canine ventricular myocardium. Effects of sympathetic stimulation. *Cardiovasc Res* 1993; 27:1954-1960.
13. Wu TJ, Lin SF, Hsieh YC, Ting CT, Chen PS: Ventricular Fibrillation During No-Flow Global Ischemia in Isolated Rabbit Hearts. *J Cardiovasc Electrophysiol* 2006;17:1-9
14. Bethell HW, Vandenberg JI, Smith GA, Grace AA: Changes in ventricular repolarization during acidosis and low-flow ischemia. *Am J Physiol Heart Circ Physiol* 1998; 275:H551-H561.
15. Jennings RB, Murry CE, Steenbergen C, Reimer KA: Development of cell injury in sustained acute ischemia. *Circulation* 1990; 82:II-2-II-12.
16. Kleber AG: Resting membrane potential, extracellular potassium activity, and intracellular sodium activity during acute global ischemia in isolated perfused guinea pig hearts. *Circ Res* 1983; 52:442-450.
17. Kettlewell S, Walker NL, Cobbe SM, Burton FL, Smith GL: The electrophysiological and mechanical effects of 2,3-butane-dione monoxime and cytochalasin-D in the Langendorff perfused rabbit heart. *Exp Physiol* 2004; 89:163-172.
18. Choi BR, Salama G: Simultaneous maps of optical action potentials and calcium transients in guinea-pig hearts: mechanisms underlying concordant alternans. *J. Physiol (Lond)* 2000; 529:171-188.
19. Banville I, Chattipakorn N, Gray RA: Restitution dynamics during pacing and arrhythmias in isolated pig hearts. *J Cardiovasc Electrophysiol* 2004; 15:455-463.
20. Qu Z, Weiss JN: Effects of Na⁺ and K⁺ channel blockade on vulnerability to and termination of fibrillation in simulated normal cardiac tissue. *Am J Physiol Heart Circ Physiol* 2005; 289:H1692-H1701.
21. Wit AL, Janse MJ: Electrophysiological effect of acute myocardial ischemia: The Ventricular Arrhythmias of Ischemia and Infarction. New York: Futura, 1993, pp, 174-222.
22. Kleber,AG, Janse MJ, Wilms-Schopmann FJ, Wilde AA, Coronel R: Changes in conduction velocity during acute ischemia in ventricular myocardium of the isolated porcine heart. *Circulation* 1986; 73:189-198.
23. Kagiya Y, Hill JL, Gettes LS: Interaction of acidosis and increased extracellular potassium on action potential characteristics and conduction in guinea pig ventricular muscle. *Circ Res* 1982; 51:614-623.
24. Nygren A, Giles WR: Mathematical simulation of slowing of cardiac conduction velocity by elevated extracellular potassium. *Ann.Biomed.Eng* 2000; 28:951-957.

25. Huang JL, Tai CT, Lin YJ, Ting CT, Chen YT, Chang MS, Lin FY, Lai WT, Chen SA: The Mechanisms of an Increased Dominant Frequency in the Left Atrial Posterior Wall During Atrial Fibrillation in Acute Atrial Dilatation. *J Cardiovasc Electrophysiol* 2006; 17:178-188.
26. Gettes LS, Reuter H: Slow recovery from inactivation of inward currents in mammalian myocardial fibres. *J Physiol* 1974; 240:703-724.
27. Cobbe SM, Manley BS, Alexopoulos D: Interaction of the effects of hypoxia, substrate depletion, acidosis and hyperkalemia on the class III antiarrhythmic properties of sotalol. *Cardiovasc Res* 1985; 19:668-673.
28. Downar E, Janse MJ, Durrer D: The effect of acute coronary artery occlusion on subepicardial transmembrane potentials in the intact porcine heart. *Circulation* 1977; 56:217-224.
29. Han JAOK, Moe GK: Nonuniform Recovery of Excitability in Ventricular Muscle. *Circ Res* 1964; 14:44-60.
30. Janse MJ, Capucci A, Coronel R, Fabius MA: Variability of recovery of excitability in the normal canine and the ischaemic porcine heart. *Eur Heart J* 1985; 6 Suppl D:41-52.
31. Elharrar V, Foster PR, Jirak TL, Gaum WE, Zipes DP: Alterations in canine myocardial excitability during ischemia. *Circ Res* 1977; 40:98-105.
32. Sutton, P. M. I., Taggart, P., Opthof, T., Coronel, R., Trimlett, R., Pugsley, W., and Kallis, P.: Repolarisation and refractoriness during early ischemia in humans. *Heart* 2000; 84:365-369.
33. Sidorov VY, Woods MC, Wikswo JP: Effects of Elevated Extracellular Potassium on the Stimulation Mechanism of Diastolic Cardiac Tissue. *Biophys.J.* 2003; 84:3470-3479.
34. Chen C, Bharucha V, Chen Y, Westenbroek RE, Brown A, Malhotra JD, Jones D, Avery C, Gillespie PJ, Kazen-Gillespie KA., Kazarinova-Noyes K, Shrager P, Saunders TL, Macdonald RL, Ransom BR, Scheuer T, Catterall WA, Isom LL: Reduced sodium channel density, altered voltage dependence of inactivation, and increased susceptibility to seizures in mice lacking sodium channel beta 2-subunits. *PNAS* 2002; 99:17072-17077.
35. Mandapati R, Asano Y, Baxter WT, Gray R, Davidenko J, Jalife J: Quantification of effects of global ischemia on dynamics of ventricular fibrillation in isolated rabbit heart. *Circulation* 1998; 98:1688-1696.
36. Warren M, Guha PK, Berenfeld O, Zaitsev A, Anumonwo JMB, Dhamoon AS, Bagwe S, Taffet SM, Jalife J: Blockade of the inward rectifying potassium current terminates ventricular fibrillation in the guinea pig heart. *J Cardiovasc Electrophysiol* 2003; 14:621-631.
37. Nerbonne JM, Kass RS: Molecular Physiology of Cardiac Repolarization. *Physiol.Rev.* 2005; 85:1205-1253.

38. Fahmi AI, Patel M, Stevens EB, Fowden AL, John JE, Lee K, Pinnock R, Morgan K, Jackson AP, Vandenberg JI: The sodium channel beta-subunit SCN3b modulates the kinetics of SCN5a and is expressed heterogeneously in sheep heart. *J Physiol (Lond)* 2001; 537:693-700.

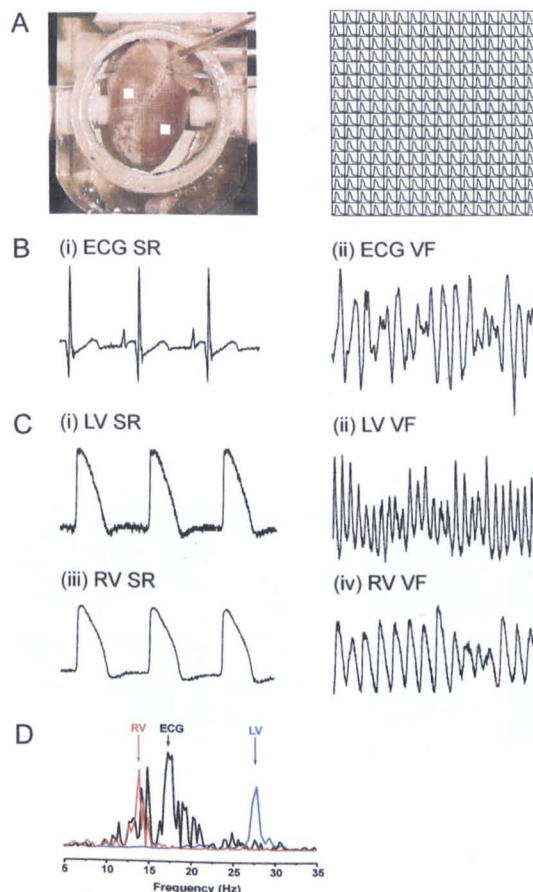


Figure 1 Panel A: (i) Langendorff-perfused rabbit heart in optical mapping chamber. The superimposed grid represents the area of the myocardium (16x16 pixel) visualised by the photodiode array. Panel A (ii) optically recorded action potentials (pacing cycle length 300ms). Panel B: ECG recording during (i) sinus rhythm and (ii) ventricular fibrillation (VF). Panel C: optical pixel recordings from: (i) the LV in sinus rhythm, (ii) the LV in VF, (iii) the RV in sinus rhythm and (iv) the RV in VF. Panel D: superimposed power spectra of ECG [B(ii)], LV [C(ii)] and RV [C(iv)] signals in VF.

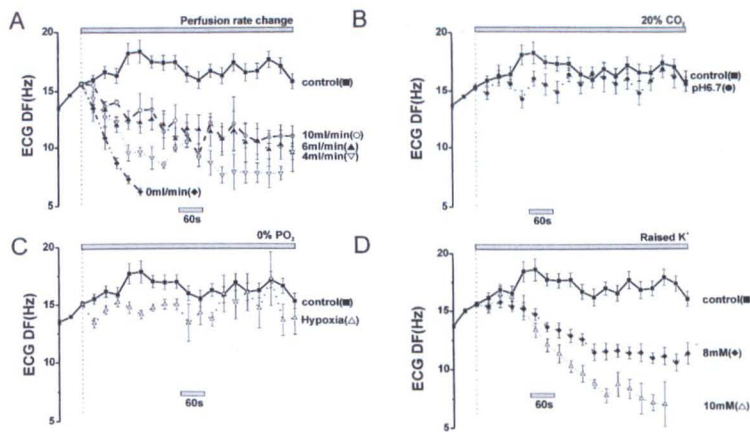


Figure 2 Progressive changes of ECG DF during VF. ECG dominant frequency (DF) are shown under a range of conditions. Panel A: at varying perfusion rates. Panel B: reduced extracellular pH (pH 6.7). Panel C: hypoxia. Panel D: raised extracellular $[K^+]$.

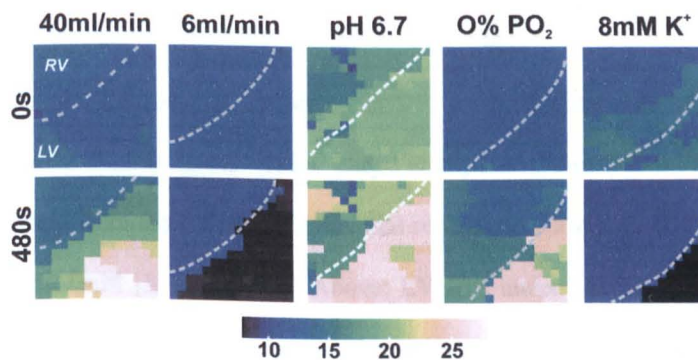


Figure 3 Dominant frequency maps. Spatial distributions of DF are demonstrated using by a colour code scale from 8-30Hz. Snapshots of typical DF distribution are shown at VF onset (0s) and after 480s. The LV-RV border is indicated by a dotted white line. Maps are shown under the flowing conditions: Control (40ml/min); Low-flow global ischemia (6ml/min); Acidic pH (pH 6.7; 20% CO_2 , 80% O_2); Hypoxia (0% PO_2 ; 5% CO_2 , 95% N_2); Raised K^+ (8mM).

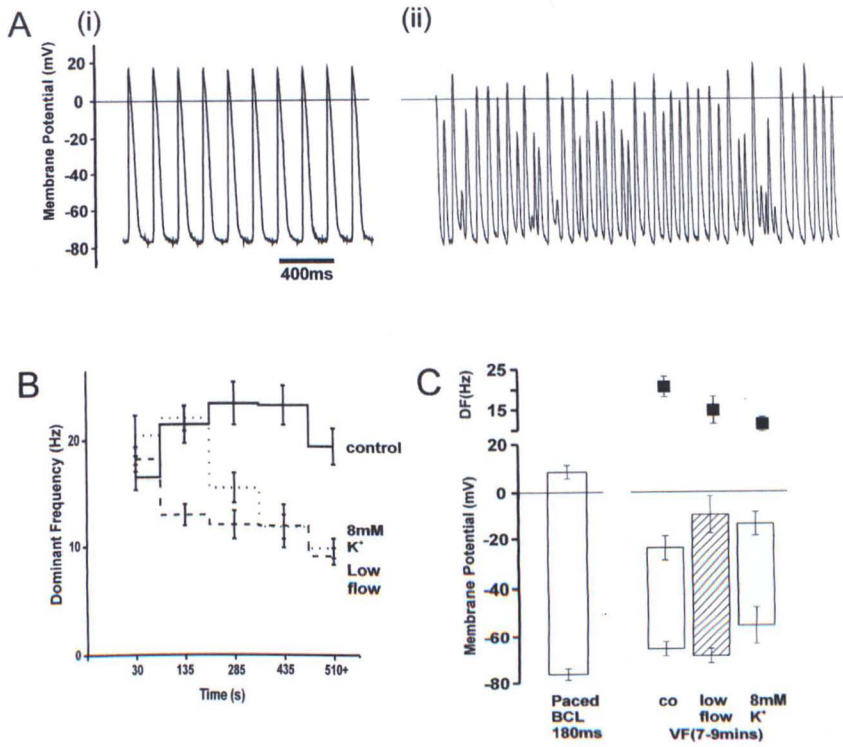


Figure 4 Measurements of transmembrane potential in VF. Panel A: Transmembrane potential recording from anterior LV epicardial surface during: (i) RV paced at BCL of 180ms and (ii) in VF. Panel B: Plot of DF progression as assessed from transmembrane potential recordings during VF in control (40ml/min), low-flow global ischemia and 8mM $[K^+]_o$. Panel C: Above: LV DFs under control conditions (co) and during low-flow global ischemia and 8mM $[K^+]_o$. Below: Mean diastolic potential (bottom) and systolic potential (top) during RV pacing and VF (7-9 minutes).

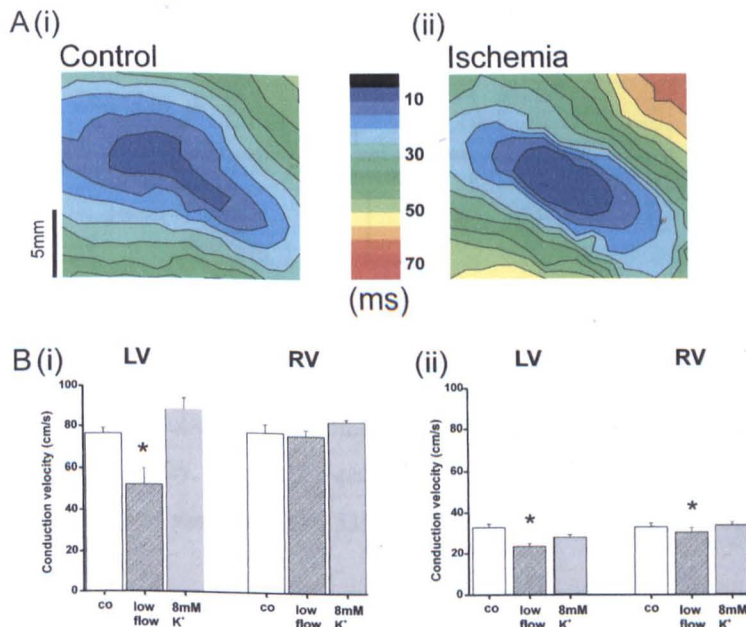


Figure 5 Conduction Velocity Panel A: Typical LV isochronal activation maps during epicardial stimulation in control conditions (co) (i) and after 6-7 mins low-flow global ischemia (ii). Panel B: (i) Mean longitudinal CV; (ii) mean transverse CV. * indicates significant difference from control ($p < 0.05$).

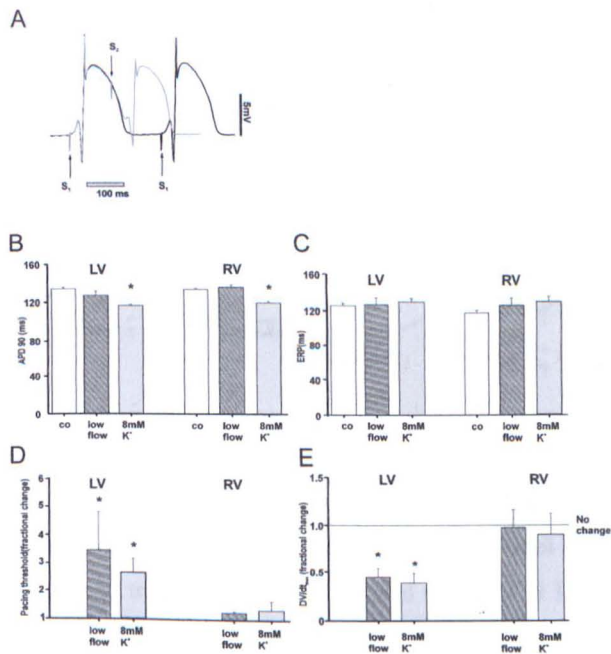
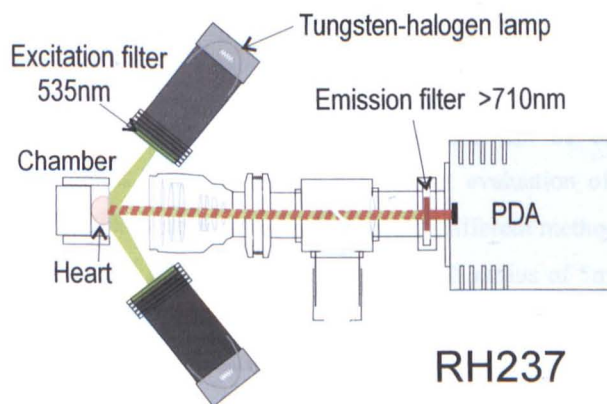
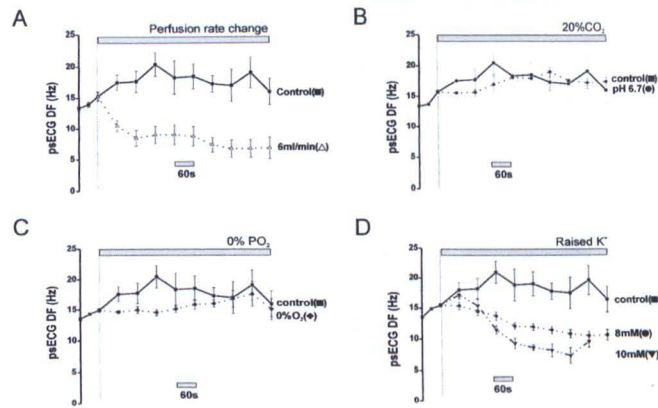


Figure 6 MAP studies Panel A: Two superimposed LV MAP recordings S₁ and S₂ stimuli are indicated by arrows: black line is a control trace (BCL 300ms); grey line is record in response to an S₂ stimulus 140ms after S₁. Panel B: mean APD₉₀ of LV and RV under control (co), low-flow global ischemia (6ml/min) and raised [K⁺]_o (8mM). Panel C: mean ERP of LV and RV. Panel D: Fractional change of threshold voltage required to capture the respective ventricle at BCL 300ms. Panel E: Percentage change in upstroke velocity of MAP under low-flow global ischemia (6ml/min) and raised [K⁺]_o (8mM). * indicates significant difference from control (p<0.05).



Online Figure 1 Optical Mapping Set-up Diagrammatic representation of optical mapping apparatus. Only 2 Tungsten lamps are shown for clarity. The second pair of lights was parallel such that the 4 lights formed a square around the heart. Light was shone through 535±25nm interference filters and recorded after filtering through a 695nm long-pass filter.



Online Figure 2 Progression of psECG DF in VF Panel A: progression during differing perfusion rates. PseudoECG DF during 40ml/min and 6ml/min protocol ($p < 0.005$). Panel B: progression under reduced extracellular pH (pH 6.7) compared to control (pH 7.4). Panel C: ps ECG DF progression during hypoxia compared to control. Again this global assessment showed no significant difference of DF in hypoxia compared to control. Panel D: psECG[#] progression with raised extracellular $[K^+]$ compared to control. DF is profoundly reduced compared to control ($^{\#}p < 0.05$). This assessment of global DF progression was indistinguishable from 6ml/min low-flow global ischemia.

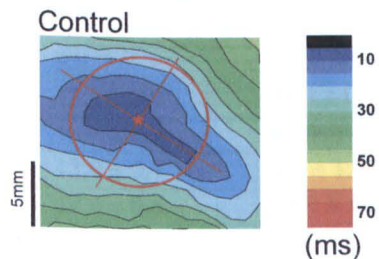
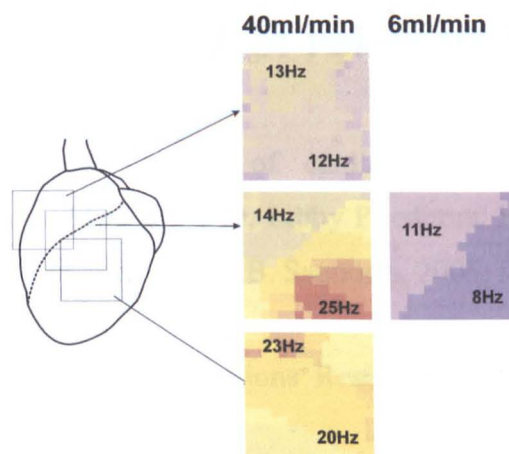


Figure 3 Conduction Velocity Conduction velocity measurements can be contaminated by intramural conduction or close pacing stimulus. Thus, to ensure the correct evaluation of conduction velocity, both transverse and longitudinal velocities were assessed using several different methods: (i) Circular method: CV was measured around a circle centred on the stimulation point *. A radius of 5mm was chosen to avoid the central area of instantaneous activation and more remote areas where transmural conduction can produce spuriously elevated values. Peak velocity was identified and the angle of the axis of fastest (longitudinal) conduction measured. CV at 90° to this axis (transverse) was also measured, yielding an estimate of conduction anisotropy. (ii) Linear method, using isochronal activation maps, CV was calculated along a straight line from the pacing site through the fastest advancing point of the wavefront. Longitudinal CV was determined as the value of the low plateau velocity between the peaks of stimulus artefact and intramural conduction. Transverse velocity was similarly assessed on a perpendicular line. Both methods produced similar results.



Online Figure 4 Ventricular Heterogeneity. The discrete LV-RV nature of the DF heterogeneity was demonstrated by rotating the heart and recording just from the LV or RV. Illustrated are typical DF maps at 480s at 40ml/min control perfusion. No frequency alteration was observed on moving further into the LV or RV. Within the same ventricle statistics on mean DF were performed on two sets of 3×3 pixels. These sets were located at sites on the array identical to those used in standard experiments. There was no difference in DF between these sites at 480s (LV 1 - 24.4±2.7, LV 2 - 27.6±3.6, RV1 12.2±0.65, RV2 11.7±0.1).

Time	Dominant frequency of VF (Hz)			
	0s		480s	
	LV	RV	LV	RV
40ml/min (n=7)	16.7 ± 1.4	13.4 ± 0.9	26.1 ± 1.9* [#]	15.6 ± 1.3 [#]
6ml/min (n=7)	15.2 ± 1.0	13.4 ± 0.9	8.6 ± 1.0* [#]	12.3 ± 0.84 [#]
8mM K ⁺ (n=5)	16.5 ± 1.9	13.0 ± 0.7	9.2 ± 1.0** [#]	12.5 ± 1.5 [#]
Hypoxia (n=5)	14.7 ± 1.0	12.4 ± 0.5	21.9 ± 1.0** [#]	14.7 ± 0.9 [#]
pH 6.7 (n=7)	15.4 ± 1.3	13.5 ± 1.0	20.0 ± 1.2**	17.8 ± 1.1**

Table 1 Mean ventricular DFs calculated using 3×3 pixels. * indicates significant differences of VF DF, 0s vs. 480s *p<0.01, ** p<0.0001. [#] indicates significant LV-RV differences at 480s p<0.001.

13 List of reference

- (1) Rubart M, Zipes D. Genesis of cardiac arrhythmias: Electrophysiological considerations. In: Braunwald E, Zipes D, Libby P, editors. Heart Disease: a textbook of cardiovascular medicine. Philadelphia: W.B. Saunders, 2005: 803-861.
- (2) British Heart Foundation Promotions Research Group. Coronary Heart Disease Statistics 2004.
- (3) Janse MJ, Wit AL. Electrophysiological mechanisms of ventricular arrhythmias resulting from myocardial ischemia and infarction. *Physiol Rev* 1989; 69(4):1049-1169.
- (4) Burton FL, McPhaden AR, Cobbe SM. Ventricular fibrillation threshold and local dispersion of refractoriness in isolated rabbit hearts with left ventricular dysfunction. *Basic Res Cardiol* 2000; 95(5):359-367.
- (5) Podrid PJ, Myerburg RJ. Epidemiology and stratification of risk for sudden cardiac death. *Clin Cardiol* 2005; 28(11 Suppl 1):I3-11.
- (6) Pell JP, Sirel JM, Marsden AK, Ford I, Cobbe SM. Effect of reducing ambulance response times on deaths from out of hospital cardiac arrest: Cohort study. *BMJ* 2001; 322(7299):1385-1388.
- (7) Ross P, Nolan J, Hill E, Dawson J, Whimster F, Skinner D. The use of AEDs by police officers in the City of London. *Resuscitation* 2001; 50(2):141-146.
- (8) Valenzuela TD, Roe DJ, Nichol G, Clark LL, Spaite DW, Hardman RG. Outcomes of rapid defibrillation by security officers after cardiac arrest in casinos. *N Engl J Med* 2000; 343(17):1206-1209.
- (9) Cobb LA, Fahrenbruch CE, Walsh TR, Copass MK, Olsufka M, Breskin M, Hallstrom AP. Influence of cardiopulmonary resuscitation prior to defibrillation in patients with out-of-hospital ventricular fibrillation. *JAMA* 1999; 281(13):1182-1188.
- (10) Garcia LA, Allan JJ, Kerber RE. Interactions between CPR and defibrillation waveforms: effect on resumption of a perfusing rhythm after defibrillation. *Resuscitation* 2000; 47(3):301-305.

- (11) Kolarova J, Ayoub IM, Yi Z, Gazmuri RJ. Optimal timing for electrical defibrillation after prolonged untreated ventricular fibrillation. *Cri Care Med* 2003; 31(7):2022-2028.
- (12) Niemann JT, Cairns CB, Sharma J, Lewis RJ. Treatment of prolonged ventricular fibrillation. Immediate countershock versus high-dose epinephrine and CPR preceding countershock. *Circulation* 1992; 85(1):281-287.
- (13) Wik L, Hansen TB, Fylling F, Steen T, Vaagenes P, Auestad BH, Steen PA. Delaying defibrillation to give basic cardiopulmonary resuscitation to patients with out-of-hospital ventricular fibrillation: a randomized trial. *JAMA* 2003; 289(11):1389-1395.
- (14) Resuscitation Council (UK). Adult advanced life support: Resuscitation guidelines 2005. 2005. Resuscitation Council (UK).
- (15) Weisfeldt ML, Becker LB. Resuscitation after cardiac arrest: a 3-phase time-sensitive model. *JAMA* 2002; 288(23):3035-3038.
- (16) Gilmore CM, Rea TD, Becker LJ, Eisenberg MS. Three-phase model of cardiac arrest: Time-dependent benefit of bystander cardiopulmonary resuscitation. *Am J Cardiol* 2006; 98(4):497-499.
- (17) Gazmuri RJ. Acidosis during cardiac arrest: a manifestation of inadequate perfusion. *Crit Care Med* 1999; 27(9):2055-2056.
- (18) Wenzel V, Idris AH, Banner MJ, Fuerst RS, Tucker KJ. The composition of gas given by mouth-to-mouth ventilation during CPR. *Chest* 1994; 106(6):1806-1810.
- (19) Weaver WD, Cobb LA, Dennis D, Ray R, Hallstrom AP, Copass MK. Amplitude of ventricular fibrillation waveform and outcome after cardiac arrest. *Ann Intern Med* 1985; 102(1):53-55.
- (20) Gazmuri RJ, Ayoub IM, Shakeri SA. Ventricular fibrillation waveform analysis for guiding the time of electrical defibrillation. *Crit Care Med* 2001; 29(12):2395-2397.
- (21) Carlisle EJ, Allen JD, Kernohan WG, Leahey W, Adgey AA. Pharmacological analysis of established ventricular fibrillation. *Br J Pharmacol* 1990; 100(3):530-534.

- (22) Carlisle EJ, Allen JD, Kernohan WG, Anderson J, Adgey AA. Fourier analysis of ventricular fibrillation of varied aetiology. *Eur Heart J* 1990; 11(2):173-181.
- (23) Stewart AJ, Allen JD, Adgey AA. Frequency analysis of ventricular fibrillation and resuscitation success. *Q J Med* 1992; 85(306):761-769.
- (24) Strohmenger HU, Eftestol T, Sunde K, Wenzel V, Mair M, Ulmer H, Lindner KH, Steen PA. The predictive value of ventricular fibrillation electrocardiogram signal frequency and amplitude variables in patients with out-of-hospital cardiac arrest. *Anesth Analg* 2001; 93(6):1428-1433.
- (25) Achleitner U, Wenzel V, Strohmenger HU, Lindner KH, Baubin MA, Krismer AC, Mayr VD, Amann A. The beneficial effect of basic life support on ventricular fibrillation, mean frequency and coronary perfusion pressure. *Resuscitation* 2001; 51(2):151-158.
- (26) Achleitner U, Wenzel V, Strohmenger HU, Krismer AC, Lurie KG, Lindner KH, Amann A. The effects of repeated doses of vasopressin or epinephrine on ventricular fibrillation in a porcine model of prolonged cardiopulmonary resuscitation. *Anesth Analg* 2000; 90(5):1067-1075.
- (27) Strohmenger HU, Hemmer W, Lindner KH, Schickling J, Brown CG. Median fibrillation frequency in cardiac surgery: influence of temperature and guide to countershock therapy. *Chest* 1997; 111(6):1560-1564.
- (28) Strohmenger HU, Lindner KH, Prengel AW, Pfenninger EG, Bothner U, Lurie KG. Effects of epinephrine and vasopressin on median fibrillation frequency and defibrillation success in a porcine model of cardiopulmonary resuscitation. *Resuscitation* 1996; 31(1):65-73.
- (29) Strohmenger HU, Lindner KH, Brown CG. Analysis of the ventricular fibrillation ECG signal amplitude and frequency parameters as predictors of countershock success in humans. *Chest* 1997; 111(3):584-589.
- (30) Strohmenger HU, Lindner KH, Keller A, Lindner IM, Pfenninger EG. Spectral analysis of ventricular fibrillation and closed-chest cardiopulmonary resuscitation. *Resuscitation* 1996; 33(2):155-161.

- (31) Martin DR, Brown CG, Dzwonczyk R. Frequency analysis of the human and swine electrocardiogram during ventricular fibrillation. *Resuscitation* 1991; 22(1):85-91.
- (32) Brown CG, Griffith RF, Hoekstra J, Nejman G, Mitchell L, Dzwonczyk R. Median Frequency - a parameter for predicting defibrillation success rate. *Ann Emerg Med* 1991; 20(7):787-789.
- (33) Brown CG, Dzwonczyk R, Werman HA, Hamlin RL. Estimating the duration of ventricular fibrillation. *Ann Emerg Med* 1989; 18(11):1181-1185.
- (34) Marn-Pernat A, Weil MH, Tang W, Pernat A, Bisera J. Optimizing timing of ventricular defibrillation. *Crit Care Med* 2001; 29(12):2360-2365.
- (35) Jalife J. Ventricular fibrillation: mechanisms of initiation and maintenance. *Annu Rev Physiol* 2000; 62:25-50.
- (36) Wiggers CJ. The mechanism and nature of ventricular fibrillation. *Am Heart J* 1940; 20:399-412.
- (37) Chen PS, Wolf PD, Dixon EG, Danieleley ND, Frazier DW, Smith WM, Ideker RE. Mechanism of ventricular vulnerability to single premature stimuli in open-chest dogs. *Circ Res* 1988; 62(6):1191-1209.
- (38) Antzelevitch C. Basic mechanisms of reentrant arrhythmias. *Curr Opin Cardiol* 2001; 16(1):1-7.
- (39) Jalife J, Delmar M, Davidenko J, Anumonwo JMB. Cardiac arrhythmias. Basic cardiac electrophysiology for the clinician. Futura publishing company, 1999: 197-245.
- (40) Bers DM. Excitation-contraction coupling and cardiac force. 2 ed. Dordrecht/Boston/London: Kluwer Academic Press, 2001.
- (41) Nuss HB, Kaab S, Kass DA, Tomaselli GF, Marban E. Cellular basis of ventricular arrhythmias and abnormal automaticity in heart failure. *Am J Physiol Heart Circ Physiol* 1999; 277(1):H80-H91.

- (42) Bers DM, Pogwizd SM, Schlotthauer K. Upregulated Na/Ca exchange is involved in both contractile dysfunction and arrhythmogenesis in heart failure. *Basic Res Cardiol* 2002; 97 Suppl 1:I36-I42.
- (43) de Bakker JMT, Stein M, van Rijen HVM. Three-dimensional anatomic structure as substrate for ventricular tachycardia/ventricular fibrillation. *Heart Rhythm* 2005; 2(7):777-779.
- (44) Burton FL, Cobbe SM. Dispersion of ventricular repolarization and refractory period. *Cardiovasc Res* 2001; 50(1):10-23.
- (45) Ng GA, Brack KE, Coote JH. Effects of direct sympathetic and vagus nerve stimulation on the physiology of the whole heart--a novel model of isolated Langendorff perfused rabbit heart with intact dual autonomic innervation. *Exp Physiol* 2001; 86(3):319-329.
- (46) Burton FL, Cobbe SM. Effect of sustained stretch on dispersion of ventricular fibrillation intervals in normal rabbit hearts. *Cardiovasc Res* 1998; 39(2):351-359.
- (47) Gettes L, Cascio W, Johnson T, Muller-Borer B. Characteristics and causes of conduction changes associated with 1a and 1b arrhythmias in acute ischaemia. In: Spooner P, Joyner R, Jalife J, editors. *Discontinuous conduction in the heart*. Futura Publishing Co, 1997: 441-452.
- (48) Choi BR, Salama G. Simultaneous maps of optical action potentials and calcium transients in guinea-pig hearts: mechanisms underlying concordant alternans. *J Physiol* 2000; 529 Pt 1:171-188.
- (49) Pak HN, Hong SJ, Hwang GS, Lee HS, Park SW, Ahn JC, Moo RY, Kim YH. Spatial dispersion of action potential duration restitution kinetics is associated with induction of ventricular tachycardia/fibrillation in humans. *J Cardiovasc Electrophysiol* 2004; 15(12):1357-1363.
- (50) Weiss JN, Chen PS, Qu Z, Karagueuzian HS, Lin SF, Garfinkel A. Electrical restitution and cardiac fibrillation. *J Cardiovasc Electrophysiol* 2002; 13(3):292-295.

- (51) Koller ML, Riccio ML, Gilmour RF, Jr. Dynamic restitution of action potential duration during electrical alternans and ventricular fibrillation *Am J Physiol Heart Circ Physiol* 1998; 275(5 Pt 2):H1635-H1642.
- (52) Banville I, Gray RA. Effect of action potential duration and conduction velocity restitution and their spatial dispersion on alternans and the stability of arrhythmias. *J Cardiovasc Electrophysiol* 2002; 13(11):1141-1149.
- (53) Riccio ML, Koller ML, Gilmour RF, Jr. Electrical restitution and spatiotemporal organization during ventricular fibrillation. *Circ Res* 1999; 84(8):955-963.
- (54) Omichi C, Zhou S, Lee MH, Naik A, Chang CM, Garfinkel A, Weiss JN, Lin SF, Karagueuzian HS, Chen PS. Effects of amiodarone on wave front dynamics during ventricular fibrillation in isolated swine right ventricle. *Am J Physiol Heart Circ Physiol* 2002; 282(3):H1063-H1070.
- (55) Wu TJ, Lin SF, Weiss JN, Ting CT, Chen PS. Two types of ventricular fibrillation in isolated rabbit hearts: importance of excitability and action potential duration restitution. *Circulation* 2002; 106(14):1859-1866.
- (56) Weiss JN, Garfinkel A, Karagueuzian HS, Qu Z, Chen PS. Chaos and the transition to ventricular fibrillation: a new approach to antiarrhythmic drug evaluation. *Circulation* 1999; 99(21):2819-2826.
- (57) Rosen MR, Cohen IS, Danilo J, Steinberg SF. The heart remembers. *Cardiovasc Res* 1998; 40(3):469-482.
- (58) Choi BR, Liu T, Salama G. Adaptation of cardiac action potential durations to stimulation history with random diastolic intervals. *J Cardiovasc Electrophysiol* 2004; 15(10):1188-1197.
- (59) Huang J, Zhou X, Smith WM, Ideker RE. Restitution properties during ventricular fibrillation in the In Situ Swine Heart. *Circulation* 2004; 110(20):3161-3167.
- (60) Gray RA, Jalife J, Pertsov AM. Spatial and temporal organization during cardiac fibrillation. *Nature* 1998; 392:75-78.

- (61) Chen J, Mandapati R, Berenfeld O, Skanes AC, Jalife J. High-frequency periodic sources underlie ventricular fibrillation in the isolated rabbit heart. *Circ Res* 2000; 86(1):86-93.
- (62) Mandapati R, Asano Y, Baxter WT, Gray R, Davidenko J, Jalife J. Quantification of effects of global ischemia on dynamics of ventricular fibrillation in isolated rabbit heart. *Circulation* 1998; 98(16):1688-1696.
- (63) Samie FH, Berenfeld O, Anumonwo J, Mironov SF, Udassi S, Beaumont J, Taffet S, Pertsov AM, Jalife J. Rectification of the background potassium current: a determinant of rotor dynamics in ventricular fibrillation. *Circ Res* 2001; 89(12):1216-1223.
- (64) Valderrabano M, Yang J, Omichi C, Kil J, Lamp ST, Qu Z, Lin SF, Karagueuzian HS, Garfinkel A, Chen PS, Weiss JN. Frequency analysis of ventricular fibrillation in swine ventricles. *Circ Res* 2002; 90(2):213-222.
- (65) Choi BR, Liu T, Salama G. The distribution of refractory periods influences the dynamics of ventricular fibrillation. *Circ Res* 2001; 88(5):E49-E58.
- (66) Choi BR, Nho W, Liu T, Salama G. Life span of ventricular fibrillation frequencies. *Circ Res* 2002; 91(4):339-345.
- (67) Wu TJ, Lin SF, Baher A, Qu Z, Garfinkel A, Weiss JN, Ting CT, Chen PS. Mother rotors and the mechanisms of D600-induced type 2 ventricular fibrillation. *Circulation* 2004;01.
- (68) Chen PS, Wu TJ, Ting CT, Karagueuzian HS, Garfinkel A, Lin SF, Weiss JN. A tale of two fibrillations. *Circulation* 2003; 108(19):2298-2303.
- (69) Wu TJ, Lin SF, Hsieh YC, Ting CT, Chen PS. Ventricular fibrillation during no-flow global ischemia in isolated rabbit hearts. *J Cardiovasc Electrophysiol* 2006; 17(10):1-9.
- (70) Liu YB, Pak HN, Lamp ST, Okuyama Y, Hayashi H, Wu TJ, Weiss JN, Chen PS, Lin SF. Coexistence of two types of ventricular fibrillation during acute regional ischemia in rabbit ventricle. *J Cardiovasc Electrophysiol* 2004; 15(12):1433-1440.

- (71) Martin G, Cosin J, Such M, Hernandez A, Llamas P. Relation between power spectrum time course during ventricular fibrillation and electromechanical dissociation. Effects of coronary perfusion and nifedipine. *Eur Heart J* 1986; 7(7):560-569.
- (72) Chorro FJ, Guerrero J, Canoves J, Martinez-Sober M, Mainar L, Sanchis J, Calpe J, Llavador E, Espi J, Lopez-Merino V. Quantification of the modifications in the dominant frequency of ventricular fibrillation under conditions of ischemia and reperfusion: an experimental study. *Pacing Clin Electrophysiol* 1998; 21(9):1716-1723.
- (73) Barton CW, Cascio WE, Batson DN, Engle CL, Johnson TA. Effect of rates of perfusion on dominant frequency and defibrillation energy in isolated fibrillating hearts. *Pacing Clin Electrophysiol* 2000; 23(4 Pt 1):504-511.
- (74) Jennings RB, Murry CE, Steenbergen C, Reimer KA. Development of cell injury in sustained acute ischemia. *Circulation* 1990; 82(supplement II):II-2-II-12.
- (75) Idris AH, Wenzel V, Becker LB, Banner MJ, Orban DJ. Does hypoxia or hypercarbia independently affect resuscitation from cardiac arrest? *Chest* 1995; 108(2):522-528.
- (76) Idris AH, Becker LB, Fuerst RS, Wenzel V, Rush WJ, Melker RJ, Orban DJ. Effect of ventilation on resuscitation in an animal model of cardiac arrest. *Circulation* 1994; 90(6):3063-3069.
- (77) Idris AH, Staples ED, O'Brien DJ, Melker RJ, Rush WJ, Del Duca KD, Falk JL. Effect of ventilation on acid-base balance and oxygenation in low blood-flow states. *Crit Care Med* 1994; 22(11):1827-1834.
- (78) Tucker KJ, Idris AH, Wenzel V, Orban DJ. Changes in arterial and mixed venous blood gases during untreated ventricular fibrillation and cardiopulmonary resuscitation. *Resuscitation* 1994; 28(2):137-141.
- (79) Bethell HW, Vandenberg JI, Smith GA, Grace AA. Changes in ventricular repolarization during acidosis and low-flow ischemia. *Am J Physiol Heart Circ Physiol* 1998; 275(2):H551-H561.
- (80) Kette F, Weil MH, Gazmuri RJ, Bisera J, Rackow EC. Intramyocardial hypercarbic acidosis during cardiac arrest and resuscitation. *Crit Care Med* 1993; 21(6):901-906.

- (81) Kleber AG. Resting membrane potential, extracellular potassium activity, and intracellular sodium activity during acute global ischemia in isolated perfused guinea pig hearts. *Circ Res* 1983; 52(4):442-450.
- (82) Ehlert FA, Goldberger JJ. Cellular and pathophysiological mechanisms of ventricular arrhythmias in acute ischemia and infarction. *Pacing Clin Electrophysiol* 1997; 20(4 Pt 1):966-975.
- (83) Niemann JT, Cairns CB. Hyperkalemia and ionized hypocalcemia during cardiac arrest and resuscitation: possible culprits for postcountershock arrhythmias? *Ann Emerg Med* 1999; 34(1):1-7.
- (84) Akiyama T. Intracellular recording of in situ ventricular cells during ventricular fibrillation. *Am J Physiol Heart Circ Physiol* 1981; 240(4):H465-H471.
- (85) Stewart AJ, Allen JD, Devine AB, Adgey AA. Effects of blockade of fast and slow inward current channels on ventricular fibrillation in the pig heart. *Heart* 1996; 76(6):513-519.
- (86) Jones DL, Kim YH, Natale A, Klein GJ, Varin F. Bretylium decreases and verapamil increases defibrillation threshold in pigs. *Pacing Clin Electrophysiol* 1994; 17(8):1380-1390.
- (87) Taggart P, Sutton P, Chalabi Z, Boyett MR, Simon R, Elliott D, Gill JS. Effect of adrenergic stimulation on action potential duration restitution in humans. *Circulation* 2003; 107(2):285-289.
- (88) Gonzalez Rebollo JM, Hernandez MA, Garcia A, Garcia dC, Mejias A, Moro C. Recurrent ventricular fibrillation during a febrile illness in a patient with the Brugada syndrome. *Rev Esp Cardiol* 2000; 53(5):755-757.
- (89) Brugada J, Brugada R, Brugada P. Right bundle-branch block and ST-segment elevation in leads V1 through V3: A marker for sudden death in patients without demonstrable structural heart disease. *Circulation* 1998; 97(5):457-460.
- (90) Priori SG, Napolitano C, Schwartz DJ. Genetics of cardiac arrhythmias. In: Braunwald E, Zipes D, Libby P, editors. *Heart Disease: a textbook of cardiovascular medicine*. Philadelphia: Saunders, 2005: 689-696.

- (91) Walls RM. Fundamental clinical concepts. In: Marx JA, Hockberger RS, Walls RM, Adams J, Barkin RM, Barsan WG, Danzl DF, Gausche-Hill M, Hamilton GC, Ling LJ, Newton E, editors. *Rosen's Emergency Medicine*. St Louis: Mosby, Inc., 2002: 1-241.
- (92) Ideker RE, Chattipakorn TN, Gray RA. Defibrillation mechanisms: the parable of the blind men and the elephant. *J Cardiovasc Electrophysiol* 2000; 11(9):1008-1013.
- (93) Ideker RE, Walcott GP, Epstein AE, Plumb VJ, Kay N. Ventricular fibrillation and defibrillation. What are the major unresolved issues? *Heart Rhythm* 2005; 2(5):555-558.
- (94) Wharton JM, Wolf PD, Smith WM, Chen PS, Frazier DW, Yabe S, Daniele N, Ideker RE. Cardiac potential and potential gradient fields generated by single, combined, and sequential shocks during ventricular defibrillation. *Circulation* 1992; 85(4):1510-1523.
- (95) Frazier DW, Wolf PD, Wharton JM, Tang AS, Smith WM, Ideker RE. Stimulus-induced critical point. Mechanism for electrical initiation of reentry in normal canine myocardium. *J Clin Invest* 1989; 83(3):1039-1052.
- (96) Efimov IR, Cheng Y, Van Wagoner DR, Mazgalev T, Tchou PJ. Virtual Electrode-Induced Phase Singularity: A Basic Mechanism of Defibrillation Failure. *Circ Res* 1998; 82(8):918-925.
- (97) Sharifov OF, Fast VG. Intramural Virtual Electrodes in Ventricular Wall: Effects on epicardial polarizations. *Circulation* 2004; 109(19):2349-2356.
- (98) Bourn DW, Gray RA, Trayanova NA. Characterization of the relationship between preshock state and virtual electrode polarization-induced propagated graded responses resulting in arrhythmia induction. *Heart Rhythm* 2006; 3(5):583-595.
- (99) Porter WT. On results of ligation of the coronary arteries. *J Physiol (Lond)* 1894; 15:121-138.
- (100) McWilliam JA. Fibrillar contraction of the heart. *J Physiol* 1887; 8:296-310.
- (101) Gazmuri RJ, Deshmukh S, Shah PR. Myocardial effects of repeated electrical defibrillations in the isolated fibrillating rat heart. *Crit Care Med* 2000; 28(8):2690-2696.

- (102) Qu Z. Critical mass hypothesis revisited: role of dynamical wave stability in spontaneous termination of cardiac fibrillation. *Am J Physiol Heart Circ Physiol* 2006; 290(1):H255-H263.
- (103) Zipes DP, Fischer J, King RM, Nicoll B, Jolly WW. Termination of ventricular fibrillation in dogs by depolarizing a critical amount of myocardium. *Am J Cardiol* 1975; 36(1):37-44.
- (104) Shibata N, Chen PS, Dixon EG, Wolf PD, Danieley ND, Smith WM, Ideker RE. Epicardial activation after unsuccessful defibrillation shocks in dogs. *Am J Physiol Heart Circ Physiol* 1988; 255(4):H902-H909.
- (105) Tovar OH, Jones JL. Relationship between "extension of refractoriness" and probability of successful defibrillation. *Am J Physiol Heart Circ Physiol* 1997; 272(2 Pt 2):H1011-H1019.
- (106) Sweeney RJ, Gill RM, Steinberg MI, Reid PR. Ventricular refractory period extension caused by defibrillation shocks. *Circulation* 1990; 82(3):965-972.
- (107) Jones JL, Tovar OH. The mechanism of defibrillation and cardioversion. *Proc IEEE* 1996; 84(3):392-403.
- (108) Chattipakorn N, Fotuhi PC, Chattipakorn SC, Ideker RE. Three-dimensional mapping of earliest activation after near-threshold ventricular defibrillation shocks. *J Cardiovasc Electrophysiol* 2003; 14(1):65-69.
- (109) Chattipakorn N, Banville I, Gray RA, Ideker RE. Effects of shock strengths on ventricular defibrillation failure. *Cardiovasc Res* 2004; 61(1):39-44.
- (110) Chattipakorn N, Kenknight BH, Rogers JM, Walker RG, Walcott GP, Rollins DL, Smith WM, Ideker RE. Locally propagated activation immediately after internal defibrillation. *Circulation* 1998; 97(14):1401-1410.
- (111) Gray RA. Global mechanisms of defibrillation. In: Zipes DP, Jalife J, editors. *Cardiac Electrophysiology: From cell to bedside*. Philadelphia, USA: Saunders, 2006: 417-425.

- (112) Sepulveda NG, Roth BJ, Wikswo JP, Jr. Current injection into a two-dimensional anisotropic bidomain. *Biophys J* 1989; 55(5):987-999.
- (113) Wikswo JP, Jr., Lin SF, Abbas RA. Virtual electrodes in cardiac tissue: a common mechanism for anodal and cathodal stimulation. *Biophys J* 1995; 69(6):2195-2210.
- (114) Muzikant AL, Henriquez CS. Bipolar stimulation of a three dimensional bidomain incorporating rotational anisotropy. *IEEE Trans Biomed Eng* 1998; 45(4):449-462.
- (115) Sepulveda NG, Wikswo JP, Jr. Bipolar stimulation of cardiac tissue using an anisotropic bidomain model. *J Cardiovasc. Electrophysiol* 1994; 5(3):258-267.
- (116) Nikolski VP, Sambelashvili AT, Efimov IR. Mechanisms of make and break excitation revisited: paradoxical break excitation during diastolic stimulation. *Am J Physiol Heart Circ Physiol* 2002; 282(2):H565-H575.
- (117) Sobie EA, Susil RC, Tung L. A generalized activating function for predicting virtual electrodes in cardiac tissue. *Biophys J* 1997; 73(3):1410-1423.
- (118) Efimov IR, Cheng YN, Biermann M, Van Wagoner DR, Mazgalev TN, Tchou PJ. Transmembrane voltage changes produced by real and virtual electrodes during monophasic defibrillation shock delivered by an implantable electrode. *J Cardiovasc Electrophysiol* 1997; 8(9):1031-1045.
- (119) Shibata N, Chen PS, Dixon EG, Wolf PD, Danieley ND, Smith WM, Ideker RE. Influence of shock strength and timing on induction of ventricular arrhythmias in dogs. *Am J Physiol Heart Circ Physiol* 1988; 255(4):H891-H901.
- (120) Chen PS, Shibata N, Dixon EG, Martin RO, Ideker RE. Comparison of the defibrillation threshold and the upper limit of ventricular vulnerability. *Circulation* 1986; 73(5):1022-1028.
- (121) Efimov I, Ripplinger CM. Virtual electrode hypothesis of defibrillation. *Heart Rhythm* 2006; 3(9):1100-1102.

(122) Yashima M, KIM YH, Armin S, Wu TJ, Miyauchi Y, Mandel WJ, Chen PS, Karagueuzian HS. On the mechanism of the probabilistic nature of ventricular defibrillation threshold. *Am J Physiol Heart Circ Physiol* 2003; 284(1):H249-H255.

(123) Irnich W. Threshold measurements: ten rules for good measuring practice. *Pacing Clin Electrophysiol* 2003; 26(8):1738-1746.

(124) Warner ED, Dahl C, Ewy GA. Myocardial injury from transthoracic defibrillator countershock. *Arch Pathol* 1975; 99(1):55-59.

(125) Tokano T, Bach D, Chang J, Davis J, Souza JJ, Zivin A, Knight BP, Goyal R, Man KC, Morady F, Strickberger SA. Effect of ventricular shock strength on cardiac hemodynamics. *J Cardiovasc Electrophysiol* 1998; 9(8):791-797.

(126) Walcott GP, Melnick SB, Chapman FW, Jones JL, Smith WM, Ideker RE. Relative efficacy of monophasic and biphasic waveforms for transthoracic defibrillation after short and long durations of ventricular fibrillation. *Circulation* 1998; 98(20):2210-2215.

(127) Jones JL, Jones RE, Balasky G. Improved cardiac cell excitation with symmetrical biphasic defibrillator waveforms. *Am J Physiol Heart Circ Physiol* 1987; 253(6 Pt 2):H1418-H1424.

(128) Blanchard SM, Ideker RE. Mechanisms of electrical defibrillation: impact of new experimental defibrillator waveforms. *Am Heart J* 1994; 127(4 Pt 2):970-977

(129) Tovar OH, Jones JL. Electrophysiologic deterioration after one-minute fibrillation increases relative biphasic defibrillation efficacy. *J Cardiovasc Electrophysiol* 2000; 11(6):645-651.

(130) Jones JL, Tovar OH. Electrophysiology of ventricular fibrillation and defibrillation. *Crit Care Med* 2000; 28(11 Suppl):N219-N221.

(131) Eftestol T, Sunde K, Ole AS, Husoy JH, Steen PA. Predicting outcome of defibrillation by spectral characterization and nonparametric classification of ventricular fibrillation in patients with out-of-hospital cardiac arrest. *Circulation* 2000; 102(13):1523-1529.

- (132) Patwardhan A, Moghe S, Wang K, Wright H, Leonelli F. Correlation between defibrillation shock outcome and coherence in electrocardiograms. *Pacing Clin Electrophysiol* 2001; 24(9 Pt 1):1354-1362.
- (133) Amann A, Achleitner U, Antretter H, Bonatti JO, Krismer AC, Lindner KH, Rieder J, Wenzel V, Voelckel WG, Strohmer HU. Analysing ventricular fibrillation ECG-signals and predicting defibrillation success during cardiopulmonary resuscitation employing N(alpha)-histograms. *Resuscitation* 2001; 50(1):77-85.
- (134) Opthof T, Misier AR, Coronel R, Vermeulen JT, Verberne HJ, Frank RG, Mouljn AC, van Capelle FJ, Janse MJ. Dispersion of refractoriness in canine ventricular myocardium. Effects of sympathetic stimulation. *Circ Res* 1991; 68(5):1204-1215.
- (135) Opthof T, Coronel R, Vermeulen JT, Verberne HJ, van Capelle FJ, Janse MJ. Dispersion of refractoriness in normal and ischaemic canine ventricle: effects of sympathetic stimulation. *Cardiovasc Res* 1993; 27(11):1954-1960.
- (136) Wolk R, Kane KA, Cobbe SM, Hicks MN. Facilitation of spontaneous defibrillation by moxonidine during regional ischaemia in an isolated working rabbit heart model. *Eur J Pharmacol* 1999; 367(1):25-32.
- (137) Mechanisms for the early mortality reduction produced by beta-blockade started early in acute myocardial infarction: ISIS-1. ISIS-1 (First International Study of Infarct Survival) Collaborative Group. *Lancet* 1988; 1(8591):921-923.
- (138) Ganong WF. Origin of the heartbeat and the electrical activity of the heart. In: Ganong WF, editor. *Review of medical physiology*. Norwalk: Appleton & Lange, 1991: 504-520.
- (139) Hayashi H, Miyauchi Y, Chou CC, Karagueuzian HS, Chen PS, Lin SF. Effects of cytochalasin D on electrical restitution and the dynamics of ventricular fibrillation in isolated rabbit heart. *J Cardiovasc Electrophysiol* 2003; 14(10):1077-1084.
- (140) Czarnecka M, Lewartowski B, Prokopczuk A. Intracellular recording from the in situ working dog heart in physiological conditions and during acute ischemia and fibrillation. *Acta Physiol Pol* 1973; 24(2):331-337.

- (141) Culling W, Penny WJ, Sheridan DJ. Effects of sotalol on arrhythmias and electrophysiology during myocardial ischaemia and reperfusion. *Cardiovasc Res* 1984; 18(7):397-404.
- (142) Franz MR. Long-term recording of monophasic action potentials from human endocardium. *The Am J Cardiol* 1983; 51(10):1629-1634.
- (143) Kondo M, Nesterenko V, Antzelevitch C. Cellular basis for the monophasic action potential. Which electrode is the recording electrode? *Cardiovasc Res* 2004; 63(4):635-644.
- (144) Franz MR. What is a monophasic action potential recorded by the Franz contact electrode? *Cardiovasc Res* 2005; 65(4):940-941.
- (145) Vigmond EJ. The electrophysiological basis of MAP recordings. *Cardiovasc Res* 2005; 68(3):502-503.
- (146) Franz MR. Current status of monophasic action potential recording: theories, measurements and interpretations. *Cardiovasc Res* 1999; 41(1):25-40.
- (147) Ino T, Karagueuzian HS, Hong K, Meesmann M, Mandel WJ, Peter T. Relation of monophasic action potential recorded with contact electrode to underlying transmembrane action potential properties in isolated cardiac tissues: a systematic microelectrode validation study. *Cardiovasc Res* 1988; 22(4):255-264.
- (148) Tille J. Electrotonic Interaction between Muscle Fibers in the Rabbit Ventricle. *J Gen Physiol* 1966; 50(1):189-202.
- (149) Knisley SB, Neuman MR. Simultaneous electrical and optical mapping in rabbit hearts. *Ann Biomed Eng* 2003; 31(1):32-41.
- (150) Efimov IR, Nikolski VP, Salama G. Optical Imaging of the Heart. *Circ Res* 2004; 95(1):21-33.
- (151) Optical mapping of cardiac excitation and arrhythmias. New York: Futura Publishing Company, 2001.

- (152) Loew LM. Mechanisms and principles of voltage-sensitive fluorescence. In: Rosenbaum DS, Jalife J, editors. *Optical mapping of cardiac excitation and arrhythmias*. New York: Futura, 2001: 33-46.
- (153) Laurita KR, Libbus I. Optics and detectors. In: Rosenbaum DS, Jalife J, editors. *Optical mapping of cardiac excitation and arrhythmias*. New York: Future, 2001: 61-78.
- (154) Qin H, Kay MW, Chattipakorn N, Redden DT, Ideker RE, Rogers JM. Effects of heart isolation, voltage-sensitive dye, and electromechanical uncoupling agents on ventricular fibrillation. *Am J Physiol Heart Circ Physiol* 2003; 284(5):H1818-H1826.
- (155) Cheng Y, Li L, Nikolski V, Wallick DW, Efimov IR. Shock-induced arrhythmogenesis is enhanced by 2,3-butanedione monoxime compared with cytochalasin D. *Am J Physiol Heart Circ Physiol* 2004; 286(1):H310-H318.
- (156) Salama G. Optical mapping: Background and historical perspective. In: Rosenbaum DS, Jalife J, editors. *Optical mapping of cardiac excitation and arrhythmias*. New York: Futura, 2001: 9-31.
- (157) Dillon SM. Optical recordings in the rabbit heart show that defibrillation strength shocks prolong the duration of depolarization and the refractory period. *Circ Res* 1991; 69(3):842-856.
- (158) Choi BR, Hatton WJ, Hume JR, Liu T, Salama G. Low osmolarity transforms ventricular fibrillation from complex to highly organized, with a dominant high-frequency source. *Heart Rhythm* 2006; 3(10):1210-1220.
- (159) Kirchhof PF, Fabritz CL, Behrens S, Franz MR. Induction of ventricular fibrillation by T-wave field-shocks in the isolated perfused rabbit heart: role of nonuniform shock responses. *Basic Res Cardiol* 1997; 92(1):35-44.
- (160) Sharma AD, Fain E, O'Neill PG, Skadsen A, Damle R, Baker J, Chauhan V, Mazuz M, Ross T, Zhang X. Shock on T versus direct current voltage for induction of ventricular fibrillation: A randomized prospective comparison. *Pacing Clin Electrophysiol* 2004; 27(1):89-94.

- (161) Hohnloser S, Weirich J, Antoni H. Influence of direct current on the electrical activity of the heart and on its susceptibility to ventricular fibrillation. *Basic Res Cardiol* 1982; 77(3):237-249.
- (162) Zima E, Gergely M, Soos P, Geller LA, Nemes A, Acsady G, Merkely B. The effect of induction method on defibrillation threshold and ventricular fibrillation cycle length. *J Cardiovasc Electrophysiol* 2006; 17(4):377-381.
- (163) Hooker DR. On the recovery of the heart in electric shock. *Am J Physiol* 1929; 91(1):305-328.
- (164) Peirce EC. Potassium reversion of hypothermic ventricular fibrillation. *J Thorac Cardiovasc Surg* 1964;(48):996-1006.
- (165) Muller W, Windisch H, Tritthart HA. Fluorescent styryl dyes applied as fast optical probes of cardiac action potential. *Eur Biophys J* 1986; 14(2):103-111.
- (166) Windisch H, Muller W, Tritthart HA. Fluorescence monitoring of rapid changes in membrane potential in heart muscle. *Biophys J* 1985; 48(6):877-884.
- (167) Anderson RH, Janse MJ, van Capelle FJ, Billette J, Becker AE, Durrer D. A combined morphological and electrophysiological study of the atrioventricular node of the rabbit heart. *Circ Res* 1974; 35(6):909-922.
- (168) Mazgalev TN, Efimov IR. Optical Mapping of Impulse Propagation in the Atrioventricular Node:1. In: Rosenbaum DS, Jalife J, editors. *Optical Mapping of Cardiac Excitation and Arrhythmias*. New York: Future, 2001: 157-176.
- (169) Rogers JM, Bayly PV. Quantitative analysis of complex rhythms. In: Cabo C, Rosenbaum DS, editors. *Quantitative cardiac electrophysiology*. New York: Marcel Dekker, 2002: 403-428.
- (170) Bracewell RN. The Fourier transform. *Scientific American* 1992; 260(6):86-89.
- (171) Dataq Instruments. Waveform analysis using the fourier transform. Internet. 2003.
- (172) Cooley JW, Turkey JW. An algorithm for the machine calculation of complex fourier series. *Mathematics of Computation* 1965; 19(90):297-301.

- (173) Gray RA, Jalife J, Panfilov A, Baxter WT, Cabo C, Davidenko JM, Pertsov AM. Nonstationary vortexlike reentrant activity as a mechanism of polymorphic ventricular tachycardia in the isolated rabbit heart. *Circulation* 1995; 91(9):2454-2469.
- (174) Zaitsev AV, Berenfeld O, Mironov SF, Jalife J, Pertsov AM. Distribution of excitation frequencies on the epicardial and endocardial surfaces of fibrillating ventricular wall of the sheep heart. *Circ Res* 2000; 86(4):408-417.
- (175) Bernus O, Wellner M, Pertsov AM. Intramural wave propagation in cardiac tissue: asymptotic solutions and cusp waves. *Phys Rev E Stat Nonlin Soft Matter Phys* 2004; 70(6 Pt 1):061913.
- (176) Bayly PV, Kenknight BH, Rogers JM, Hillsley RE, Ideker RE, Smith WM. Estimation of conduction velocity vector fields from epicardial mapping data. *IEEE Trans Biomed Eng* 1998; 45:563-571.
- (177) Jalife J, Delmar M, Davidenko J, Anumonwo JMB. Propagation through cardiac muscle. *Basic cardiac electrophysiology for the clinician*. New York: Futura, 1999: 97-122.
- (178) Kalb SS, Dobrovolny HM, Tolkacheva EG, Idriss SF, Krassowska W, Gauthier DJ. The restitution portrait: a new method for investigating rate-dependent restitution. *J Cardiovasc Electrophysiol* 2004; 15(6):698-709.
- (179) McIntosh MA, Cobbe SM, Smith GL. Heterogeneous changes in action potential and intracellular Ca^{2+} in left ventricular myocyte sub-types from rabbits with heart failure. *Cardiovasc Res* 2000; 45(2):397-409.
- (180) Ng GA, Cobbe SM, Smith GL. Non-uniform prolongation of intracellular Ca^{2+} transients recorded from the epicardial surface of isolated hearts from rabbits with heart failure. *Cardiovasc Res* 1998; 37(2):489-502.
- (181) Pye MP, Black M, Cobbe SM. Comparison of in vivo and in vitro haemodynamic function in experimental heart failure: use of echocardiography. *Cardiovasc Res* 1996; 31(6):873-881.
- (182) Walker NL. Optical mapping of cardiac electrophysiology in transmural myocardial infarction and global acidosis. PhD thesis, University of Glasgow, 2004.

- (183) Garrey WE. The nature of fibrillary contraction of the heart - its relation to tissue mass and form. *Am J Physiol* 1914; 33(3):397-414.
- (184) Garfinkel A, Kim YH, Voroshilovsky O, Qu Z, Kil JR, Lee MH, Karagueuzian HS, Weiss JN, Chen PS. Preventing ventricular fibrillation by flattening cardiac restitution. *PNAS* 2000; 97(11):6061-6066.
- (185) Taggart P, Sutton PMI, Boyett MR, Lab M, Swanton H. Human ventricular action potential duration during short and long cycles: rapid modulation by ischemia. *Circulation* 1996; 94(10):2526-2534.
- (186) Kurz RW, Ren XL, Franz MR. Dispersion and delay of electrical restitution in the globally ischaemic heart. *Eur Heart J* 1994; 15(4):547-554.
- (187) Pye MP, Cobbe SM. Arrhythmogenesis in experimental models of heart failure: the role of increased load. *Cardiovasc Res* 1996; 32(2):248-257.
- (188) Ng GA. Mechanical performance, intracellular Ca^{2+} handling and ventricular repolarisation in isolated hearts for rabbits with heart failure. PhD thesis, University of Glasgow, 1998.
- (189) Joel SE, Hsia PW. Discovery of gradient pattern in dominant frequency maps during fibrillation: implication of rotor drift and epicardial conduction velocity changes. *J Electrocardiol* 2005; 38(4, Supplement 1):159-165.
- (190) Warren M, Guha PK, Berenfeld O, Zaitsev A, Anumonwo JMB, Dhamoon AS, Bagwe S, Taffet SM, Jalife J. Blockade of the inward rectifying potassium current terminates ventricular fibrillation in the guinea pig heart. *J Cardiovasc Electrophysiol* 2003; 14(6):621-631.
- (191) Jalife J. Dynamics and molecular mechanisms of ventricular fibrillation in normal hearts. In: Zipes DP, Jalife J, editors. *Cardiac Electrophysiology; From cell to bedside*. Philadelphia, USA: Saunders, 2006: 390-398.
- (192) Newton JC, Smith WM, Ideker RE. Estimated global transmural distribution of activation rate and conduction block during porcine and canine ventricular fibrillation. *Circ Res* 2004; 94:836-842.

- (193) Huang J, Walcott GP, Killingsworth CR, Melnick SB, Rogers JM, Ideker RE. Quantification of activation patterns during ventricular fibrillation in open-chest porcine left ventricle and septum. *Heart Rhythm* 2005; 2(7):720-728.
- (194) Sorota S. Insights into the structure, distribution and function of the cardiac chloride channels. *Cardiovasc Res* 1999; 42(2):361-376.
- (195) Vandenberg JI, Bett GC, Powell T. Contribution of a swelling-activated chloride current to changes in the cardiac action potential. *Am J Physiol Cell Physiol* 1997; 273(2):C541-C547.
- (196) Hiraoka M, Kawano S, Hirano Y, Furukawa T. Role of cardiac chloride currents in changes in action potential characteristics and arrhythmias. *Cardiovasc Res* 1998; 40(1):23-33.
- (197) Nerbonne JM, Kass RS. Molecular physiology of cardiac repolarization. *Physiol Rev* 2005; 85(4):1205-1253.
- (198) Fahmi AI, Patel M, Stevens EB, Fowden AL, John JEI, Lee K, Pinnock R, Morgan K, Jackson AP, Vandenberg JI. The sodium channel beta-subunit SCN3b modulates the kinetics of SCN5a and is expressed heterogeneously in sheep heart. *J Physiol (Lond)* 2001; 537(3):693-700.
- (199) Quail AW, Cottee DB, Porges WL, White SW. Recent views on integrated coronary control: significance of non-uniform regional control of coronary flow conductance. *Clin Exp Pharmacol Physiol* 2000; 27(12):1039-1044.
- (200) Gautier M, Hyvelin JM, De Crescenzo V, Eder V, Bonnet P. Heterogeneous Kv1 function and expression in coronary myocytes from right and left ventricles in rat. *Am J Physiol Heart Circ Physiol* 2006;00774.
- (201) Trautwein W, Gottstein U, Dudel J. Der Aktionsstrom der Myokardfaser im Sauerstoffmangel. *Pflugers Arch* 1954; 260(1):40-60.
- (202) Tissier C, Bes S, Vandroux D, Fantini E, Rochette L, Athias P. Specific electromechanical responses of cardiomyocytes to individual and combined components of ischemia. *Can J Physiol Pharmacol* 2002; 80(12):1145-1157.

- (203) Kodama I, Wilde A, Janse MJ, Durrer D, Yamada K. Combined effects of hypoxia, hyperkalemia and acidosis on membrane action potential and excitability of guinea-pig ventricular muscle. *J Mol Cell Cardiol* 1984; 16(3):247-259.
- (204) Ruiz-Ceretti E, Ragault P, Leblanc N, Ponce Zumino AZ. Effects of hypoxia and altered K_o on the membrane potential of rabbit ventricle. *J Mol Cell Cardiol* 1983; 15(12):845-854.
- (205) Wit AL, Janse MJ. Electrophysiological effect of acute myocardial ischemia. The ventricular arrhythmias of ischemia and infarction. New York: Futura, 1993: 174-222.
- (206) MacLeod DP, Daniel EE. Influence of glucose on the transmembrane action potential of anoxic papillary muscle. *J Gen Physiol* 1965; 48(5):887-899.
- (207) MacLeod DP, Prasad K. Influence of glucose on the transmembrane action potential of papillary muscle: Effects of concentration, phlorizin and insulin, nonmetabolizable sugars, and stimulators of glycolysis. *J Gen Physiol* 1969; 53(6):792-815.
- (208) Allen DG, Orchard CH. Myocardial contractile function during ischemia and hypoxia. *Circ Res* 1987; 60(2):153-168.
- (209) Trautwein W, Dudel J. Aktionspotential und Kontraktion des Herzmuskels im Sauerstoffmangel. *Pflugers Arch* 1956; 263(1):23-32.
- (210) MacDonald TF, MacLeod DP. Metabolism and the electrocal activity of anoxic ventricular muscle. *J Physiol (Lond)* 1973; 229(3):559-582.
- (211) Morena H, Janse MJ, Fiolet JW, Krieger WJ, Crijns H, Durrer D. Comparison of the effects of regional ischemia, hypoxia, hyperkalemia, and acidosis on intracellular and extracellular potentials and metabolism in the isolated porcine heart. *Circ Res* 1980; 46(5):634-646.
- (212) Shivkumar K, Deutsch NA, Lamp ST, Khuu K, Goldhaber JJ, Weiss JN. Mechanism of hypoxic K^+ loss in rabbit ventricle. *J Clin Invest* 1997; 100(7):1782-1788.
- (213) Orchard CH, Cingolani HE. Acidosis and arrhythmias in cardiac muscle. *Cardiovasc Res* 1994; 28(9):1312-1319.

- (214) Wilde AM. Myocardial ischaemia and hypoxia. Amsterdam: Rodopi, 1988.
- (215) Choi HS, Trafford AW, Orchard CH, Eisner DA. The effect of acidosis on systolic Ca^{2+} and sarcoplasmic reticulum calcium content in isolated rat ventricular myocytes. *J Physiol (Lond)* 2000; 529(3):661-668.
- (216) Omichi C, Lamp ST, Lin SF, Yang J, Baher A, Zhou S, Attin M, Lee MH, Karagueuzian HS, Kogan B, Qu Z, Garfinkel A, Chen PS, Weiss JN. Intracellular Ca dynamics in ventricular fibrillation. *Am J Physiol Heart Circ Physiol* 2004.
- (217) Wu ST, Weiss JN, Chou CC, Attin M, Hayashi H, Lin SF. Dissociation of membrane potential and intracellular calcium during ventricular fibrillation. *J Cardiovasc Electrophysiol* 2005; 16(2):186-192.
- (218) Kagiya Y, Hill JL, Gettes LS. Interaction of acidosis and increased extracellular potassium on action potential characteristics and conduction in guinea pig ventricular muscle. *Circ Res* 1982; 51(5):614-623.
- (219) Sato R, Noma A, Kurachi Y, Irisawa H. Effects of intracellular acidification on membrane currents in ventricular cells of the guinea pig. *Circ Res* 1985; 57(4):553-561.
- (220) Spitzer KW, Hogan PM. The effects of acidosis and bicarbonate on action potential repolarization in canine cardiac Purkinje fibers. *J Gen Physiol* 1979; 73(2):199-218.
- (221) Orchard CH, Houser SR, Kort AA, Bahinski A, Capogrossi MC, Lakatta EG. Acidosis facilitates spontaneous sarcoplasmic reticulum Ca^{2+} release in rat myocardium. *J Gen Physiol* 1987; 90(1):145-165.
- (222) Skinner RB, Jr., Kunze DL. Changes in extracellular potassium activity in response to decreased pH in rabbit atrial muscle. *Circ Res* 1976; 39(5):678-683.
- (223) Brown RH, Jr., Cohen I, Noble D. The interactions of protons, calcium and potassium ions on cardiac Purkinje fibres. *J Physiol (Lond)* 1978; 282(1):345-352.
- (224) Warren M, Pandit SV, Moreno J, Zaitsev A, Mironov S, Kalifa J, Jalife J. Contrasting effect of high extracellular K on left and right ventricular excitation frequencies during fibrillation. *Heart Rhythm* 1(1),S52. 2004.

- (225) Roden DM, Balsar JR, George AL, Angelos M. Cardiac ion channels. *Annu Rev Physiol* 2002; 64:431-475.
- (226) Dhamoon AS, Pandit SV, Sarmast F, Parisian KR, Guha P, Li Y, Bagwe S, Taffet SM, Anumonwo JMB. Unique Kir2.x properties determine regional and species differences in the cardiac inward rectifier K⁺ current. *Circ Res* 2004; 94(10):1332-1339.
- (227) Weidmann S. Shortening of the cardiac action potential due to a brief injection of KCl following the onset of activity. *J Physiol* 1956; 132(1):157-163.
- (228) Kleber AG, Janse MJ, van Capelle FJ, Durrer D. Mechanism and time course of S-T and T-Q segment changes during acute regional myocardial ischemia in the pig heart determined by extracellular and intracellular recordings. *Circ Res* 1978; 42(5):603-613.
- (229) Volders PGA, Sipido KR, Carmeliet E, Spatjens RLHM, Wellens HJJ, Vos MA. Repolarizing K⁺ currents I_{TO1} and I_{Ks} are larger in right than left canine ventricular midmyocardium. *Circulation* 1999; 99(2):206-210.
- (230) Weiss J, Shine KI. [K⁺]_o accumulation and electrophysiological alterations during early myocardial ischemia. *Am J Physiol Heart Circ Physiol* 1982; 243(2):H318-H327.
- (231) Kettlewell S, Walker NL, Cobbe SM, Burton FL, Smith GL. The electrophysiological and mechanical effects of 2,3-butane-dione monoxime and cytochalasin-D in the Langendorff perfused rabbit heart. *Exp Physiol* 2004; 89(2):163-172.
- (232) Cao JM, Qu Z, Kim YH, Wu TJ, Garfinkel A, Weiss JN, Karagueuzian HS, Chen PS. Spatiotemporal heterogeneity in the induction of ventricular fibrillation by rapid pacing: importance of cardiac restitution properties. *Circ Res* 1999; 84(11):1318-1331.
- (233) Chen X, Fenton FH, Gray RA. Head-tail interactions in numerical simulations of reentry in a ring of cardiac tissue. *Heart Rhythm* 2005; 2(8):851-859.
- (234) Banville I, Chattipakorn N, Gray RA. Restitution dynamics during pacing and arrhythmias in isolated pig hearts. *J Cardiovasc Electrophysiol* 2004; 15(4):455-463.
- (235) Wan X, Bryant SM, Hart G. The effects of [K⁺]_o on regional differences in electrical characteristics of ventricular myocytes in guinea-pig. *Exp Physiol* 2000; 85(6):769-774.

- (236) Gettes LS, Reuter H. Slow recovery from inactivation of inward currents in mammalian myocardial fibres. *J Physiol* 1974; 240(3):703-724.
- (237) Cobbe SM, Manley BS, Alexopoulos D. Interaction of the effects of hypoxia, substrate depletion, acidosis and hyperkalaemia on the class III antiarrhythmic properties of sotalol. *Cardiovasc Res* 1985; 19(11):668-673.
- (238) Downar E, Janse MJ, Durrer D. The effect of acute coronary artery occlusion on subepicardial transmembrane potentials in the intact porcine heart. *Circulation* 1977; 56(2):217-224.
- (239) Han J, MoeOE GK. Nonuniform recovery of excitability in ventricular muscle. *Circ Res* 1964; 14(1):44-60.
- (240) Grant AO, Starmer CF, Strauss HC. Antiarrhythmic drug action: Blockade of the inward sodium current. *Circ Res* 1984; 55(4):427-439.
- (241) Huang JL, Tai CT, Lin YJ, Ting CT, Chen YT, Chang MS, Lin FY, Lai WT, Chen SA. The Mechanisms of an increased dominant frequency in the left atrial posterior wall during atrial fibrillation in acute atrial dilatation. *J Cardiovasc Electrophysiol* 2006; 17(2):178-188.
- (242) Elharrar V, Foster PR, Jirak TL, Gaum WE, Zipes DP. Alterations in canine myocardial excitability during ischemia. *Circ Res* 1977; 40(1):98-105.
- (243) Stewart JR, Burmeister WE, Burmeister J, Lucchesi BR. Electrophysiologic and antiarrhythmic effects of phentolamine in experimental coronary artery occlusion and reperfusion in the dog. *J Cardiovasc Pharmacol* 1980; 2(1):77-91.
- (244) Penny WJ. The deleterious effects of myocardial catecholamines on cellular electrophysiology and arrhythmias during ischaemia and reperfusion. *Eur Heart J* 1984; 5(12):960-973.
- (245) Janse MJ, Capucci A, Coronel R, Fabius MA. Variability of recovery of excitability in the normal canine and the ischaemic porcine heart. *Eur Heart J* 1985; 6 Suppl D:41-52.

- (246) Sutton PMI, Taggart P, Opthof T, Coronel R, Trimlett R, Pugsley W, Kallis P. Repolarisation and refractoriness during early ischaemia in humans. *Heart* 2000; 84(4):365-369.
- (247) Sidorov VY, Woods MC, Wikswo JP. Effects of elevated extracellular potassium on the stimulation mechanism of diastolic cardiac tissue. *Biophys J* 2003; 84(5):3470-3479.
- (248) Chen C, Bharucha V, Chen Y, Westenbroek RE, Brown A, Malhotra JD, Jones D, Avery C, Gillespie PJ, III, Kazen-Gillespie KA, Kazarinova-Noyes K, Shrager P, Saunders TL, Macdonald RL, Ransom BR, Scheuer T, Catterall WA, Isom LL. Reduced sodium channel density, altered voltage dependence of inactivation, and increased susceptibility to seizures in mice lacking sodium channel beta 2-subunits. *PNAS* 2002; 99(26):17072-17077.
- (249) Wit AL, Janse MJ. *The Ventricular arrhythmias of ischaemia and infarction*. First ed. New York: Futura Publishing Company, 1993.
- (250) Nygren A, Giles WR. Mathematical simulation of slowing of cardiac conduction velocity by elevated extracellular potassium. *Ann Biomed Eng* 2000; 28(8):951-957.
- (251) Salama G, Kanai A, Efimov IR. Subthreshold stimulation of Purkinje fibers interrupts ventricular tachycardia in intact hearts. Experimental study with voltage-sensitive dyes and imaging techniques. *Circ Res* 1994; 74(4):604-619.
- (252) Wiegerinck RF, Verkerk AO, Belterman CN, van Veen TAB, Baartscheer A, Opthof T, Wilders R, de Bakker JMT, Coronel R. Larger cell size in rabbits with heart failure increases myocardial conduction velocity and QRS duration. *Circulation* 2006; 113(6):806-813.
- (253) Aya AG, Robert E, Bruelle P, Lefrant JY, Juan JM, Peray P, Eledjam JJ, de La Coussaye JE. Effects of ketamine on ventricular conduction, refractoriness, and wavelength: potential antiarrhythmic effects: a high-resolution epicardial mapping in rabbit hearts. *Anesthesiology* 1997; 87(6):1417-1427.

- (254) Qu Z, Weiss JN. Effects of Na⁺ and K⁺ channel blockade on vulnerability to and termination of fibrillation in simulated normal cardiac tissue. *Am J Physiol Heart Circ Physiol* 2005; 289(4):H1692-H1701.
- (255) Bishop MJ, Rodriguez B, Eason J, Whiteley JP, Trayanova N, Gavaghan DJ. Synthesis of voltage-sensitive optical signals: Application to panoramic optical mapping. *Biophys J* 2006; 90(8):2938-2945.
- (256) Pertsov AM, Zemlin CW, Hyatt CJ, Bernus O. What can we learn from the optically recorded epicardial action potential? *Biophys J* 2006; 91(10):3959-3960.
- (257) Hyatt CJ, Mironov SF, Vetter FJ, Zemlin CW, Pertsov AM. Optical action potential upstroke morphology reveals near-surface transmural propagation direction. *Circ Res* 2005; 97(3):277-284.
- (258) Yan GX, Shimizu W, Antzelevitch C. Characteristics and distribution of M cells in arterially perfused canine left ventricular wedge preparations. *Circulation* 1998; 98(18):1921-1927.
- (259) Antzelevitch C, Fish J. Electrical heterogeneity within the ventricular wall. *Basic Res Cardiol* 2001; 96(6):517-527.
- (260) Sosunov EA, Anyukhovskiy EP, Rosen MR. Effects of quinidine on repolarization in canine epicardium, midmyocardium, and endocardium: I. In vitro study. *Circulation* 1997; 96(11):4011-4018.
- (261) Ujhelyi MR, Creazzo TL. Action potentials that mimic fibrillation activate sodium current. *J Mol Cell Cardiol* 1999; 31(9):1673-1684.
- (262) Chorro FJ, Canoves J, Guerrero J, Mainar L, Sanchis J, Such L, Lopez-Merino V. Alteration of ventricular fibrillation by flecainide, verapamil, and sotalol: an experimental study. *Circulation* 2000; 101(13):1606-1615.
- (263) Chorro FJ, Guerrero J, Ferrero A, Tormos A, Mainar L, Millet J, Canoves J, Porres JC, Sanchis J, Lopez-Merino V, Such L. Effects of acute reduction of temperature on ventricular fibrillation activation patterns. *Am J Physiol Heart Circ Physiol*. 2002; 283(6):H2331-H2340.

- (264) Kardesch M, Hogancamp CE, Bing RJ. The Effect of complete ischemia on the intracellular electrical activity of the whole mammalian heart. *Circ Res* 1958; 6(6):715-720.
- (265) Knisley SB, Justice RK, Kong W, Johnson PL. Ratiometry of transmembrane voltage-sensitive fluorescent dye emission in hearts. *Am J Physiol Heart Circ Physiol* 2000; 279(3):H1421-H1433.
- (266) Witkowski FX, Leon LJ, Penkoske PA, Giles WR, Spano ML, Ditto WL, Winfree AT. Spatiotemporal evolution of ventricular fibrillation. *Nature* 1998; 392(6671):78-82.
- (267) Neubauer S, Newell JB, Ingwall JS. Metabolic consequences and predictability of ventricular fibrillation in hypoxia. A ³¹P- and ²³Na- nuclear magnetic resonance study of the isolated rat heart. *Circulation* 1992; 86(1):302-310.
- (268) Kusuoka H, Chacko VP, Marban E. Myocardial energetics during ventricular fibrillation investigated by magnetization transfer nuclear magnetic resonance spectroscopy. *Circ Res* 1992; 71(5):1111-1122.
- (269) Lawrence JH, Yue DT, Rose WC, Marban E. Sodium channel inactivation from resting states in guinea-pig ventricular myocytes. *J Physiol* 1991; 443:629-650.
- (270) Garlick PB, Radda GK, Seeley PJ. Studies of acidosis in the ischaemic heart by phosphorus nuclear magnetic resonance. *Biochem J* 1979; 184(3):547-554.
- (271) Rogers JM, Huang J, Smith WM, Ideker RE. Incidence, evolution, and spatial distribution of functional reentry during ventricular fibrillation in pigs. *Circ Res* 1999; 84(8):945-954.
- (272) Huang J, Rogers JM, Killingsworth CR, Singh KP, Smith WM, Ideker RE. Evolution of activation patterns during long-duration ventricular fibrillation in dogs. *Am J Physiol Heart Circ Physiol* 2004; 286(3):H1193-H1200.
- (273) Efimov I, Cheng Y. Mechanisms of internal defibrillation. In: Rosenbaum DS, Jalife J, editors. *Optical mapping of cardiac excitation and arrhythmias*. New York: Futura, 2001: 407-431.

- (274) Komukai K, Brette F, Pascarel C, Orchard CH. Electrophysiological response of rat ventricular myocytes to acidosis. *Am J Physiol Heart Circ Physiol* 2002; 283(1):H412-H422.
- (275) Ujhelyi MR, Sims JJ, Miller AW. Induction of electrical heterogeneity impairs ventricular defibrillation: an effect specific to regional conduction velocity slowing. *Circulation* 1999; 100(25):2534-2540.
- (276) Goto Y, Suzuki I, Inaba H. Frequency of ventricular fibrillation as predictor of one-year survival from out-of-hospital cardiac arrests. *Am J Cardiol* 2003; 92(4):457-459.
- (277) Brown CG, Dzwonczyk R. Signal analysis of the human electrocardiogram during ventricular fibrillation: frequency and amplitude parameters as predictors of successful countershock. *Ann Emerg Med* 1996; 27(2):184-188.
- (278) Eftestol T, Wik L, Sunde K, Steen PA. Effects of cardiopulmonary resuscitation on predictors of ventricular fibrillation defibrillation success during out-of-hospital cardiac arrest. *Circulation* 2004; 110(1):10-15.
- (279) Callihan J, Roeder R, Geddes LA, Otlewski M, Kemeny A. Ventricular fibrillation frequency. *Pacing Clin Electrophysiol* 2005; 28(7):610-612.
- (280) Niemann JT, Cruz B, Garner D, Lewis RJ. Immediate countershock versus cardiopulmonary resuscitation before countershock in a 5-minute swine model of ventricular fibrillation arrest. *Ann Emerg Med* 2000; 36(6):543-546.
- (281) Berg RA, Hilwig RW, Ewy GA, Kern KB. Precountershock cardiopulmonary resuscitation improves initial response to defibrillation from prolonged ventricular fibrillation: A randomized, controlled swine study. *Crit Care Med* 2004; 32(6):1352-1357.
- (282) Menegazzi JJ, Wang HE, Lightfoot CB, Fertig KC, Chengelis NL, Sherman LD, Callaway CW. Immediate defibrillation versus interventions first in a swine model of prolonged ventricular fibrillation. *Resuscitation* 2003; 59(2):261-270.
- (283) Behrens S, Li C, Franz MR. Effects of myocardial ischemia on ventricular fibrillation inducibility and defibrillation efficacy. *J Am Coll Cardiol* 1997; 29(4):817-824.

- (284) Rodriguez B, Tice BM, Eason JC, Aguel F, Ferrero Jr JM, Trayanova N. Effect of acute global ischemia on the upper limit of vulnerability: a simulation study. *Am J Physiol Heart Circ Physiol* 2004; 286(6):H2078-H2088.
- (285) Rodriguez B, Tice BM, Eason JC, Aguel F, Trayanova N. Cardiac vulnerability to electric shocks during phase 1A of acute global ischemia. *Heart Rhythm* 2004; 1(6):695-703.
- (286) Hwang C, Swerdlow CD, Kass RM, Gang ES, Mandel WJ, Peter CT, Chen PS. Upper limit of vulnerability reliably predicts the defibrillation threshold in humans. *Circulation* 1994; 90(5):2308-2314.
- (287) Chen PS, Feld GK, Mower MM, Peters BB. Effects of pacing rate and timing of defibrillation shock on the relation between the defibrillation threshold and the upper limit of vulnerability in open chest dogs. *J Am Coll Cardiol* 1991; 18(6):1555-1563.
- (288) Chattipakorn N, Ideker RE. Delayed afterdepolarization inhibitor: a potential pharmacologic intervention to improve defibrillation efficacy. *J Cardiovasc Electrophysiol* 2003; 14(1):72-75.
- (289) Qin H, Walcott GP, Killingsworth CR, Rollins DL, Smith WM, Ideker RE. Impact of myocardial ischemia and reperfusion on ventricular defibrillation patterns, energy requirements, and detection of recovery. *Circulation* 2002; 105(21):2537-2542.
- (290) Walcott GP, Killingsworth CR, Smith WM, Ideker RE. Biphasic waveform external defibrillation thresholds for spontaneous ventricular fibrillation secondary to acute ischemia. *J Am Coll Cardiol* 2002; 39(2):359-365.
- (291) Arredondo MT, Armayor MR, Valentinuzzi ME. Electrical defibrillation thresholds with transventricular simple-capacitor discharge under conditions of ischemia by acute coronary occlusion. *Med Prog Technol* 1982; 8(4):175-181.
- (292) Jones DL, Sohla A, Klein GJ. Internal cardiac defibrillation threshold: effects of acute ischemia. *Pacing Clin Electrophysiol* 1986; 9(3):322-331.
- (293) Ruffy R, Schwartz DJ, Hieb BR. Influence of acute coronary artery occlusion on direct ventricular defibrillation in dogs. *Med Instrum* 1980; 14(1):23-26.

- (294) Kerber RE, Pandian NG, Hoyt R, Jensen SR, Koyanagi S, Grayzel J, Kieso R. Effect of ischemia, hypertrophy, hypoxia, acidosis, and alkalosis on canine defibrillation. *Am J Physiol Heart Circ Physiol* 1983; 244(6):H825-H831.
- (295) Cheng Y, Mowrey KA, Nikolski V, Tchou PJ, Efimov IR. Mechanisms of shock-induced arrhythmogenesis during acute global ischemia. *Am J Physiol Heart Circ Physiol* 2002; 282(6):H2141-H2151.
- (296) Swerdlow CD, Lin SF. Optimizing defibrillation waveforms. *J Cardiovasc Electrophysiol* 2002; 13(4):371-373.
- (297) Malkin RA. Large sample test of defibrillation waveform sensitivity. *J Cardiovasc Electrophysiol* 2002; 13(4):361-370.
- (298) Guan D, Malkin R. Analysis of the defibrillation efficacy for 5-ms waveforms. *J Cardiovasc Electrophysiol* 2004; 15(4):447-454.
- (299) Natale A, Sra J, Krum D, Dhala A, Deshpande S, Jazayeri M, Newby K, Wase A, Axtell K, VanHout WL, Akhtar M. Relative efficacy of different tilts with biphasic defibrillation in humans. *Pacing Clin Electrophysiol* 1996; 19(2):197-206.
- (300) Yamanouchi Y, Brewer JE, Olson KF, Mowrey KA, Mazgalev TN, Wilkoff BL, Tchou PJ. Fully Discharging Phases: A new approach to biphasic waveforms for external defibrillation. *Circulation* 1999; 100(8):826-831.
- (301) Plank G, Leon LJ, Kimber S, Vigmond EJ. Defibrillation depends on conductivity fluctuations and the degree of disorganization in reentry patterns. *J Cardiovasc Electrophysiol* 2005; 16(2):205-216.
- (302) Hillebrenner MG, Eason JC, Trayanova NA. Mechanistic inquiry into decrease in probability of defibrillation success with increase in complexity of preshock reentrant activity. *Am J Physiol Heart Circ Physiol* 2004; 286(3):H909-H917.
- (303) Yakaitis RW, Thomas JD, Mahaffey JE. Influence of pH and hypoxia on the success of defibrillation. *Crit Care Med* 1975; 3(4):139-142.

- (304) Babbs CF, Whistler SJ, Yim GK, Tacker WA, Geddes LA. Dependence of defibrillation threshold upon extracellular/intracellular K^+ concentrations. *J Electrocardiol* 1980; 13(1):73-78.
- (305) Salama G, Kanai AJ, Huang D, Efimov IR, Girouard SD, Rosenbaum DS. Hypoxia and hypothermia enhance spatial heterogeneities of repolarization in guinea pig hearts: analysis of spatial autocorrelation of optically recorded action potential durations. *J Cardiovasc Electrophysiol* 1998; 9(2):164-183.
- (306) Sims JJ, Miller AW, Ujhelyi MR. Regional hyperkalemia increases ventricular defibrillation energy requirements: role of electrical heterogeneity in defibrillation. *J Cardiovasc Electrophysiol* 2000; 11(6):634-641.
- (307) Moubarak JB, Karasik PE, Fletcher RD, Franz MR. High dispersion of ventricular repolarization after an implantable defibrillator shock predicts induction of ventricular fibrillation as well as unsuccessful defibrillation. *J Am Coll Cardiol* 2000; 35(2):422-427.
- (308) Coetzee WA, Opie LH. Effects of components of ischemia and metabolic inhibition on delayed afterdepolarizations in guinea pig papillary muscle. *Circ Res* 1987; 61(2):157-165.
- (309) Kerber RE, Sarnat W. Factors influencing the success of ventricular defibrillation in man. *Circulation* 1979; 60(2):226-230.
- (310) Tang W. Hypercarbia decreases effectiveness of electrical defibrillation during CPR. *Crit Care Med* 20, s24. 1992.
- (311) Maldonado FA, Weil MH, Tang W, Bisera J, Gazmuri RJ, Johnson B, D'Alessio A. Myocardial hypercarbic acidosis reduces cardiac resuscitability. *Anesthesiology* 1993; 78(2):343-352.
- (312) von Planta, I, Weil MH, von Planta M, Gazmuri RJ, Duggal C. Hypercarbic acidosis reduces cardiac resuscitability. *Crit Care Med* 1991; 19(9):1177-1182.
- (313) Coraboeuf E, Deroubaix E, Hoerter J. Control of ionic permeabilities in normal and ischemic heart. *Circ Res* 1976; 38(5 Suppl 1):I92-I98.

- (314) Coraboeuf E, Deroubaix E, Coulombe A. Acidosis-induced abnormal repolarization and repetitive activity in isolated dog Purkinje fibers. *J Physiol (Paris)* 1980; 76(2):97-106.
- (315) Coulombe A, Coraboeuf E, Deroubaix E. Computer simulation of acidosis-induced abnormal repolarization and repetitive activity in dog Purkinje fibers. *J Physiol (Paris)* 1980; 76(2):107-112.
- (316) Kurachi Y. The effects of intracellular protons on the electrical activity of single ventricular cells. *Pflügers Archiv* 1982; 394(3):264-270.
- (317) Orchard CH, McCall E, Kirby MS, Boyett MR. Mechanical alternans during acidosis in ferret heart muscle. *Circ Res* 1991; 68(1):69-76.
- (318) McCall E, Orchard CH. The effect of acidosis on the interval-force relation and mechanical restitution in ferret papillary muscle. *J Physiol* 1991; 432:45-63.
- (319) Veenstra RD, Joyner RW, Wiedmann RT, Young ML, Tan RC. Effects of hypoxia, hyperkalemia, and metabolic acidosis on canine subendocardial action potential conduction. *Circ Res* 1987; 60(1):93-101.
- (320) Eloff BC, Gilat E, Wan X, Rosenbaum DS. Pharmacological modulation of cardiac gap junctions to enhance cardiac conduction: Evidence supporting a novel target for antiarrhythmic therapy. *Circulation* 2003; 108(25):3157-3163.
- (321) Burt JM. Block of intercellular communication: interaction of intracellular H^+ and Ca^{2+} . *Am J Physiol Cell Physiol* 1987; 253(4):C607-C612.
- (322) Pressler ML. Effects of pCa_i and pH_i on cell-to-cell coupling. *Experientia* 1987; 43(10):1084-1091.
- (323) Marban E, Robinson SW, Wier WG. Mechanisms of arrhythmogenic delayed and early afterdepolarizations in ferret ventricular muscle. *J Clin Invest* 1986; 78(5):1185-1192.
- (324) Loughrey CM, MacEachern KE, Neary P, Smith GL. The relationship between intracellular Ca^{2+} and Ca^{2+} wave characteristics in permeabilised cardiomyocytes from the rabbit. *J Physiol* 2002; 543(Pt 3):859-870.

- (325) Kojima S, Wu ST, Wikman-Coffelt J, Parmley WW. Acute amiodarone terminates ventricular fibrillation by modifying cellular Ca^{2+} homeostasis in isolated perfused rat hearts. *J Pharmacol Exp Ther* 1995; 275(1):254-262.
- (326) Zaugg CE, Wu ST, Barbosa V, Buser PT, Wikman-Coffelt J, Parmley WW, Lee RJ. Ventricular fibrillation-induced intracellular Ca^{2+} overload causes failed electrical defibrillation and post-shock reinitiation of fibrillation. *J Mol Cell Cardiol* 1998; 30(11):2183-2192.
- (327) Chattipakorn N, Banville I, Gray RA, Ideker RE. Mechanism of ventricular defibrillation for near-defibrillation threshold shocks: a whole-heart optical mapping study in swine. *Circulation* 2001; 104(11):1313-1319.
- (328) Spear JF, Moore EN. A comparison of alternation in myocardial action potentials and contractility. *Am J Physiol* 1971; 220(6):1708-1716.
- (329) Allen DG, Lee JA, Smith GL. The consequences of simulated ischaemia on intracellular Ca^{2+} and tension in isolated ferret ventricular muscle. *J Physiol* 1989; 410:297-323.
- (330) Pastore JM, Girouard SD, Laurita KR, Akar FG, Rosenbaum DS. Mechanism linking T-wave alternans to the genesis of cardiac fibrillation. *Circulation* 1999; 99(10):1385-1394.
- (331) Qu Z, Garfinkel A, Chen PS, Weiss JN. Mechanisms of discordant alternans and induction of reentry in simulated cardiac tissue. *Circulation* 2000; 102(14):1664-1670.
- (332) Pastore JM, Laurita KR, Rosenbaum DS. Importance of spatiotemporal heterogeneity of cellular restitution in mechanism of arrhythmogenic discordant alternans. *Heart Rhythm* 2006; 3(6):711-719.
- (333) Shiferaw Y, Sato D, Karma A. Coupled dynamics of voltage and calcium in paced cardiac cells. *Phys Rev E Stat Nonlin Soft Matter Phys* 2005; 71(2 Pt 1):021903.
- (334) Brown RH, Jr., Noble D. Displacement of activator thresholds in cardiac muscle by protons and calcium ions. *J Physiol (Lond)* 1978; 282(1):333-343.

- (335) Weiss JN, Karma A, Shiferaw Y, Chen PS, Garfinkel A, Qu Z. From pulsus to pulseless: the saga of cardiac alternans. *Circ Res* 2006; 98(10):1244-1253.
- (336) Ovrum E, Tangen G, Holen EA, Ringdal MA, Istad R. Conversion of postischemic ventricular fibrillation with intraaortic infusion of potassium chloride. *Ann Thorac Surg* 1995; 60(1):156-159.
- (337) Zipes DP, Wellens HJJ. Sudden cardiac death. *Circulation* 1998; 98(21):2334-2351.
- (338) Pinto JMB, Boyden PA. Electrical remodeling in ischemia and infarction. *Cardiovasc Res* 1999; 42(2):284-297.
- (339) Camelliti P, Devlin GP, Matthews KG, Kohl P, Green CR. Spatially and temporally distinct expression of fibroblast connexins after sheep ventricular infarction. *Cardiovasc Res* 2004; 62(2):415-425.
- (340) Smith JH, Green CR, Peters NS, Rothery S, Severs NJ. Altered patterns of gap junction distribution in ischemic heart disease. An immunohistochemical study of human myocardium using laser scanning confocal microscopy. *Am J Pathol* 1991; 139(4):801-821.
- (341) Peters NS, Green CR, Poole-Wilson PA, Severs NJ. Reduced content of connexin 43 gap junctions in ventricular myocardium from hypertrophied and ischemic human hearts. *Circulation* 1993; 88(3):864-875.
- (342) Peters NS, Coromilas J, Severs NJ, Wit AL. Disturbed connexin 43 gap junction distribution correlates with the location of reentrant circuits in the epicardial border zone of healing canine infarcts that cause ventricular tachycardia. *Circulation* 1997; 95(4):988-996.
- (343) Li L, Nikolski V, Wallick DW, Efimov IR, Cheng Y. Mechanisms of enhanced shock-induced arrhythmogenesis in the rabbit heart with healed myocardial infarction. *Am J Physiol Heart Circ Physiol* 2005; 289(3):H1054-H1068.
- (344) Tomaselli GF, Marban E. Electrophysiological remodeling in hypertrophy and heart failure. *Cardiovasc Res* 1999; 42(2):270-283.

- (345) Olivetti G, Capasso JM, Meggs LG, Sonnenblick EH, Anversa P. Cellular basis of chronic ventricular remodeling after myocardial infarction in rats. *Circ Res* 1991; 68(3):856-869.
- (346) Anversa P, Loud AV, Levicky V, Guideri G. Left ventricular failure induced by myocardial infarction. I. Myocyte hypertrophy. *Am J Physiol Heart Circ Physiol* 1985; 248(6):H876-H882.
- (347) Cox MM, Berman I, Myerburg RJ, Smets MJD, Kozlovskis PL. Morphometric mapping of regional myocyte diameters after healing of myocardial infarction in cats. *J Mol Cell Cardiol* 1991; 23(2):127-135.
- (348) Santos PE, Barcellos LC, Mill JG, Masuda MO. Ventricular action potential and L-type calcium channel in infarct-induced hypertrophy in rats. *J Cardiovasc Electrophysiol* 1995; 6(11):1004-1014.
- (349) Kaprielian R, Sah R, Nguyen T, Wickenden AD, Backx PH. Myocardial infarction in rat eliminates regional heterogeneity of AP profiles, Ito K⁺ currents, and [Ca²⁺]_i transients. *Am J Physiol Heart Circ Physiol* 2002; 283(3):H1157-H1168.
- (350) Pak PH, Nuss HB, Tunin RS, Kaab S, Tomaselli GF, Marban E, Kass DA. Repolarization abnormalities, arrhythmia and sudden death in canine tachycardia-induced cardiomyopathy. *J Am Coll Cardiol* 1997; 30(2):576-584.
- (351) Friedman PA, Foley DA, Christian TF, Stanton MS. Stability of the defibrillation probability curve with the development of ventricular dysfunction in the canine rapid paced model. *Pacing Clin Electrophysiol* 1998; 21(2):339-351.
- (352) Huang J, Rogers JM, Killingsworth CR, Walcott GP, KenKnight BH, Smith WM, Ideker RE. Improvement of defibrillation efficacy and quantification of activation patterns during ventricular fibrillation in a canine heart failure model. *Circulation* 2001; 103(10):1473-1478.
- (353) Ideker RE, Zhou X, Knisley SB. Correlation among fibrillation, defibrillation, and cardiac pacing. *Pacing Clin Electrophysiol* 1995; 18(3):512-525.

- (354) Schuger C, Ellenbogen KA, Faddis M, Knight BP, Yong P, Sample R. Defibrillation energy requirements in an ICD population receiving cardiac resynchronization therapy. *J Cardiovasc Electrophysiol* 2006; 17(3):247-250.
- (355) Khalighi K, Daly B, Leino EV, Shorofsky SR, Kavesh NG, Peters RW, Gold MR. Clinical predictors of transvenous defibrillation energy requirements. *Am J Cardiol* 1997; 79(2):150-153.
- (356) Trayanova N, Plank G, Rodriguez B. What have we learned from mathematical models of defibrillation and postshock arrhythmogenesis? Application of bidomain simulations. *Heart Rhythm* 2006; 3(10):1232-1235.
- (357) Opthof T, Coronel R, Shander GS, Wilms-Schopman FJG, Janse MJ. Electrophysiologic changes and ventricular fibrillation in acute regional ischaemia in the porcine heart. *J Cardiovasc Electrophysiol* 1992; 3:128-140.
- (358) Rogers JM, Huang J, Pedoto RW, Walker RG, Smith WM, Ideker RE. Fibrillation is more complex in the left ventricle than in the right ventricle. *J Cardiovasc Electrophysiol* 2000; 11(12):1364-1371.
- (359) Weiss JN, Qu Z, Chen PS, Lin SF, Karagueuzian HS, Hayashi H, Garfinkel A, Karma A. The Dynamics of Cardiac Fibrillation. *Circulation* 2005; 112(8):1232-1240.
- (360) Chudin E, Goldhaber J, Garfinkel A, Weiss J, Kogan B. Intracellular Ca^{2+} dynamics and the stability of ventricular tachycardia. *Biophys J* 1999; 77(6):2930-2941.
- (361) Lakkireddy V, Bub G, Baweja P, Syed A, Boutjdir M, El Sherif N. The kinetics of spontaneous calcium oscillations and arrhythmogenesis in the in vivo heart during ischemia/reperfusion. *Heart Rhythm* 2006; 3(1):58-66.
- (362) Samie FH, Mandapati R, Gray RA, Watanabe Y, Zuur C, Beaumont J, Jalife J. A mechanism of transition from ventricular fibrillation to tachycardia: Effect of calcium channel blockade on the dynamics of rotating waves. *Circ Res* 2000; 86(6):684-691.
- (363) Kawahara K, Takase M, Yamauchi Y, Kimura H. Spectral and correlation analyses of the verapamil-induced conversion of ventricular fibrillation to tachycardia in isolated rat hearts. *J Electrocardiol* 2004; 37(2):89-100.

- (364) Adams JN, Sirel J, Marsden K, Cobbe SM. Heartstart Scotland: the use of paramedic skills in out of hospital resuscitation. *Heart* 1997; 78(4):399-402.
- (365) Bar-Joseph G, Weinberger T, Castel T, Bar-Joseph N, Laor A, Bursztein S, Ben Haim S. Comparison of sodium bicarbonate, Carbicarb, and THAM during cardiopulmonary resuscitation in dogs. *Crit Care Med* 1998; 26(8):1397-1408.
- (366) Leong ECM, Bendall JC, Boyd AC, Einstein R. Sodium bicarbonate improves the chance of resuscitation after 10 minutes of cardiac arrest in dogs. *Resuscitation* 2001; 51(3):309-315.
- (367) Kette F, Weil MH, von Planta M, Gazmuri RJ, Rackow EC. Buffer agents do not reverse intramyocardial acidosis during cardiac resuscitation. *Circulation* 1990; 81(5):1660-1666.
- (368) Kirchhof P, Borggrefe M, Breithardt G. Effect of electrode position on the outcome of cardioversion. *Cardiac Electrophysiology Review* 2003; 7(3):292-296.
- (369) Kirchhof P, Eckardt L, Loh P, Weber K, Fischer RJ, Seidl KH, Bocker D, Breithardt G, Haverkamp W, Borggrefe M. Anterior-posterior versus anterior-lateral electrode positions for external cardioversion of atrial fibrillation: a randomised trial. *Lancet* 2002; 360(9342):1275-1279.
- (370) Botto GL, Politi A, Bonini W, Broffoni T, Bonatti R. External cardioversion of atrial fibrillation: role of paddle position on technical efficacy and energy requirements. *Heart* 1999; 82(6):726-730.
- (371) Lown B. Electrical reversion of cardiac arrhythmias. *Br Heart J* 1967; 29(4):469-489.
- (372) Lown B, Kleigher R, Wolff G. The technique of cardioversion. *Am Heart J* 1964; 67:282-284.
- (373) Siaplaouras S, Buob A, Rotter C, Bohm M, Jung J. Randomized comparison of anterolateral versus anteroposterior electrode position for biphasic external cardioversion of atrial fibrillation. *Am Heart J* 2005; 150(1):150-152.

- (374) Alp NJ, Rahman S, Bell JA, Shahi M. Randomised comparison of antero-lateral versus antero-posterior paddle positions for DC cardioversion of persistent atrial fibrillation. *Int J Cardiol* 2000; 75(2-3):211-216.
- (375) Atwood C, Eisenberg MS, Herlitz J, Rea TD. Incidence of EMS-treated out-of-hospital cardiac arrest in Europe. *Resuscitation* 2005; 67(1):75-80.
- (376) Kleber AG, Janse MJ, Wilms-Schopmann FJ, Wilde AA, Coronel R. Changes in conduction velocity during acute ischemia in ventricular myocardium of the isolated porcine heart. *Circulation* 1986; 73(1):189-198.